Université de Montréal

Paramétrisation de la rétrodiffusion ultrasonore érythrocytaire haute fréquence et pertinence comme facteur de risque de la thrombose veineuse

par

François Tchi-Ho Yu

Institut de génie biomédical

Faculté de médecine

Thèse présentée à la Faculté des études supérieures
en vue de l'obtention du grade de Philosophiae Doctor (Ph.D.)
en génie biomédical

Décembre 2009

Université de Montréal

Faculté des études supérieures

Cette thèse intitulée :

Paramétrisation de la rétrodiffusion ultrasonore érythrocytaire haute fréquence et pertinence comme facteur de risque de la thrombose veineuse

présentée par :

François Tchi-Ho Yu

a été évaluée par un jury composé des personnes suivantes :

Alain Vinet
président-rapporteur

Guy Cloutier
directeur de recherche

André Denault
membre du jury

Michael Kolios
examinateur externe

Vasile Diaconu
représentant du doyen de la FES

Résumé

L'agrégation érythrocytaire est le principal facteur responsable des propriétés non newtoniennes sanguines pour des conditions d'écoulement à faible cisaillement. Lorsque les globules rouges s'agrègent, ils forment des rouleaux et des structures tridimensionnelles enchevêtrées qui font passer la viscosité sanguine de quelques mPa.s à une centaine de mPa.s. Cette organisation microstructurale érythrocytaire est maintenue par des liens inter-globulaires de faible énergie, lesquels sont brisés par une augmentation du cisaillement. Ces propriétés macroscopiques sont bien connues. Toutefois, les liens étiologiques entre ces propriétés rhéologiques générales et leurs effets pathophysiologiques demeurent difficiles à évaluer *in vivo* puisque les propriétés sanguines sont dynamiques et fortement tributaires des conditions d'écoulement. Ainsi, à partir de propriétés rhéologiques mesurées *in vitro* dans des conditions contrôlées, il devient difficile d'extrapoler leurs valeurs dans un environnement physiologique. Or, les thrombophlébites se développent systématiquement en des *loci* particuliers du système cardiovasculaire. D'autre part, plusieurs études cliniques ont établi que des conditions hémorhéologiques perturbées constituent des facteurs de risque de thrombose veineuse mais leurs contributions étiologiques demeurent hypothétiques ou corrélatives. En conséquence, un outil de caractérisation hémorhéologique applicable *in vivo* et *in situ* devrait permettre de mieux cerner et comprendre ces implications.

Les ultrasons, qui se propagent dans les tissus biologiques, sont sensibles à l'agrégation érythrocytaire. De nature non invasive, l'imagerie ultrasonore permet de caractériser *in vivo* et *in situ* la microstructure sanguine dans des conditions d'écoulements physiologiques. Les signaux ultrasonores rétrodiffusés portent une information sur la microstructure sanguine reflétant directement les perturbations

hémorhéologiques locales. Une cartographie *in vivo* de l'agrégation érythrocytaire, unique aux ultrasons, devrait permettre d'investiguer les implications étiologiques de l'hémorhéologie dans la maladie thrombotique vasculaire.

Cette thèse complète une série de travaux effectués au Laboratoire de Biorhéologie et d'Ultrasonographie Médicale (LBUM) du centre de recherche du Centre hospitalier de l'Université de Montréal portant sur la rétrodiffusion ultrasonore érythrocytaire et menant à une application *in vivo* de la méthode. Elle se situe à la suite de travaux de modélisation qui ont mis en évidence la pertinence d'un modèle particulaire tenant compte de la densité des globules rouges, de la section de rétrodiffusion unitaire d'un globule et du facteur de structure. Ce modèle permet d'établir le lien entre la microstructure sanguine et le spectre fréquentiel du coefficient de rétrodiffusion ultrasonore. Une approximation au second ordre en fréquence du facteur de structure est proposée dans ces travaux pour décrire la microstructure sanguine. Cette approche est tout d'abord présentée et validée dans un champ d'écoulement cisaillé homogène. Une extension de la méthode en 2D permet ensuite la cartographie des propriétés structurelles sanguines en écoulement tubulaire par des images paramétriques qui mettent en évidence le caractère temporel de l'agrégation et la sensibilité ultrasonore à ces phénomènes. Une extrapolation menant à une relation entre la taille des agrégats érythrocytaires et la viscosité sanguine permet l'établissement de cartes de viscosité locales. Enfin, il est démontré, à l'aide d'un modèle animal, qu'une augmentation subite de l'agrégation érythrocytaire provoque la formation d'un thrombus veineux. Le niveau d'agrégation, la présence du thrombus et les variations du débit ont été caractérisés, dans cette étude, par imagerie ultrasonore. Nos résultats suggèrent que des paramètres hémorhéologiques, préférablement mesurés *in vivo* et *in situ*, devraient faire partie du profil de risque thrombotique.

Mots-clés : ultrasons, coefficient de rétrodiffusion ultrasonore, agrégation érythrocytaire, diffusion non-Rayleigh, facteur de structure, caractérisation *in vivo*, modification des énergies d'interaction érythrocytaire par Pluronics, carte de viscosité locale, thrombophlébite.

Abstract

The aggregation of erythrocytes is the main determinant of blood non Newtonian behaviour under low shearing flow conditions. When red blood cells (RBCs) aggregate, they form « *rouleaux* » and complex tridimensional structures that increase blood viscosity from a few mPa.s to a hundred mPa.s. The reversible RBC aggregation phenomenon is attributed to weak adhesive links between erythrocytes that are readily broken by increasing flow shearing. Blood bulk rheological properties have been comprehensively studied. However, the *in vivo* physiological impacts of abnormal clustering of RBCs are more difficult to assess. Clinical studies have identified altered hemorheology as a risk factor for thrombosis, but a clear etiological relationship between abnormal aggregation and thrombosis has not yet been established, in part because clinical conclusions were derived from correlative findings. It is to note that cardiovascular diseases such as deep venous thrombosis generally occur at specific locations within the vascular bed, suggesting a hemodynamic contribution to the development of this disease. Consequently, it is postulated that *in vivo* hemorheological characterization may help shed some light on the role of RBC hyper-aggregation on cardiovascular disorders.

Ultrasound imaging, a non-invasive method relying on the propagation of mechanical waves within biological tissues, is sensitive to RBC aggregation. Indeed, the study of backscattered waves allows characterizing blood microstructure *in vivo* and *in situ* under physiological flow conditions.

The work described in this thesis is based on prior simulation studies, performed at the Laboratory of Biorheology and Medical Ultrasonics of the University of Montreal Hospital Research Center, in which the backscattering of ultrasound from aggregating RBCs was modeled by considering a particle scattering

strategy. In this approach, each RBC is a weak ultrasound scatterer (Born assumption) and the backscattering coefficient is modeled as the product of the RBC number density, the RBC backscattering cross section and a structure factor. This model relates variations in the backscattering coefficient to the RBC spatial organisation through the structure factor, which is the only parameter that changes during the aggregation process. A second order expansion in frequency of the structure factor was used to describe blood microstructure in terms of a packing factor *W* and an ensemble averaged aggregate diameter *D*. The model was first presented and validated by considering a homogenous shear flow condition using three broadband mono-element transducers. It was then extended in 2D to allow computation of parametric images in tube flow. An extrapolation based on the assumption that viscosity is related to the level of aggregation was used to compute local viscosity maps. Finally, a last contribution was the demonstration that a sudden increase in aggregation tendency directly promoted the formation of venous thrombosis in an experimental animal model. In that study, RBC aggregation, thrombus formation and flow variations were monitored longitudinally for two weeks using ultrasound. The results reported in this thesis suggest that rheological parameters on RBC clustering, ideally assessed *in vivo* and *in situ*, should be included in thrombosis risk profiling.

Keywords : Ultrasound, backscatter coefficient, erythrocyte aggregation, non Rayleigh scattering, structure factor, *in vivo* validation, modification of erythrocyte aggregation properties with Pluronics, local viscosity map, thrombosis.

Table des matières

Liste des tableaux

Liste des figures

Liste des symboles et abréviations

a : rayon d'un globule rouge (m)

α : coefficient d'atténuation (dB/MHz/cm)

α_0 : coefficient d'atténuation total (dB/MHz)

B : biais expérimental sur *H*

B/A : le coefficient de non linéarité ultrasonore (adimensionnel)

BH : phénomène du « trou noir » (« *black hole* »)

BSC : coefficient de rétrodiffusion (« *backscattering coefficient* ») ($sr^{-1}.cm^{-1}$)

$\overline{BSC}$: coefficient de rétrodiffusion moyenné sur la bande passante

c : vitesse du son ($m.s^{-1}$)

CV : coefficient de variation

d : dimension fractale (adimensionnel)

d0,d1,…,d_n : Jour 0, 1,…, n (« *day* »)

D : diamètre normalisé d'un agrégat isotrope (nombre de globules)

dP : intensité diffusée (V^2)

dΩ : angle solide (sr^{-1})

dV : volume élémentaire (m^3)

DVT : thrombophlébite (« *deep vein thrombosis* »)

EA : agrégation érythrocytaire (« *erythrocyte aggregation* »)

f : fréquence (MHz)

F_{max} : borne fréquentielle maximale utilisée dans le SFSE

g(r) : fonction de corrélation de paire

$\dot{\gamma}$ = SR: taux de cisaillement (« *shear rate* ») (s^{-1})

γ_z : contraste d'impédance acoustique

γ_κ : contraste de compressibilité

γ_ρ : contraste de densité

H : hématocrite

H6 : suspension saline de globules rouges (non agrégeante) à H = 6%

H40 : suspension saline de globules rouges (non agrégeante) à H = 40%

IVUS : imagerie ultrasonore intra-vasculaire (« *intravascular ultrasound* »)

$\vec{t}$: vecteur unitaire

$I_{incident}$: intensité incidente (V^2)

k : nombre d'onde ($rad.m^{-1}$)

K : index d'uniformité d'écoulement ($Pa.s^n$)

K_b : constante de Boltzmann

κ : compressibilité (Pa^{-1})

κ_e : compressibilité d'un érythrocyte (Pa^{-1})

κ_p : compressibilité plasmatique (Pa^{-1})

LDL : lipoprotéines de basse densité (« *low density lipoproteins* »)

λ : longueur d'onde (m)

m : densité volumique (nombre de globules par volume unitaire)

M1 : index d'agrégation (sans unité) mesuré en transmission laser. M1 augmente avec l'agrégation mesuré avec l'érythroagregamètre Myrenne (voir paragraphe 1.4.4).

μ : viscosité (Pa.s)

μ_p : viscosité plasmatique (Pa.s)

n : index de comportement d'écoulement (adimensionnel)

N : nombre de globules par agrégat

$N(x,y)$: densité microscopique

P_{H6} : spectre du signal rétrodiffusé par la solution H6

P_{H40} : spectre du signal rétrodiffusé par la solution H40

P_{T6} : spectre du signal rétrodiffusé par la solution T6

P_{T40} : spectre du signal rétrodiffusé par la solution T40

PBS : solution saline (« *phosphate buffered saline* ») (0.9%)

PV : viscosité plasmatique (« *plasmatic viscosity* ») (Pa.s)

PVA : Cryogel d'alcool de polyvinlyle (« *polyvinyl alcohol cryogel* ») écho transparent

PVDF : poly(vinylidene fluoride)

ρ : densité ($kg.m^{-3}$)

ρ_e : densité d'un érythrocyte ($kg.m^{-3}$)

ρ_p : densité plasmatique ($kg.m^{-3}$)

r : distance radiale (m)

R : rayon d'un agrégat (m)

r^2 : coefficient de corrélation

RBC : globule rouge (« *red blood cell* »)

RF(t) : Signal radio fréquence provennant directement du transducteur

R_g : rayon de gyration (m)

RS : taux de cisaillement résiduel (« *residual shear rate* ») (s^{-1})

R_t : rayon d'un tube (m)

S_0, S_1, S_2 : constantes de l'approximation en série de Taylor du facteur de structure

$S(-2k) = S_b(k)$: facteur de structure (adimensionnel)

SE : erreur type (« *standard error* »)

SFSE : « *Structure factor size estimator »*

SFSAE : « *Structure factor size and attenuation estimator »*

SNR : rapport signal sur bruit (« *signal to noise ratio* »)

SR = $\dot{\gamma}$: Taux de cisaillement (« *shear rate* ») (s^{-1})

$\sigma(k, \theta)$: section de diffusion ($m^2.sr^{-1}$)

$\sigma_R(k,\theta)$: section de diffusion d'un diffuseur Rayleigh ($m^2.sr^{-1}$)

$\sigma(-2k) = \sigma_b(k)$: section de rétrodiffusion ($m^2.sr^{-1}$)

$\sigma_R(-2k) = \sigma_{Rb}(k)$: section de rétrodiffusion d'un diffuseur Rayleigh ($m^2.sr^{-1}$)

t : temps (s)

T : température absolue (°K)

T6 : globules suspendus dans du plasma (agrégeants) à *H* = 6%

T40 : globules suspendus dans du plasma (agrégeants) à *H* = 40%

Tab. : tableau

Θ : angle de diffusion (rad)

UTC caractérisation ultrasonore tissulaire (« *ultrasound tissue characterization* »)

V : volume d'un diffuseur (m^3)

VCAM 1: molécule d'adhésion cellulaire vasculaire

W : facteur d'entassement (adimensionnel)

WBV : viscosité du sang complet (« *whole blood viscosity* ») ($Pa.s^{-1}$)

ξ_T : compressibilité isothermale

Z : impédance acoustique ($kg.m^{-2}.s^{-1}$)

À Isabelle

Remerciements

Voici venu le temps de tracer un bilan :
Cinq ans mémorables, six en fait, véritables
À plancher sur l'écho : « Est-ce modélisable ?
Le problème inverse ? Microstructure du sang ? »

Ma gratitude entière à un homme inspirant.
Minutieux, rigoureux, il vous guide, conseille,
Bon père de famille, il sait tendre l'oreille.
Un grand merci pour tout, comment dire autrement ?

Coup de chapeau sincère aux amis du labo.
Avec des gens sympas, c'est la fête au bureau !
Impossible en un vers, de vous nommer ici.

À vous tous et chacun, vos idées, vos lumières,
Ceux présents aujourd'hui, ceux qui m'ont guidé hier,
À tous et toutes merci, des souvenirs pour la vie !!

À mon directeur Guy Cloutier, j'offre toute ma gratitude pour m'avoir accueilli dans son laboratoire et m'avoir guidé, aidé, soutenu. Enthousiaste, dynamique, chaleureux et infatigable, il vous inspire tel « un vrai capitaine d'équipe de hockey » (sic). Je tiens à remercier les professeurs Herbert J. Meiselman, Yves Goussard, Sophie Lerouge et Gilles Soulez pour avoir siégé sur mon comité d'examen prédoctoral et m'avoir aiguillé sur la direction à donner à mon travail. Aux professeurs Herbert J. Meiselman et Jon K. Armstrong de l'University of Southern California, mes remerciements pour m'avoir accueilli à Los Angeles et formé sur l'utilisation des Pluronics. Merci à Roch L. Maurice pour son soutien, ses conseils et son optimisme. Merci à Louise Allard pour ses conseils et son soutien administratif, moral et scientifique. Merci au personnel de l'animalerie et tout particulièrement au Dr Hélène Héon, vétérinaire, et à Nancy Beauchemin, technicienne en animalerie, sans lesquelles la phase d'expérimentation animale aurait été impossible. Merci aussi à mon mentor de la première heure, David Savéry, pour les discussions et démonstrations sur le facteur de structure et pour m'avoir légué une thèse - que dis-je, une bible - à consulter et décortiquer. Et bien entendu merci à tous les collègues du labo. À ceux de la première heure, Michel Daronat et Audrey Zimmer qui m'ont initié au rituel de la manipulation du sang. À Marie Hélène Roy Cardinal, Ékathérina Stoyanova, Cédric Schmitt et François Treyve pour leur amitié. À Jean-Luc coach Gennisson et Marianne Fenech pour leur bonne humeur. Mention spéciale à Émilie Franceschini pour avoir travaillé sur le SFSAE, une contribution inestimable à l'avancement de ces travaux. Et aussi à tous ceux et celles que je ne pourrais nommer ici. Sachez qu'il a été bon de se sentir épaulé autant dans les bons moments que dans les moments de crise, dans la fête que dans les maux de tête, dans la joie que dans les inéluctables phases d'introspection.

Enfin un gigantissime merci à mon entourage immédiat sans lesquels cette longue et interminable vie étudiante n'auraient pu être complété avec succès. À ma femme Isabelle pour son soutien et ses encouragements. Merci à mes beaux parents Gisèle et Yves pour leur gentillesse et leur soutient et qui m'ont convaincu de persévérer lorsque la montagne a semblé la plus insurmontable. À mes sœurs Myriam et Mathilde, qui ont aussi accouché durant ces cinq années, de deux magnifiques neveux et d'une nièce époustouflante, qui me rendent si fier jour après jour et illuminent mon quotidien – et mes soirées de babysitting… Merci à mon papa pour ses encouragements et sa persévérance. Merci à Sing, la force tranquille, pour sa présence apaisante et son indéfectibilité. Et par-dessus tout, merci à ma mère, pour m'avoir élevé, gâté, nourri, logé, aimé, encouragé, et qui aura appris et récité, au bout de cinq années, le titre de ma thèse à ses amis.

Ce travail a été possible grâce à des bourses du Conseil de recherches en sciences naturelles et en génie du Canada, des Fonds de recherche sur la nature et les technologies du Québec, de la Faculté des études supérieures et postdoctorales de l'Université de Montréal, de l'Institut de génie biomédical de l'Université de Montréal ainsi qu'à des subventions de recherche des Instituts de recherche en santé du Canada octroyées au laboratoire.

Avant-propos généraux

Cette thèse portant sur la caractérisation ultrasonore de l'agrégation érythrocytaire a été réalisée au Laboratoire de Biorhéologie et d'Ultrasonographie Médicale (LBUM) sous la supervision du professeur Guy Cloutier. Cet objet d'étude constitue une des thématiques originales du laboratoire. Ce travail s'ajoute, de ce fait, à une longue lignée d'investigations remontant aux expérimentations post-doctorales du professeur Cloutier au début des années 1990. Depuis, de nombreux étudiants et post-doctorants ont apportés leurs contributions respectives, permettant de faire avancer la compréhension de l'interaction entre l'onde ultrasonore et les agrégats de globules rouges. Je tiens ici à souligner la contribution de tous ces individus. Sans eux et le travail qu'ils ont accompli, cette thèse n'aurait évidemment pu naître.

1 Chapitre 1 : Introduction

Ce chapitre décrit l'agrégation érythrocytaire comme objet d'étude et positionne la méthode ultrasonore comme un outil unique permettant le suivi et la quantification *in vivo* et *in situ* de ce phénomène.

1.1 Le sang

Ce n'est qu'au XVII^{e} siècle que le fonctionnement de la circulation sanguine est démystifié par William Harvey (1578 - 1657), alors médecin attitré du roi d'Angleterre. Scientifique acharné et épris d'anatomie, il démontre envers et contre tous que le cœur est au centre de la circulation sanguine et qu'il agit telle une pompe dans un réseau fermé formé par les artères et les veines. Le paradigme à l'époque consistait plutôt en une transformation des aliments en sang par le foie, ce sang servant lui-même de carburant qui était donc consumé par le corps. Il publie *Exercitatio anatomica de motu cordis et sanguinis in animalibus* ou « Traité anatomique sur les mouvements du cœur et du sang chez les animaux » en 1628, ouvrage qui a posé les fondements de l'anatomie vasculaire moderne. On sait aujourd'hui que le sang est un fluide physiologique non homogène et non newtonien[1] composé principalement par une suspension de cellules dans du plasma. Le plasma peut être considéré comme un fluide newtonien contenant des lipides, des protéines, des glucides et des ions. Dans le plasma baignent également des cellules : les globules rouges (Figure 1-1) ou érythrocytes servent au transport de l'oxygène et du dioxyde de carbone, les globules blancs assurent une fonction immunitaire alors que les plaquettes interviennent dans la cascade de coagulation permettant de contrôler et minimiser les pertes sanguines en cas d'hémorragie. Le Tab. 1-1 décrit plus précisément la composition sanguine.

[1] La viscosité d'un fluide non newtonien varie en fonction du taux de cisaillement appliqué.

	Constituants	*Concentration*	*Fonction*
Cellules **40% du volume**		<u>Nombre (% volumique)</u>	
	Globules rouges	4 - 5 × 10^6 mm^{-3} (35-45%)	Transport O_2/CO_2
	Globules blancs	5 - 10 × 10^3 mm^{-3}(0.3-0.5%)	Fonction immunitaire
	Plaquettes	1 - 2 × 10^6 mm^{-3}(1-3%)	Système hémostatique
Plasma **60% du volume**	*Eau*	93% de la masse	Médium de transport
	Ions inorganiques	Total < 1% de la masse	Maintient de la pression osmotique transmembranaire; tampon; système hémostatique
	Na^+	145 mM	
	K^+	4 mM	
	Ca^{2+}	2.5 mM	
	Mg^{2+}	1.5 mM	
	H^+	0.0004 mM	
	Cl^-	103 mM	
	Principales protéines	7% de la masse	Tampon; transport moléculaire;; précurseurs d'enzymes; anticorps; système hormonal
	Albumines	4.2 g/100 mL de plasma	
	Globulines	2.8 g/100 mL de plasma	
	Fibrinogènes	0.3 g/100 mL de plasma	
	Nutriments		Structure cellulaire; fonctions protéiques; régulation; métabolisme; énergie
	Hydrates de carbone		
	Acides aminés		
	Lipides		
	Cholestérols		
	Vitamines		

Tab. 1-1: Composition du sang. Adapté de [174].

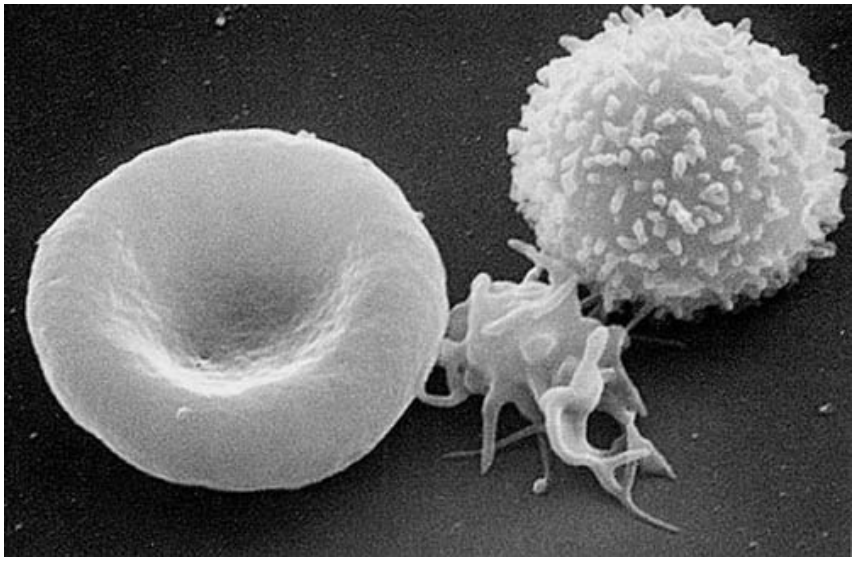

Figure 1-1 : Microscopie électronique d'un érythrocyte, d'un thrombocyte et d'un leucocyte. Image provenant de NCI-Frederick, en reproduction libre.

Au repos, le corps humain contient en moyenne 5 L de sang circulant à un débit moyen de 5 $L.min^{-1}$ sous l'action du muscle cardiaque qui bat à un rythme moyen de 70 contractions par minute [174].

1.2 L'agrégation érythrocytaire

Au niveau macroscopique, les caractéristiques mécaniques du sang ont été décrites avec précision dans les travaux de Chien et al. [36;37]. Puisque les globules rouges, qui comptent pour environ 40% de la fraction volumique sanguine (aussi appelé hématocrite *H*), sont plus gros que les plaquettes et plus nombreux que les globules blancs (ils représentent en effet 99% de la fraction volumique cellulaire sanguine), les plaquettes et les globules blancs peuvent généralement être négligées lorsqu'on s'intéresse aux propriétés non newtoniennes sanguines. L'augmentation de

la viscosité globale[2] du sang à bas taux de cisaillement est liée à la formation d'agrégats en forme de rouleaux alors qu'elle est liée, à haut taux de cisaillement, à la déformabilité des hématies (Figure 1-2). Dans les deux cas, un retour à des conditions de flot modéré ramène les globules à une forme individuelle biconcave « normale ». On parle donc ici de processus réversibles. On remarque que des globules normaux suspendus dans une solution d'albumine ne s'agrègent pas (NA, Figure 1-2) et que des globules durcis dans une solution de glutharaldéhyde ne se déforment pas (HA, Figure 1-2). Il faut distinguer l'agrégation réversible des globules rouges, qui modifie la rhéologie sanguine en fonction des conditions du flot, de la coagulation sanguine, qui fait partie du système hémostatique (agrégation plaquettaire et cascade de coagulation permettant la formation d'un réseau de fibrine) et qui mène à la formation d'un thrombus. Nous verrons au chapitre 5 que l'agrégation peut directement être impliquée dans la formation d'un thrombus. Cette démonstration constitue une contribution importante de cette thèse.

L'agrégation érythrocytaire est également modulée par les énergies de liaisons électrostatiques répulsives (puisque la glycocalyx membranaire est chargée négativement) et par des forces d'attraction induites par l'entremise de macromolécules plasmatiques dont le fibrinogène, la céruloplasmine, les immuglobulines G, A et M, l'haptoglobine et certaines macroglobulines. Des polymères synthétiques, tels les polysaccharides (dextrans), le polyvinylpyrrolidone et le polyoxyéthylène, modulent également l'agrégation lorsqu'ils sont ajoutés à la phase liquide sanguine [9]. Il existe deux modèles opposés qui expliquent la nature de la

[2] Cette notion est traduite librement de l'anglais « bulk viscosity» et s'obtient par une mesure *in vitro* dans un viscosimètre, par opposition à la viscosité locale ou microscopique, abordée au chapitre 4.

force d'agrégation : d'un coté, la théorie de l'adsorption moléculaire ou « *bridging model* », et de l'autre, le model de déplétion osmotique ou « *depletion model* ».

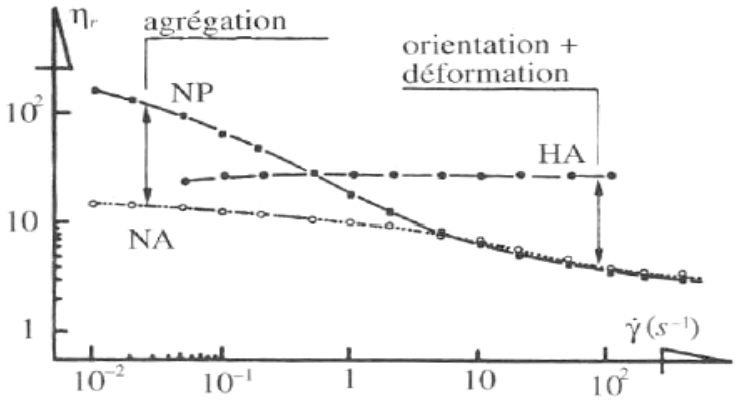

Figure 1-2 : Caractéristiques non newtoniennes du sang et relation avec l'agrégation et la déformabilité des globules rouges. η est la viscosité du sang total; η_p celle du plasma; $\dot{\gamma}$ est le taux de cisaillement; *t* le temps; *H* représente les érythrocytes durcis (*« Hardened »*); N représente les érythrocytes normaux; A est une solution d'albumine; et P est une solution de plasma. Adapté de [37].

1.2.1 L'adsorption moléculaire

Selon la théorie de l'adsorption moléculaire, les forces de Van der Waals permettent l'adsorption (adhésion de surface) de la molécule d'interaction par les membranes cellulaires de deux globules avoisinant, ce qui maintient les globules à proximité. Les forces de Van der Waals regroupent les forces intermoléculaires de nature inductive et dispersive. Les forces inductives naissent des interactions dues aux répartitions anisotropes des charges dans les molécules même, si ces dernières sont globalement électriquement neutres. Elles sont aussi dites forces de polarisation. Les forces dispersives sont, quant à elles, dues aux interactions de dipôles instantanés créés par la présence d'une molécule polarisée, l'eau H_2O par exemple. Les forces de

Van der Waals sont à faible énergie, de nature anisotrope et dépendent fortement des conformations géométriques moléculaires [100]. Cette théorie permet d'expliquer que la concentration et la taille des molécules modulent l'agrégation puisqu'ils permettent la formation de plus de liens entre les globules avoisinants [27;28]. Cependant la nature non spécifique des molécules impliquées dans l'agrégation sème le doute sur la pertinence de ce modèle puisque des grandes différences dans la composition et la structure existent entre les protéines pro-agrégeantes et des polymères synthétiques qui induisent toutes l'agrégation érythrocytaire lorsqu'elles atteignent une certaine masse molaire [9] (voir Tab. 1-2 et Tab. 1-3).

1.2.2 Modèle de la déplétion moléculaire

Le modèle de la déplétion a reçu une plus grande attention ces dernières années et offre une explication plus inclusive des phénomènes observés. L'énergie d'adhésion proviendrait plutôt d'une diminution localisée de la concentration de la protéine ou du polymère près de la membrane du globule dans la glycocalyx. Lorsque des globules se rapprochent, par mouvement brownien ou selon l'écoulement, cette déplétion entraine un gradient osmotique qui maintient les deux membranes à proximité. Cette théorie est directement inspirée du domaine de la chimie colloïdale sous la nomenclature de « *flocculation depletion* » [47] et semble bien s'appliquer à l'agrégation érythrocytaire [19;123;124]. Si ce modèle semble moins intuitif, il offre une explication directe de la nature non spécifique des molécules qui induisent l'agrégation des globules. En effet, la force d'attraction est directement liée à la taille hydratée de la macromolécule [9] et à la concentration de la macromolécule dans la phase suspendante. Ces deux grandeurs déterminent la pénétration des macromolécules en suspension dans la glycocalyx. Une petite molécule pénètre plus facilement la glycocalyx et la zone de déplétion est moins importante [123], ce qui

explique que des molécules de petite taille inhibent l'agrégation, même lorsque des molécules agrégeantes sont présentes. La pénétration de la glycocalyx semble limitée pour des molécules dont le rayon hydrodynamique est supérieur à 4 nm [9] (voir Tab. 1-2 et Tab. 1-3), ce qui permet la formation d'une zone de déplétion et d'un gradient osmotique. La déplétion augmente avec la concentration jusqu'à un point de saturation où une très forte concentration augmente la pénétration et réduit l'agrégation, ce qui explique la forme unimodale de l'agrégation en fonction de la concentration. Des équations permettant de déterminer l'épaisseur de la zone de déplétion, l'énergie d'interaction entre deux surfaces et la profondeur de pénétration ont été proposées, en fonction de la composition du solvant et du polymère en suspension [123], et validées par des résultats expérimentaux sur du dextran. La dépendance unimodale de l'agrégation en fonction du poids moléculaire qui atteint un maximum autour de 500 kDa est aussi expliquée par ce modèle [124]. Cela explique sans doute pourquoi le fibrinogène globulaire (680 kDa), bien que de masse molaire plus importante que le fibrinogène fibreux (340 kDa), n'induit pas d'agrégation [153]. D'autres expériences utilisant des globules rouges recouverts de polymères agrégeants tendent également à valider le modèle de la déplétion [7]. En effet ces globules rouges pour lesquels une moitié de la liaison entre les globules est déjà préformée présentent moins d'agrégation que des globules rouges non traité alors qu'une agrégation similaire ou supérieure serait attendue selon la théorie de l'adsorption, puisqu'une moitiée du lien est déjà formée. Plusieurs protéines plasmatiques et polymères qui induisent ou inhibent l'agrégation sont résumés aux Tab. 1-2 et Tab. 1-3 où l'on retrouve la masse molaire et le rayon hydrodynamique de plusieurs macromolécules hydratées.

1.2.3 Rôle et influence physiologiques de l'agrégation

Le rôle de l'agrégation érythrocytaire dans l'organisme n'est pas clairement élucidé à ce jour. Certaines remarques et conjectures ont cependant été avancées. Tout d'abord, il est intéressant de remarquer que les mammifères présentent des niveaux de viscosité et d'agrégation très variables [14;15;32;182]. Quelques exemples d'études inter-espèces sont présentés au Tab. 1-4 ainsi qu'aux Figure 1-3 et Figure 1-4.

Protéine	*Masse molaire (kDa)*	*Rayon hydro-dynamique (nm)*	*Tendance agrégeante*
Hémoglobine A	65	3.18	inhibition
Albumine	66	3.51	inhibition
Glycoprotéine acide α-1	100-140	3.64	0
Transferrine	60-100	3.72	0
Antitrypsine α-1	51	3.81	0
PC- réactive (pentamère)	125	4.03	+
Céruloplasmine	100-140	4.56	+
IgG	140- 200	5.29	+
IgA (monomer)	162	6.50	++
Haptoglobine (multiples isoformes)	100 – 900	4.7-25.0	+++
IgM	950	12.65	+++
Macroglobuline α-2	725	9.22	+++
TumorNecrosisFactor-α	51.9	10	Non documenté
Pentastarch	260	10.80	Non documenté
Fibrinogène fibreux	340	10.95	+++
Fibrinogène globulaire	680		0

Tab. 1-2 : Protéines plasmatiques et leur effet sur l'agrégation érythrocytaire. Adapté de [9].

Polymère	*Masse molaire (kDa)*	*Rayon hydro-dynamique (nm)*	*Tendance agrégeante*
polyvinylpyrrolidones	2.5	1.2	inhibition
	10.0	2.2	inhibition
	360.0	19.0	+++
polyoxyéthylènes	2.0	1.4	inhibition
	11.8	3.5	inhibition
	100.0	11.9	+++
Polysaccharides	9.5	1.9	Inhibition
(Dextran)	39.1	4.8	0
	73.0	6.5	++
	500.0	15.9	+++

Tab. 1-3 : Polymères et leur effet sur l'agrégation érythrocytaire. Adapté de [9].

	Viscosité sang complet (mPa.s)			**Viscosité**
	0.7 s^{-1}	**2.4 s^{-1}**	**94 s^{-1}**	**plasmatique (mPa.s)**
Cheval	38.17	20.18	5.17	1.66
Porc	24.69	14.86	4.94	1.58
Chien	22.88	14.58	5.59	1.61
Chat	30.19	15.35	4.44	1.71
Rat	35.40	19.75	6.29	1.59
Lapin	8.31	7.44	4.04	1.30
Souris	13.17	10.56	4.88	1.31
Homme	33.49	18.53	5.99	1.24

Tab. 1-4 : Viscosité sanguine et plasmatiqur à différents taux de cisaillement chez plusieurs mammifères. Adapté de [182].

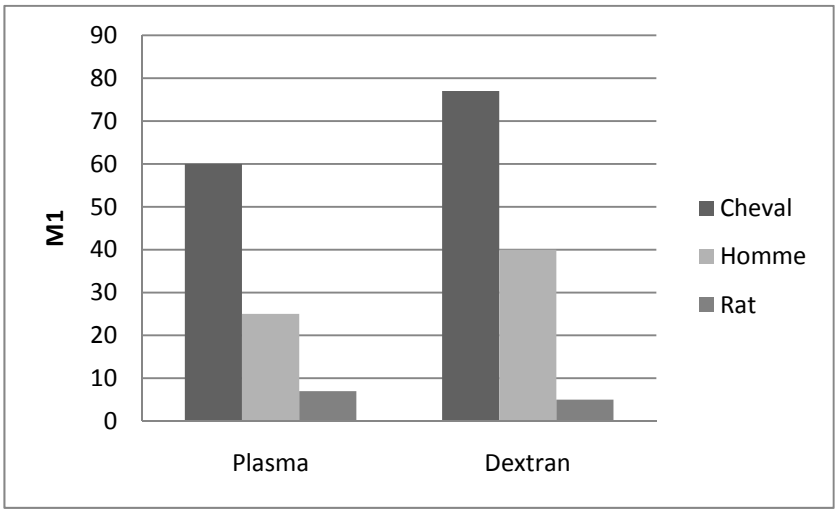

Figure 1-3 : Indice d'agrégation érythrocytaire M1 mesuré par rétrodiffusion laser (voir paragraphe 1.4.4) chez le cheval, l'Homme et le rat. M1 est un index sans unité qui augmente avec l'agrégation. Adapté de [15].

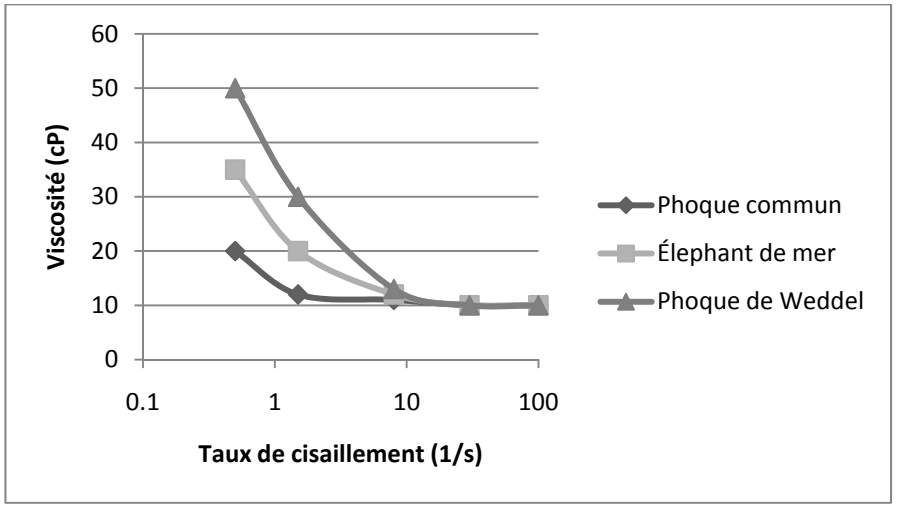

Figure 1-4 : Viscosité en fonction du taux de cisaillement pour le phoque commun, l'éléphant de mer et le phoque de Weddell. Typiquement, la viscosité du sang humain se retrouve au niveau de celle de l'éléphant de mer. Adapté de [54].

La comparaison de mesures de viscosité et d'agrégation entre les espèces place à une extrémité du spectre les mammifères marins, les équins et les félins qui présentent des niveaux d'agrégation élevés, alors que les rongeurs et les ovins ne présentent presque aucune agrégation. L'Homme et les espèces porcines et canines sont dans le milieu du peloton. Le rat est un cas particulier puisqu'il présente une viscosité importante mais très peu d'agrégation. Une structure particulière de la glycocalyx fortement chargée négativement pourrait expliquer la faible agrégation chez le rat [15]. Il a été avancé hypothétiquement que les performances athlétiques [132] pourraient expliquer cette gradation, sans toutefois identifier de mécanisme justifiant une telle hypothèse. Une explication plus fondamentale est proposée par l'équipe du professeur Johnson [29]: avec une préparation sur le muscle gastrocnémien chez le chat, l'étude démontre que le niveau d'agrégation physiologique permet de réguler la chute de pression dans le réseau musculaire, alors qu'une augmentation ou une diminution de l'agrégation entraine de plus grandes variations du gradient de pression veineux (Figure 1-5). Ainsi, lorsque le flot veineux augmente, lors d'un effort physique par exemple, la diminution de la résistance circulatoire (Figure 1-6) due à la rhéofluidification sanguine permettrait de diminuer l'impact sur le gradient de pression veineux, ce qui assurerait une régulation de la pression capillaire et le maintient de la perfusion [29]. On rappelle que la conductance s'obtient par l'inverse de la résistance.

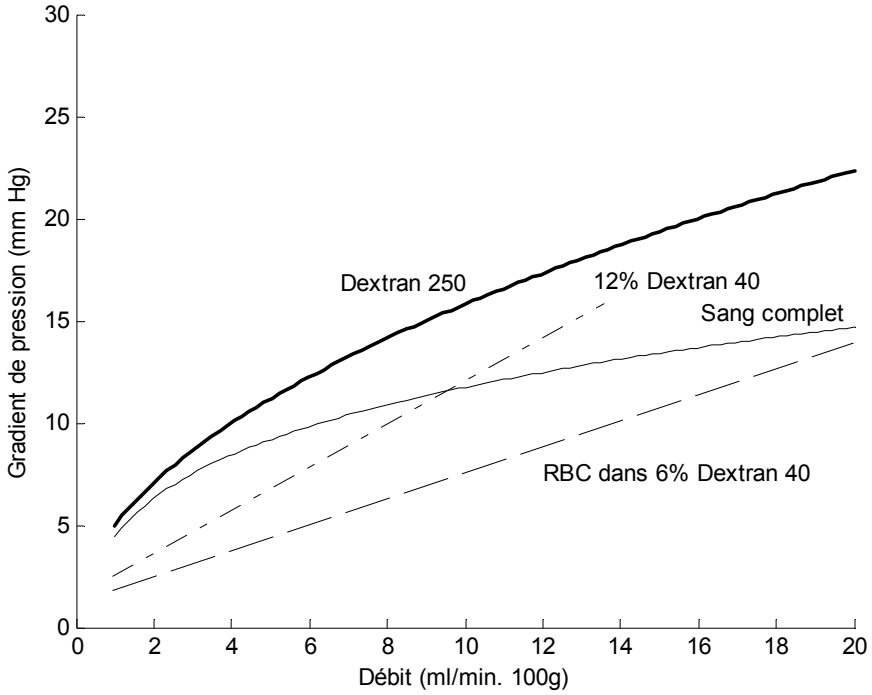

Figure 1-5 : Chute de pression dans le réseau du muscle gastrocnémien chez le chat en fonction du débit et du type de sang. Le sang normal permet le maintient de la pression capillaire dans le muscle. « *RBC dans 6% Dextran 40 »* (suspension de globules rouges non agrégeants); « *12% Dextran 40 »* (solution de viscosité newtonienne équivalente à du sang non agrégeant); « *Sang complet »* (sang total félin); « *Dextran 250 »* (sang hyperagrégeant). Adapté de [29].

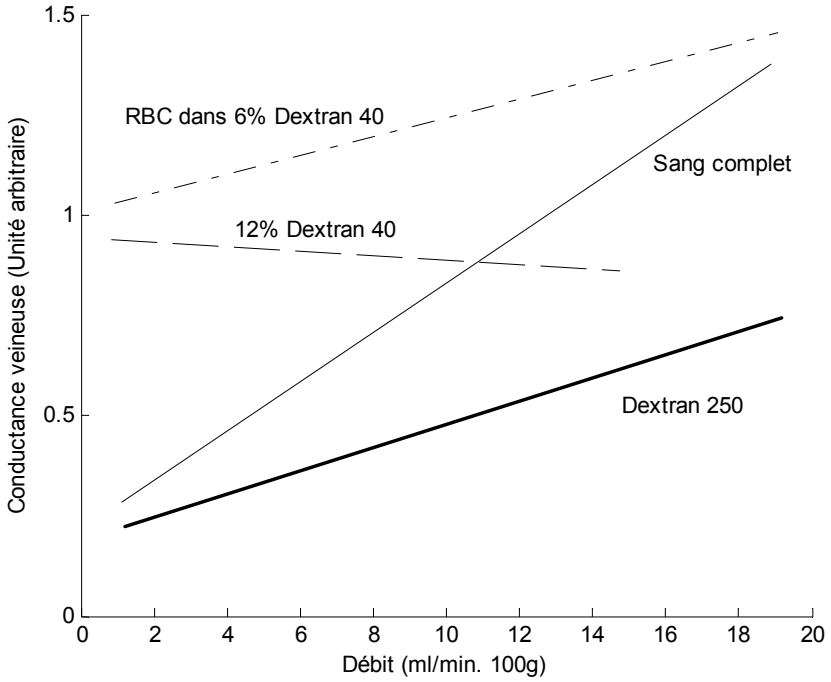

Figure 1-6 : Conductance vasculaire dans le muscle gastrocnémien chez le chat en fonction du débit pour différents types de sang. On constate que la plus grande variation est observée pour le sang total. Cette augmentation de conductance avec le débit, qui est permise par la désagrégation des agrégats avec l'augmentation du flot, permet la régulation de la chute de pression (voir Figure 1-5). Adapté de [29].

L'absence d'une telle régulation veineuse chez les espèces présentant moins d'agrégation indique qu'il existe vraisemblablement d'autres mécanismes régulateurs de la perfusion. On peut évidemment penser à la vasoconstriction par exemple. L'observation de niveaux d'agrégation différents selon les espèces suggère également que plusieurs équilibres physiologiques différents ont pu être atteints au cours de l'évolution. Cette grande variabilité inter-espèce est souvent soulevée contre l'argument de l'hyperagrégation comme marqueur pathologique. Nous verrons plus

loin que chez l'Homme, une augmentation de la viscosité est souvent reliée à un état pathologique, même si le rôle étiologique de la perturbation hémorhéologique n'est pas clairement établi à ce jour. Ces questions complexes n'ont sans doute pas de réponses simples et sont l'objet d'un secteur de recherche foisonnant. Les effets de variations hémorhéologiques sont investigués notamment au niveau de leurs impacts sur la macro- et la micro-circulation dans les domaines de la biorhéologie et de l'hémorhéologie clinique [117].

1.2.3.1 En macro-circulation

En macro-circulation, l'agrégation entraîne principalement une augmentation de la viscosité systémique. Elle peut être décrite, par exemple, à l'aide du modèle de viscosité de Casson (Eq. 1.1) ou par une loi de puissance (Eq. 1.2).

$$\mu = \left(1.53\sqrt{\mu_p} + \frac{2\sqrt{\mu_p}}{\sqrt{\dot{\gamma}}} \right)^2 \tag{1.1}$$

$$\mu = K\left|\dot{\gamma}\right|^{n-1} \tag{1.2}$$

où
μ est la viscosité (Pa.s),
μ_p la viscosité plasmatique (Pa.s),
$\dot{\gamma}$ le taux de cisaillement (s^{-1}),
K est l'index d'uniformité d'écoulement ($Pa.s^n$), et
n est l'index de comportement d'écoulement (sans dimension).

Ces relations décrivent le changement de viscosité sanguine en fonction du cisaillement et peuvent être vérifiées expérimentalement par des mesures en régime permanent dans un viscosimètre de Couette. Dans un tube, l'agrégation érythrocytaire à bas débit provoque un écrasement « *blunted flow* » du profil de vitesse. Dans un

écoulement laminaire stationnaire en régime permanent, il est possible, en mesurant expérimentalement le profil de vitesse, de déterminer la loi de viscosité sous l'hypothèse que le fluide suit un comportement de Casson ou de puissance. La loi de puissance, bien que peu réaliste, est souvent utilisée car une solution de l'équation de Navier-Stokes pour un écoulement cylindrique peut être calculée analytiquement (voir Eq. 4.3). *In vitro,* ce genre d'analyse peut être effectué sur des séquences vidéo d'images ultrasonores [154], ce qui a inspiré certaines expériences menant aux résultats du chapitre 4 (Figure 4-7, par exemple). Ce genre d'analyse pour d'autres lois de viscosité peut être effectué *in silico* [71]. Cette approche est cependant difficilement applicable *in vivo* car même dans les veines, les bifurcations, aux sites de courbure des vaisseaux et la présence de valves veineuses entrainent des perturbations qui invalident l'hypothèse du régime permanent. En effet le sang est un fluide thixotrope, ce qui signifie que la viscosité varie également en fonction du temps.

Certains modèles s'attaquent à cette propriété rhéologique mais demeurent limités et l'implication clinique de la thixotropie est peu connue [59]. Dans les artères, les débits élevés permettent de considérer le sang comme un fluide newtonien, ce qui simplifie fortement le problème. Toutefois, cette simplification pourrait être critiquée surtout pour les sangs hyperagrégeants ou dans certaines zones de flot réduit, telles que les zones de recirculation (e.g., derrière une valve veineuse ou en aval d'une sténose artérielle). *In vivo*, l'effet de l'agrégation est souvent abordé à un niveau systémique puisqu'aucune technique ne permet une mesure locale de l'agrégation (sauf la technique ultrasonore développée dans ce travail). En conséquence, l'apport de la viscosité sanguine (agrégation) sur la résistance à l'écoulement est souvent ignoré. La résistance d'un organe à la circulation est établie en considérant principalement la pression et le débit. Le problème se complexifie cependant puisque la résistance *in vivo* est tributaire de la vasoconstriction. En effet, les cellules endothéliales sont dotées de mécano-transducteurs qui sont sensibles à l'étirement

(donc à la pression) ainsi qu'au cisaillement à la paroi (donc au flot). L'effet d'une augmentation du flot dépendant de l'agrégation provoque donc une cascade d'évènements confondants qui font augmenter, diminuer ou induisent peu d'effet sur la résistance à l'écoulement [29;33;82;83;176]. Les résultats contradictoires de ces études sont difficiles à synthétiser car les protocoles, les organes et les méthodes diffèrent d'une étude à l'autre. L'orientation principale de la circulation dans l'organe semble également influencer les résultats. De manière très générale, on peut dire qu'une augmentation modérée de l'agrégation (par l'ajout de dextran par exemple) n'entraine que peu de changements sur la perfusion tissulaire et la résistance à l'écoulement. En effet, la vasodilatation semble compenser adéquatement pour l'augmentation de viscosité. Par contre, lorsque la régulation vasoactive est déficiente ou que la réserve vasculaire régulatrice est épuisée, des complications plus sérieuses se font sentir [117]. Une méthode permettant de quantifier la distribution spatiale de la viscosité instantanée *in vivo* et *in situ,* abordée au chapitre 4, pourrait apporter des réponses à ces questionnements.

1.2.3.2 En micro-circulation

En micro-circulation, une augmentation de l'agrégation n'entraîne pas directement une augmentation de la résistance à l'écoulement. En effet, la viscosité sanguine effective diminue lorsqu'on fait circuler du sang dans des microtubes dont le diamètre varie entre 1 mm et ~ 7 µm puis augmente à nouveau pour de plus petits diamètres (Figure 1-7). C'est l'effet Fahraeus-Lindqvist [58] (ou effet sigma). Le regroupement des hématies au centre des vaisseaux permet une lubrification de la microcirculation par une couche de plasma à la paroi. Cet effet se superpose et s'explique en partie par l'effet Fahraeus, qui consiste en une diminution de

l'hématocrite effectif dans les petits capillaires. L'hématocrite veineux et artériel en fonction du diamètre des vaisseaux est résumé à la Figure 1-8.

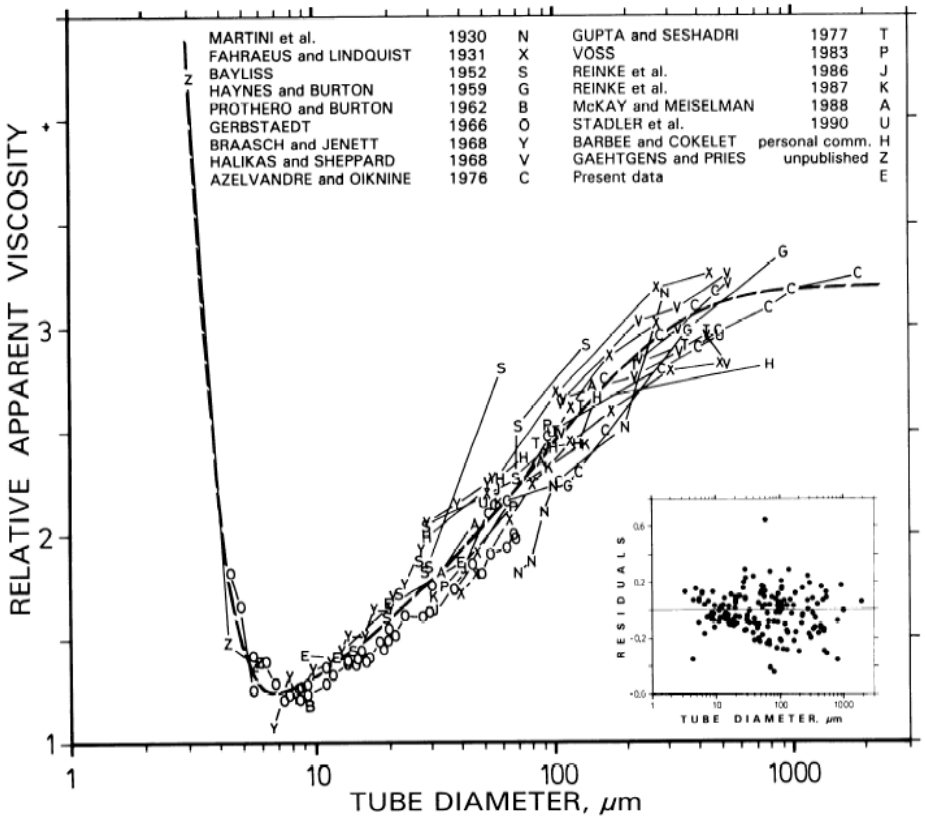

Figure 1-7 : Viscosité apparente du sang (H = 45%) circulant dans des capillaires en vitre de différents diamètres [135] [3].

[3] Reproduite avec permission "fair use" de AJP - Heart and Circulatory Physiology, Vol 263, Issue 6 1770-H1778, Copyright © 1992 by American Physiological Society (http://ajpheart.physiology.org).

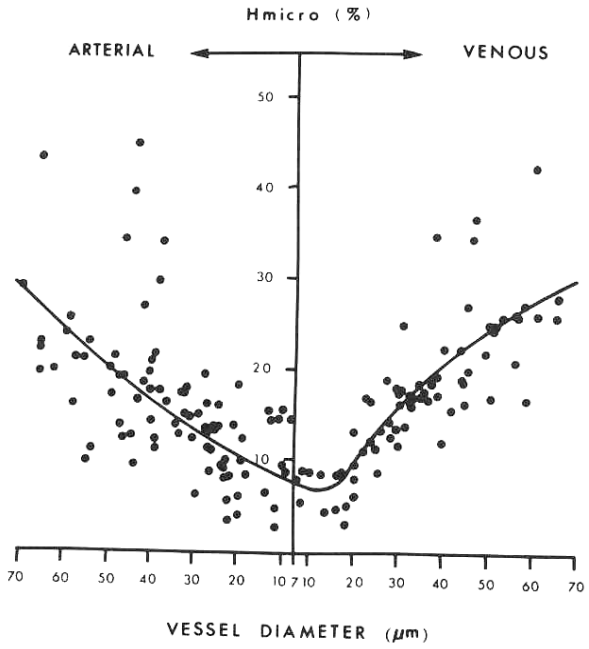

Figure 1-8 : Répartition de l'hématocrite en fonction du diamètre luminal mesuré dans le mésentère de chats sous microscopie intravitale. La vitesse plus rapide des érythrocytes situés au centre du vaisseau et la couche lubrifiante plasmatique près de la paroi (absence d'érythrocytes) expliquent ce phénomène. Extrait de [69][4].

Les effets Fahraeus-Lindqvist et Fahraeus ont été abondamment étudiés à l'aide de modèles numériques. Il semble que la déformabilité globulaire soit un des mécanismes de la migration vers le centre des érythrocytes dans les petits vaisseaux [13] et ce phénomène augmente avec l'agrégation [24], ce qui contribue à la diminution de l'hématocrite dans les embranchements successifs menant à une diminution en diamètre de l'arbre vasculaire. L'analyse des profils de vitesse est aussi utilisée en microscopie intravitale pour évaluer l'effet de l'agrégation sur la circulation.

[4] Reproduite avec permission de Springer Science+Business Media - Fung, Y. C., Biomechanics: circulation, pp. 283 figure 5.5.2, 2nd ed. New York, Berlin, Heidelberg Springer © 1997

L'approche consiste en l'analyse de films acquis sous microscope sur un mince tissu translucide à même l'animal anesthésié. Souvent, le crémaster ou le péritoine sont utilisés à ces fins. Une augmentation modérée de l'agrégation érythrocytaire provoque un écrasement du profil de vitesse et une augmentation de l'épaisseur de la couche plasmatique sans cellules « *cell free layer* » [22;24]. Cependant, la migration cellulaire vers le centre du vaisseau diminue lorsque le nombre d'embranchements augmente (« mixing effect ») [24].

En résumé, on retiendra que l'hémorhéologie participe à un équilibre régulateur complexe de la circulation aux niveaux macro et microscopiques. La compréhension des mécanismes impliqués requiert une meilleure connaissance de la fonction endothéliale, des mécanismes de migration luminale des globules, de leur effet sur les autres cellules sanguines ainsi que des mesures précises de la viscosité à l'intérieur des vaisseaux.

1.3 Hémorhéologie et maladies cardiovasculaires

Les implications pathophysiologiques de l'hémorhéologie dans les maladies circulatoires sont relativement peu connues. Les mécanismes et les marqueurs pathologiques aujourd'hui reconnus considèrent rarement les perturbations hémorhéologiques (viscosité plasmatique, viscosité du sang total à faible ou fort cisaillement, indices d'agrégation). Si l'implication directe de l'hémorhéologie n'a pas été démontrée, son implication dans la création d'un environnement propice au développement pathologique est en croissance, tant pour son rôle dans la formation de la plaque athéromateuse que dans la formation du thrombus veineux. Plusieurs coïncidences ont amené une recrudescence d'études en ce sens. En effet, comment expliquer autrement que les maladies circulatoires tant au niveau artériel que veineux

se manifestent systématiquement en des endroits spécifiques dans l'arborescence vasculaire? Certains auteurs parlent même de négligence par rapport à d'autres facteurs de risque [50]. L'hyperviscosité plasmatique et l'hyperagrégation érythrocytaire sont reconnus par certaines études comme des facteurs indépendants de risque tant du coté artériel [53;111;112;186] que veineux [52;138].

1.3.1 Maladies artérielles athéromateuses

L'étiologie de la plaque athéromateuse est directement liée à l'hyperlipidémie et à l'inflammation. Lorsque le corps accumule le mauvais cholestérol (LDL ou « *low density lipoproteins* »), les cellules endothéliales, normalement résistantes à l'adhésion des leucocytes, expriment des VCAM1 (« *vascular cell adhesion molecule 1* ») qui fixent les monocytes et les lymphocytes T. Ces derniers pénètrent dans l'intima par diapédèse, se transforment en macrophage « *scavenger* » et internalisent les lipoprotéines présentes. Elles sont alors transformées en cellules spumeuses qui sont dégradées par apoptose pour former le corps nécrotique ou lipidique « *lipid pool* » de la plaque d'athérome [104]. Cette chaine d'événements est résumée à la Figure 1-9.

Bien que le lien entre l'hémodynamie et l'initiation de la plaque ne soit pas explicitement soulevé par l'auteur [104], il est souligné dans cet article de synthèse que la plaque ne se développe pas dans les régions de flot laminaire mais seulement près des bifurcations où le flot est perturbé. Il émet l'hypothèse que la réponse inflammatoire (expression de VCAM1 et recrutement de leucocytes) peut être inhibée par l'oxyde nitrique synthase (NOS) exprimée par la cellule endothéliale. Or, il est connu que l'agrégation érythrocytaire inhibe l'expression de la NOS par mécanotransduction [18;184]. Une augmentation de l'agrégation pourrait donc inhiber l'expression de NOS et provoquer une réponse inflammatoire.

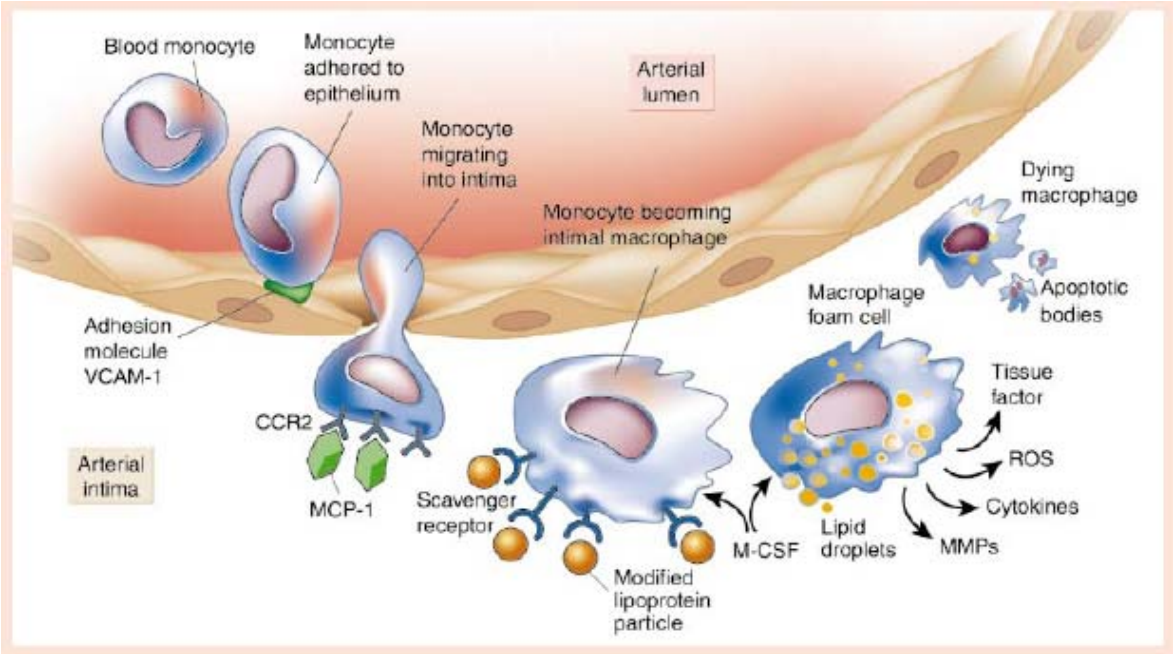

Figure 1-9 : Initiation de la plaque athéromateuse par le recrutement de leucocytes dans l'intima, causée par une accumulation de LDL dans la paroi vasculaire [104] [5].

En microcirculation, le lien entre l'inflammation et l'agrégation érythrocytaire a été démontré uniquement dans les veinules post-capillaires mésentériques du rat : l'agrégation érythrocytaire augmente la margination et l'adhésion des leucocytes à la paroi [131]. Ce lien encore peu étudié pourrait s'avérer primordial dans la compréhension de l'étiologie de la plaque athéromateuse.

1.3.2 Maladies veineuses thrombotiques

L'incidence de la thrombose veineuse est de 1 à 2 événements pour 1000 patients par année [128]. Elle se manifeste principalement sous la forme de

[5]Reproduite avec permission de Macmillan Publishers Ltd : Nature (www.nature.com) (Libby, P., Inflammation in atherosclerosis, Nature, 420 (2002), pp. 868-874), copyright 2002.

thrombophlébite (« deep vein thrombosis », DVT) dont la complication principale est l'embolie pulmonaire. La thrombose est un état de déséquilibre du système hémostatique. Un thrombus qui se forme normalement à l'extérieur du vaisseau pour prévenir l'hémorragie se manifeste intraluminalement. C'est une complication médicale très commune, qui se produit seule ou en conséquence à d'autres procédures et son origine demeure souvent idiopathique (jusqu'à 47% des cas [1]). La triade de Virchow regroupe trois éléments généralement impliqués dans l'apparition de la maladie : la stase veineuse, l'hypercoagulabilité et une blessure endothéliale. La thrombose peut être vue comme un problème multifactoriel qui est déclenché par l'accumulation de plusieurs facteurs de risque : immobilisation, chirurgie, cancer, puerpéralité, hormones féminines exogènes, protéine C réactive, protéine S, niveau élevé de facteur de coagulation VIII, IX ou XI, déficience en antithrombine, facteur V Leiden, et hyperfibrinogénémie [38;99;143]. Cliniquement, ces facteurs de risques sont classifiés comme transitoires (risque limité dans le temps) ou permanents (risque lié à un état chronique). Cette catégorisation est importante car le risque de récurrence de la maladie, et donc la durée de l'administration d'anticoagulant prophylactique, en dépend directement. En effet, les risques de récurrence thrombotique sont plus faibles lorsque le premier épisode est dû à des facteurs transitoires (6.7%) que lorsqu'il est d'origine permanente ou idiopathique (18.1%) [1;38;152].

D'autre part, une association corrélative a pu être établie entre l'apparition de troubles rhéologiques et l'existence d'une thrombose. En effet, une augmentation de l'agrégation érythrocytaire, de la viscosité plasmatique et du fibrinogène a été répertoriée chez des patients atteints de DVT en comparaison de sujets contrôles [6]. Or, tous ces paramètres étaient retournés à des valeurs normales chez les patients aux facteurs de risque transitoires mais pas chez les patients aux facteurs de risque permanents. Ces constatations soulèvent plusieurs questionnements : les facteurs

rhéologiques sont-ils impliqués dans l'étiologie de la thrombose veineuse ou est-ce uniquement une association corrélative? Quels sont les mécanismes reliant les désordres rhéologiques aux DVT d'origine idiopathique? Les facteurs rhéologiques sont-ils à la source des complications post-phlébitiques [99] ou de la récurrence des DVT?

La littérature est claire sur l'impact des désordres hémorhéologiques comme facteur de risque de la maladie thrombotique [51;52;110;195], cependant ces faits ont eu peu d'impact sur la pratique clinique [50]. Les mécanismes impliquant l'hémorhéologie dans la pathogénèse thrombotique incluent la réduction du débit sanguin qui induit une augmentation de la viscosité, l'augmentation de la margination des plaquettes et des globules blancs vers les parois [77], et l'activation plaquettaire (augmentation de la fréquence de collision plaquettaire [20;74]) causée par une migration des agrégats de globules rouges vers le centre du vaisseau [57]. Cependant, le lien de causalité entre les désordres hémorhéologiques et la maladie thrombotique n'a jamais été clairement établi. En effet, l'hyperviscosité sanguine et l'hyperfibrinogénémie accompagnent la plupart des autres facteurs de risque de la maladie thrombotique (e.g., chirurgie, infarctus du myocarde, déshydratation, accident cérébro-vasculaire, leucémie). Ils n'ont donc pas pu être clairement identifié comme facteur de risque indépendant de la DVT. De plus, pour ajouter à la confusion possible, l'hyper-fibrinogénémie, identifiée dès 1973 comme facteur de risque de la DVT [50;52], particulièrement chez les patients âgés [173], n'est pas prédictif de la maladie chez les jeunes ou chez les patients présentant des niveaux de fibrinogène génétiquement élevés [50]. Il persiste donc un doute justifié sur le rôle que jouent les désordres rhéologiques dans la maladie thrombotique. En conséquence, une évaluation locale de l'agrégation érythrocytaire permettrait-elle de répondre à ces interrogations? Serait-il possible que des conditions locales d'écoulement chez certains

patients expliqueraient ces confusions? L'objectif de cette thèse est d'offrir des outils rhéologiques de caractérisation permettant de répondre à certaines de ces questions.

1.4 Méthodes de mesures de l'agrégation érythrocytaire

La plupart des méthodes d'analyse de l'agrégation érythrocytaire nécessite le prélèvement d'un échantillon sanguin par ponction veineuse. Une approche *ex vivo* permet d'obtenir un index de tendance d'agrégation systémique moyen. Ces analyses ne peuvent tenir compte des conditions d'écoulement et sont rarement effectuées au niveau du vaisseau d'intérêt. Ceci constitue une autre limitation puisqu'il existe des variations locales d'agrégation. En effet, il a été démontré que la tendance d'agrégation diffère entre des échantillons prélevés au niveau du bras et de la jambe ainsi qu'avant et après 2 heures d'attente en position assise [85]. Ces variations locales et temporelles soulignent l'intérêt d'une mesure *in situ* et illustrent les avantages d'une mesure *in vivo*.

1.4.1 Taux de sédimentation

La manière la plus ancienne et celle utilisée en clinique pour quantifier l'agrégation érythrocytaire est le taux de sédimentation. La méthode mise au point par Westergren [181] consiste à maintenir un échantillon sanguin verticalement dans une éprouvette maintenue à 37°C et de mesurer la longueur de la colonne de plasma après une heure d'attente. Ce taux, mesuré en mm/h, est une fonction du rayon de Stokes - ou rayon hydrodynamique - des agrégats. La simplicité de la méthode explique qu'elle soit utilisée comme marqueur d'inflammation et pour le diagnostic de certaines maladies dont l'artérite temporale et la polymyalgia rheumatica. Toutefois, cette

méthode souffre d'une grande variabilité car elle est sensible à plusieurs facteurs dont la température, l'orientation de l'éprouvette, la viscosité plasmatique et les vibrations de l'environnement.

1.4.2 Microscopie

Il est possible de caractériser l'agrégation en observant du sang au microscope sous lumière blanche à des grossissements standards (10× à 100×). Certains index géométriques ont été proposés pour quantifier le niveau d'agrégation dans de tels montages [35]. Cependant, la forte densité des globules rouges oblige une dilution de l'échantillon pour permettre leur observation à des hématocrites de l'ordre de 1 à 10 %. L'extrapolation des résultats à un hématocrite physiologique n'est pas sans difficultés. Certains chercheurs sont parvenus à extraire l'hémoglobine des globules rouges les rendant ainsi transparents à la lumière (« *ghost cells* ») pour les filmer et mesurer leur migration axiale en présence ou non d'agrégation [75;76].

1.4.3 Viscosimétrie

Un échantillon sanguin est soumis à un cisaillement constant et un capteur mesure la contrainte de cisaillement sur une des parois du montage. Le taux de cisaillement est une fonction des caractéristiques géométriques du montage. Le ratio de la contrainte et du taux de cisaillement permet de déterminer la viscosité sanguine. Une limitation de ce type de mesure est la formation d'une couche de plasma (« *plasma skimming* ») à la paroi supérieure du montage par la sédimentation des globules, ce qui peut induire un biais dans les mesures. Cependant, cette approche a été et demeure très utilisée en rhéologie et en hémorhéologie clinique.

1.4.4 Rétrodiffusion laser

La méthode de référence pour quantifier l'agrégation érythrocytaire est une mesure fondée sur la diffusion de la lumière laser par les globules rouges. Un faisceau lumineux est envoyé dans un échantillon sanguin et la rétrodiffusion (appareil Regulest, Florange, France; ou LORCA, Amsterdam, Pays-Bas) ou la transmission (appareil Myrenne, Roetgen, Allemagne) de la lumière est mesurée à l'aide d'une photodiode. L'échantillon est soumis à des cycles de désagrégation et d'agrégation à faible cisaillement ou en stase permettant de calculer des indices de cinétiques et d'énergie d'adhésion. L'inconvénient principal de la méthode est la nature *ex vivo* et *ex situ* de la mesure.

1.4.5 Permittivité électrique

La permittivité électrique du sang est aussi déterminée par l'agrégation érythrocytaire. La résistance mais surtout la capacitance sanguine à 0.2 et 14 MHz varient avec l'agrégation [133;134]. Cependant, la relation entre ces propriétés électriques et l'agrégation demeure très complexe. Cette méthode est peu utilisée, même dans les laboratoires spécialisés de rhéologie.

1.4.6 Rétrodiffusion ultrasonore : avantages et limites

Les interactions entre les ondes ultrasonores et les globules rouges agrégeants sont connus depuis les années 1970 et forment, en mode B, des images texturées (« *speckle patterns* ») dont l'intensité varie avec l'agrégation des hématies. L'image

mode B est formée en juxtaposant les variations de l'enveloppe de l'intensité du signal de radiofréquence capté par le transducteur sur une échelle de niveaux de gris. La possibilité d'évaluer la rhéologie sanguine *in vivo* et *in situ* représente un atout de taille lorsqu'on connait la dépendance des propriétés mécaniques sanguines à l'écoulement. Pourtant, les ultrasons sont très peu utilisés dans le domaine de l'hémorhéologie. La faible résolution de 150 µm à 10 MHz et de 50 µm à 30 MHz, et la dépendance non linéaire de l'intensité rétrodiffusée en fonction de l'hématocrite expliquent sans doute cet état de faits. En effet, les globules rouges sont trop petits pour permettre de les distinguer directement sur une image ultrasonore et leur très grande densité introduit des interactions complexes menant à la génèse des ondes rétrodiffusées. Ces interactions destructives et constructives sont aujourd'hui mieux comprises. Nous exposons dans ce travail comment ces propriétés échogènes peuvent être exploitées de manière quantitative et ainsi permettre une caractérisation rigoureuse et objective de l'agrégation.

1.5 Objectifs et descriptifs de la thèse

L'objectif premier de ce travail consiste dans le développement un outil quantitatif permettant la caractérisation locale de l'agrégation érythrocytaire par la méthode ultrasonore. Nous posons l'hypothèse que les propriétées spectrales non Rayleigh de la rétrodiffusion ultrasonore par du sang agrégeant peuvent être modélisées par le « *Structure Factor Size Estimator* », une approximation au second ordre en fréquence du facteur de structure. Nous démontrons qu'une approche spectrale limitée à une largeur de bande finie (ici considérée principalement entre 9 et 28 MHz) permet la paramétrisation du problème par deux grandeurs physiques menant à une cartographie bidimentionnelle de la microstructure sanguine. Les

propriétés de ces deux paramètres sont étudiées et leurs sens physiques respectifs sont établis.

L'applicabilité *in vivo* d'un tel outil constitue le second objectif de ce travail. Nous posons l'hypothèse que la caractérisation ultrasonore locale de l'agrégation érythrocytaire devrait contribuer à élucider l'implication des perturbations hémorhéologiques dans le développement des complications circulatoires. Des travaux en collaboration avec le D^{r} Franceschini portant sur la compensation de l'atténuation des ondes ultrasonores par les tissus interposés entre la sonde et le sang ont permis d'atteindre cet objectif. Les avantages d'une caractérisation locale *in vivo* de l'agrégation et les implications cliniques potentielles d'un tel outil sont illustrés dans une étude expérimentale animale sur l'implication de l'hyperviscosité sanguine, mesurée localement, dans la formation des thrombus veineux.

Le chapitre 2 est un chapitre méthodologique présentant la modélisation spectrale du coefficient de rétrodiffusion érythrocytaire par le « *Structure Factor Size Estimator* ». Le corps de cette thèse est composé de trois articles. Le chapitre 3 (article 1) expose essentiellement la validation du modèle en 1D dans un champ cisaillé homogène et s'attarde sur certaines propriétés des paramètres microstructuraux. Le chapitre 4 (article 2) consiste en l'extension de la méthode en 2D permettant l'obtention d'images paramétriques dans différents types d'écoulement et l'établissement de cartes de viscosité locales. Le chapitre 5 (article 3) présente une étude *in vivo* de la méthode dans une expérimentation animale mettant en évidence l'implication étiologique de l'agrégation érythrocytaire sur le déclenchement de la thrombose veineuse chez le lapin. L'originalité, la portée et les perspectives de ce travail sont discutés dans le chapitre 6.

2 Chapitre 2 : Ultrasons et agrégation érythrocytaire

L'étude des interactions des ultrasons avec le sang s'inscrit dans le domaine de la caractérisation tissulaire acoustique. Des grandeurs telles la vitesse du son, l'atténuation, le coefficient de non linéarité *B/A* ou le coefficient de rétrodiffusion *BSC* sont utilisés pour imager des variations mécaniques et structurelles dans la composition des tissus. Ces paramètres permettent, entre autres, le diagnostic du cancer de la prostate [60], la différenciation entre fibroadénomes et carcinomes chez les rongeurs [127], la quantification de l'apoptose cellulaire [98] et l'étendue de l'ostéoporose [101]. La grandeur d'intérêt exploitée dans ce travail est le *BSC*. Une modélisation du *BSC* à l'aide du facteur de structure permet de relier la microstructure sanguine au spectre du *BSC*. Le facteur de structure est le paramètre qui décrit les variations spectrales du *BSC* lorsque les globules rouges s'agrègent. Souvent négligé en caractérisation tissulaire, il est nécessaire dans notre problème en raison des interactions partiellement cohérentes qui surgissent en raison de la très grande densité des diffuseurs (les globules rouges). La paramétrisation du modèle élaboré dans ce travail par une approximation au second ordre en fréquence permet de décrire la microstructure sanguine à l'aide de deux paramètres, d'une part, le facteur d'entassement *W* qui est relié à la thermodynamique statistique du système, et d'autre part, le paramètre *D* qui permet d'approximer la taille moyenne isotrope des agrégats. Le cadre théorique et la paramétrisation du modèle sont décrits dans ce chapitre.

2.1 Sensibilité des ultrasons à l'agrégation érythrocytaire et limites de l'imagerie mode B

L'agrégation érythrocytaire augmente visiblement l'intensité du signal dans un vaisseau sanguin en mode B (Figure 2-1) lorsque, par exemple, un garrot est apposé pour diminuer la circulation sanguine.

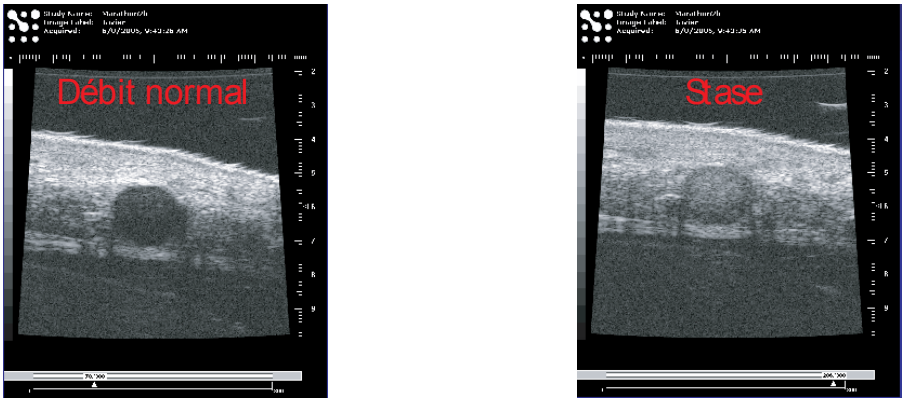

a) b)

Figure 2-1 : Échographie en mode B d'une veine sous cutanée de l'avant bras : (a) en circulation normale; (b) lorsqu'un garrot est apposé en aval de la veine sous cutanée, entrainant une augmentation d'échogénicité. Le rétablissement de la circulation entraîne la désagrégation sanguine et une diminution de l'intensité du signal sanguin.

Ce phénomène est attribué à la formation réversible d'agrégats érythrocytaires qui est fonction de la diminution du taux de cisaillement [160]. Kitamura démontre que cette augmentation d'intensité est corrélée avec la concentration plasmatique en fibrinogène et les concentrations sériques de cholestérol et de triglycérides [96]. Une étude sur

l'intensité ultrasonore sanguine dans la carotide, mesurée directement depuis l'intérieur du vaisseau en IVUS (« *IntraVascular UltraSound* ») [48], montre des variations temporelles cycliques attribuables à la dynamique de formation et de brisure des agrégats. La présence d'échos spontanés dans l'oreillette gauche lors d'un examen transœsophagien est un marqueur de stase sanguine causée par la présence d'une sténose mitrale [21;87;88] et d'anomalies hémorhéologiques dans la maladie cérébrovasculaire [26;46]. Leur présence dans l'aorte descendante est indicative de la présence de calcification de la paroi aortique, d'un taux de cisaillement maximal réduit, de dysfonction ventriculaire gauche, d'hypertrophie aortique [49;92].

Deux termes sont utilisés dans la littérature pour définir les propriétés échogènes des tissus. L'échoicité ultrasonore, introduite par Yuan et Shung [193], représente la capacité apparente d'un tissu à générer des échos ultrasonores en mode B. Ce terme a été introduit pour marquer la distinction entre cette propriété et l'échogénicité, qui est la capacité réelle d'un tissu à générer des échos ultrasonores, une grandeur quantifiable et indépendante de l'instrumentation. La confusion entre les deux termes est très largement répandue dans la littérature où le terme échogénicité est souvent employé à tort pour sa contrepartie. Cette distinction lexicale est mentionnée ici pour marquer l'importance des limitations inhérentes au mode B, qui sont des mesures semi quantitatives d'échoicité.

Une augmentation de puissance observée en mode B permet une évaluation qualitative ou au mieux une quantification relative de l'augmentation d'échogénicité. Ces quantités sont en effet biaisées par les algorithmes de post traitements des images mode B, par l'atténuation des signaux acoustiques par les tissus interposés, par les caractéristiques du transducteur (fréquence, bande passante, focalisation) et de l'électronique qui diffèrent entre appareils et *a fortiori* entre manufacturiers. La détermination de paramètres quantitatifs permettant une caractérisation ultrasonore de l'agrégation est l'un des objectifs de ce travail. Celle-ci passe essentiellement par une

normalisation permettant de calculer le *BSC*. Ce paramètre est la grandeur qui quantifie l'échogénicité. La seconde étape permettant une évaluation objective de l'agrégation consiste en une modélisation et une résolution d'un problème inverse assurant le lien entre le *BSC* et la microstructure des tissus. Des travaux inspirés de la cristallographie par rayon X et de la physique des milieux colloïdaux ont été menés préalablement au laboratoire par Beng-Ghee Teh [166], Isabelle Fontaine [62-64] et David Savéry [147;148]. Ils ont permi d'atteindre certains acquis permettant la modélisation de la rétrodiffusion érythrocytaire à l'aide du facteur de structure et une paramétrisation du problème.

2.2 Définitions

2.2.1 Propagation de l'onde ultrasonore

Une onde ultrasonore de compression d'intensité $I_{incidente}$, de nombre d'onde *k*, est générée dans un tissu. Elle se propage dans le milieu à la vitesse *c* dans la direction $\vec{\imath}$. Lorsqu'elle rencontre un volume élémentaire *dV* contenant des diffuseurs présentant un contraste d'impédance γ_z, elle est diffusée dans toutes les directions (Figure 2-2).

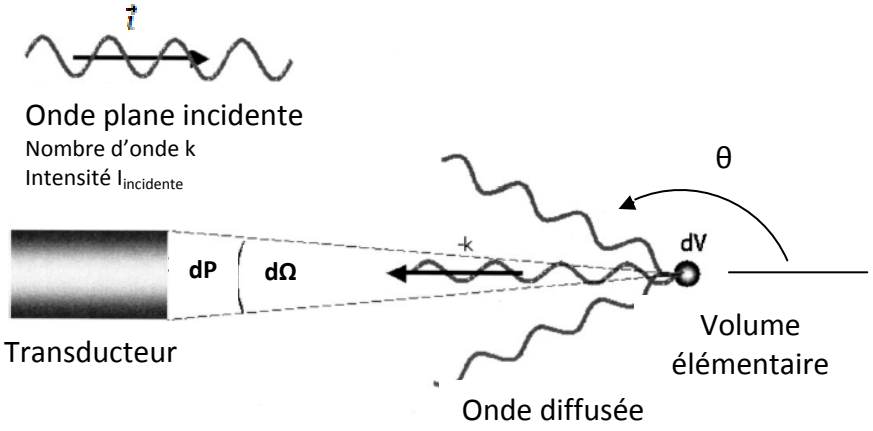

Figure 2-2 : Propagation et diffusion d'une onde de compression ultrasonore. Adapté de [147].

La vitesse du son *c* est déterminée par $c = \frac{1}{\sqrt{\kappa\rho}}$ où κ et ρ sont respectivement la compressibilité et la densité du milieu de propagation. Dans les tissus mous, la vitesse du son est généralement approximée à 1540 m/s alors que les vitesses réelles dans les tissus mammaliens s'étalent de 1400 à 1650 m/s, pour une marge d'erreur de moins de 5% [78]. La longueur d'onde λ est définie par le ratio $\lambda = \frac{2\pi}{k}$. La fréquence *f* est reliée au nombre d'onde et à la longueur d'onde par $k = \frac{2\pi}{\lambda} = \frac{2\pi f}{c}$.

Si les diffuseurs sont caractérisés par κ_e et ρ_e (indice *e* pour érythrocyte), et le milieu suspendant par κ_p et ρ_p (indice *p* pour plasma), les contrastes de compressibilité $\gamma_\kappa$et de densité γ_ρ sont définis par :

$$\gamma_\kappa = \frac{\kappa_e - \kappa_p}{\kappa_p} \text{ et } \gamma_\rho = \frac{\rho_e - \rho_p}{\rho_e}. \quad (2.1)$$

Puisque l'impédance acoustique *Z* est définie par $Z = \sqrt{\frac{\rho}{\kappa}}$, le contraste d'impédance acoustique γ_Z est donc donné par [147;149] :

$$\gamma_z = \frac{Z_e - Z_p}{Z_p} \approx \frac{1}{2}(\gamma_\rho - \gamma_\kappa)\,. \quad (2.2)$$

2.2.2 Coefficient de rétrodiffusion *BSC*

Le coefficient de rétrodiffusion ultrasonore *BSC* d'un tissu est défini par :

$$BSC = \frac{dP}{I_{incident} d\Omega dV}\,, \quad (2.3)$$

soit l'intensité rétrodiffusée vers le transducteur par un volume élémentaire de diffuseurs par angle solide $d\Omega$ pour une onde incidente unitaire $I_{incident}$. Il se mesure en $sr^{-1}.cm^{-1}$ et est une signature acoustique de l'échogénicité d'un tissu.

Le *BSC* est dépendant de la fréquence et se note *BSC(k)*. La mesure du *BSC* à plusieurs fréquences permet evidemment de déterminer *BSC(k)*. Toutefois, l'utilisation de transducteurs large bande permet une exploitation spectrale plus élégante et efficace du signal rétrodiffusé par une transformée de Fourier. *BSC(k)* s'obtient alors expérimentalement par une étape de normalisation du spectre du signal *RF(t)* provenant du tissu d'intérêt. Une approche, dite de substitution modifiée, est décrite en détail au paragraphe 3.5.2 et s'applique bien aux transducteurs large bande focalisés utilisés dans nos études [177]. Elle repose essentiellement sur une mesure de référence obtenue dans un milieu diffus (ici une suspension non agrégeante de globules rouges diluée à 6%) dont le *BSC* est soit connu théoriquement (voir paragraphe 2.3.2 et équations 3.1 et 3.4), soit déterminé expéritalement (voir équation 3.11). Le ratio des spectres des deux signaux, P_{Blood} et P_{H6}, obtenus par transformée de Fourier, permet alors le calcul de *BSC(k)* (voir équation 3.12). Il est à noter que les coefficients d'atténuation du sang α_{blood} et du milieu de référence ici α_{H6} doivent aussi être connus dans l'équation 3.12.

2.3 Modélisation analytique de *BSC(k)*

2.3.1 Intéraction de l'onde avec un globule : section de rétrodiffusion $\sigma_b(k)$

Un diffuseur est caractérisé par sa section de diffusion $\sigma(k, \theta)$ qui est, par définition, la surface d'un réflecteur plan idéal renvoyant la même énergie que la particule dans la direction θ. La section de diffusion d'une particule de Rayleigh ($\gamma_Z \ll 1, kV^{1/3} \ll 1$) est exprimée par [158]:

$$\sigma_R(k,\theta) = \frac{k^4 V^2}{16\pi^2}\left(\gamma_\kappa + \gamma_\rho \cos(\theta)\right)^2 . \qquad (2.4)$$

où
V est le volume d'un diffuseur,
γ_κ est le contraste entre les compressibilités du diffuseur et du milieu suspendant,
γ_ρ est le contraste entre les densités du diffuseur et du milieu suspendant.

Lorsque la diffusion est mesurée avec un angle θ de 180°, on parle de rétrodiffusion (indice *b* pour « *backscattering* ») pour laquelle la section de rétrodiffusion Rayleigh $\sigma_{Rb}(k)$ est donnée par :

$$\sigma_{Rb}(k) = \frac{1}{4\pi^2} k^4 V^2 {\gamma_Z}^2. \quad (2.5)$$

Dans notre problème, le globule rouge est le diffuseur acoustique élémentaire. Aux fréquences médicales couramment utilisées en clinique (< 10 MHz), le globule rouge suspendu dans du plasma est essentiellement un diffuseur de Rayleigh [158]. Sa section de rétrodiffusion est donnée par l'équation 2.5 où l'on remarque que $\sigma_{Rb}(k)$ est indépendante de la forme du globule rouge, qui est donc généralement associée à une sphère de volume $V = \frac{4}{3}\pi a^3 = 87\mu m^3$ où *a* est le rayon du diffuseur équivalent. Cette approximation est valide lorsque $ka < \frac{\pi}{10}$, ce qui correspond pour un globule avec *c* = 1540 m/s à f < 28.5 MHz. Au-delà de cette fréquence limite, la forme du diffuseur modifie sa section de rétrodiffusion $\sigma_b(k)$, ce qui peut être pris en compte par un facteur de forme $F(k)$ défini par :

$$F(k) = {\sigma_b(k)}\Big/{\sigma_{Rb}(k)}. \quad (2.6)$$

Des facteurs de formes pour une sphère, un cylindre et une ellipsoïde sont comparés à un globule rouge à la Figure 2-3, en fonction du rayon *a* du diffuseur prototype. Il a été démontré dans une étude semi-analytique [149] qu'une erreur de moins de 5% était commise sur $\sigma_b(k)$ en approximant un globule rouge par une sphère

lorsque $ka < 0.24$, ce qui correspond à $f < 21\ MHz$. Au-delà de cette fréquence, la forme et l'orientation des globules modifient $\sigma_b(k)$ de manière importante.

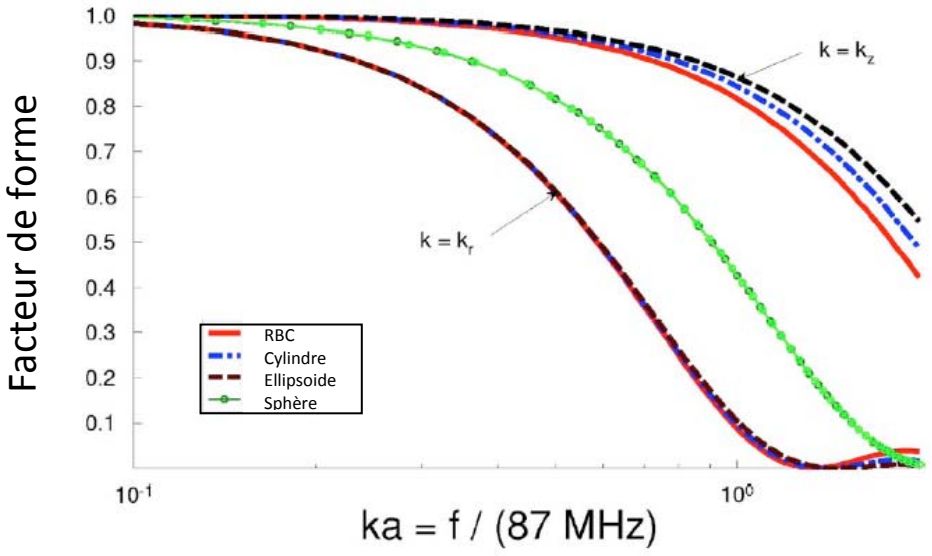

Figure 2-3 : Facteur de forme en fonction de la fréquence selon différents angles d'insonification *r* et *z*. L'erreur commise par l'approximation d'un globule rouge par ces formes géométriques est graphiquement représentée en fonction de l'orientation et de la grandeur *ka*. Adapté de [149].

Toutefois, en pratique, lorsqu'un ensemble de globules rouges orientés aléatoirement est insonifié, l'approximation de $\sigma_b(k)$ par une sphère induit une erreur moindre que celle indiquée à la Figure 2-3. En effet, le facteur de forme moyen de l'ensemble des globules orientés aléatoirement devrait se situer entre les facteurs de forme correspondant à $k = k_r$ *et* $k = k_z$. Cela fait donc augmenter la limite de fréquence au-delà de 21 MHz pour une erreur inférieure à 5%. En fait, cette remarque explique sans doute pourquoi des globules non agrégeants montrent expérimentalement des caractéristiques de diffusion Rayleigh jusqu'à des fréquences de 30 MHz [177] ou même jusqu'à 90 MHz lorsque l'hématocrite est inférieur à 15% [116]. L'approximation par une

sphère pour $f < 30\,MHz$ semble donc raisonnable et a été retenue dans ces travaux. Une orientation privilégiée des globules rouges (par exemple à haut cisaillement) pourrait toutefois entraîner des erreurs supérieures à 5% sur $\sigma_b(k)$.

2.3.2 Interactions de l'onde avec une suspension de globules non agrégeants – rétrodiffusion de Rayleigh

Complexifions quelque peu le problème en considérant maintenant une concentration de *m* globules rouges non agrégeants dans un volume unitaire. Sous l'hypothèse de Born ($|\gamma_z| \ll 1$, pas de diffusions multiples), lorsque les particules sont positionnées aléatoirement dans l'espace, la diffusion est strictement incohérente et *BSC* est tout simplement proportionnel à *m*. Cela est le cas pour de très faibles hématocrites de l'ordre de 5% et moins. La distribution spatiale des érythrocytes peut être modélisée par un processus de point de Poisson car aucune structure cohérente n'est présente dans le tissu (milieu aléatoire) [147]. Lorsque l'hématocrite augmente, le principe de superposition de s'applique plus et *BSC* n'est plus proportionnel à *m* car les positions ne sont plus indépendantes: les globules interagissent par répulsion stérique car on atteint déjà des concentrations de l'ordre de 400 000 globules par mm^3 pour un hématocrite de 10%. Cette dépendance non linéaire du *BSC* pour du sang non agrégeant est modélisée par *W*, le facteur d'entassement ou « *packing factor* ».

Le facteur d'entassement *W* est relié à la fonction de corrélation de paires *g(r)* par :

$$W = 1 + m \int [g(r) - 1\,] dr. \qquad (2.7)$$

La fonction *g*(*r*) est une densité de probabilité qui décrit la probabilité de trouver une particule à la position *r* étant donné une première particule fixée. Elle permet donc de tenir compte de la corrélation dans la structure du tissu. Lorsqu'il n'y a pas d'organisation spatiale et que les positions sont indépendantes (processus de Poisson), *g*(*r*) = 1 et *W* = 1

[147]. La Figure 2-4 illustre graphiquement une fonction *g*(*r*) pour un tissu bidimensionnel formé de disques durs lorsque la densité augmente.

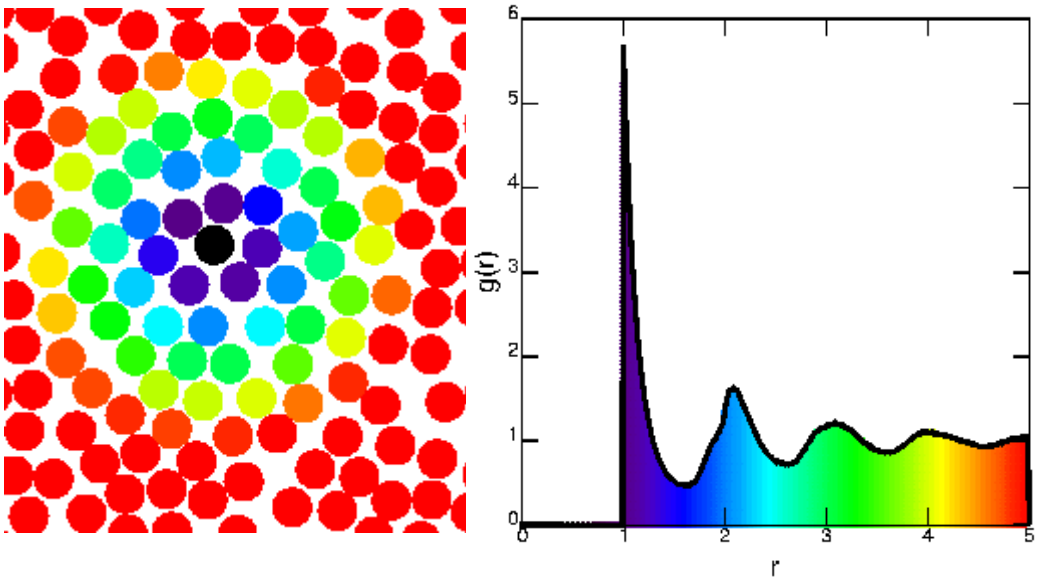

Figure 2-4 : Organisation spatiale et fonction de corrélation de paires.[6]

Puisque les sphères sont impénétrables, il ne peut y avoir de sphère à une distance inférieure à 1 (répulsion stérique). À *r* = 1, plusieurs particules sont présentes (présence d'un pic dans *g*(*r*)) mais leur entassement est à l'origine d'un creux à r = 1.5. *g*(*r*) oscille ensuite et converge asymptotiquement vers 1 lorsque *r* augmente. Analysons intuitivement l'effet de l'hématocrite *H* sur *g*(*r*) et sur *W*. Si l'on se rapporte à l'équation 2.7, lorsque *H* est faible, *m* est petit, *donc* $m\int(g(r)-1)dr$ tend vers 0 et *W* tend vers 1. Lorsque *H* augmente, *m* augmente, et *g*(*r*) présente des oscillations autour de 1. Il a été démontré que pour des particules de Rayleigh, *W* est compris entre 1 et 0 lorsque *H* augmente [169]. On peut en déduire que $m\int(g(r)-1)dr$ est compris entre 0 et -1. Sans agrégation, *g*(*r*) présente donc beaucoup de creux et peu de pics, les creux s'accentuant lorsque m augmente. Twersky [169] a déterminé sous les hypothèses de

[6] Figures extraites de http://www.physics.emory.edu/~weeks/idl/gofr.html, consultée 25 avril 2009

Rayleigh, des expressions analytiques pour *W* en fonction de *H* pour des sphères W_s et des cylindres W_c :

$$W_s = \frac{(1-H)^4}{(1+2H)^2} \tag{2.8}$$

$$W_c = \frac{(1-H)^3}{1+H} \tag{2.9}$$

Ces fonctions sont représentées à la Figure 2-5. On retrouve bien le comportement attendu soit une diminution de *W* de 1 vers 0 lorsque *H* augmente. Remarquons que lorsque *H* = 100%, ce qui est théoriquement possible puisque les globules rouges sont déformables, ce modèle prévoit que *BSC* = 0, ce qui est cohérent avec la théorie acoustique puisqu'il n'y a alors plus de diffuseurs mais seulement un milieu continu de globules, et donc aucune diffusion possible de l'onde acoustique transmise.

On obtient donc une expression du coefficient de rétrodiffusion pour une suspension non agrégeante de globules rouges qui s'écrit :

$$BSC(k) = m\sigma_b(k)W. \tag{2.10}$$

Dans cette équation, on constate que *W* peut être considéré comme un facteur de correction tenant compte de la structure du tissu (ici la densité) pour un milieu formé de particules identiques de faible diffusion (conditions de Born). *W* est donc une propriété structurelle du tissu.

Il peut être démontré que

$$W = \frac{Var(m)}{m}, \tag{2.11}$$

où *m* est le nombre de diffuseurs dans un voxel unitaire et *Var* la variance de ce nombre [120]. Pour une suspension non agrégeante, l'interprétation physique de cette équation est cohérente avec les conclusions précédentes : lorsque *H* augmente, *m* augmente et *Var*(m) diminue ce qui entraine une diminution de *W*.

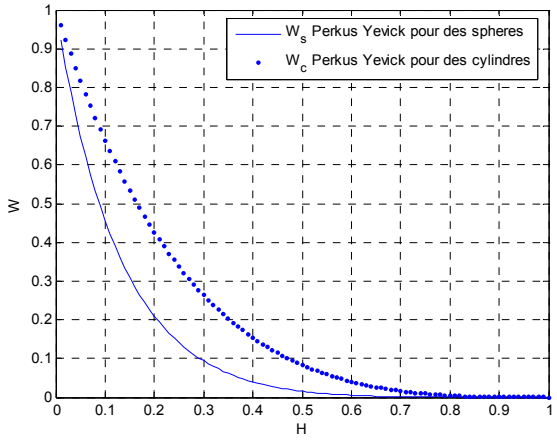

Figure 2-5 : Facteur d'entassement pour des sphères et des cylindres durs en fonction de l'hématocrite *H.*

2.3.3 Interaction de l'onde avec des globules rouges agrégeants – rétrodiffusion de Rayleigh versus non Rayleigh

2.3.3.1 Agrégation et modèle de Rayleigh

Lorsque les fréquences ultrasonores sont typiquement inférieures à 10 MHz, une agrégation faible (moins de 4 globules par agrégat [106;120]) permet d'évoquer l'hypothèse d'une rétrodiffusion de Rayleigh (ka<<1). Des simulations ont alors montré que l'agrégation provoque une augmentation de la variance du nombre de diffuseurs dans un volume élémentaire alors que *m* demeure constant, ce qui entraîne une augmentation de *W* (équation 2.11) et donc de *BSC* (équation 2.10). Cette formulation élégante concilie deux paradigmes expliquant l'augmentation de *BSC* avec l'agrégation : d'une part, elle illustre l'influence de la microstructure des diffuseurs de Rayleigh sur *BSC* à travers *W*; d'autres part elle est compatible avec l'idée que l'agrégation fait augmenter le volume des diffuseurs (maintenant des agrégats), ce qui pour la théorie de diffusion de Rayleigh se

traduit aussi par une augmentation de *BSC*. Cette approche de modélisation a été considérée par d'autres auteurs, toujours sous l'hypothèse de diffuseurs de Rayleigh, selon lesquels la dépendance de l'intensité du *BSC* à l'hématocrite est reliée à la taille des agrégats par des notions d'entassement de globules dans les agrégats et d'entassement des agrégats dans la suspension [25;84]. Étrangement toutefois, les tailles d'agrégats de 240 globules sont rapportées, ce qui dépasse fortement les limites de diffusion Rayleigh.

2.3.3.2 Agrégation et modèle non-Rayleigh

Il a été démontré expérimentalement que le sang agrégeant ne présentait pas la dépendance fréquentielle en f^4, caractéristique de la diffusion de Rayleigh [65;109;192] (voir équation 2.5). Cela concorde avec l'idée que les agrégats de globules de taille grandissante ne peuvent plus être considérés comme des diffuseurs de Rayleigh. Ceci est particulièrement vrai lorsque la fréquence du transducteur augmente, ce qui est désirable pour améliorer la résolution spatiale. Le modèle fondé sur le facteur d'entassement et les équations 2.8, 2.9 et 2.10 exprimant *W* en fonction de *H* n'est pas adapté pour le sang agrégeant. Nous avons vu à la section précédente qu'il est possible de modéliser une rétrodiffusion par de petits agrégats, cependant une complexification est nécessaire pour considérer des agrégats physiologiques, tels que rencontrés dans le système veineux.

L'absence d'un modèle théorique adapté à un milieu dense de diffuseurs non Rayleigh a incité la communauté scientifique à quantifier l'agrégation à l'aide de paramètres descriptifs tels que la pente spectrale *SS* (pente de la dépendance fréquentielle du *BSC* sur une échelle log-log) ou le coefficient *IBSC* « *Integrated BSC* » (la moyenne du *BSC* sur la bande passante du transducteur, aussi notée $\overline{BSC}$). Ces paramètres peuvent s'avérer fort utiles et suffisants pour distinguer, classifier ou caractériser le niveau d'agrégation pour une plage de fréquence prédéterminée, cependant de telles mesures peuvent dépendre des caractéristiques de l'instrument

choisi. De tels paramètres ont été utilisés pour caractériser des types de sangs aux tendances agrégeantes différentes [172], pour montrer l'hyper-agrégation chez des sujets diabétiques [43], pour comparer des variations relatives d'intensité du *BSC* en fonction de la fréquence [125], pour suivre des cinétiques d'agrégation avec la méthode ultrasonore [187;188], ou même pour quantifier la formation et l'évolution d'un thrombus au cours du temps [86;105]. Cependant, si de tels paramètres fondés sur le *BSC* sont meilleurs que le mode B (car se sont des mesures d'échogénicité et non plus d'échoicité), ils demeurent difficiles à interpréter car ils sont fortement dépendants de la fréquence, de la largeur de bande du transducteur et de l'atténuation du milieu insonifié. La comparaison entre ces études est donc complexe lorsque des fréquences différentes sont utilisées ou lorsque l'atténuation du milieu insonifié varie.

Un modèle théorique fondé sur le facteur de structure a été proposé pour expliquer le comportement non Rayleigh de la rétrodiffusion ultrasonore érythrocytaire. Sous les conditions de Born (diffusions simples), pour une répartition de diffuseurs identiques dans un volume élémentaire de densité moyenne *m*, Twersky [170] définit le facteur de structure $S(-2k)$ par :

$$S(-2k) = S_b(k) = 1 + m \int [g(r) - 1]\, e^{-2ikr} dr \,. \qquad (2.12)$$

On remarque que le cas désagrégé dans les conditions de Rayleigh est un cas particulier du facteur de structure, i.e. lorsque $k = 0$. On reconnait alors le facteur d'entassement W défini à l'équation 2.7. On vérifie bien que $S(k \to 0) = W$ dans les conditions de Rayleigh.

Sous l'hypothèse qu'il n'y a pas de diffusions multiples (conditions de Born), le facteur de structure est intéressant car il permet de modéliser la rétrodiffusion non Rayleigh d'un milieu dense agrégeant pour des diffuseurs structurés, ce qui est bien adapté pour des globules rouges agrégeants. La variation de la dépendance fréquentielle

du *BSC* en présence d'agrégation (diminution de *SS*, augmentation de $\overline{BSC}$ est entièrement prise en compte par le facteur de structure:

$$BSC(k) = m\sigma_b(k)S(-2k) \tag{2.13}$$

Ce facteur $S(-2k)$ tient compte de l'effet de la microstructure sur le coefficient de rétrodiffusion, puisque les deux autres paramètres, *m* et $\sigma(-2k)$ sont constants quel que soit le niveau d'agrégation.

Il a été démontré par des travaux de simulation [64;145;147;148] que $S(-2k)$ est directement relié à la densité microscopique des diffuseurs $N(x, y)$ par :

$$S(-2k) = \frac{1}{n}|\mathcal{F}(N(x, y))|^2, \tag{2.14}$$

où

$$N(x, y) = \sum_{i=1}^{n} \delta(x - x_i, y - y_i) \tag{2.15}$$

et *n* représente le nombre de diffuseurs. Une telle démarche théorique a permis de simuler l'effet de la structure spatiale des agrégats sur la dépendance fréquentielle du *BSC*. En changeant seulement la position des globules, le facteur de structure induit des variations de puissance et des changements de pentes spectrales [64;148]. L'effet de l'agrégation sur la fonction de corrélation de paire *g*(*r*) est illustré aux Figure 2-6 et Figure 2-7. La Figure 2-7 représente une coupe de la Figure 2-6 selon les axes x = 0 et y = 0. Ces résultats de simulation montrent qu'une augmentation de la tendance agrégeante et une diminution du taux de cisaillement entraînent une augmentation de l'agrégation, ce qui fait apparaître des pics concentriques dans *g(r)*. Si l'on se rapporte à la Figure 2-4 et à l'équation 2.7, l'agrégation des globules provoque une augmentation de l'intégrale $m\int(g(r) - 1)dr$ (la surface sous la courbe *g(r)*) et donc une augmentation de *W*. L'apparition de ces pics dans *g(r)* provoque également une augmentation de la valeur moyenne de *g(r),* ce qui se traduit dans le domaine fréquentiel par une augmentation de

$S(k \to 0) = W$, soit, par définition, de *W* (voir équations 2.7 et 2.12). (On rappelle que la valeur moyenne d'une fonction est la valeur de sa transformée de Fourier à f=0). Il est démontré dans ces travaux de simulation [64] que les positions de ces pics sont aussi reliées à la taille des agrégats. L'importance de ces travaux consiste en ce qu'ils démontrent que *W* n'est plus strictement compris entre 0 et 1 (tel que prédit par les équations 2.8 et 2.9) mais peut prendre des valeurs supérieures à 1 lorsqu'il y a agrégation, soit un changement dans l'organisation spatiale des globules.

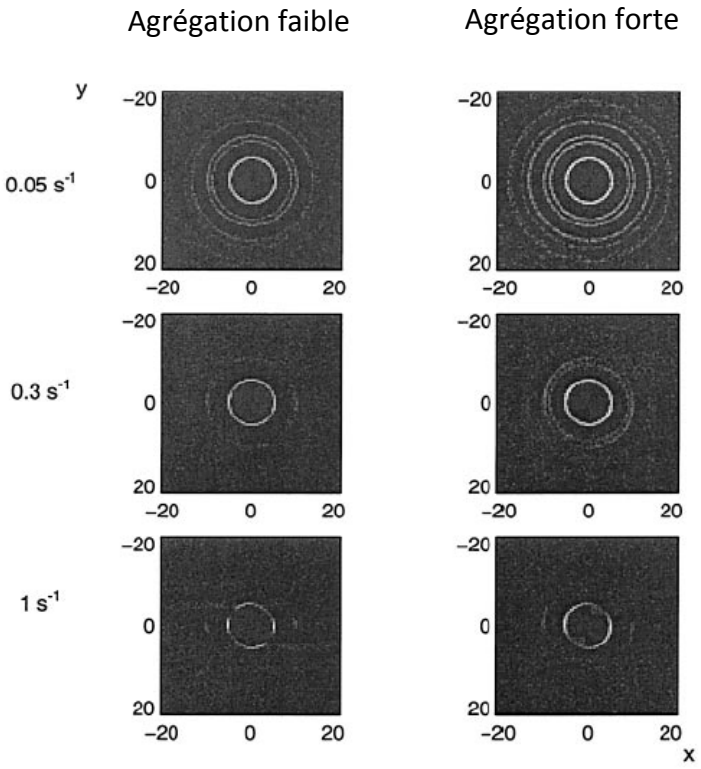

Figure 2-6 : Effet de l'agrégation sur la fonction de corrélation de paire *g*(*r*) dans un plan bidimensionnel. L'amplitude de *g(r)* est codée sur une échelle en ton de gris. Les axes x et y sont exprimés en µm. Une augmentation de l'agrégabilité ou une diminution du taux de cisaillement entraîne une augmentation de l'agrégation, ce qui se traduit par la présence de pics concentriques dans la fonction *g*(*r*). Adapté de [64].

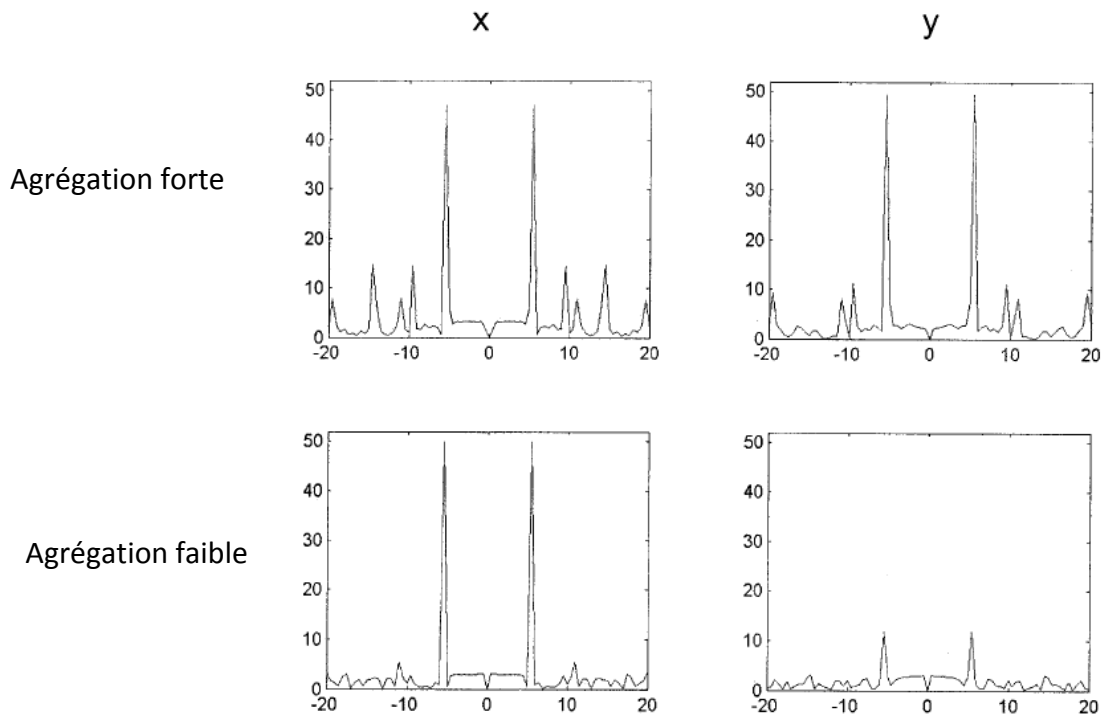

Figure 2-7 : Amplitude de *g*(*r*) selon l'axe des x (y = 0) et y (x = 0) pour une agrégation forte (tendance agrégeante forte et taux de cisaillement faible) et une agrégation faible (tendance agrégeante faible et taux de cisaillement plus élevé). On remarque l'apparition de pics importants selon les deux axes dans le case d'une agrégation forte. Les axes des x et y sont exprimés en µm. Adapté de [64].

Pour des suspensions à faible hématocrite (< 5%), un processus de point de Neyman Scott possède une formulation analytique de *g*(*r*) si bien que $S(-2k)$ peut être déterminé exactement. Cette approche de modélisation fut utilisée par Savéry et Cloutier [147]. Elle permet d'illustrer l'effet de la structure des diffuseurs sur *BSC*(*f*) de manière convaincante (Figure 2-8).

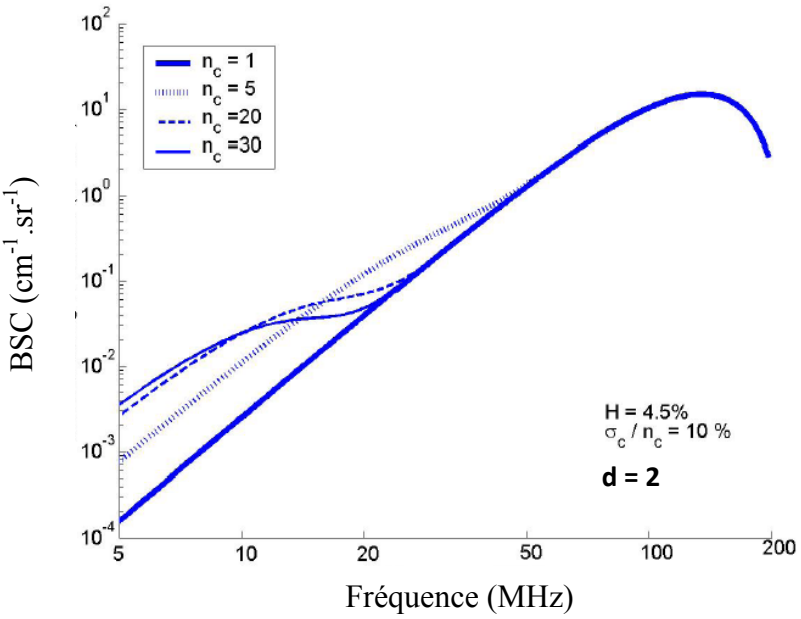

Figure 2-8 : Coefficient de rétrodiffusion (*BSC)* pour du sang porcin agrégeant tel que prédit par le processus de point de Neyman Scott pour un hématocrite de 4.5%. Pour une dimension fractale d de 2, une polydispersité de taille $^{\sigma_c}/_{n_c}$ de 10%, l'effet de différentes tailles d'agrégats n_c sur la dépendance fréquentielle du *BSC* y est décrit. Adapté de [147].

Des variations de pente spectrales très marquées sont observables entre 10 et 20 MHz. Dans le même article, le modèle est aussi appliqué pour résoudre le problème inverse qui consiste à extraire des paramètres structurels (facteur d'entassement *W* et taille normalisée de l'agrégat $D = {}^{\sigma}/_{a}$) à partir de données expérimentales (voir Figure 2-9). On remarque encore une fois que *W*, le facteur d'entassement, restreint à l'intervalle [0, 1] pour des particules non agrégeantes, peut, lorsqu'il y a agrégation, prendre des valeurs supérieures à 1. Nous reviendrons sur cette propriété de *W* dans le paragraphe 6.2.1.1. Cette approche analytique est fort attrayante mais ne peut être appliquée à plus haut hématocrite (hématocrite physiologique typiquement de 20 à 50%) car le processus

de point de Neyman Scott repose sur un positionnement indépendant des particules, ce qui n'est plus respecté lorsque *H* augmente au delà de 5%.

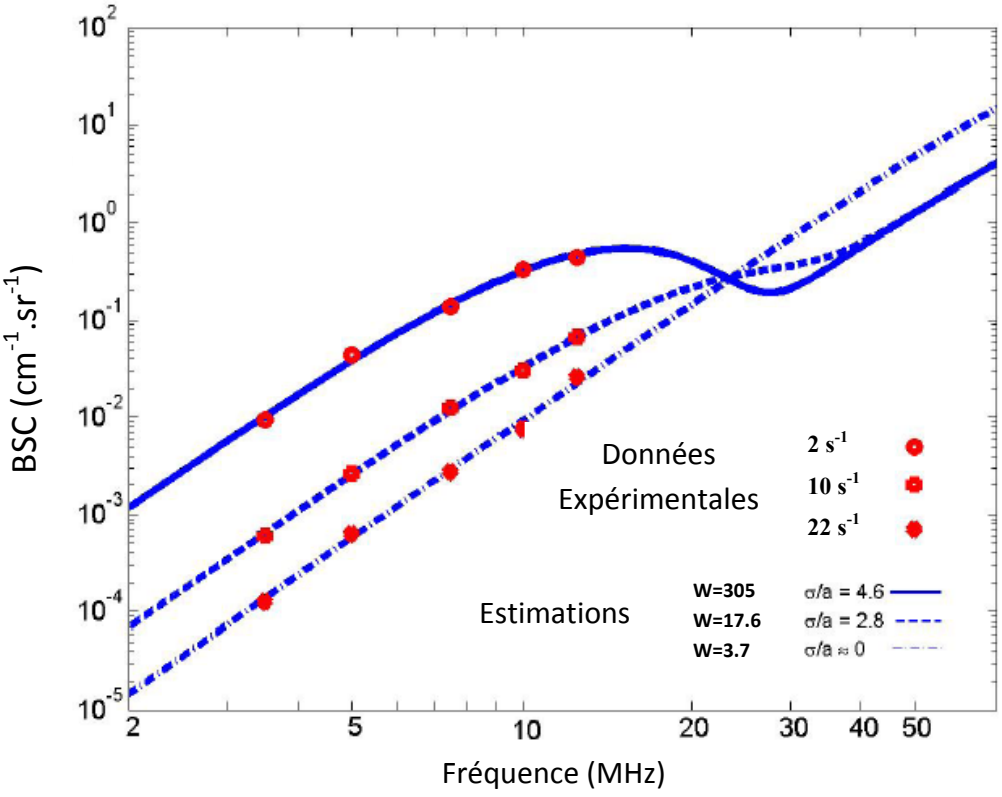

Figure 2-9 : Extraction de paramètres de structures *W* et $D = {}^{\sigma}/_{a}$ à partir de données expérimentales à l'aide du facteur de structure évalué avec le processus de point de Neyman Scott applicable à faibles hématocrites. Adapté de [147].

Les développements du facteur d'entassement et du facteur de structure selon des formulations relevant de la mécanique statistique des milieux denses se retrouvent dans la thèse de David Savéry [146].

2.4 Paramétrisation expérimentale de *BSC(k)*

2.4.1 SFSE : une approximation polynomiale au second ordre en *k*

Sur une largeur de bande infinie, *g(r)* et *N(x,y)* pourraient théoriquement être déterminés par une transformée de Fourier inverse de $S(-2k)$ (voir équations 2.12 et 2.14). Rappelons que *S(-2k)* peut être calculé à partir de *BSC(k)* (voir équation 2.13*)*. En pratique, la largeur de bande n'est pas infinie si bien que ce concept demeure purement théorique. Il est proposé, dans une implémentation pratique du modèle fondé sur le facteur de structure, d'approximer $S(-2k)$ par une série de Taylor du second ordre en *k*, soit

$$S(-2k) = S_0 + (-2k)S_1 + (-2k)S_2k^2 \tag{2.16}$$

où S_0, S_1 et S_2 sont les constantes du développement de Taylor. On a vu précédemment que lorsque *k = 0, S(0) = W*. On a donc $S_0 = W$. Pour des raisons de symétrie, i.e. si l'on retourne l'échantillon sanguin de 180°, $S(-2k)$ ne doit pas changer car tant la structure que l'asymmétrie des agrégats érythrocytaires demeurent identiques, ce qui implique que $S_1 = 0$. Une analyse dimensionnelle montre que S_2 est homogène à une surface. En notant R_g le rayon de giration[7] de l'agrégat, *R* son rayon et en prenant $R_g = \sqrt{\frac{3}{5}}R$ (approximation pour des agrégats isotropes) [81], on peut déterminer que $S_2 = -{R_g}^2 = -\frac{3}{5}(R)^2$. Enfin, en notant *a* le rayon d'un globule, on définit $D = {R}/{a}$ le rayon de l'agrégat en nombre de rayon de globules, ce qui correspond plus simplement au diamètre de l'agrégat en nombre de globules. On obtient alors :

$$S(-2k) \approx W - \frac{12}{5}(Da)^2k^2 \tag{2.17}$$

[7] Le rayon de gyration d'un objet est la distance moyenne quadratique des composantes de l'objet à son barycentre

En remplaçant cette expression dans l'équation 2.13, on obtient le modèle appelé « *Structure Factor Size Estimator* » ou SFSE :

$$BSC(k) = m\sigma_b(k)\left(W - \frac{12}{5}(Da)^2k^2\right) \quad (2.18)$$

Dans cette équation, *m* peut être obtenu par microcentrifugation ($m = {}^{H}/_{V}$, où *H* est l'hématocrite et *V* le volume d'un globule rouge) et $\sigma_b(k)$ peut être calculé selon l'équation 2.5. Lorsque *BSC* est déterminé expérimentalement sur une largeur de bande raisonnable, il est possible par minimisation de la fonction de coût $F_{coût}$, selon le critère des moindres carrés, de déterminer le couple *(W, D)* qui caractérise la microstructure du tissu sanguin insonifié.

$$F_{coût}(W, D) = min \left\| BSC_{exp}(k) - m\sigma_b(k)\left(W - \frac{12}{5}(kDa)^2\right)\right\|^2 \quad (2.19)$$

W et D sont des paramètres microstructurels du tissu et, de ce fait, ne dépendent théoriquement pas de la largeur de bande ou de la fréquence de transducteur. Nous verrons au paragraphe 6.2.2 dans quelle mesure cette affirmation peut s'appliquer. Les résultats expérimentaux et la validation de cette méthode font l'objet de l'article qui compose le chapitre 3 de cette thèse. Ce modèle est ensuite utilisé sur divers types de sang et divers types d'écoulements au chapitre 4, dans lequel des images paramétriques de *W* et *D* sont présentées.

2.4.2 SFSAE : une approximation tenant compte de l'atténuation du milieu

Le problème de la compensation des distortions fréquentielles des ondes ultrasonores, causées par les caractéristiques des tissus situés entre la sonde et le sang, a également été abordé au laboratoire, par D[r] Emilie Franceschini, en utilisant le formalisme du SFSE. En effet, *in vivo*, les mesures de rétrodiffusion sanguine sont biaisées par

l'atténuation de la peau, celle des tissus conjonctifs et des corps gras sous cutanés. Le SFSAE, ou « *Structure Factor Size and Attenuation Estimator* » est une méthode de minimisation permettant d'évaluer simultanément *W*, *D* et α_0, ce dernier paramètre étant l'atténuation totale des tissus situés entre la sonde et le sang [66]. Une nouvelle fonction de coût $F_{coût}(W, D, \alpha_0)$ a donc été introduite et minimisée selon le critère des moindres carrés:

$$F_{coût}(W, D, \alpha_0) = \left\| BSC_{exp}(k) - m\sigma(k)\left(W - \frac{12}{5}(kDa)^2\right)e^{-4\alpha_0 f}\right\|^2 \qquad (2.20)$$

pour obtenir des estimations de *W, D* et α_0. Dans cette fonction, α_0 est le coefficient d'atténuation total exprimé en Np/MHz. Il correspond à $\alpha_0 = \sum \alpha_i e_i$ où α_i et e_i sont respectivement le coefficient d'atténuation exprimé en Np/MHz/m et l'épaisseur des *i* tissus traversés. Une approximation linéaire en fréquence pour le produit $\alpha_0 f$ est une est raisonnable pour des tissus biologiques [79;80]. Plusieurs stratégies de minimisation de $F_{coût}(W, D, \alpha_0)$ ont été envisagées : une première approche non linéaire à l'aide de la fonction LSQNONLIN de Matlab fondée sur des descentes de gradients (voir [66] reproduit dans l'annexe B); une seconde approche fondée sur une recherche exhaustive du minimum global en balayant sur un intervalle de α_0 (article [67], soumis au « *Journal of the Acoustical Society of America »*). Puisque α_0 devient une constante dans la minimisation, le problème quadratique peut se résoudre analytiquement par la méthode de Cramer, ce qui assure du minimum global de cette étape de la minimisation. La recherche du minimum de la fonction $F_{coût}(W, D, \alpha_0)$ en fonction de α_0 permet de déterminer le trio (W, D, α_0) final. Cette nouvelle méthode de minimisation a le mérite d'être très rapide et d'assurer que la minimisation est globale [67]. Cette deuxième approche de minimisation appliquée au modèle SFSAE a été utilisée pour les résultats du chapitre 5, soit l'étude *in vivo* sur le lapin. En effet une méthode permettant de compenser les effets de l'atténuation par les tissus interposés entre la sonde et le sang est essentielle *in vivo*.

3 Chapitre 3 : Le « *Structure Factor Size Estimator* » : une paramétrisation du problème au second ordre en fréquence

3.1 Avant-propos

Ce chapitre reprend l'article « *Experimental ultrasound characterization of red blood cell aggregation using the structure factor size estimator* » publié dans le « *Journal of Acoustical Society of America* »[8]. Cet article constitue les premiers résultats de validation du SFSE, l'approximation au second ordre en fréquence de la modélisation du coefficient de rétrodiffusion érythrocytaire par le facteur de structure. Dans cette étude expérimentale, la méthode de normalisation permettant la détermination de *BSC(f)* est présentée. Trois transducteurs mono-éléments de fréquences différentes sont utilisés pour déterminer *BSC(f)* sur une large bande fréquentielle. Une étude de la cinétique de formation des agrégats est présentée, ce qui témoigne de la stabilité de la méthode. Deux hématocrites sont étudiés : un échantillon à hématocrite physiologique de 40% et un échantillon à faible hématocrite. La dilution permet une validation des estimations de taille *D* par une méthode optique, qui, malgré les limitations géométriques (3D - méthode ultrasonore vs 2D - méthode optique) montre une bonne corrélation entre les tailles mesurées.

[8] *Reprinted with permission from Yu F.T.H et al., J. Acoust. Soc. Am., vol. 122, issue 1, pages 645-656, 2007. Copyright 2009. Acoustical Society of America.*

Experimental ultrasound characterization of red blood cell aggregation using the Structure Factor Size Estimator (SFSE)

François T.H. Yu and Guy Cloutier

Laboratory of Biorheology and Medical Ultrasonics, University of Montreal Hospital Research Center, Pavilion J.A de Sève (room Y-1619), 2099 Alexandre de Sève, Montréal, Québec, H2L 2W5, Canada.

3.2 Abstract

The frequency dependence of the ultrasonic backscattering coefficient (*BSC*) was studied to assess the level of red blood cell (RBC) aggregation. Three mono-element focused wideband transducers were used to insonify porcine blood sheared in a Couette flow from 9 to 30 MHz. A high shear rate was first applied to promote disaggregation. Different residual shear rates were then used to promote formation of RBC aggregates. The Structure Factor Size Estimator (SFSE), a 2nd order data reduction model based on the structure factor, was applied to the frequency dependent *BSC*. Two parameters were extracted from the model to describe the level of aggregation at 6% and 40% hematocrits: *W*, the packing factor, and *D* the aggregate diameter, expressed in number of RBCs. Both parameters closely matched theoretical values for non aggregated RBCs. *W* and *D* increased during aggregation with stabilized values modulated by the applied residual shear rate. Furthermore, parameter *D* during the kinetics of aggregation at 6% hematocrit under static conditions correlated with an optical RBC aggregate size estimation from microscopic images (r^2 = 0.76). To conclude, the SFSE presents an interesting framework for tissue characterization of partially correlated dense tissues such as aggregated RBCs.

3.3 Introduction

Ultrasonic tissue characterization (UTC) is emerging as a unique non invasive tool to characterize red blood cell (RBC) aggregation *in vivo*. UTC is an imaging modality that takes advantage of quantitative ultrasonic parameters (backscattering, attenuation, speed of sound, tissue nonlinearity, statistics) to reveal intrinsic tissue properties. Major advances in this field have been recently accomplished in the areas of prostate cancer

diagnosis [60], cell apoptosis monitoring [98;168], osteoporosis characterization [129], rat fibroadenomas and mouse mammary carcinomas characterization [115;127], and in early Duchenne muscular dystrophy diagnosis [70]. In most cases, the spectral content (integrated backscatter coefficient, spectral slope, *y*-intercept, mid-band fit) of the radio-frequency (RF) ultrasound signal backscattered by the tissue is used to extract its acoustic properties and to reveal its microstructure and composition.

In the ultrasonic blood characterization (UBC) field, the objective is to obtain quantitative parameters that reflect the aggregation state of blood elements. It is well known that RBCs aggregate to form complex three-dimensional (3D) rouleaux structures depending mainly on an equilibrium between aggregating forces, which are mediated by RBC membrane factors and concentrations of plasmatic high molecular weight proteins such as fibrinogen, and disaggregating forces induced by the shear effects of the flow and the electrostatic and steric interactions between RBCs [37]. This phenomenon is normal, reversible and it occurs in the circulation of many mammalian species. RBC hyper-aggregation, however, is a pathological state; clinical and epidemiological studies identified it as an independent risk factor of circulatory related disorders such as deep venous thrombosis [6], atherosclerosis [103] and diabetes mellitus [102], to name a few. Because these diseases are characterized by localized blood and blood vessel impairments, this suggests that flow-dependent rheological parameters, such as RBC aggregation, could be involved in their respective pathogenesis. It would thus be of great interest to elucidate the role of RBC aggregation in the etiology of these pathologies *in vivo* and *in situ* with UBC techniques.

One difficulty in UBC resides in the fact that blood is an extremely dense medium (5 million erythrocytes / mm^3) that introduces a non linear relationship between the backscattered power and the scatterer concentration. In fact, non linear effects become important above 10% hematocrit (*H*, which is the RBC volume concentration),

approximately [156]. The physiological hematocrits normally range from 35% to 45%, which is clearly in the non linear regime. This particularity is a major difficulty in blood acoustic characterization compared to other UTC fields such as the study of the eye and liver, where the number density of scatterers in the targeted tissues rarely exceeds 100 scatterers / mm^3 [89;108]. Note that in the study of cell apoptosis, the group of D^r Kolios has shown evidence of packing effects in tissue like pellets of acute myeloid leukemia cells and concentrated cell suspensions [10]. Particular to UBC however is the consideration of particles clustering as RBC aggregates.

The non-linear hematocrit dependence of the *BSC* has been thoroughly studied with non aggregating RBC suspensions. It is well described for Rayleigh scatterers at frequencies up to 90 MHz by the Perkus Yevick packing factor W_{PY} [116;177], and it is supported by quantitative experimental data [156;158]. In the frequency domain, the spectrum of non aggregating RBCs presents a spectral slope (SS) of 4 (SS is the linear slope of the backscatter as a function of frequency on a log-log scale). When considering aggregating RBCs, an increase in the effective scatterer size (caused by RBC rouleaux formation) or in the insonifying ultrasound (US) frequency (to achieve better resolution) both increase the *ka* product and restrain the validity of the Rayleigh scattering theory (*k* is the ultrasonic wave number, and *a* is the mean radius of individual scatterers or RBCs). Nevertheless, numerous experimental quantification of the effect of RBC aggregation on the *BSC* and its frequency dependence can be found in the literature [39;42;65;144;172;188;192]. Previously, our group reported different simulation models based on the structure factor, *S(-2k),* that could explain the frequency dependence of aggregating RBCs in the non-Rayleigh regime [62-64;148]. It is the purpose here to validate those models with experimental results. The objective of the present study was thus to use an inverse approach of data reduction, using the Structure Factor Size Estimator (SFSE), to analyze experimental results obtained from three different wideband

focused transducers covering the bandwidth from 9 to 30 MHz. Two parameters that describe the structure of aggregated RBCs were extracted from the 2nd order Taylor expansion of the structure factor. The first parameter *W* translates acoustically into variations of the *BSC*, whereas *D* reflects reductions of SS from its Rayleigh value of 4.

The theoretical framework behind modeling of the structure factor is first described in section 3.4. Section 3.5 explains the experimental setup followed by section 3.6 that gives results on the kinetics of 6% and 40% hematocrit aggregating RBCs, sheared in a Couette flow at residual shear (RS) rates of 0, 2, 10 and 30 s^{-1}. For the static residual shear rate (RS0) at 6% hematocrit, results are compared to aggregate sizes estimated by optical microscopic image segmentation. The validation of the method is discussed in section 3.7.

3.4 Theory : the structure factor size estimator

Suspended RBCs in a saline solution (no aggregation) can be acoustically considered as a dense collection of partially correlated weak scatterers embedded in a homogeneous medium [120]. Using the Born approximation, the backscattered power is given for Rayleigh scatterers (*ka* << 1) by [156]:

$$BSC(k) = m\sigma_b(k)W\,, \tag{3.1}$$

where *m* is the number density of scatterers, σ_b is the backscattering cross section of a single RBC, *W* is the packing factor and *k* is the wave vector. For suspended RBCs in saline, all parameters in Eq. 3.1 can be determined analytically. When the hematocrit is known by micro centrifugation, *m* is given by $m = H/V_s$, where V_s is the volume of a RBC

(typically 87 μm^3). The backscattering cross-section σ_b of a Rayleigh scatterer can be estimated by [89]:

$$\sigma_b(k) = \frac{1}{4\pi^2} V_s^2 \gamma_Z^{\,2} k^4 \left(3 \frac{\sin(2ka) - 2ka\cos(2ka)}{(2ka)^3} \right)^2 , \qquad (3.2)$$

where γ_Z is the acoustical relative impedance mismatch between the RBC and its suspending medium, hence $\gamma_Z = \frac{Z_{RBC} - Z_{Plasma}}{Z_{Plasma}}$ (see Tab. 3-1).

	ρ (kg.m^{-3})	κ (Pa^{-1})	Z (kg.m^{-2}.s^{-1})
RBC	1078	3.50×10^{-10}	1.755×10^6
Plasma	1021	4.09×10^{-10}	1.580×10^6
Relative impedance contrast γ_Z	-	-	0.11

Tab. 3-1: Some physical properties of blood at 23 ± 1 °C [191]. The density is noted ρ, the adiabatic compressibility κ and the acoustic impedance *Z*.

The packing factor *W* has been extensively studied for non aggregating scatterers [169;170]. It was shown to reflect the decrease in backscattered power with the increase in spatial correlation among particles with increasing particle crowding. *W* can be seen as a correction factor that accounts for increasing destructive phase interference (coherent field) introduced by the increase in correlation between particles. The detailed development of this approach can be found in Twersky's paper [170]. In the same manuscript, expressions of the Perkus Yevick packing factor W_{PY} (hard particles) were

proposed for packed spheres (W_{PYs}) and cylinders (W_{PYc}). They are functions of the hematocrit *H*.

$$W_{PYs}(H) = \frac{(1-H)^4}{(1+2H)^2} \quad (3.3) \qquad W_{PYc}(H) = \frac{(1-H)^3}{(1+H)} \quad (3.4)$$

The cylinder prototype (Eq. 3.4) provided the best fitting with experimental measurements for suspended RBCs up to physiological hematocrits under Rayleigh conditions [156]. However, this Rayleigh theoretical approach cannot be used when aggregating RBCs is considered and non-Rayleigh scattering occurs. Looking at Eq. 3.1, one can consider different ways to model the power increase with RBC aggregation. The effect of aggregation can be considered by an increase in the effective scatterer cross-section (rouleaux formation) combined to a decrease in the number of scatterers at a constant hematocrit [166]. A comprehensive study of the effect of aggregation on *W* should then be pursued, as it would not be a simple function of *H.* A different approach [62-64;148] introduced the structure factor *S(-2k)* as an alternative way to model the backscatter power in the non–Rayleigh regime. These last models were based upon the generalized form of Eq. 3.1, also introduced in [170], namely:

$$BSC(k) = m\sigma_b(k)S(-2k). \quad (3.5)$$

With this formalism, the number density of scatterers *m* and the backscattering cross-section of a single red cell σ_b remain constant, and changes in backscattered power are entirely caused by variations of the structure factor *S(-2k)*, which is by definition the Fourier transform of the pair correlation function *g(r)* [170]:

$$S(-2k) = 1 + m\int (g(r)-1)e^{-j2kr}dr\,. \quad (3.6)$$

In this expression, *g(r)* represents the probability of finding two particles separated by a distance *r* (see Figs 9 and 10 of [64] for a visual interpretation of this parameter). This

formula shows that a variation in the microscopic organization of particles, and thus of *g(r)*, modifies *S*(-2*k*) and therefore also the *BSC*. It is proper to emphasize here that the low frequency limit of *S*(-2*k*) is by definition [170] the packing factor *W*:

$$S(-2k)\big|_{k\to 0} = 1 + m\int (g(r)-1)dr = W \,. \tag{3.7}$$

Under Rayleigh conditions (non aggregated RBCs), Eq. 3.5 therefore directly reduces to Eq. 3.1 .

A 2nd order Taylor approximation of *S*(-2*k*) is proposed here to extract two geometrical parameters from the RF frequency dependent backscattered *US* data. The 2nd order Taylor expansion in *k* of *S*(-2*k*) is of the form :

$$S(-2k) \approx C_0 + (-2k)C_1 + (-2k)^2 C_2 \,, \tag{3.8}$$

where C_0, C_1 and C_2 are simply the series coefficients. We have shown earlier that $C_0 = S(-2k)\big|_{k=0}$ is the packing factor *W* (see eq. 3.7). The second constant C_1 is necessarily equal to zero because of parity (i.e., if the blood sample is turned around 180 degrees, the tissue remains the same). Since *S*(-2*k*) is a non dimensional number, the third constant C_2 must be a surface in m^2. This inference is well known in crystallography, using small angle neutron, light, and X-ray scattering to determine polymer and protein radius of gyration. C_2 is negative and $-C_2$ is related to the square of the radius of gyration (R_g) of scatterers. This 2nd order approximation is valid in the Guinier region [81], named after the pioneering work of that scientist in X-rays scattering and is discussed in paragraph 3.7. In the current paper, we consider that $C_2 = -R_g^2$, hence

$$S(-2k) \approx W - 4R_g{}^2 k^2 \,. \tag{3.9}$$

For identical spherical scatterers of radius *a* (i.e, individual RBCs), and recombining Eqs 3.2, 3.5 and 3.9, we find that:

$$BSC(k) = \frac{1}{3\pi} H\gamma_Z{}^2 k^4 a^3 \left(3\frac{\sin(2ka) - 2ka\cos(2ka)}{(2ka)^3} \right)^2 \times \left(W - 4R_g{}^2 k^2 \right) \qquad (3.10)$$

By replacing $k = \frac{2\pi f}{c}$, Eq. 3.10 becomes a polynomial approximation of the frequency dependence of the backscatter for aggregating RBCs, which can model the decrease in spectral slope observed experimentally in the non-Rayleigh regime. By considering an isotropic 3D aggregate of radius *R*, R_g is related to *R* by $R_g = \sqrt{\frac{3}{5}} R$ [81]. Hence, $D = \sqrt{\frac{5}{3}} R_g \Big/ a$, where *D* is the isotropic diameter of an aggregate (expressed in number of RBCs).

In the current study, the Structure Factor Size Estimator (SFSE) was used to achieve data reduction of experimental *BSC* measurements on aggregating RBCs. Estimated values of *W* and *D* were deduced from Eq. 3.10 by least mean squared polynomial fitting of the *BSC* as a function of frequency.

3.5 Materials and Methods

3.5.1 Blood preparation

Fresh porcine whole blood was obtained from a local slaughter house. It was anti-coagulated with 3 g/L of ethylene diamine tetra acetic acid (EDTA). The buffy coat was removed after centrifugation at $2000 \times g$ and four 60 mL samples were prepared as described in Tab. 3-2. These samples were introduced and sheared in a Couette flow system, as in [65;172], where *US* measurements were performed. All experiments were made at room temperature.

3.5.2 Ultrasonic setup and normalization algorithm for *BSC*

The use of focused transducers allow to overcome the limited signal to noise ratio consequent to increased attenuation in high frequency characterization of blood (>20 MHz), especially at physiological hematocrits. However, it was shown that with a focused transducer, the standard substitution method can yield erroneous *BSC* results [190].

Label	Hematocrit	Suspending medium
H6	6%	Isotonic saline
T6	6%	Porcine plasma
H40	40%	Isotonic saline
T40	40%	Porcine plasma

Tab. 3-2 : Labeling of the different types of blood samples studied.

One normalization technique with focused transducers was suggested using a low density 6% hematocrit RBC suspension, with the condition that the *BSC* of the reference suspension is known or can be determined [177]. Accordingly, the methodology that follows was utilized to first determine the 6% hematocrit reference BSC_{H6}, which was then used for assessing the backscattering coefficients of blood with the Couette flow apparatus.

Three broadband transducers were used in these experiments. Their general characteristics are summarized in Tab. 3-3. The pulse-echo acquisition system was

composed of an Avtech pulse generator (model AVB2-TA-C-CRIMA, Ottawa, CANADA), a Ritec diplexer (model RDX-6, Warwick, RI, USA), a 10 dB Mitec linear amplifier (model AU-A3-0120, Hauppauge, NY, USA), a Panametric pulser-receiver that was used as a wideband receiver (model 5900 PR, Waltham, MA, USA), and an 8 bits 500 MHz sampling frequency GageScope acquisition board (model 8500CS, Montreal, CANADA).

Type (manufacturer)	Center frequency (MHz)	-3 dB bandwidth (MHz)	Transducer radius (mm)	Focal length (mm)
V313-SM (Panametrics, MA, USA)	15	9 -14 [a)]	4.5	12
V317-SM (Panametrics, MA, USA)	20	15 – 26	4.5	12
PVDF (VisualSonics, Toronto, CANADA)	35	26 – 40 [b)]	1.5	6

Tab. 3-3 : Characteristics of each transducer used to collect RF *US* data. a) The 15 MHz transducer was excited at a lower frequency to cover a different frequency band than the 20 MHz transducer. b) For the 35 MHz transducer, according to the Guinier plot of Figure 3-11, only the data under 30 MHz was used.

The first step consisted in determining the BSC_{H6}. The H6 sample was stirred in a beaker with a magnetic agitator to avoid sedimentation. One hundred RF lines were acquired and stored; the procedure was repeated on a stainless steel plane reflector submerged in degassed water and positioned in the focal plane of each transducer to provide normalization data. A window of 1024 points in each line was selected in the focal zone of the transducer and Fourier transformed; the amplitude was squared to get the

power spectrum P of the backscattered signal. These data were then averaged over 100 acquisitions to provide $\overline{P_{H6B}}$ and $\overline{P_{plane}}$, where subscripts *B* and *plane* mean "beaker" and "planar reflector", respectively. The absolute backscatter BSC_{H6} of Rayleigh diffusers was measured by the substitution method with attenuation compensations, as suggested in [171]:

$$BSC_{H6} = \frac{\overline{P_{H6B}(f,F)}}{\overline{P_{plane}(f,F)}} \times \frac{R_p{}^2 k^2 r^2}{8\pi d\left[1+\left(\frac{kr^2}{4F}\right)^2\right]} \times e^{(4\alpha_{H6}d)} \ , \qquad (3.11)$$

where R_p, k, r, d, F and α_{H6} are, respectively, the reflection coefficient of the planar reflector (assumed to 1), the wave vector, the transducer radius, the inspected depth, the transducer focal length, and the H6 attenuation coefficient. This equation is valid in the focal zone of focused transducers for Rayleigh scatterers [171]. Such is the case for non aggregated RBCs in our setup in the frequency range 9-30 MHz [177]. Since this step was not performed with non focused transducers, the results for BSC_{H6} are presented in Figure 3-1a for validation.

Following the beaker and plane reflector measurements, each transducer was then successively placed in the Couette apparatus with its focal plane matching the center of the 2 mm gap between both concentric cylinders filled with blood. An agar gel was used to fill the hole that was made to position the transducer within the static cylinder; the solidified gel was cut to match the curvature of the cylinder in order to minimize any flow disturbance. The non-aggregating H6 sample was filled and gently sheared at 50 s^{-1} while acquiring 100 RF lines for each transducer. The shear rate was precisely controlled by the rotation speed of the moving Couette cylinder. The H6 data provided $\overline{P_{H6}}$ for the modified substitution method described below in Eq. 3.12. Following these measures, the H6 sample was removed and the Couette apparatus was washed with saline. H40 was

then introduced and rotated at the same shear rate of 50 s^{-1} in the Couette system. BSC_{H40} was computed also using Eq. 3.12 (with $\overline{P}_{Blood} = \overline{P}_{H40}$) to provide comparison data for non-aggregating conditions at 40% hematocrit. Then, T6 and T40 whole blood samples were successively introduced in the Couette apparatus.

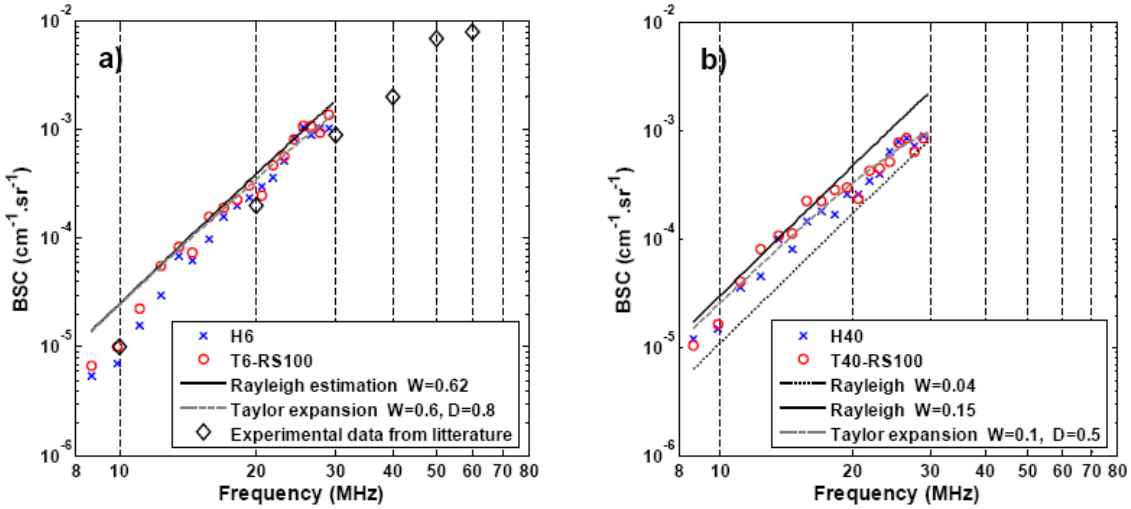

Figure 3-1 : a) Backscatter coefficient for H6 blood gently stirred in a beaker and T6 blood sheared at 100 s^{-1} in the Couette flow apparatus. The theoretical Rayleigh prediction (Eq. 3.1), the 2nd order Taylor model with $W = 0.6$ and $D = 0.8$ (Eq. 3.10), and H6 experimental data obtained by using non focused transducers [116;177] are also plotted. b) Backscatter coefficient for H40 blood sheared at 50 s^{-1} and T40 blood sheared at 100 s^{-1} in the Couette flow apparatus. The theoretical Rayleigh prediction with $W = 0.04$ and $W = 0.11$, and the 2nd order Taylor model with $W = 0.1$ and $D = 0.5$ are also plotted (see Table IV). Standard deviations are not shown for clarity.

For each aggregation kinetic experiment, the blood was first sheared at 100 s^{-1} for 2 minutes to disrupt RBC rouleaux. The shear rate was then changed to residual values of 0, 2, 10 and 30 s^{-1} for 3 minutes. During each experiment, 20 RF lines were acquired every

2 s for 190 s, starting 10 s before the application of the residual shear. At each time instant, a power spectrum was averaged over 20 RF lines to obtain $\overline{P}_{Blood}$ in Eq. 3.12. The *BSC* of H6, H40, T6 and T40 samples, sheared in Couette flow, was computed as:

$$BSC_{Blood} = BSC_{H6} \times \frac{\overline{P_{Blood}}}{\overline{P_{H6}}} \times e^{4d(\alpha_{Blood} - \alpha_{H6})}, \quad (3.12)$$

where BSC_{H6} is given by Eq. 3.11 and α_{Blood} is the attenuation coefficient of the investigated samples. Values of $\alpha_{H6} \approx \alpha_{T6}$ = 0.03 dB/cm/MHz [177], and $\alpha_{H40} \approx \alpha_{T40}$ = 0.22 dB/cm/MHz [79;80] were selected for all shear rates.

Finally, since suspended RBCs are Rayleigh scatterers in the range of frequencies considered here [116;177], theoretical values of BSC_{H6} and BSC_{H40} were also computed using Eqs 3.1, 3.2 and 3.4. This 2nd approach was used to confirm the experimental Couette flow measures of *BSC*. They are identified as "Rayleigh estimations" in Figure 3-1. Using the H6 sample as a reference in the Couette rather than the beaker insured that the focused beams were rigorously identical for both spectra in the modified substitution method, as well as providing automatic attenuation compensation for the agar gel.

3.5.3 Microscopy analysis of RBC aggregates and segmentation

Aggregation kinetics of whole blood at 6% hematocrit (T6 sample) under static conditions were also quantified using an optical method. Blood was shaken using a pipette by cyclic aspiration and a drop was deposited on a glass lamella. It was covered by a micro lamella for visualization. Images were taken at an optical magnification of 40X (1 pixel = 0.6 × 0.6 μm) at intervals of 15 s during 3 minutes. This procedure was repeated 3 times with the same blood sample. A H6 non aggregating suspension was also imaged for comparison. Grayscale images were processed offline to determine the size of each

aggregate. The same algorithm was used on all images. First, a segmentation threshold was determined using images normalized in intensity between [0, 1]. The threshold minimized the intra-class variance of the black and white pixels by using the Otsu method (Matlab function "Graythresh", version 7.0.1.24704, Natick, MA, USA). From the binary images obtained by thresholding, all elements smaller than 7 pixels in diameter were eliminated since they were smaller than a single RBC (a typical single RBC had a diameter of 12 pixels). The size of each cluster of aggregates was normalized by a 12 pixels diameter circular prototype to obtain the number of RBCs per aggregate. Following this pre-processing, the histogram of the number of RBCs per aggregate was traced and fitted to an exponential distribution of mean *b*, the mean number of RBCs per aggregate. Assuming isotropic 2D circular aggregates, as a first approximation, the surface occupied by *b* RBCs is given by π $(D_{OPT} / 2)^2$. An optical equivalent of parameter *D*, given above after Eq. 3.10, was thus given by :

$$D_{OPT} = \sqrt{\frac{4}{\pi} b} \ . \qquad (3.13)$$

3.6 Results

3.6.1 Ultrasonic characterization of RBC suspensions

Figure 3-1a shows *BSC* obtained with the three transducers on H6, the 6% hematocrit RBC suspension reference medium (Eq. 3.11). The *BSC* on T6 computed with Eq. 3.12 at 100 s^{-1} (T6-RS100, where RS means "residual shear") is also presented. The fitted Taylor model expansion (Eq. 3.10) and the theoretical Rayleigh estimation (Eq. 3.1) are also represented, along with experimental results from [116;177]. Figure 3-1b shows *BSC* obtained on H40, the 40% hematocrit RBC suspension, the theoretical Rayleigh *BSC*

with W = 0.04 and W = 0.11 (Eq. 3.4) and the Taylor model. Values of W obtained with the Taylor model for suspended non aggregating RBCs at 6% and 40% hematocrits are very close to the theoretical Perkus Yevick predictions (see Tab. 3-4). In addition, the estimated value of $D = 0.78 \pm 0.09$ for H6 is fairly close to the expected result of 1 RBC / aggregate, whereas the size estimation appears underestimated for H40 ($D = 0.5 \pm 0.1$).

	H6		H40	
	W	*D*	*W*	*D*
Experimental values	0.60 ± 0.03	0.78 ± 0.09	0.10 ± 0.01	0.5 ± 0.1
Theoretical W_{PYs}	0.62	-	0.04	-
Theoretical W_{PYc}	0.74	-	0.11	-
Theoretical D	-	1	-	1

Tab. 3-4 : Experimental and theoretical values of W and D for disaggregated RBCs suspended in an isotonic saline solution at 6% and 40% hematocrits. W_{PYs} and W_{PYc} were calculated using Eqs 3.3 and 3.4.

3.6.2 Kinetics of RBC aggregation

Figure 3-2 presents the mean *BSC* over the respective transducers' bandwidth (see Tab. 3-3) during the kinetics of rouleaux formation for (a) T6 and (b) T40 blood samples. At both studied hematocrits, the rouleaux formation kinetic profiles had similar shapes. For instance, at all frequencies, *BSC* first had a low value, when blood was sheared at 100 s^{-1}, which corresponds to the disaggregated state. *BSC* then gradually increased and stabilized

at different levels depending on the applied residual shear rates and on the *US* frequency. The highest *BSC* levels were achieved at a residual shear rate of 2 s^{-1} for all experiments (RS2 curves). As expected, higher shearing (RS10 and RS30) partially disrupted RBC aggregates and smaller *BSC* were thus obtained. Under static conditions (RS0) and for all transducers, the *BSC* reached an intermediate level near that of RS10. For T40, faster kinetics were observed in the first few seconds at increasing frequencies. Figure 3-3 shows the evolution of parameters *W* and *D* during the process of aggregate formation.

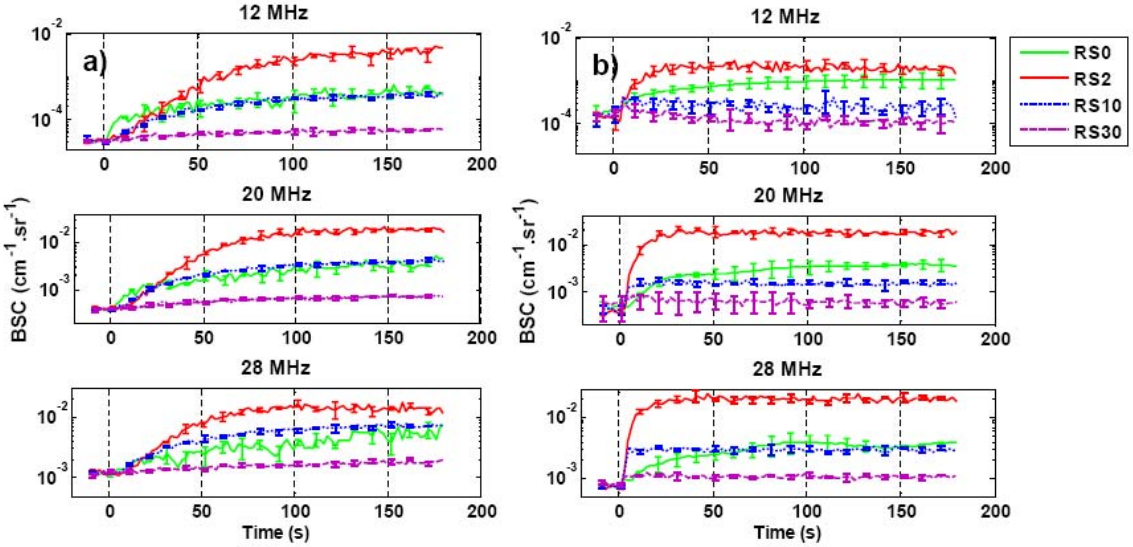

Figure 3-2 : *BSC* during the kinetics of rouleaux formation for (a) T6 and (b) T40 blood at different residual shear rates of 0, 2, 10 and 30 s^{-1}. A high shear rate of 100 s^{-1} was first applied during the first 10 s (before t = 0 s). *BSC* is taken as the mean value over the transducer bandwidth (see Tab. 3-3). Results are expressed as means ± one standard deviation over three experiments.

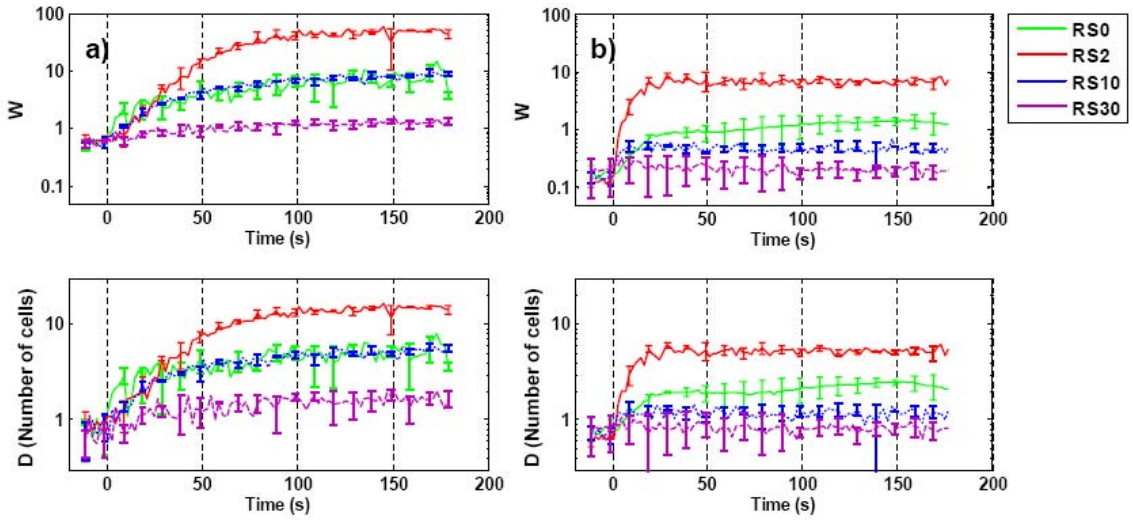

Figure 3-3 : Time variations of fitted parameters *W* and *D* during the kinetics of RBC aggregation for experiments with (a) T6 blood and (b) T40 blood at different residual shear rates (RS = 0, 2, 10 and 30 s^{-1}). A high shear of 100 s^{-1} was applied during the first 10 s of each acquisition. Results are expressed as means ± one standard deviation over three experiments.

As observed, *W* and *D* increased as a function of time for residual shear rates promoting RBC aggregation. The comparison of results at both hematocrits suggests that aggregates formed at 40% hematocrit are smaller in size than those obtained at 6% hematocrit, at each respective residual shear rate. Mean values at the plateau of the kinetic curves for all applied shear rates are summarized in Tab. 3-5.

Residual	T6		T40	
shear rate	*W*	*D*	*W*	*D*
RS0	6.8 ± 2.4	4.9 ± 1.4	1.4 ± 0.1	2.4 ± 0.1
RS2	48.9 ± 5.7	15.0 ± 1.0	6.8 ± 1.1	5.3 ± 0.6
RS10	8.4 ± 0.7	5.3 ± 0.4	0.5 ± 0.1	1.1 ± 0.1
RS30	1.3 ± 0.2	1.6 ± 0.3	0.2 ± 0.1	0.7 ± 0.1
RS100	0.60 ± 0.09	0.87 ± 0.27	0.2 ± 0.03	0.8 ± 0.1

Tab. 3-5 : T6 and T40 blood fitting parameters *W* and *D* at different residual shear rates (averaged values were computed between *t* = 170 s and 180 s). RS100 data were averaged between *t* = 0 s and 10 s. Results are expressed as means $\pm$ one standard deviation over three experiments.

3.6.3 Frequency dependence of the *BSC*

Figure 3-4 shows *BSC* as a function of frequency for different residual shear rates and at the plateau of the kinetics of aggregation (temporal means between *t* = 170 s and *t* = 180 s). Standard deviations are not shown for clarity. It can be observed that *BSC* increases with the level of aggregation promoted by different residual shears. The *BSC* is Rayleigh at low frequencies and high shear rates, and becomes non Rayleigh (drop in SS) with decreasing RS. Also represented on this figure are fitted curves based on the Taylor model. Respective values of *W* and *D* were reported earlier in Tab. 3-5.

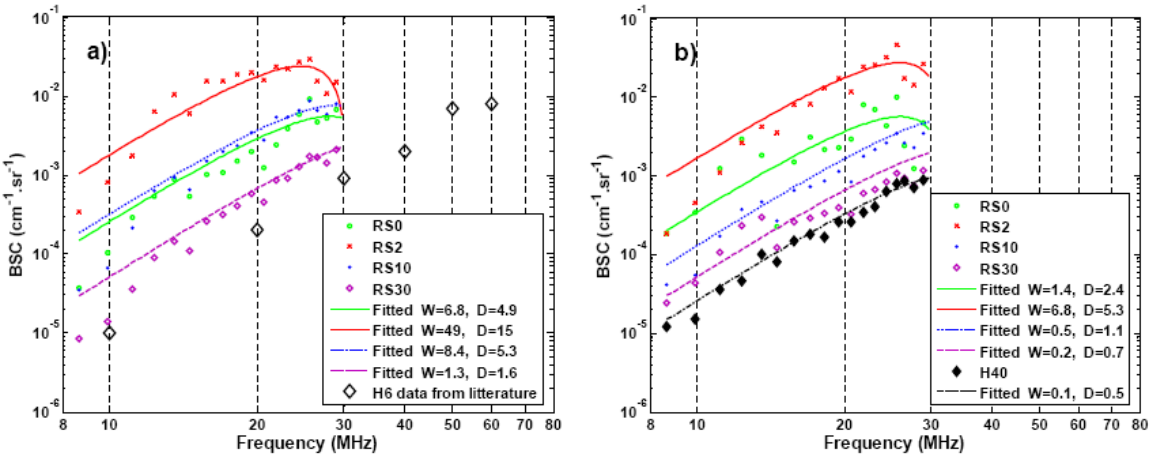

Figure 3-4 : Frequency dependencies of (a) T6 and (b) T40 blood samples sheared at different residual shear rates (RS = 0, 2, 10 and 30 s^{-1}), and corresponding fitted models. H6 experimental data taken from [116;177] are also displayed. The standard deviations are not shown for clarity.

3.6.4 Comparison of *US* and optical methods

The *US* data obtained under static conditions (RS0) are compared in this section with microscopic images acquired at the same hematocrit of 6%. Images were taken with a time resolution of 15 s during 3 minutes. The first row of Figure 3-5 shows typical microscopic images during the aggregation kinetics promoted by Brownian motion. The actual treated images were bigger, only the central 300×400 pixels of the whole 960×1280 pixels are shown on this figure.

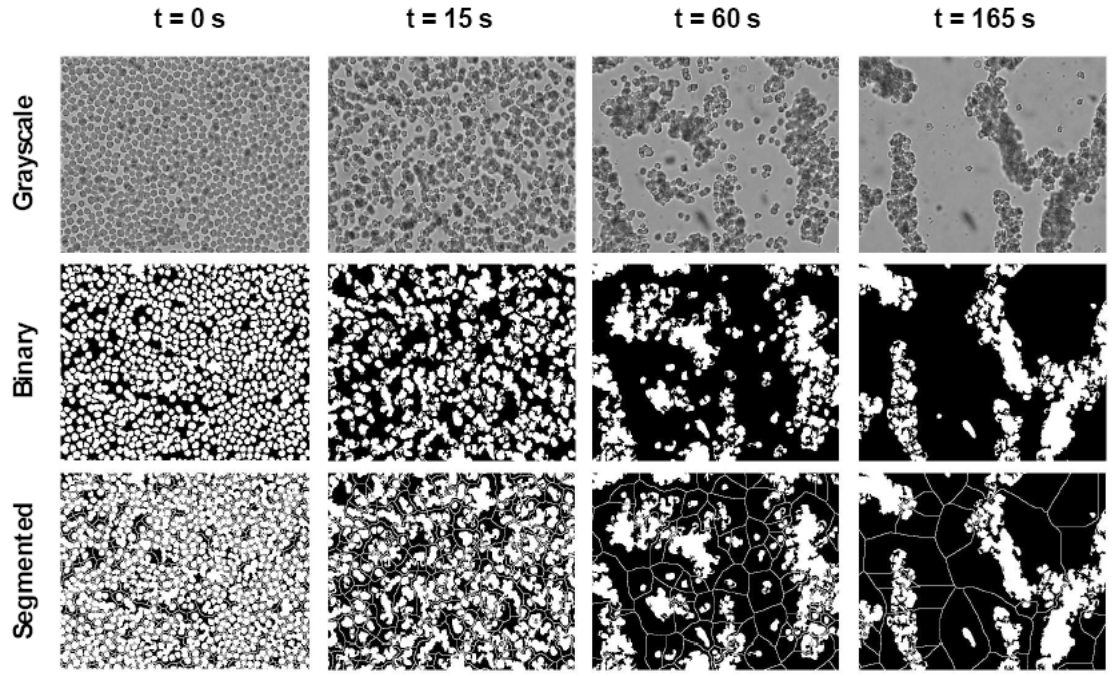

Figure 3-5 : In columns are represented typical microscopic images and image processing at a particular time during the kinetics of aggregation of a T6 sample. In rows are represented grayscale images, binary images and segmented images. Actual processed images (960×1280 pixels) were bigger than those represented here (300×400 pixels). Resolution is 1 pixel = $0.6\ \mu m \times 0.6\ \mu m$.

Binary thresholded images are presented in the second row. Segmented objects are given in the third row. Histograms of the number of RBCs per aggregate, arbitrarily partitioned in 15 logarithmically spaced bins, are displayed in Figure 3-6.

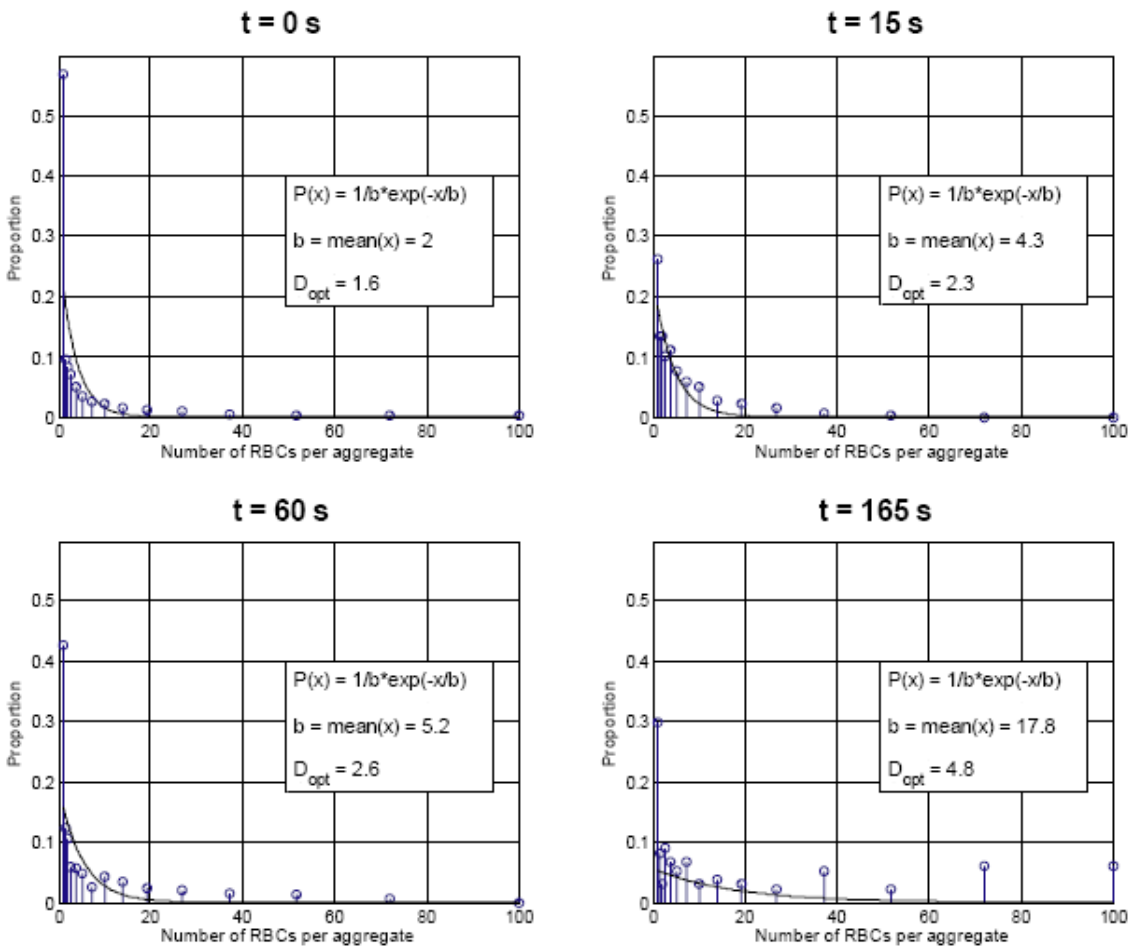

Figure 3-6 : Histograms of the aggregate dimension in number of cells at time 0, 15, 60 and 165 s. Cell count was arbitrarily separated in 15 logarithmically spaced bins to allow better resolution for small sizes. The distributions were fitted by an exponential function of mean *b* defined by $P(x) = \frac{1}{b}\exp^{(-\frac{x}{b})}$. D_{opt} was determined using Eq. 3.13.

Each distribution was fitted to an exponential function defined by $P(x) = \frac{1}{b}e^{\left(-\frac{x}{b}\right)}$, where *b* = mean(*x*) and *x* is the number of RBCs per aggregate. Parameter *b* is thus an

estimation of the mean number of RBCs per 2D aggregate. D_{OPT} was computed using Eq. 3.13. Optical and acoustical estimations of *D* are compared in Tab. 3-6.

Time (s)	0	30	60	90	120	150	180
D_{OPT}	1.5 ± 0.3	2.4 ± 0.3	3.1 ± 0.5	3.5 ± 0.4	4.2 ± 0.2	4.5 ± 0.1	4.7 ± 0.1
D_{US}	0.8 ± 0.1	3.9 ± 0.1	3.8 ± 0.6	5.3 ± 0.4	4.9 ± 1.0	4.8 ± 1.0	6.2 ± 1.1

Tab. 3-6: Estimations of *D* with the optical and ultrasonic methods. Microscopic images were acquired with a time resolution of 15 s. A time resolution of 30 s was used here to reduce the size of the table. *US* data taken from Figure 3-3 (RS0, *H* = 6%) at corresponding time were used for comparison.

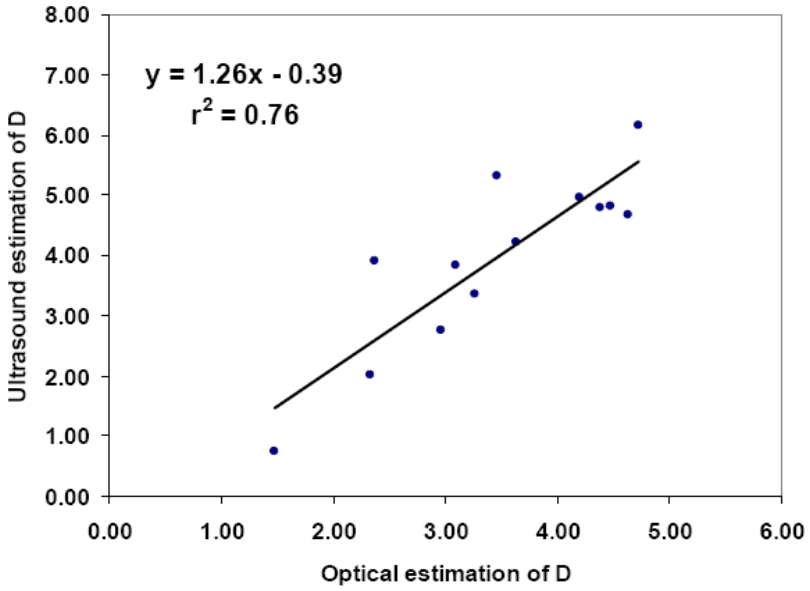

Figure 3-7 : Comparison of *D* estimated with the optical and *US* methods. Each point is the mean over three experiments at a particular time during the kinetics of aggregation.

Both methods show an increase of the aggregate size with time under static condition. The linear regression of D_{OPT} with D_{US} (see Figure 3-7) resulted in an index of correlation $r^2 = 0.76$, reflecting that both methods followed the dimension of aggregates over time. In Figure 3-7, the optical method generally predicted lower values of *D*.

3.7 Discussion

3.7.1 On the quality of the data normalization

One concern when pursuing UTC is the quality and reliability of the normalization algorithm. A recent interlaboratory study [178] suggested that improvements in data normalization needed to be pursued, especially for *BSC* intensity measurements. However, that study also suggested that measurements of backscatter frequency dependent parameters, such as the spectral slope, were more consistent. We therefore tried, in the current study, to take advantage of *BSC* frequency dependent information, while emphasizing on the validation of the normalization procedure to achieve proper UTC.

First, we used three different transducers to obtain frequency dependent backscatter measurements. The continuity in frequency can be appreciated in Figure 3-1 and Figure 3-4. Second, values of *W* obtained with our model for suspended non aggregating RBCs at 6% and 40% hematocrits are very close to the theoretical Perkus Yevick predictions. The estimated value of $D = 0.78 \pm 0.09$ for H6 is also fairly close to the expected number of 1 RBC / aggregate, whereas the size estimation seems slightly underestimated for H40 ($D = 0.5 \pm 0.1$, see Tab. 3-6). Lastly, as another validation step, one can note that the increases in *BSC* reported in this study as a function of the level of aggregation are comparable with published data from the literature. For instance, Yuan

and Shung [192] reported aggregating pig blood backscattered power as a function of frequency at mean shear rates of 2, 10 and 22 s^{-1} using 5 unfocused transducers from 3.5 to 12.5 MHz. Hematocrits of 4.5%, 25% and 45% were investigated in that study. The limitation of the Rayleigh scattering theory could be clearly observed as the spectral slope decreased for strongly aggregating RBCs at 10 MHz and higher, as it can be noted with our data (Figure 3-4). Our low hematocrit data (Figure 3-4a) are also in agreement with those shown in Figure 4 of [192]. In that same study, an increase of 11.5 dB at 12.5 MHz was reported when the shear rate was decreased from 22 s^{-1} to 2 s^{-1} at 45% hematocrit. Our data (T40-RS2 – Figure 3-2b) suggests an increase of 12 dB from 30 s^{-1} to 2 s^{-1} at 12 MHz. In addition, a 13 dB increase at 30 MHz was measured between low and high shearing conditions for whole blood at physiological hematocrits in [172] and [65]. Our data (T40-RS2 – Figure 3-2b) at 28 MHz shows a 14 dB increase with shear rate variations from 100 s^{-1} to 2 s^{-1}. It must be noted, nevertheless, that the former results were obtained on human blood rather that porcine blood. Other experimental studies have also found similar relative increases of the *BSC* with aggregation [42;144;188]. All these results tend to demonstrate the validity of Eq. 3.11 (normalization with BSC_{H6}) and of Eq. 3.12 that were used to obtain BSC_{T6}, BSC_{H40} and BSC_{T40}.

3.7.2 *BSC* rate of increase during RBC aggregation kinetics

As observed in Figure 3-2, the *BSC* increase in the first few seconds following flow reduction was faster as the frequency was increased; this is especially evident for a hematocrit of 40% and for residual shear rates promoting the largest aggregates. These results confirm previous observations at 40% hematocrit [39] where the rate of increase of the backscattered power as a function of time following flow stoppage was significantly faster at 58 and 36 MHz than at 10 MHz. It was postulated in that study that increasing the ultrasound frequency improved the sensitivity of the method to rapid changes in RBC aggregate sizes. When comparing in Figure 3-2 results at 6% and 40% hematocrits, the

more rapid increase of *BSC* at the highest hematocrit is not surprising if one considers that the probability of two RBCs to be in proximity is higher at 40% hematocrit.

3.7.3 Frequency dependent data and 2nd order Taylor model

The SFSE can be seen as an implementation of form factors used in other tissue characterization fields [159], adapted to the problem of RBC aggregation. In that sense, it takes into consideration the structure of the tissue rather than the shape of a single scatterer. $S(-2k) = W - 4 R_g^2 k^2$ is a decreasing function of k from W to minus infinity.

The parallel is straightforward when illustrated with scarce scatterer concentration: in this case, W is equal to 1 and using $R_g = \sqrt{\frac{3}{5}}R$, then $S(-2k) = 1 - \frac{12}{5}R^2k^2$. With non aggregated RBCs and for f < 30 MHz (ka < 0.33), $S(-2k)$ behaves similarly to the spherical Gaussian and to the exponential form factor, as shown in Figure 3-8 (The notation R is used in this study but the notation a_{eff} is often found in the literature).

The structure factor is a decreasing function in ka that translates a variation in scatterer organization but that can have a low frequency limit W different from unity. As Gaussian, fluid sphere or spherical shell form factors describe the amplitude of the backscattered intensity due to a single scatterer as a function of the frequency, the structure factor describes the effect of aggregation on the backscattered intensity of increasingly organized weak scatterers. The main advantage is that the SFSE can be applied to dense media where the scatterers' positions are partially correlated. If scatterers in the tissue are independently positioned, W = 1 and the SFSE is very similar to a form factor.

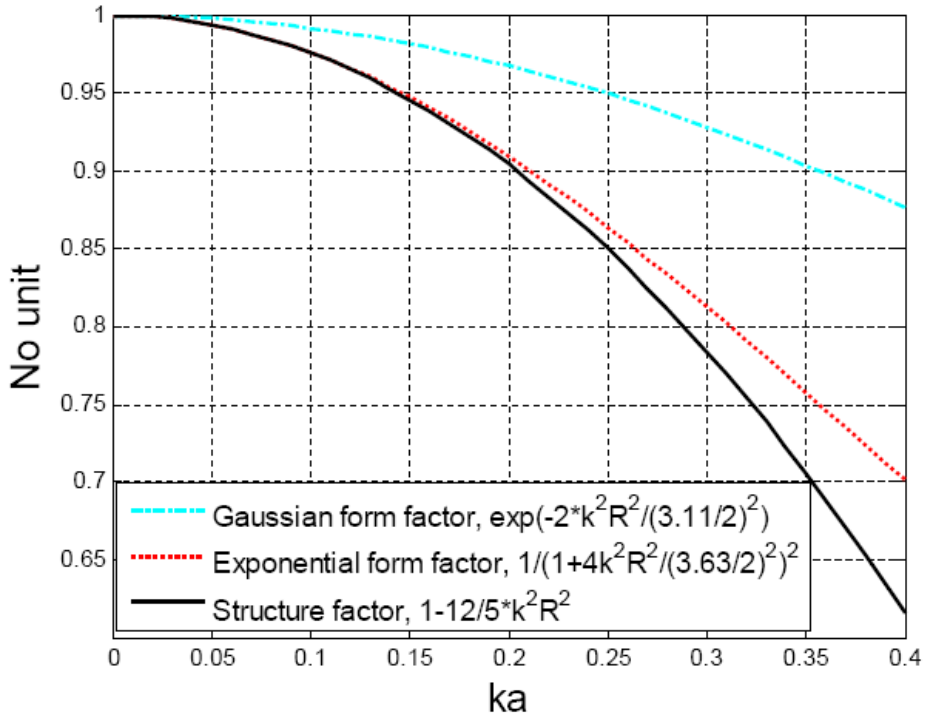

Figure 3-8 : Spherical Gaussian form factor, exponential form factor and the second order Taylor expansion of the structure factor as a function of *ka*, for diluted scatterers (*W* = 1). R, the effective radius of the scatterer, is often noted a_{eff} in the litterature.

One might wonder why we limited our model to a 2nd order Taylor expansion in Eq. 3.10. If it is mathematically true that a higher polynomial order would provide a better fitting with the experimental data, we found that the physical pertinence of the model was lost when a higher order was used. For instance, the 2nd order model allowed the estimation of *W* and *D*, which have a physical meaning.

Also, one might question the physical meaning of $W > 1$. In fact, Eqs. 3.3 and 3.4 are function of *H* and are strictly limited to $0 < W \leq 1$. It is important to emphasize that the above equations were derived for non aggregating particles. Moreover, our results for non

aggregated RBCs were consistent with these equations. As mentioned earlier, the packing factor *W* can be generalized for aggregating particles as the low frequency limit of the structure factor. This concept has been used earlier in the field of colloidal suspensions. The Baxter sticky hard sphere model was used to describe the effect of aggregation within the Perkus Yevick approximation of the structure factor and its low frequency limit *W* [140]. The adhesive sphere model predicts values of *W* that decrease from 1 to 0 with increasing hematocrits for low adhesion energy, but presents values of $W > 1$ when the adhesion energy is increased. Values of *W* up to 50 were reported at a volumic fraction of 12%. The structure factor at a frequency of 0 Hz (i.e., $S(0) = W$) is thermodynamically described in this model as $W = mK_bT\xi_T$ with K_b being the Boltzmann's constant, *T* the absolute temperature and ξ_T the isothermal compressibility, as in Twersky's work [170]. It is also interesting to remark that an increase of *W* with aggregation is also consistent with an increase in variability of the number of scatterers per elemental scattering voxel, as it was suggested in [119].

3.7.4 Validation

There is no known way to the authors to experimentally characterize the real size of three-dimensional RBC aggregates at a physiological hematocrit and hence to validate the dimensions reported here. For instance, microscopic observations can only be done with diluted blood; this is why we limited the optical validation to a hematocrit of 6%. Although the correlation between the *US* and optical methods was good ($r^2 = 0.76$), it is clear that the comparison has limitations. We can consider the 2D nature of the wet mounts for microscopy versus the 3D structure of real aggregates sensed with US, the isotropic nature of the estimators versus the anisotropic shape of real rouleaux networks, and the limitation of the optical method that only considered a static condition. However, some quantitative information could be deduced with our 2nd order model. The estimated parameters *W* and *D* were modulated in a predictable manner by the applied residual

shear rate: higher shear rates produced smaller values of those measures due to the reversible disruption of RBC clusters. The fact that aggregates were smaller under static conditions is not surprising. Others have reported that a minimal level of shear is necessary to promote aggregation, as it increases RBC interactions [136;150;154]. Further increasing the shear rate results in the breaking of rouleaux. Furthermore, our model showed smaller values of *W* and *D* at 40% versus 6% hematocrit. This observation was made earlier in [162], where the radius of gyration of concentrated cluster suspensions was studied. Stronger aggregate interpenetrations at high hematocrit were hypothesized in that study to explain this observation. Another group reported size estimations from computerized image analysis of RBC aggregates in a small flow chamber [34]. With a diluted 10% hematocrit blood, they measured aggregates of about 6-12 RBCs / aggregate at stasis (~ 0 dyne/cm^2) and of about 24-48 RBCs / aggregate at a low shear stress of ~ 0.1 dyne/cm^2 (corresponding to a shear rate of 10 s^{-1} considering plasma as a Newtonian fluid of viscosity = 1 cP).

3.7.5 Respective effect of *W* and *D* on the 2nd order Taylor model - relation $(D)^2$- *W*

To help interpreting the acoustical meaning of *W* and *D* and the relation between these two physical parameters, we first present in Figure 3-9 for T6-RS100 the respective effect of varying *W* and *D* on the *BSC*; we arbitrarily selected a shear rate of 100 s^{-1}, the same interpretation applies to the other shear rates.

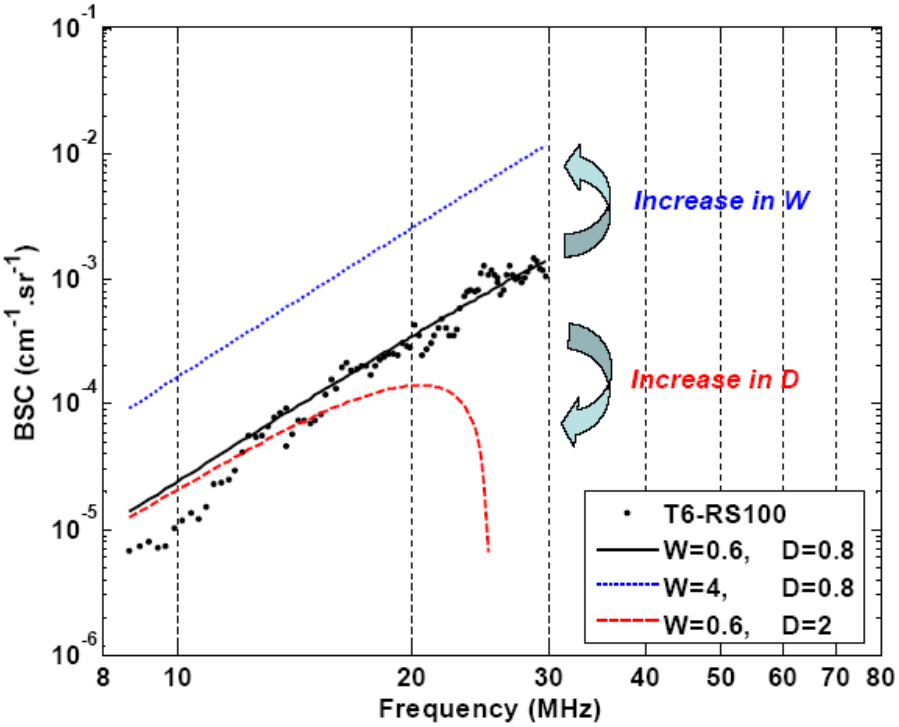

Figure 3-9 : Effect of increasing *W* and *D* on the *BSC* in the 2nd order model.

An increase in *W* has the effect of increasing the amplitude of the *BSC* at all frequencies. In terms of standard UTC measures, it can be seen as an analogue to the mean *BSC* [107]. Increasing *D* has an effect on the frequency dependence and it thus modulates the spectral slope SS.

Another interesting aspect of parameters *W* and *D*, apart from their physical interpretability ("packing factor" and "normalized mean aggregate size") is the fact that they are not independent from one another. In Figure 3-10 are plotted *W* as a function of $(D)^2$ for all blood samples during the entire kinetics of aggregation for 6% and 40% hematocrits and for all applied shear rates.

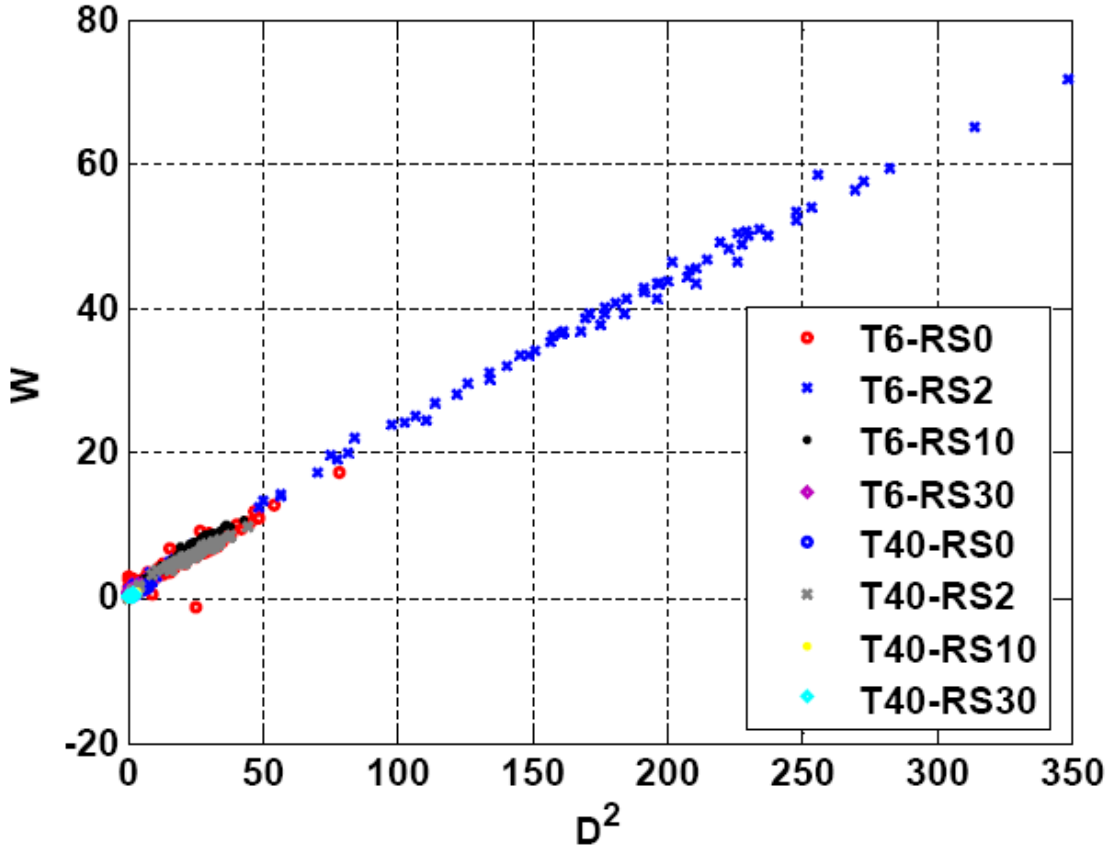

Figure 3-10 : Quadratic relationship between *D* and *W* for all shear rates at both 6% and 40% whole blood hematocrits. The high frequency limit was fixed to 30 MHz.

It can be clearly observed that a quadratic relation exists between *W* and *D*. Although this observation could have led us to eliminate one parameter in our data reduction model, we chose not to, as *D* brings a physical dimension and *W* is a parameter largely studied in UBC. The fact that the 40% hematocrit scales in the same way as the 6% hematocrit brings further confidence in the 2^{nd} order approximation model. The relation between both parameters should be further investigated in future studies.

3.7.6 Guinier plot

One convenient way to determine the higher frequency limit of our 2nd order approximation is to use the Guinier plot. This plot is frequently used in X-ray, neutron and light scattering characterization. It consists in plotting $k^2 \rightarrow \log S(-2k)$. Since we are dealing with a 2nd order model, the quadratic approximation is valid when the slope is linear and is called the Guinier region. In Figure 3-11 are plotted Guinier results for T6 and T40 blood samples at a residual shear of 2 s^{-1}.

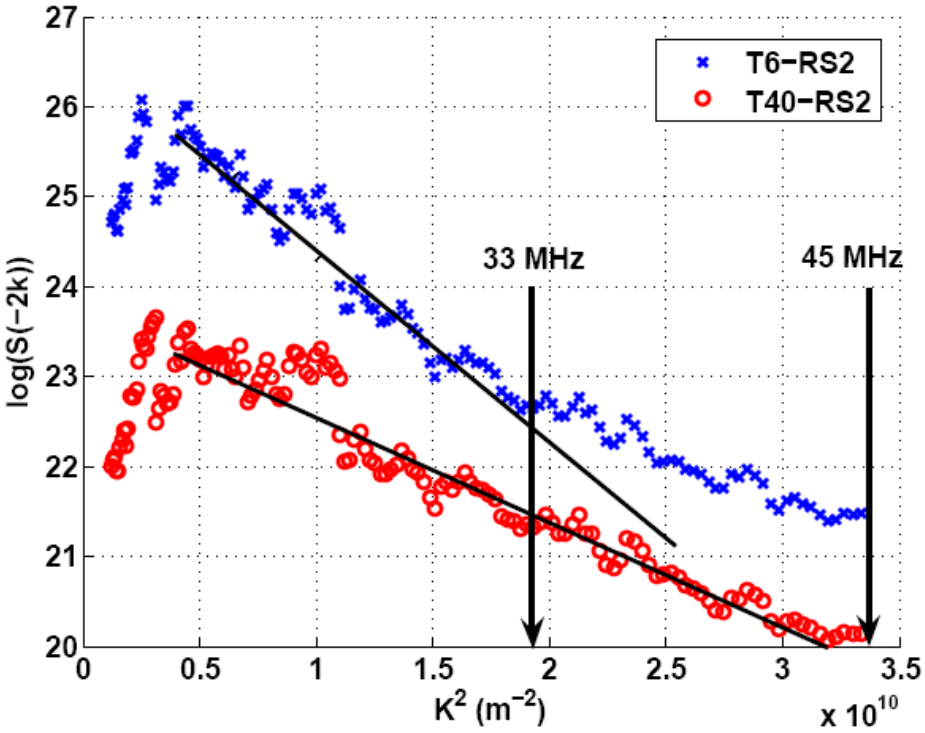

Figure 3-11 : Guinier plots extended to 45 MHz for T6-RS2 and T40-RS2. The linear slope transition indicates the limit of the Guinier domain.

The frequency correspondence of the abscissa is indicated by arrows on the figure. Very interesting information can be deduced from Figure 3-11. First, the T6-RS2 Guinier plot

diverges from a linear slope at frequencies higher than 33 MHz. This observation signifies that the 2nd order approximation is no longer valid for big aggregates at frequencies above 33 MHz. For this reason, we limited our 2nd order approximation to 30 MHz (see the Method section). The same cannot be said about the Guinier plot of T40-RS2 that was still linear through 45 MHz. This observation also supports the preceding observation that aggregates formed at 40% hematocrit were smaller that those at 6% hematocrit, for any given residual shear rate.

3.8 Conclusion

Experimental and theoretical results on *BSC* variations during the kinetics of RBC aggregation determined by modulating the shear rate in a Couette flow apparatus were presented. Different samples of whole blood and RBC suspensions at 6% and 40% hematocrits were prepared and quantitatively characterized at room temperature using three focused wideband transducers covering the bandwidth from 9 to 30 MHz. A 2nd order Taylor approximation of the structure factor, the SFSE, was proposed to achieve data reduction of the *BSC* measurements, to extract two physical parameters, namely the packing factor (*W*) and the mean normalized dimension of isotropic aggregates (*D*). The *D* parameter was validated by an optical imaging method at 6% hematocrit under static conditions. The SFSE presents an interesting framework for ultrasonic characterization of partially correlated tissues, such as aggregating blood. For instance, it more closely mimics the frequency dependence of *BSC* and it is physically interpretable in a non frequency dependent manner.

3.9 Acknowledgments

This work was supported by grant #MOP-36467 from the Canadian Institutes of Health Research. The salary of Mr. F.T.H. Yu is partially supported by a Ph.D. studentship from the Natural Sciences and Engineering Research Council of Canada, and Dr. G. Cloutier is recipient of the National Scientist Award from the 'Fonds de la Recherche en Santé du Québec'. We are also thankful to Mr. G. Leblond for his help in the segmentation of the microscopic images, and 'Les Viandes ULTRA Meats Inc.', Saint-Esprit, Québec, Canada for blood supply.

4 Chapitre 4 : Extension de la méthode en 2D: images paramétriques de *W* et *D* et extrapolation de la viscosité locale

4.1 Avant-propos

Ce chapitre est constitué par l'article « *Ultrasonic parametric imaging of erythrocyte aggregation using the structure factor size estimator* » publié au journal « *Biorheology* »[9]. Cet article étend la validation du SFSE en 2D avec une seule sonde ultrasonore large bande. Les paramètres ultrasonores sont ensuite utilisés pour extrapoler des cartes de viscosité locale dans un écoulement tubulaire. Différents types de sang sont étudiés dont deux échantillons traités avec des revêtements de polymères membranaires (Pluronics F68 et F98). Ces polymères permettent de moduler l'agrégation érythrocytaire en variant la concentration et la longueur de la chaine polymérique : le F98 induit une forte agrégation alors que F68 est un contrôle. Ce type de traitement est particulièrement intéressant car il est applicable *in vivo* par transfusion car ne modifie pas la phase plasmatique contrairement au Dextran qui augmente la viscosité plasmatique. Ces traitements sont hautement novateurs mais leurs effets sur la rétrodiffusion ultrasonore n'ont jamais été étudiés. Cette étude *in vitro* a plusieurs objectifs : (1) la démonstration que le SFSE permet la caractérisation de plusieurs types de sang ayant des tendances

[9] *Reprinted from Biorheology, Yu F.T.H. et al., Ultrasonic parametric imaging of erythrocyte aggregation using the structure factor size estimator, 46(4), pp.434-464, Copyright 2009, with permission from IOS Press.*

d'agrégation différentes (incluant deux échantillons traités aux Pluronics) dans un écoulement de cisaillement homogène; (2) la comparaison des indices *W* et *D* préalablement déterminés avec ceux obtenus dans un écoulement tubulaire plus réaliste; (3) l'extrapolation de cartes de viscosité locale à partir des relations entre le niveau d'agrégation et la viscosité établies par des mesures de viscosite globales (« *bulk viscosity* »).

Ultrasonic parametric imaging of erythrocyte aggregation using the Structure Factor Size Estimator*

François T.H. Yu[a], Émilie Franceschini[a], Boris Chayer[a], Jonathan K. Armstrong[b], Herbert J. Meiselman[b] and Guy Cloutier[a,c**]

[a] *Laboratory of Biorheology and Medical Ultrasonics, Centre de Recherche, Centre Hospitalier de l'Université de Montréal* (*CRCHUM*)*, Montréal, Québec, Canada.*

[b] *Department of Physiology and Biophysics, Keck School of Medicine, University of Southern California, Los Angeles, California, USA.*

[c] *Department of Radiology, Radio-Oncology and Nuclear Medicine and Institute of Biomedical Engineering, Université de Montréal, Montréal, Québec, Canada.*

Running Title: Ultrasound imaging of erythrocyte aggregation.

Keywords: ultrasound backscattering coefficient, ultrasound tissue characterization, packing factor, Born approximation, non-Rayleigh scattering, hemorheology, local viscosity.

---

* This article is based on a paper given by Dr. Guy Cloutier in Symposium 31 at the 13th International Congress of Biorheology and 6th International Conference on Clinical Hemorheology, Penn State University, PA, USA, July 9–14, 2008.

**Address for correspondence: Guy Cloutier, Director LBUM-CRCHUM, 2099 Alexandre de Sève, Pavilion J.A. de Sève (room Y-1619), Montréal, Québec, Canada, H2L 2W5. Tel: +1 514 890-8000 (24703); Fax: +1 514 412-7505; Web: http://lbum-crchum.com;

4.2 Abstract

Ultrasound characterization of erythrocyte aggregation (EA) is attractive because it is a non-invasive imaging modality that can be applied *in vivo* and *in situ*. An experimental validation of the Structure Factor Size Estimator (SFSE), a non-Rayleigh scattering model adapted for dense suspensions, was performed on 4 erythrocyte preparations with different aggregation tendencies. Erythrocyte preparations were circulated in Couette and tube flows while acoustically imaged over a bandwidth of 9-28 MHz. Two acoustically derived parameters, the packing factor (*W*) and ensemble averaged aggregate size (*D*), predictably increased with increasing EA, a finding corroborated by bulk viscosity measurements. In tube flow, a "black hole" reflecting the absence of aggregates was observed in the center stream of some parametric images. The SFSE clearly allowed quantifying the EA spatial distribution with larger aggregates closer to the tube walls as the aggregation tendency was increased. In Couette flow, *W* and *D* were uniformly distributed across the shear field. Assuming that the viscosity increase at low shear is mainly determined by EA, viscosity maps were computed in tube flow. Interestingly, erythrocyte suspensions with high aggregabilities resulted in homogeneous viscosity distributions, whereas a "normal" aggregability promoted the formation of concentric rings with varying viscosities.

4.3 Introduction

Blood is a shear thinning non-Newtonian fluid: in steady state, the viscosity increase at low shear is predominantly caused by reversible erythrocyte aggregation (EA) [36]. The level of EA is dependent on the erythrocyte aggregability [139], on the concentration of aggregation-inducing macromolecules in plasma (primarily fibrinogen but

also immunoglobulins and other inflammatory proteins) and on mechanical shearing forces [9;37]. Indices of aggregation can be measured *in vitro* on samples obtained by venipuncture using different techniques - including viscosimetry, erythrocyte sedimentation rate, electrical impedance, light and ultrasound scattering [164]. In humans, increased bulk blood viscosity and aggregation measured *in vitro* correlate with numerous cardiovascular diseases and complications including diabetes [94;113], deep venous thrombosis and its recurrence [38;99], and ischemic heart events [112;186]. The fact that these diseases and their complications generally occur in specific locations of the vascular system suggest a pathological micro- and/or macro-circulatory hemodynamic contribution to their etiologies.

Analytical [59;137;142] and numerical [11;90;194] models have been proposed to interpret the rheological behavior of blood. However, the complexity of blood's time dependent non-Newtonian behavior and the computational loads required for transposing numerical models to real vascular and erythrocyte geometries remain important challenges for these approaches. Ultrasound (*US*) imaging, which utilizes non-invasive pressure wave propagation through biological tissues, is a tool that has the potential to measure EA for both *in vivo* and *in situ* flow conditions. This imaging modality could significantly contribute to hemorheology especially at high *US* frequencies, since it allows characterization of EA in space and in time, as demonstrated by its sensitivity to measure aggregate formation kinetics [39;43] and its ability to follow cyclic aggregation and disaggregation states under pulsatile flows [48;125]. *In situ* quantification, etiological impacts and *in vivo* monitoring are potential applications of *US* EA characterization.

4.3.1 Ultrasound and EA

The increased B-mode blood echogenicity caused by EA during clinical scans, typically performed at 2-12 MHz, is well known [96;160]. The access to radio-frequency

(*RF*) data from laboratory instruments and, increasingly, from clinical scanners allows application of a normalization procedure [114;161;177] to obtain a backscattering coefficient (*BSC*), defined as the power backscattered by a unit volume of scattering entities per unit incident intensity per unit solid angle [158]. The *BSC* is an acoustic signature of a tissue's microstructure and is therefore not dependent on the scanner and *US* probe sensitivity. This is a quantitative and reproducible absolute measure that is superior to B-mode echogenicity, which is only qualitative and relative.

It is now well established that the *BSC* for blood is modulated by the erythrocyte aggregation state that can be modified by flow or shear rate, plasma fibrinogen concentration and hematocrit *H* [40;120;156;158]. By measuring blood *BSC* at different frequencies, it has been shown that the frequency dependence *BSC*(*f*) for non-aggregated erythrocytes obeys the Rayleigh scattering theory and its 4^{th} power (f^4) frequency dependence up to $f < 30$ MHz for $H < 30\%$ [192]. However, it has also been shown that beyond these limits, the presence of EA causes a deviation of the backscattered signal from that predicted by the Rayleigh scattering mode. By using a broadband transducer, this deviation can be quantified through the spectral analysis of *BSC*(*f*). This approach has been extensively used in *US* tissue characterization to study cell apoptosis [155], for prostate cancer diagnosis [60] and to differentiate rat mammary fibroadenomas from carcinomas [127].

Our group recently introduced the Structure Factor Size Estimator (SFSE) [189], a data reduction model based on a structure factor *S*(*f*), with the objective of solving the inverse problem, i.e., extracting blood microstructural properties from *BSC*(*f*). This model, which assumes a known hematocrit, estimates two physical parameters describing the microstructure of erythrocyte clusters: 1) the packing factor (*W*) that increases with erythrocyte clustering and is related to the Boltzmann compressibility state Eq. [140], and

2) the ensemble averaged aggregate isotropic diameter (*D*), a measure of the mean spatial extent of aggregates, expressed in terms of the number of erythrocytes.

4.3.2 Control of erythrocyte aggregation tendency

In order to control the aggregation tendency of erythrocytes while maintaining a consistent suspending phase, the covalent attachment of Pluronic copolymers F68 and F98 to the erythrocyte surface was employed as previously described [8]. Pluronics are block copolymers comprised of central poly(propylene glycol) chain flanked by two poly(ethylene glycol) chains. In aqueous solution, Pluronic copolymers micellize (self-aggregate) at a critical temperature dependent on the molecular weight of the poly(propylene glycol) core and copolymer concentration. By utilizing the known micellization behavior of Pluronic copolymers, following covalent attachment of derivatized Pluronic copolymers to the erythrocyte surface, it is possible to create erythrocytes with defined aggregation tendencies. Below the micellization temperature, erythrocyte aggregation is inhibited, and above the micellization temperature, erythrocyte aggregation is augmented [8].

4.3.3 Objectives

The first objective was to demonstrate that the SFSE allows characterization of EA in homogenous Couette shear flow under steady state conditions with blood at 40% hematocrit having different aggregation tendencies promoted by F68 and F98 Pluronics. The second objective was to circulate the same blood samples in the Couette instrument and a tube flow system in order to compare *W* and *D* and their dependence on the shear rate spatial pattern. The last objective was to establish the relationships between steady

state bulk viscosity, measured with a low-shear viscometer, and steady state parameters *W* and *D* to extrapolate local viscosity maps in tube flow.

4.4 Materials and Methods

4.4.1 Blood samples

Fresh porcine blood from 4 animals was obtained from a local slaughter house. It was anticoagulated with 0.3% (w/w) EDTA. All blood samples were centrifuged (2500 g for 10 min) to separate the plasma and erythrocytes. The buffy coat was carefully removed and discarded. Plasma was centrifuged at 20,000 g for 20 min and platelet poor plasma (PPP) was kept to reconstitute blood with erythrocytes washed two times with phosphate buffered saline (PBS) and one more time with PPP. This high-speed centrifugation was necessary since we noted in preliminary experiments that platelet aggregates were echogenic in blood exposed to high shear (300 s^{-1}) in Couette flow. Hence, using PPP eliminated this confounding effect potentially affecting the interpretation of our results.

Four types of erythrocyte preparations at 40% hematocrit were then assembled: one non-aggregating erythrocytes suspended in PBS (PBS suspension), control reconstituted blood samples with erythrocytes suspended in PPP (*control*), and erythrocytes coated with tri-block copolymers termed Pluronic F68 or F98 and suspended in PPP. Briefly, the copolymer coating consisted of covalently binding a reactive succinimidyl carbonate derivative of Pluronic F68 and F98 to the primary amines on the erythrocyte membrane , in the present study, the concentration of the activated Pluronic during the coating process was 0.25 mg/ml of suspension. These tri-block copolymers form temperature-dependent micelles that are determined mainly by the length of the poly(propylene glycol) block chain and its concentration. At room temperature, F98

coating increases EA and F68 coating has essentially no effect on plasma-induced aggregation [8]. Figure 4-1 shows typical images of uncoated cells, control cells in plasma, and F68 or F98 coated cells in plasma (≈ 1% hematocrit, stasis, 25°C). In this study, all measurements were performed at 25°C.

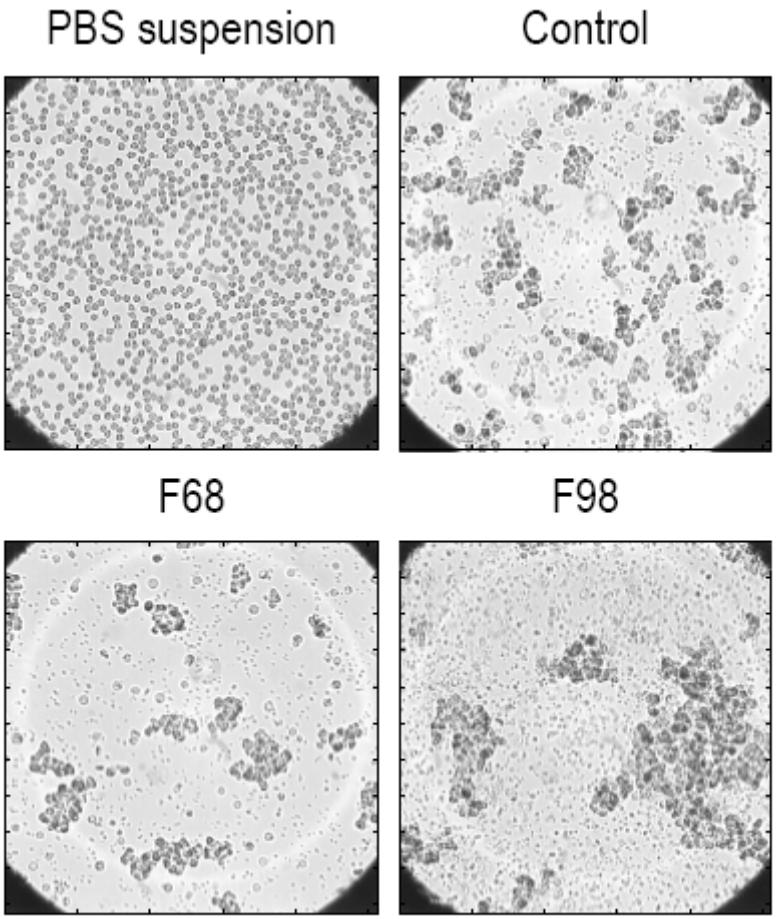

Figure 4-1: Microscopic images (40×) of diluted (≈ 1% hematocrit) PBS suspension, *control* blood, F68 and F98 Pluronics coated erythrocytes at 25°C. F98 increases erythrocyte aggregation whereas F68 has a neutral effect on the clustering organization.

4.4.2 Experimental setup

Two flow geometries were investigated in this study (see Figure 4-2).

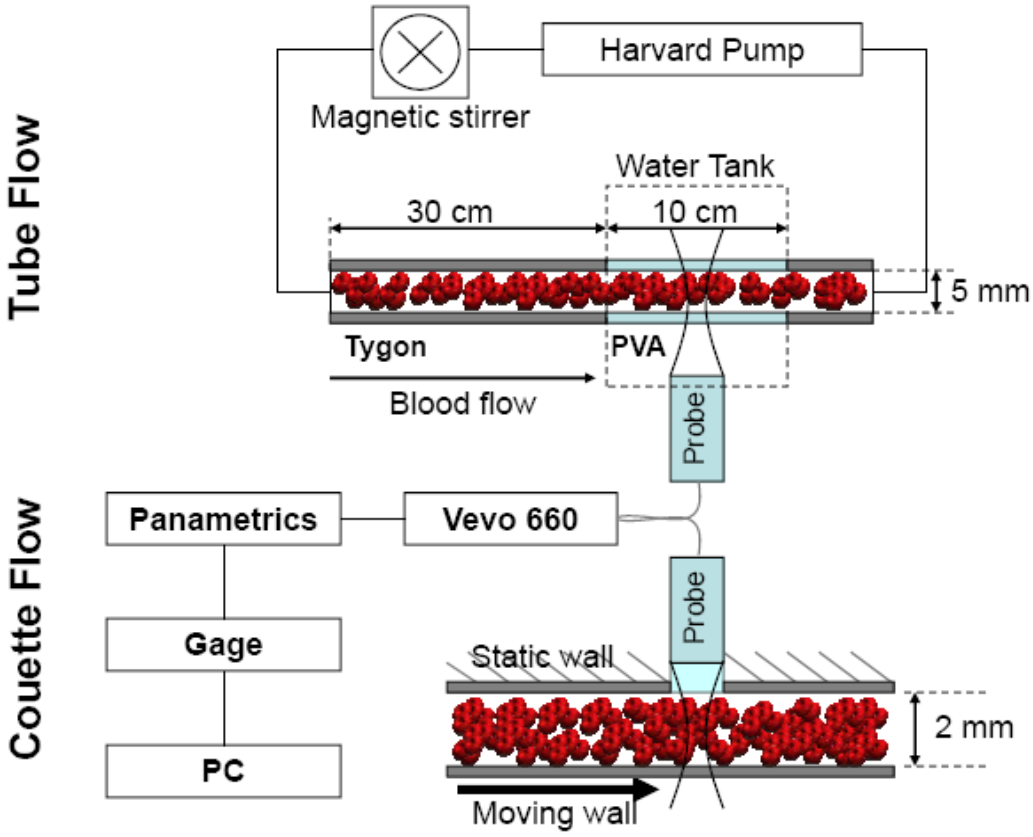

Figure 4-2: Schematics of tube and Couette flow experimental setups.

A Couette flow was created between two coaxially aligned cylinders with respective diameters of 160 and 164 mm. The inner cylinder's speed was controlled using a stepper motor (Zeta 6104, Parker Hannifin Corporation, Rohnert Park, CA). The ultrasound probe was positioned in the fixed outer wall of the Couette flow apparatus with its focal zone positioned at the center of the gap. The 2 mm gap was filled with 70 ml

of blood, which was alternatively submitted to a disaggregating cycle of 30 s at a high shear (300 s^{-1}) to initially disrupt all aggregates, and then to lower shear rates of 1, 2, 5, 10, 22, 47 and 100 s^{-1} for one minute to allow erythrocyte aggregate formation. At the one minute mark when aggregation was stabilized [189], eight ultrasound images were captured for subsequent analysis offline.

Prepared blood samples were also circulated in a horizontal straight tube submerged in degassed water at flow rates of 1, 2, 5 and 10 ml/min (5 mm inner tube diameter, 40 cm tube length). Measurements were made at 35 cm from the entrance , the required tube entry length for fully developed flow is 1.4 mm at the maximum flow rate of 10 ml/min [118], and shorter for lower flow rates. The last 10 cm section of the tube was composed of an acoustically compatible polyvinyl alcohol (PVA) cryogel tube made by applying 3 freeze-thaw cycles to the molded material [68]. A double syringe pump (model PHD2000, Harvard Apparatus, Holliston, MA) was used to simultaneously push and pull blood to minimize deformation of the PVA tube. A reservoir with a magnetic stirrer was placed upstream of the tube to disaggregate erythrocyte clusters and prevent sedimentation before entering into the tube. Prior to acquiring *US* data, the 70 ml blood sample was moved back and forth with the Harvard pump for 10 minutes to evacuate air bubbles (which increase blood echogenicity). Blood was then flowed in the forward direction at the selected flow rate to allow aggregate formation. Twenty *US* images were acquired in the longitudinal axis of the tube after one minute of steady flow to again stabilize the size of aggregates as performed for Couette flow experiments.

4.4.3 Ultrasound data acquisition and computation of the SFSE model

An ultrasound biomicroscope (Vevo 660, Visualsonics, Toronto, Canada) was used to insonify blood in B-mode with a RMV-710 probe (central frequency = 25 MHz, focal

distance = 1.5 cm, F-number = 2.1), at frame rates of 5 (Couette flow) and 20 (tube flow) images/s. As the transducer was mechanically swept across the sample, sequences of *RF* data were amplified and filtered with a wideband acoustic receiver (model 5900 PR, Panametrics, Waltham, MA), and digitized at 250 MHz with 8 bit resolution (model CS8500, Gagescope, Montreal, Canada). With these settings, one *RF* data block consisted of 8 or 20 images, with a pixel resolution of 21 μm (width) $\times$ 3 μm (depth). Each vertical line of an image was divided into overlapping segments of 400 μm with a step resolution of 30 μm (92.5% overlapping) for spectral estimation. This window length was determined as an acceptable compromise between image resolution and variance of power spectra.

BSC(*f*) was computed for every position, each 400 μm of data being Fourier transformed, averaged with corresponding segments from multiple frames and normalized across the -10 dB (9-28 MHz) spectral bandwidth of the system using a 6% hematocrit reference non-aggregating erythrocyte suspension. This normalization procedure for focused transducers is known as the modified substitution method [177]. For each *BSC*(*f*), *W* and *D* were then calculated using the SFSE method [189]. Briefly, this data reduction model is based on a second order polynomial approximation of the structure factor *S*(*f*) that describes the weakly scattering tissue's microstructure in the spectral domain. *S*(*f*) is directly related to the pair correlation function *g*(*r*) describing spatial interactions between erythrocytes through a Fourier transform [170]. The SFSE is a minimization problem in which *W* and *D* are deduced from a polynomial fit of the measured frequency dependent *BSC*(*f*) :

$$F(W,D) = \min \left\| BSC(f) - m\sigma_b(f)S(f) \right\|^2 \qquad (4.1)$$

In this expression, *m* is the scatterer number density (*m* = *H/V* with *H* the known hematocrit and *V* the volume of an erythrocyte), σ_b is the backscattering cross-section of an erythrocyte scatterer prototype of radius *a* (i.e., in the frequency range used in this

study, the error on σ_b is about 5% when using a sphere with a volume *V* rather than a typical biconcave erythrocyte [149]), and *S* is the structure factor that is approximated by the polynomial expression [189]:

$$S(f) \approx W - \frac{12}{5}(\frac{2\pi}{c})^2 (Da)^2 f^2 \quad (4.2)$$

This model considers that the increase in *BSC*(*f*) with aggregation is caused by a change in erythrocyte positions that has an effect on *S*(*f*) , both *W* and *D* increase when erythrocytes form clusters.

4.4.4 Velocity and shear rate assessments based on speckle tracking analysis

The positioning of the *US* probe in the longitudinal plane for both Couette and tube flow geometries allowed performing velocity speckle tracking analyses on sequences of B-mode images [167]. A cross correlation algorithm was used to find the translation of a 200 µm prototype square window in two successive frames across the region of interest. By measuring displacements of speckle and knowing the elapsed time between two images, spatially varying velocities could be determined. For Couette flow, a homogeneous shear rate and a linear velocity profile were measured (data not shown), whereas for tube flow, the shear rate profile was estimated from the velocity profile determined by fitting the power law

$$v(r) = v_{\max}\left[1 - \left(\frac{r}{R_t}\right)^n\right], \quad (4.3)$$

where v_{max} is the maximum velocity, r is the radial position and R_t the tube radius. A power law with $n = 2$ describes a Poiseuille parabolic flow, whereas n greater than 2 indicates the blunting of the velocity profile caused by aggregation [41;154]. The shear rate $\dot{\gamma}(r)$ was calculated at the different radial positions using

$$\dot{\gamma}(r) = -\frac{\partial v(r)}{\partial r} = n v_{\max} \frac{r^{n-1}}{R_t^{\,n}} . \qquad (4.4)$$

To simplify the data analysis of *W* and *D* as a function of the shear rate in tube flow, both indices were pooled over image areas covering different shear rate intervals. Namely, the label SR 1 was used to indicate regions with SR $\leq$ 1 s^{-1}, SR 2 regions with 1 s^{-1} < SR $\leq$ 2 s^{-1}, SR 5 regions with 2 s^{-1} < SR $\leq$ 5 s^{-1}, and SR 10 regions with 5 s^{-1} < SR $\leq$ 10 s^{-1}. (see Figure 4-9 and Figure 4-10).

4.4.5 Viscosity measurements

Viscosity measurements were performed with a low-shear viscometer (Contraves LS30, Zurich, Switzerland) at 25°C on similar pig blood samples prepared on site by Dr J.K. Armstrong in Los Angeles. PBS suspensions, *control* blood, F68 and F98 coated erythrocytes were studied at shear rates varying from 1 to 100 s^{-1}.

4.5 Results

4.5.1 Ultrasound measures in Couette flow

4.5.1.1 *BSC(f)* and SFSE model

The SFSE model allowed extracting the erythrocyte aggregation parameters *W* and *D* from the spectral content of the backscattering coefficient *BSC(f)*. Figure 4-3 illustrates typical *BSC(f)* for the four blood types at selected SR of 1, 2, 5, 22 and 100 s^{-1}.

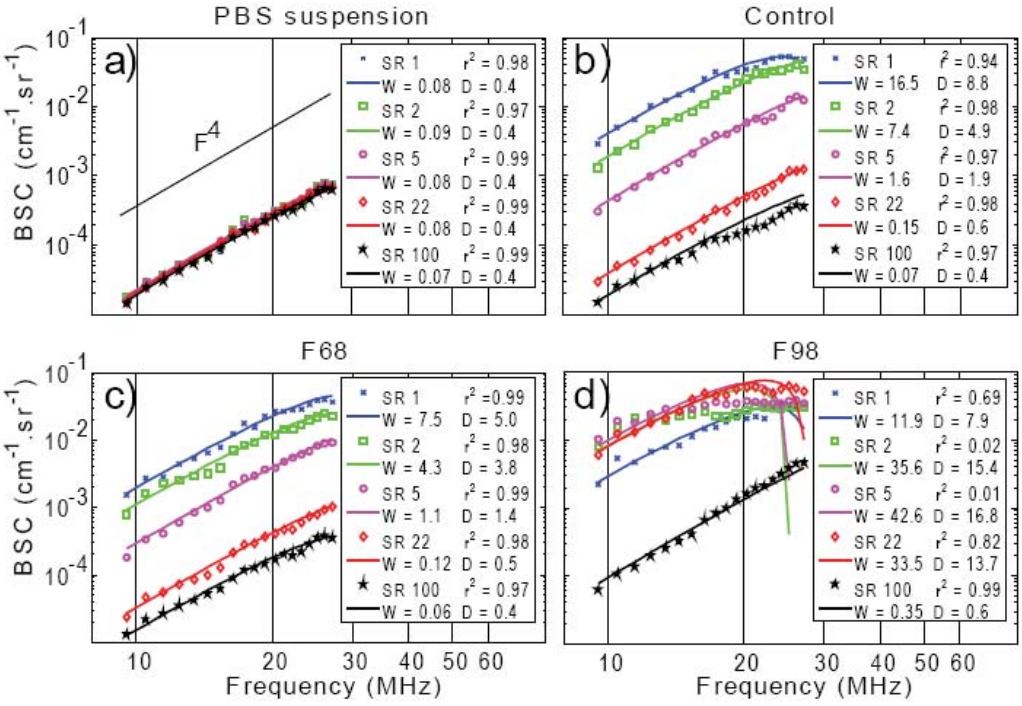

Figure 4-3: Typical experimental backscatter coefficient *BSC* as a function of the ultrasound frequency for (a) erythrocytes suspended in PBS (no aggregation), (b) *control* blood samples, (c) F68 coated blood samples and (d) F98 hyperaggregating coated blood samples under Couette flow. Lines indicate the Structure Factor Size Estimator (SFSE)

fitting of experimental data, SR is the shear rate, *W* and *D* are erythrocyte aggregation measurements, and r^2 is the correlation coefficient of the fitting.

Experimental *BSC(f)* are represented by discrete points and SFSE fittings are traced in full lines. The respective values of *W*, *D* and the correlation coefficient r^2 of the fitted model are shown in the legend. In Figure 4-3(a) for the PBS suspension, *W* and *D* were SR independent because of the absence of aggregation. With normal aggregating erythrocytes (*control*-panel b and F68-panel c), decreasing the shear rate resulted in increases in *W* and *D*. For both types of blood, the SFSE performed very well with r^2 values higher than 0.94. However, for the hyperaggregating F98-coated erythrocytes (panel d), the SFSE could not follow the frequency dependence of *BSC(f)* at shear rates of 2 and 5 s^{-1} when *D* became larger than 13.7 (value at 22 s^{-1}), as reflected by drastically lower values of r^2. The frequency dependence of aggregated erythrocytes between 9 and 28 MHz could only be efficiently modeled with the SFSE when $D < 14$, i.e., for $k*D*a < 4.3$ at $f = 28$ MHz, where *k* is the acoustic wave vector defined as $k = \frac{2\pi f}{c}$ with *c* the speed of sound in biological tissues (≈1540 m/s).

4.5.1.2 SFSE reproducibility

The reproducibility of the SFSE measurements was evaluated in the Couette homogenous shear field. *W* and *D* were computed on one control sample using 5 repetitions of the protocol at SR of 1, 2, 5, 10, 22, 47 and 100 s^{-1}. Results are presented in Figure 4-4 where both *W* and *D* are seen to decrease with increasing SR.

At a SR of 100 s^{-1}, *W* was 0.08 ± 0.01 (mean ± SE) and *D* was smaller than 1 (0.51 ± 0.04), both values corresponding to disaggregated erythrocytes [189]. *W* and *D* standard

errors increased with aggregation at the lower shear rates (logarithmic scale). Statistically different levels of *W* and *D* ($p < 0.05$) were found between all SR, except between 47 s^{-1} and 100 s^{-1} (Student-Newman-Keuls pair-wise comparisons of the mean ranks, Sigmastat 3.11, Systat Software, San Jose, CA), where erythrocyte aggregation is very low or absent.

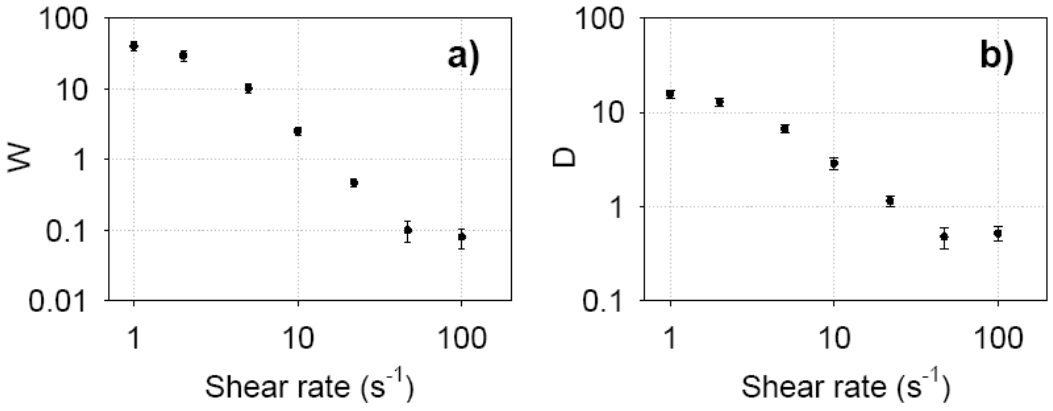

Figure 4-4: (a) *W* and (b) *D* in Couette flow as a function of the shear rate for 5 measurements realized with a control blood sample. Results are mean ± SE. Statistically different levels ($p < 0.05$) of *W* and *D* were found between all SR, except between 47 s^{-1} and 100 s^{-1}.

4.5.1.3 SFSE and viscosity shear rate dependencies

Shear rate dependencies of *W* (panel a), *D* (panel b) and apparent viscosity (panel c) for Couette flow are presented in Figure 4-5. For the PBS suspension, these three parameters were SR independent between 1 s^{-1} and 100 s^{-1}. For the *control* and F68 samples, each index showed a gradual decrease with increasing SR; at any SR, values of *W*, *D* and viscosity were similar for both types of blood. For F98, only data for SR ≥ 47 s^{-1} are presented because of the limit of SFSE model, i.e. that it was unable to fit *BSC(f)* at lower

SR. As expected, values of each rheological parameter for the F98 suspension were higher when compared with other blood types, and decreased with increasing shear rates.

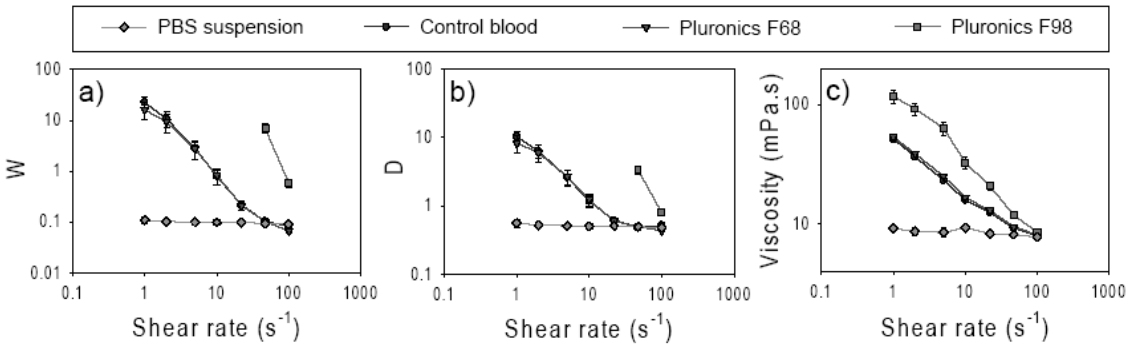

Figure 4-5 : Shear rate dependencies of (a) *W*, (b) *D* and (c) bulk viscosity (measured with a low shear viscometer) for the 4 blood samples (PBS suspension, *control* blood, F68 and F98 coated erythrocytes) collected from 4 animals. Results in Couette flow experiments are mean ± SE

Quantitative comparisons of *W* and *D* were performed between blood types using Student-Newman-Keuls pairwise statistics of the mean ranks for each SR, with $p<0.05$ considered to be significant. No differences were found at any SR between *control* and F68 groups or between *control*, F68 and PBS suspension at SR of 47 and 100 s^{-1}. Significant differences were found between normal aggregating erythrocytes (*control* and F68) and PBS suspended cells at SR of 1, 2, 5, 10 and 22 s^{-1} for *W* and at SR of 1, 2, 5 and 10 s^{-1} for *D*. Finally, *W* and *D* were significantly higher for the F98 group than for all other groups.

Based upon the results shown in Figure 4-5, the bulk viscosity of each blood type may be predicted by parameters *W* and *D* since all three indices varied similarly as a function of SR. Linear stepwise backward regressions were used to determine these relations, with linear regression equations and correlation coefficients for viscosity versus

W and *D* presented in Tab. 4-1. Based on the correlation coefficients, *D* is a somewhat better predictor of viscosity; relations between *D* and viscosity are shown in Figure 4-6. The linear regression for F98 did not reach significance (p = 0.08) even when a third point at $D \approx 17$, which is outside the limits of applicability of the SFSE model, was utilized.

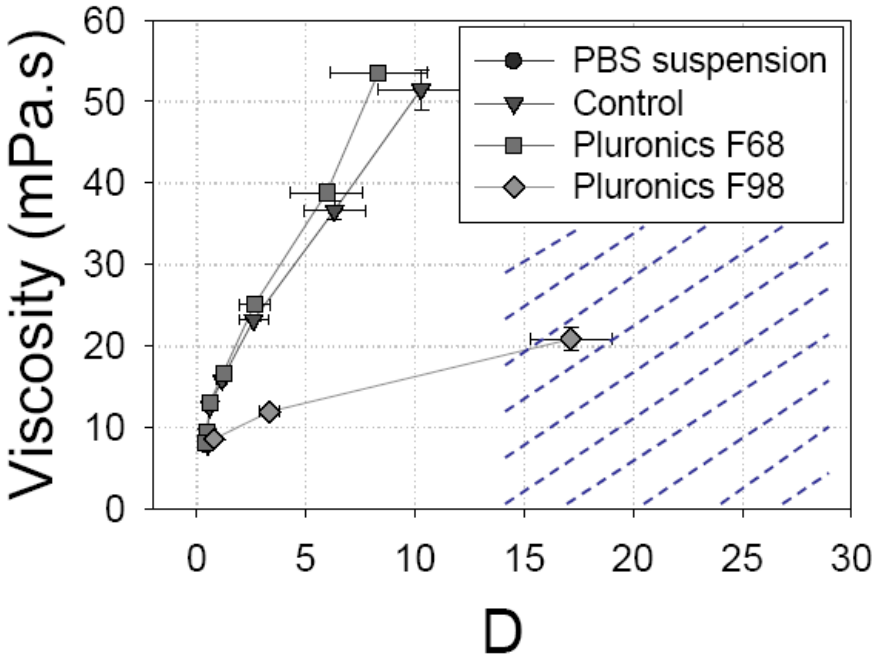

Figure 4-6 : Bulk viscosity as a function of the SFSE parameter *D* for the four blood types (PBS suspension, *control* blood, F68 and F98 coated erythrocytes) collected from four animals. Results in Couette flow experiments are mean ± SE. The dashed section marks the limits of applicability of the SFSE model.

Blood sample	Linear regression equation	Correlation coefficient r^2	p
PBS suspension	$\eta = 8.6$		
Control	$\eta = 9.12 + 4.24\ D$	0.98	< 0.001
	$\eta = 12.60 + 1.85\ W$	0.93	< 0.001
F68	$\eta = 8.41 + 5.38\ D$	0.98	< 0.001
	$\eta = 12.35 + 2.67\ W$	0.95	< 0.001
F98	$\eta = 8.72 + 0.71\ D$	0.97	NS (0.08)
	$\eta = 9.33 + 0.23\ W$	0.96	NS (0.10)

Tab. 4-1: Bulk viscosity as a function of ultrasound parameters *D* and *W.* η is the bulk viscosity (mPa.s) measured in Couette flow with a low-shear blood viscometer. *D* is the steady state acoustically determined ensemble averaged isotropic aggregate diameter, expressed in number of erythrocytes. *W* is the steady state acoustically determined ensemble averaged packing factor (no unit). NS = non significant.

4.5.2 Ultrasound measures in tube flow

4.5.2.1 Erythrocyte aggregation and impact on velocity and shear rate profiles

Typical velocity profiles estimated by the speckle tracking algorithm are presented in Figure 4-7 for flow rates of 1, 2, 5 and 10 ml/min; also shown as upward facing lines or curves are shear rate profiles calculated using Eq. 4.4.

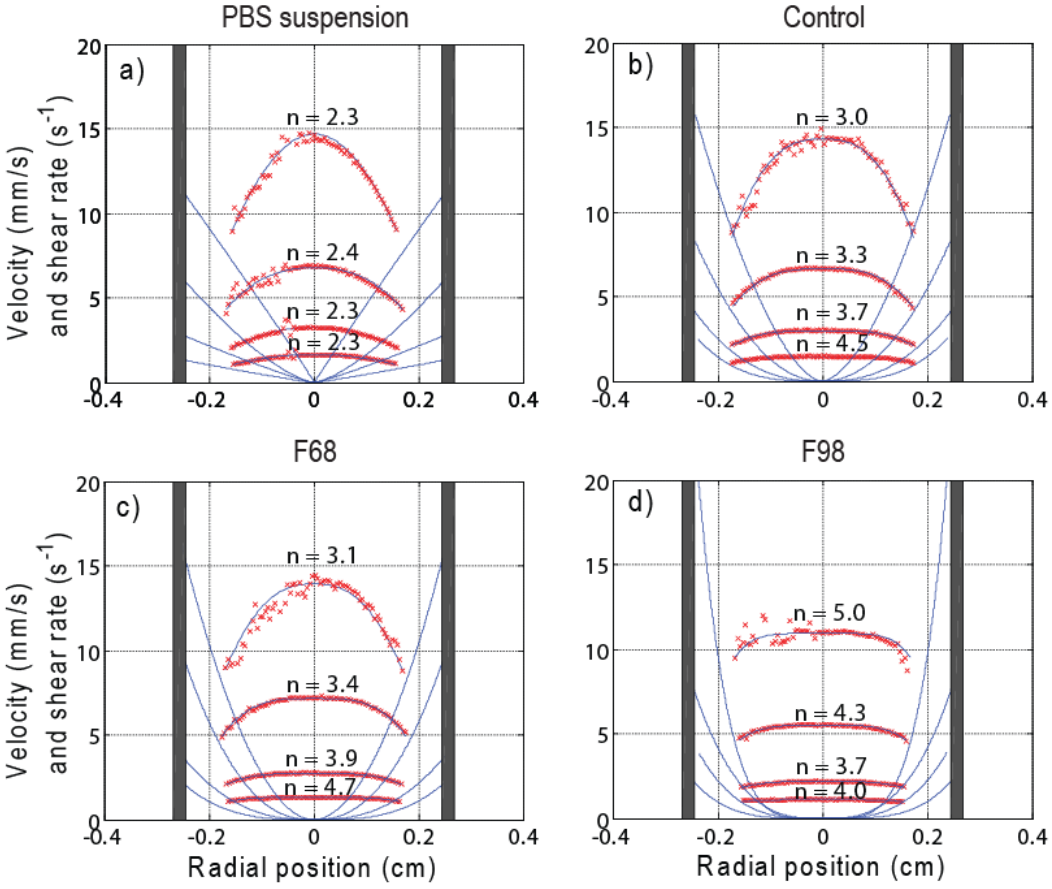

Figure 4-7: Typical speckle tracking velocity results in tube flow for flow rates of 1, 2, 5 and 10 ml/min for the four blood types (PBS suspension, *control* blood, F68 and F98 coated erythrocytes). The shear rate profiles shown as upward facing lines or curves were deduced from Eq. 4.4. *n* is the viscosity power law exponent in Eqs 4.3 and 4.4.

For the PBS suspension (a), velocity profiles were nearly parabolic ($n \approx 2$) for all shear rates. For *control* (b) and F68 (c) bloods, decreasing the flow rate provoked more blunting of velocity profiles, as reflected by monotonic increases of n. However, for F98 coated erythrocytes (d), decreasing the flow rate had the opposite effect, i.e. n decreased from 5.0 to 3.7 or 4.0 and hence less blunting occurred. As a further validation of the approach, volume integrations of velocity profiles were compared with known flow rates of the pump in Figure 4-8. The estimated flow rates were in excellent agreement for the non-aggregating PBS samples but were slightly underestimated for aggregating erythrocytes with the difference up to 10% for F98 samples.

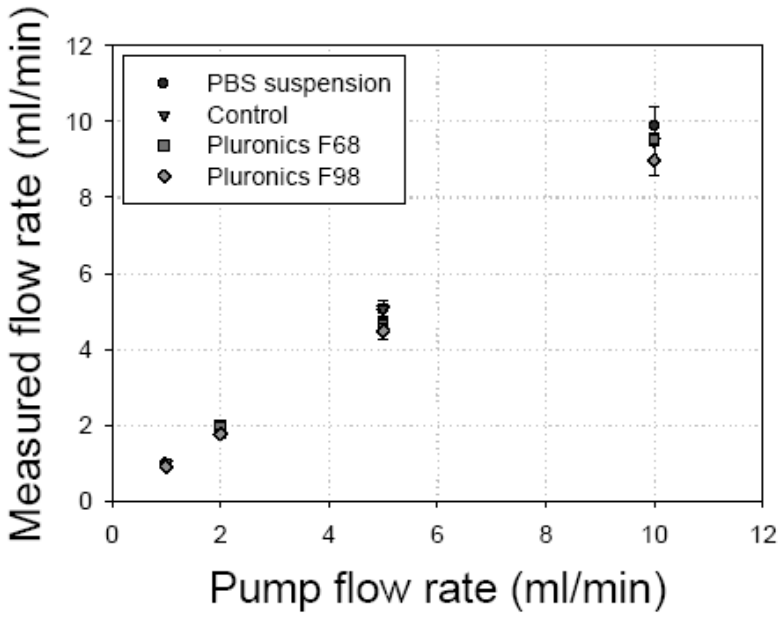

Figure 4-8 : Flow rate calculated from the volume integration of velocity profiles determined by speckle tracking as a function of the pump flow rate for the four blood types (PBS suspension, *control* blood, F68 and F98 coated erythrocytes) collected from four animals. Results in tube flow experiments are mean ± SE.

4.5.2.2 *W* and *D* shear rate dependencies in tube flow

The SFSE model was applied to determine parameters *W* and *D* as in Couette flow experiments. Figure 4-9 presents results for *control* blood and F98 coated erythrocytes of the SR dependency of *D* for flow rates of 1, 2, 5 and 10 ml/min. F68 results were very similar to *control* data, whereas for the PBS suspension *D* was SR and flow rate independent ($D = 0.42 \pm 0.02$); the SR dependency of *W* was similar to that for *D*. Note that *D* decreased with increasing SR and flow rates for *control* blood, whereas for F98 coated erythrocytes, the opposite was observed: *D* increases with increasing SR and flow rates with a similar finding for *W* (not shown).

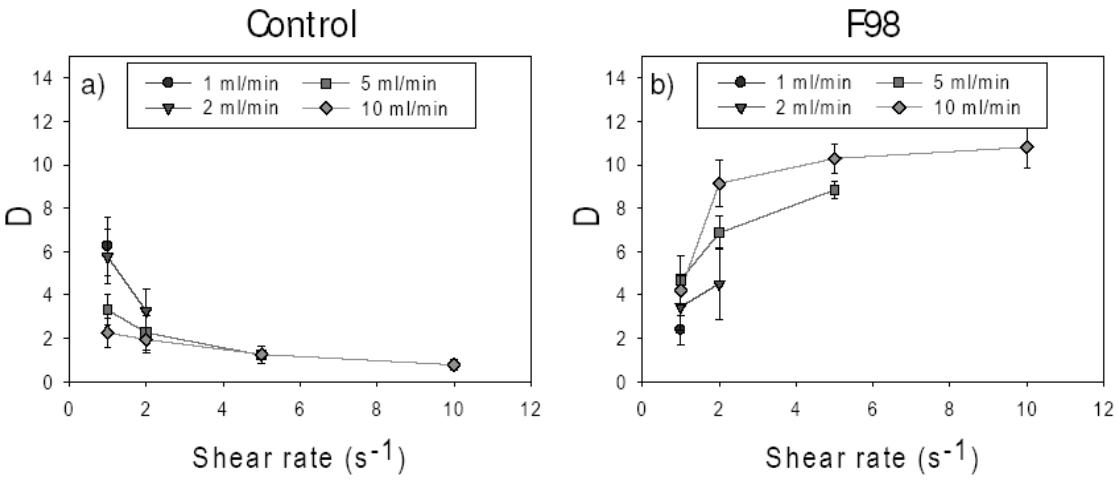

Figure 4-9 : Shear rate dependencies of *D* for (a) control blood and (b) F98 coated erythrocytes collected from four animals in tube flow rates of 1, 2, 5 and 10 ml/min. Results are mean ± SE. Tube shear rates were calculated from speckle tracking measurements.

4.5.3 Couette and tube flow comparisons

SR dependencies of *W* and *D* in both geometries are summarized in Figure 4-10.

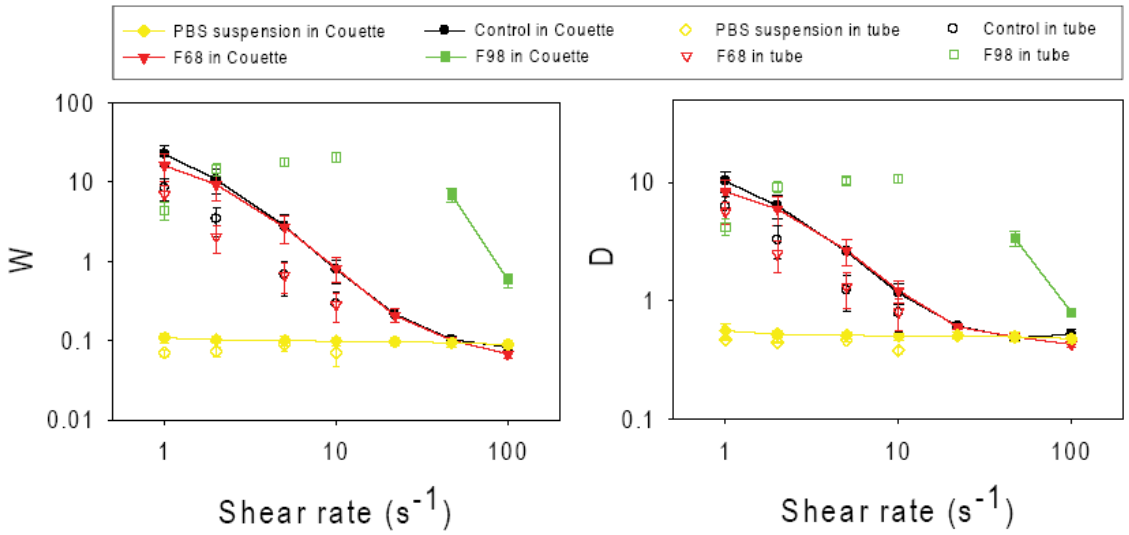

Figure 4-10 : : Shear rate dependencies of (a) *W* and (b) *D* for the four blood types (PBS suspension, *control* blood, F68 and F98 coated erythrocytes) collected from four animals and circulated in Couette and tube flows.

For clarity, only the tube flow rate providing the highest values of *W* and *D* at a given SR are shown (see Figure 4-9). Note that the SR was varied from 1 to 100 s^{-1} in Couette flow, whereas they ranged from 1 to 10 s^{-1} in tube flow. With the PBS suspension, *W* and *D* were slightly lower in tube flow and were SR independent for both geometries. For *control* and F68, lower values of *W* and *D* were also noted for tube flow, but for both geometries they decreased with increasing SR as expected. Note, however, that analysis of variance (ANOVA) tests revealed no statistical difference ($p > 0.05$) between both geometries at all SR for PBS, *control* and F68 bloods. For F98, changes of *W* and *D* with SR

were quite different (i.e., a decrease with SR in Couette flow and an increase in tube flow) but a clear comparison between both geometries was not possible because the range of SR did not overlap (Figure 4-10).

4.5.4 Parametrical images of *W* and *D* in tube flow and viscosity predictions

Typical velocity vectors determined by speckle tracking (left column), typical parametric images of *W*, *D* and predicted viscosity maps are presented for *control* (Figure 4-11) and F98 (Figure 4-12) bloods. In these figures, the parametric images are superimposed on a conventional B-mode frame. F68 images were very similar to *control*; PBS suspension images were spatially homogenous. The "black hole" (BH) phenomenon can be clearly seen for the *control* blood (Figure 4-11) as a hypoechoic zone in the tube center of B-mode and parametric images of *W* and *D* (see below for a discussion on the BH). Large BH with less contrast than *control* blood were noted at the highest flow rates for F98 samples. For *control* blood (Figure 4-11), the larger clusters of erythrocytes were concentrated in a ring located midway between the center stream and the tube wall, and corresponded to increased viscosity layers. The F98 coating also affected the radial distribution of aggregates, as illustrated in Figure 4-12: at low flow rates, the effect of the F98 coating on aggregation was not very pronounced but at higher flow rates large clusters formed close to the tube walls. Interestingly, and unexpectedly, the viscosity for F98 was not markedly increased in this region (see below).

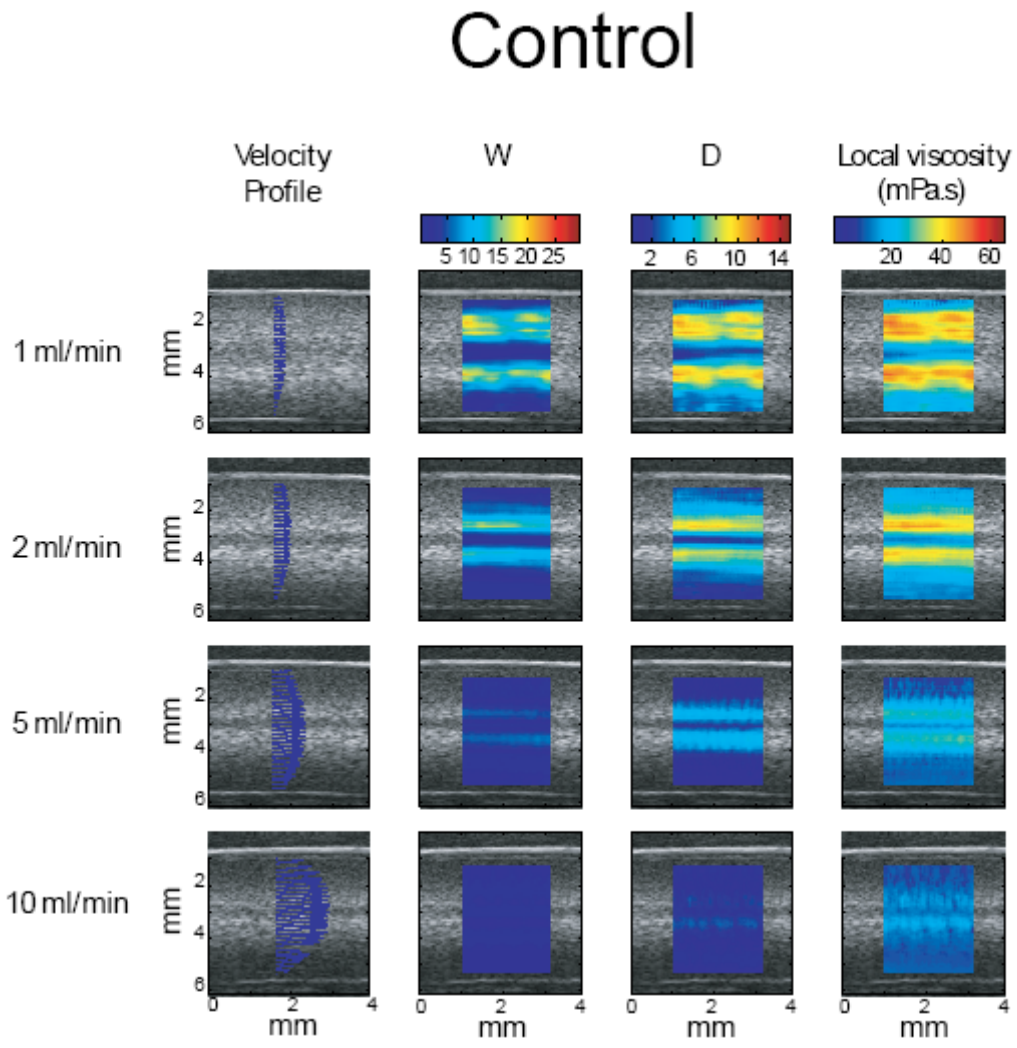

Figure 4-11 : Typical speckle tracking velocity vectors, parametric images of *W* and *D*, and local viscosity predictions for *control* blood in the tube flow geometry. For velocity scales, please refer to Figure 4-7 where the magnitude of the velocity vectors and fitted power law profiles are represented. The “black hole” phenomenon surrounded by a bright ring can be seen in the center stream of B-mode, parametric-mode (*W* and *D*) and viscosity images at the smallest flow rates.

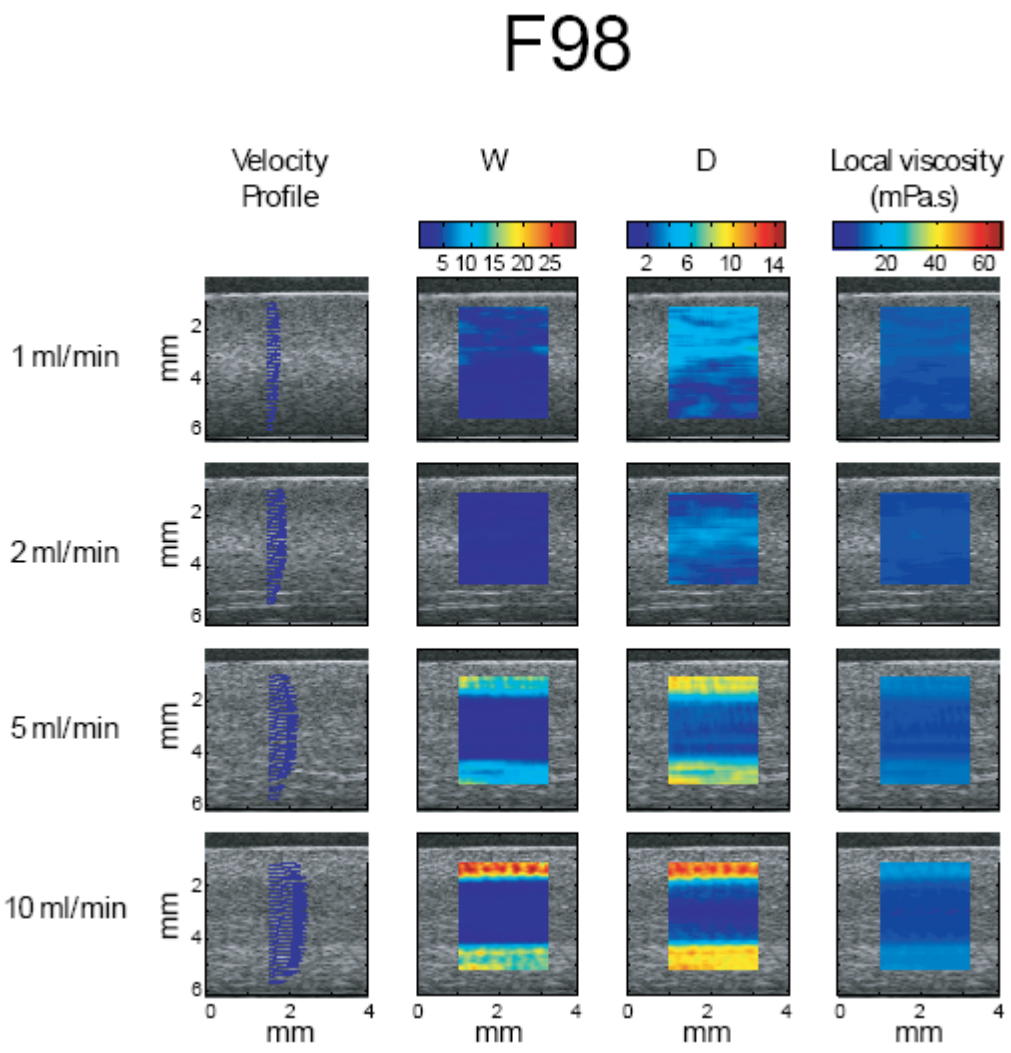

Figure 4-12 : Typical speckle tracking velocity vectors, parametric images of *W* and *D*, and local viscosity predictions for a hyperaggregating F98 blood sample in the tube flow geometry. For velocity scales, please refer to Figure 4-7 where the magnitude of the velocity vectors and fitted power law profiles are represented. Compared with Figure 4-11, a larger "black hole" can be seen in the center stream at the highest flow rates. The bright ring is now located near the wall.

4.6 Discussion

Erythrocyte aggregation (EA) can be characterized by its effect on *BSC(f)* using descriptive acoustical parameters such as the 'integrated backscatter' (i.e., mean of the *BSC* intensity within the transducer frequency bandwidth) or the 'spectral slope' (i.e., linear regression of *BSC(f)* on a log-log scale) [43;116;177]. Indeed, the use of *BSC* spectral information is commonly used because such parameters are more robust than fixed frequency *US* intensity measurements [178]. These parameters convey information on the erythrocyte spatial organization but are inherently dependent on the frequency and transducer bandwidth, which makes comparisons between studies an arduous task. Efforts to relate acoustical parameters to blood microstructure (e.g., with the structure factor) should prove to be more robust, informative and satisfying for quantitative assessment of tissue properties.

For blood, previous attempts to relate aggregate microstructures to scattering properties have generally failed when non-Rayleigh scattering and packing effects on *BSC(f)* were considered. For example, the kinetics of EA after flow stoppage were quantified in a mock flow loop by concomitant increases in "effective" scatterer size and acoustic concentration (i.e., the product of scatterer concentration and squared acoustic impedance) [97] based on changes in *BSC(f).* If an increase in scatterer size is coherent with aggregating erythrocytes, an increase in acoustic concentration is not as easily interpretable. Indeed, aggregation would rather decrease the number of "effective" scatterers, whereas the acoustic impedance would remain unchanged. The hypothesis that erythrocytes independently scatter *US* waves at a physiological hematocrit (e.g., 5 million erythrocytes/mm^3) can be questioned for this particular model. Another model, based on the Rayleigh scattering theory, established that *W* was related with the local erythrocyte concentration variance [120]. Interestingly, *W* increased with EA but the

model was limited to small aggregates with a maximum size of four erythrocytes [106]. With an empirical approach, also based on Rayleigh scattering, *BSC* dependence on hematocrit was related to the aggregate size determined by considering cell packing within aggregates and of aggregates in the suspension [25;84], but surprisingly, predicted sizes clearly exceeding Rayleigh scattering limits with aggregate sizes of up to 240 erythrocytes per aggregate.

4.6.1 Advantages of the SFSE model

The structure factor formalism was introduced by our group to describe the effects of EA on *BSC(f)* in non-Rayleigh conditions for densely packed scatterers [62;64;147]. It considers that variations of *BSC(f)* with EA are strictly related to changes in the spatial organization of erythrocytes, considered individually as weak Rayleigh scatterers much smaller than the acoustic wavelength. The SFSE is a non-Rayleigh second order approximation in *f* of the structure factor formalism that has several advantages. First, parameters *W* and *D* have a physical interpretability. *W* is related to the isothermal compressibility ξ_T of the tissue by $W = mK_bT\xi_T$, where *m* is the number density of scatterers, K_b the Boltzmann constant and *T* the absolute temperature. *W* is known to increase with the stickiness parameter of the analytical adhesive sphere model in a wide range of volume fractions [140]. This is also our observation with ultrasound, as *W* increased with aggregation, similarly to [106]. *W* also corresponds to the analytical formulation of the packing factor in the long wavelength limit [170], when there is no aggregation, which provides a lower boundary for this parameter. This lower boundary is well understood and varies with the hematocrit. At 40% hematocrit, the Perkus-Yevick approximation predicts values of *W* = 0.04 for spheres and *W* = 0.15 for cylinders [156]. In

our experiments, we obtained $W \approx 0.1$ for non-aggregated saline suspensions and, at high shear conditions, for aggregating erythrocytes (i.e., *control* and F68).

On the other hand, the parameter *D* of the SFSE model is an acoustically estimated diameter that is potentially of greater interest in hemorheology because its interpretation is easier than *W*. Nevertheless, its validation is difficult because, to the authors' knowledge, there is no means to experimentally assess aggregate sizes at 40% hematocrit. *D* is a non-dimensional number, defined as the ratio of the diameter of a fractal aggregate to the diameter of one erythrocyte, that is expected to be smaller than 1 for disaggregated erythrocytes. The apparent underestimation of the size estimate *D* for aggregated erythrocytes at 40% hematocrit has been previously discussed [189]. Nevertheless, in that prior publication it was shown that *D* was statistically correlated with the mean number of erythrocytes per aggregate, as assessed visually by microscopy at 6% hematocrit and measured acoustically at this same hematocrit.

Another advantage of the SFSE model is that *W* and *D* are parameters related to the tissue itself and should then, in theory, be independent of the frequency. In practice, because the SFSE is a second order model in *k*D*a* (see Eq. 4.2), the use of a higher frequency or increased EA degrades the performance of the model. Increasing the order of the polynomial approximation of *BSC(f)* could theoretically extend the *k*D*a* range of applicability, but unfortunately it introduces instability in the minimization fitting algorithm. Hence the following frequency trade-off had to be considered: 1) a larger bandwidth results in better *W* and *D* estimates, evidenced by a smaller variance, because more data are used for the polynomial fitting; 2) however, when *W* and *D* increase with aggregation, the *k*D*a* product also increases and the second order model reaches its limits of applicability, resulting in r^2 dropping for the curve fitting of *BSC(f)* and introducing important underestimation biases of *W* and *D.* This limit occurred for $D > 14$ for the frequency range considered in this study (9 - 28 MHz). By decreasing the upper frequency

limit from 28 MHz to 15 MHz for large aggregates in the F98 samples corrected this issue (data not shown) but introduced more variance in estimating smaller aggregates. Therefore, the frequency bandwidth to use must be appropriate for the levels of aggregation that are being characterized; this frequency range can be tested using r^2 (see Figure 4-3). Note that for clarity, in this report the bandwidth was kept constant for all results thus limiting the applicability of the SFSE to $D < 14$.

4.6.2 Steady state Couette flow relationships between *D* and measured viscosities

Multiple linear regressions showed that *W* and *D* were collinear and that *D* was linearly related with the bulk viscosity. Regressions in Tab. 4-1 suggested that the shear rate dependent viscosity was explained by the high shear viscosity and a multiple or fraction of *D*. The Flory-Fox theory [61] predicts viscosity proportional to the volume of spherical particles in suspension. The finding that the viscosity was proportional to a multiple or fraction of *D* is surprising and not fully understood. It is not clear to what extent the Flory-Fox theory for colloidal suspensions can be directly applied to dense fluid deformable corpuscles, such as erythrocytes. It seems reasonable to believe that erythrocyte deformation, interacting fractal clusters and their orientation should modify the Flory-Fox relation.

Another surprising result is that the multiplicative coefficient of *D* for F98 samples was almost six times smaller than for the other samples (see Figure 4-6). Although the linear regression did not reach statistical significance ($p = 0.08$, see Tab. 4-1), the tendency of the slope for the F98 sample was nevertheless clearly smaller. Since higher shear rates were required to obtain similar *D* values with the F98 sample, it can be speculated that

the aggregate morphology was stretched, thus provoking a lower viscosity versus size relation; validation of this hypothesis requires future studies.

4.6.3 Parametrical images in tube flow

The objectives of the tube experiments were to illustrate the performance of the SFSE in a non-homogenous shear field. The presence of the BH in tube flow images illustrates the unique imaging potential of *US* to become a rheological tool with spatial resolution and sensitivity to EA. The BH was studied by different teams [121;136;154;193] and it is now generally accepted that it is the result of a transient state of aggregation in the center stream that is dependent on the tube entry length. Indeed, the blood flowing in the center, in the low shear region, travels in the tube more quickly and has less time to form aggregates than blood on a peripheral layer. This phenomenon is also amplified by the presence of a non-zero shear on peripheral layers that promotes aggregate formation by increasing the collision frequency between erythrocytes [45]. This aggregation kinetics related effect was still present after 3 minutes of shearing in a Couette flow for zero shear conditions, as reported previously (see Figs. 2-3 in [189]). When clustering erythrocytes are insonified by the *US* probe, aggregates in the center may not have sufficient time to reach an equilibrium size as predicted by the local SR, velocity and probe position along the vessel.

The non-linear hematocrit dependence of the *BSC* was also suggested to explain the BH phenomenon. A decrease in *H* in the center axis was proposed by Yuan and Shung [193] based on the “tubular pinch” or “Segré-Silberberg” effect [31]. This behavior for fluid-like deformable corpuscles seems improbable based on earlier reports [165]: erythrocytes are rather concentrated near the center axis in that particular report. On the other hand, a local increase in hematocrit in the center axis due to erythrocyte migration

towards the vessel center could provoke a decrease in *BSC* that may not necessarily correlate with a decrease in aggregate size. Using magnetic resonance imaging, shear rate variations in the gap of a large core Couette instrument were shown to induce migration of erythrocytes away from the walls [44], but the hematocrit variations in the center of the gap remained marginal (a few hematocrits). Note that a small core Couette device was used here, which should result in even smaller hematocrit variations in our data. In another magnetic resonance study, hematocrit spatial variations were shown to be non significant in tube flow [154]. Nevertheless, in a separate experiment, a 50% hematocrit hyperaggregating blood sample was prepared and sheared at 2 s^{-1} in our Couette apparatus to provide additional evidence that hematocrit changes could not explain our results. Expected high values of W =15 and D = 9 were found. This illustrates that the SFSE could detect aggregation at an increased hematocrit. Also, if parameter H, an input in our model, is locally higher than it may be the case in the center stream, the SFSE would tend to overestimate W and D (data not shown). Moreover, an increase in H or EA in the center stream would cause a decrease in the spectral slope [116] and thus an increase in D that was not observed in our data. These results suggest that if hematocrit variations are present in the tube, such effects cannot fully explain the BH. Spectral analysis of our data thus support a dominant low EA hypothesis due to very low shears and time-dependent transient effects, as clearly shown in Figure 4-9a: at a given shear rate, the smallest flow rates promoted the largest aggregates. This also explains why W and D in tube flow were lower than the steady state Couette flow results in Figure 4-10.

Another interesting but at a first glance unexpected observation was the increase in W and D with increasing SR for the F98 tube flow experiments (Figure 4-9b and Figure 4-10), since for these suspensions, a SR increase promoted aggregate formation. Note that this effect was observed in another study [4] when horse blood, which is also characterized by very intense aggregation tendencies, was circulated in a tube flow setup.

The mechanism explaining this phenomenon may be that more SR-induced collisions between erythrocytes are necessary to promote aggregation of cells with a high tendency to aggregate. However, as with other types of erythrocyte suspensions, disaggregation occurred with further increased of the SR beyond the value inducing the maximum aggregation (see Figure 4-10, Couette and tube flow data).

The low aggregation and progressive increase in *W* and *D* as the flow rate (shear rate) was increased can be visualized in Figure 4-12 for F98 samples. This figure also shows that the maximum selected flow rate of 10 ml/min was not sufficient to induce erythrocyte disaggregation close to the tube wall, where the shear rate was maximum. Disaggregation was nonetheless noted close to the wall for *control* samples as the flow rate was increased (see Figure 4-11). Interestingly, and of potential rheological and pathophysiological impact, is the observation of a ring with large aggregates close to the wall at the highest flow rates of 5 and 10 ml/min for F98 samples (Figure 4-12), and a depleted ring with few or no aggregates close to the wall for *control* samples regardless of the flow rate (Figure 4-11). For hyperaggregating erythrocytes such as F98 samples, the presence of high EA close to the wall could influence blood/vessel wall interactions.

As discussed earlier when interpreting results of Figure 4-5 and Figure 4-6, the viscosity maps of Figure 4-12 for F98 samples did not reflect the increased EA close to the wall as the flow rate was increased. The lower slope of the viscosity versus *D* and *W* relations for the Couette experiments of Figure 4-6 can explain this observation. Likely, as mentioned before, the lower SR in tube flow ($SR < 22\ s^{-1}$ at all flow rates, see Figure 4-7(d)) compared with Couette flow, where SR were varied from 47 to 100 s^{-1}, may have biased (i.e., underestimated) the prediction. The steady state Couette flow relation between viscosity and *D* that we used in our predictions of Figure 4-12 and also Figure 4-11 were based on the hypothesis that the increase in bulk viscosity was directly caused by an increase in aggregate size. Any consideration affecting the viscosity versus particle

size relation, such as deformability, erythrocyte cluster orientation or elongation with increased flow, could not be accounted for in this simplistic approach.

4.6.4 Towards an *in vivo* assessment of the pathological impact of erythrocyte hyperaggregation

If the hematocrit is known, we have shown that precise and reproducible ultrasonic structure parameters, *W* and *D*, can be obtained with the SFSE model when an adequate *US* frequency bandwidth is available. *In vivo*, the attenuation of the pressure wave by intervening tissues such as skin, fat and vessel wall is a major difficulty that must be overcome. It is notable that the SFSE framework was used in a minimization routine called the SFSAE (Structure Factor Size and Attenuation Estimator) and allowed the simultaneous estimation of the attenuation of different phantom layers positioned between the *US* probe to study erythrocyte aggregates [66]. This approach could therefore potentially be used to characterize blood microstructure through the skin *in vivo,* although further validation is still needed.

The pathophysiological impact of erythrocyte hyperaggregation has been studied by transfusion of Pluronics coated erythrocytes by members of our group [18;183]. In the current study, it was shown that F98 coated pig erythrocytes exhibited increased clustering up to shear rates as high as 100 s^{-1}. The presence of aggregation near the tube walls was quantified with *US* parametrical imaging *in situ.* The natural next step would be to locally measure EA *in vivo* using ultrasound and quantify the physiological effect of increasing the aggregability using Pluronics coatings.

4.7 Conclusions

It was demonstrated in this study that the SFSE*,* an *US* non-Rayleigh scattering model, could adequately characterize EA for non-aggregating, aggregating and Pluronics coated erythrocytes. Two parameters, the packing factor (*W*) and ensemble averaged aggregate isotropic diameter (*D*), were compared in Couette and tube flows and predictably quantified EA with respect to SR and to blood type for $D < 14$. In Couette flow, empirical blood type dependent relationships between *D* and viscosity were established. These relationships were then used to extrapolate local viscosity maps in tube flow. In tube flow, a "black hole" (BH) appeared for aggregating bloods under some flow conditions. Analysis of the backscattered spectral information with the SFSE model supported that the BH is the consequence of a time related lower aggregation in the center stream. Increasing the aggregation tendency of erythrocytes (F98 blood) resulted in the presence of bigger aggregates near the walls at the highest flow rates (aggregates were present at shear rates up to 100 s^{-1} in Couette flow). Preliminary results also suggested that in near stasis conditions, a higher shear rate was necessary to promote aggregate formation with the F98 samples, resulting in larger BH. The *in vivo* significance of the BH remains to be established. Parametrical images, superimposed on B-mode displays, clearly illustrated the unique capacity of ultrasound to reveal spatially non-homogenous EA states*.* Ultrasound opens new perspectives for *in vivo* macrocirculatory studies on the impact of hemodynamic perturbations and complications caused by EA using high frequency *US*, which can be locally monitored and characterized non invasively thought the skin *in vivo* and *in situ*.

4.8 Acknowledgments

Supported by grants from the Canadian Institutes of Health Research (#MOP-84358 and #CMI-72323), Heart and Stroke Foundation of Canada (#PG-05-0313), National Institutes of Health of USA (#R01HL078655), and Natural Sciences and Engineering Research Council of Canada Ph.D. scholarship program (#ES D3-317051 - 2005).

5 Chapitre 5 : Application à l'étude de l'implication pathophysiologique de l'hyperagrégation sur la thrombophlébite

5.1 Avant propos

Ce chapitre est constitué par un manuscrit intitulé « *Increased red blood cell aggregation directly triggers early deep venous thrombosis* » destiné au journal « *Circulation Research* ». Il décrit l'effet d'une augmentation de l'agrégation érythrocytaire induite par une transfusion de globule traité par des Pluronics sur la thrombophlébite veineuse fémorale chez le lapin. Une augmentation significative de la fréquence de formation d'un thrombus 30 minutes après l'intervention a été constatée dans le groupe cible, de manière concomitante avec une augmentation de l'agrégation érythrocytaire (paramètres *W* et *D*) alors que les autres paramètres hématologiques demeurent pratiquement inchangés entre les deux groupes. Cet article est hautement novateur car, à la connaissance de l'auteur, le lien de causalité entre la thrombose et l'hémorhéologie sanguine n'a jamais été établi par une étude expérimentale mais plutôt suggérée par des études cliniques corrélatives aux conclusions parfois contradictoires. Cela explique pourquoi les facteurs hémorhéologiques ne sont pas exploités cliniquement dans la prédiction du risque de thrombophlébite ou de récurrence de thrombophlébite alors qu'une grande proportion de thrombose demeure d'origine idiopathique. Cette étude démontre que les perturbations hémorhéologiques locales semblent être impliquées dans

la thrombogénèse de la thrombophlébite. L'émergence de nouveaux outils de caractérisation hémorhéologiques tels que les ultrasons permet de quantifier ces perturbations localisées.

Increased Red Blood Cell Aggregation Directly Triggers Acute Deep Vein Thrombosis

François T.H. Yu[†], Jonathan K. Armstrong[§], Herbert J. Meiselman[§], Guy Cloutier[†‡10]

[†] Laboratory of Biorheology and Medical Ultrasonics, Centre de Recherche, Centre Hospitalier de l'Université de Montréal (CRCHUM), Montréal, Québec, Canada.

[§] Department of Physiology and Biophysics, Keck School of Medicine, University of Southern California, Los Angeles, California, USA.

[‡] Department of Radiology, Radio-Oncology and Nuclear Medicine and Institute of Biomedical Engineering, Université de Montréal, Montréal, Québec, Canada.

RUNNING TITLE: Blood rheology is implicated in DVT etiology.

KEYWORDS: Deep vein thrombosis, RBC aggregation, cardiovascular ultrasound imaging, ultrasound tissue characterization, rabbit model.

[10] Corresponding author :
Guy Cloutier, Director of LBUM-CRCHUM, 2099 Alexandre de Sève, Pavilion J.A. de Sève (room Y-1619), Montréal, Québec, Canada, H2L 2W5.
Tel: 514-890-8000 (24703), Fax: 514-412-7505
Web: http://lbum-crchum.com,

5.2 Abstract

Recurrent deep vein thrombosis (DVT) risk factors include a first idiopathic DVT in up to 47% of cases, strongly suggesting the existence of unidentified prothrombotic abnormalities. The present study investigated the effect of increasing erythrocyte aggregation (EA) on DVT pathogenesis in a rabbit model. DVT presence, flow and EA were measured locally with ultrasound. Greatly enhanced EA for red blood cells (RBC) in native plasma was achieved by covalent linkage of Pluronic F98 to the RBC surface; coating with Pluronic F68, which does not enhance aggregation, was used as a coating control. On day 1, endothelial damage and a partial stenosis were surgically created on the left femoral vein of each animal. A thrombus was formed within 30 minutes in 6 of 7 veins of animals receiving a 30% volume blood exchange with the F98-coated RBC, whereas a thrombus occurred in only 1 of 7 veins in the F68 transfused control group. *In vivo* EA imaging using quantitative ultrasound, based on the structure factor size and attenuation estimator, confirmed the increased aggregation in thrombosed veins of the F98 group compared with the F68 group and the contralateral vessel. For each group, 5 animals were followed for 2 weeks, then sacrificed. Femoral veins were excised and processed for histology. In the F98-transfused animals, lysis of blood clots occurred and the presence of chronic thrombi totally occluding the vein in 3 of 5 animals was confirmed by histology. Conversely, in the F68 group, only mural neointimal hyperplasia and a single disorganized blood clot was observed in 1 of 5 animals by histology. In conclusion, the marked increase in EA induced by transfusing F98-coated RBC promoted the formation of acute DVT in rabbit femoral veins, strongly suggesting a direct pathophysiological role of altered hemorheology in acute DVT formation.

5.3 Introduction

The incidence rate of deep vein thrombosis (DVT) is 1-2 events per 1000 patient-years [38], with pulmonary embolism being its major complication. DVT is a multi-factorial problem triggered when several risk conditions related to Virchow's triad contribute to a prothrombotic threshold. Identifying these factors and their etiopathological impacts are fundamental in the prediction, understanding and treatment of DVT. Risk factors for DVT are usually classified as transient/provoked (e.g., surgery, trauma, immobilization), or persistent/unprovoked (e.g., cancer, paralysis, sex, age, hormone intake), with the latter group at higher risk of recurrence [1;6]. Interestingly, an idiopathic first DVT episode increases the risk of recurrent DVT by a ratio of 1.9 compared with patients experiencing a provoked first DVT episode [38;151]; the proportion of idiopathic DVT ranges from 26 to 47% of all DVT cases [1;175]. Such findings strongly suggest the existence of yet unidentified prothrombotic abnormalities in first time and recurrent DVT patients.

Evidence of altered blood rheology playing a role in DVT pathogenesis and its recurrence is fairly scarce and mostly based on correlation studies [50;52;110;195]. Although blood viscosity and EA are raised in most clinical conditions associated with an increased risk for DVT (e.g., surgery, myocardial infarction, leukemia), these hemorheological parameters are not routinely used in DVT risk profiling since it is unclear whether they contribute to DVT pathogenesis or are merely surrogate markers of inflammation. As a typical example, hyperfibrinogenemia, which promotes EA, has long been identified as a risk factor of DVT [50;52] and recently shown to effectively increase its occurrence with a risk ratio of 4.2 for patients aged above 45 [173]. However, a similar risk ratio could not be established in younger patients [173], nor in individuals presenting genetically elevated fibrinogen [141], raising the question whether fibrinogen itself is a risk factor for DVT. In another study based on a one-year follow-up, patients with

persistent DVT risk factors had higher plasma fibrinogen, EA and plasma viscosity than patients with transient risk factors [6]. Indeed, these rheological variables returned to normal levels only in the transient risk factor group, which suggests that impaired hemorheology could contribute to maintaining DVT risk. Several questions arise from clinical observations that persistent risk factors predict DVT recurrence whereas transient ones do not: 1) could altered hemorheology be a mechanism that triggers DVT recurrence?; 2) could such alterations be directly implicated in DVT pathogenesis?; 3) should hemorheological parameters be screened more routinely to prevent DVT and DVT recurrence ?

We designed this study to experimentally assess the impact of abruptly increasing EA on the formation of a DVT in a surgically created prothrombotic environment in a rabbit model. Prior to surgery, rabbits were exchanged transfused with either hyperaggregating Pluronic F98 covalently coated red blood cells (RBC) or control RBC (Pluronic F68 covalently coated, neutral effect on aggregation). A prothrombotic environment was then created by concomitant femoral vein lumen area reduction and endothelial damage. Animals were followed for 2 weeks and were regularly monitored for thrombus formation, blood flow and EA using ultrasound imaging; a new *in vivo* approach to assessment of EA was carried out using a structure factor size and attenuation estimator (SFSAE). After sacrifice of the animals, the presence and composition of thrombi in the femoral vein were evaluated by histological analyses of excised tissue.

5.4 Materials and Methods

5.4.1 Animals and groups

Twelve New Zealand white rabbits weighting 3.3 to 3.5 kg were used, randomly assigned to either the hyperaggregating F98 group (n = 6) or to the control F68 group (n =

6). One animal in each group was studied to examine the acute response following lumen area reduction and endothelial damage of both left (LV) and right (RV) femoral veins. The other five animals per group underwent vessel stenosis and endothelial damage only on the LV with the contralateral RV used as a paired control for aggregation measurements. Within each group of five animals, longitudinal follow-up was performed for two weeks at five time points: pre-intervention (d0), 30 minutes post-intervention (d1), and on days 4 (d4), 9 (d9) and 14 (d14). All procedures were performed aseptically, and the protocol was approved by the institutional animal care committee of the Centre de Recherche du Centre Hospitalier de l'Université de Montréal, in accordance with the Canadian Council on Animal Care guidelines.

5.4.2 Blood exchange transfusion and DVT model.

Blood collection from donor animals and preparation of coated RBC were performed the day prior to the surgery and the cells stored at 4°C overnight; blood transfusions were performed the next day. The coating procedure is described in the online data supplement section 5.10. The effects of polymer coatings on EA are illustrated in Figure 5-1 where it is clear that F98 coating markedly enhances RBC aggregation.

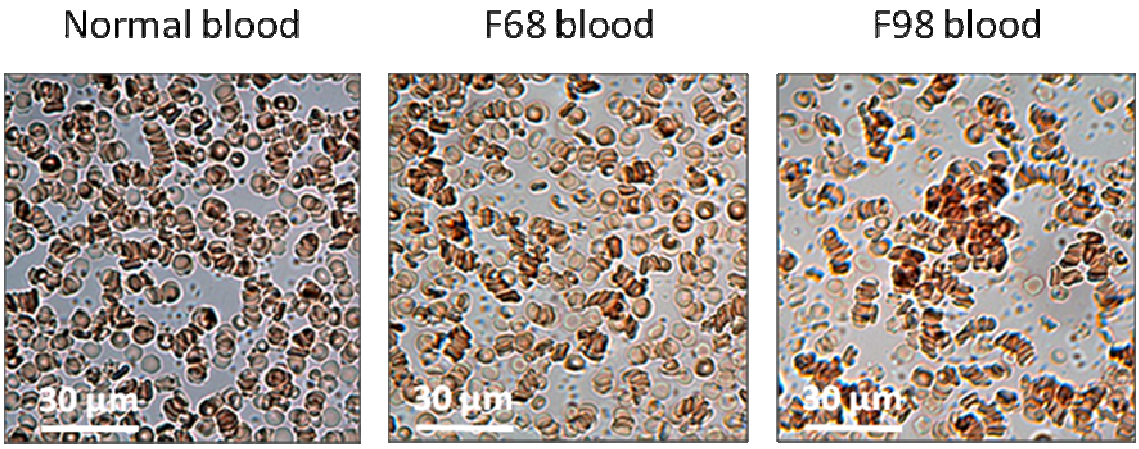

Figure 5-1 : Microscopic images of diluted (10% hematocrit) blood in native plasma for: (a) normal rabbit blood; (b) 30% Pluronic F68-coated RBC showing RBC aggregates comparable to normal blood; and (c) 30% Pluronic F98-coated RBC showing enhanced RBC aggregation. Bright field images were taken at 37°C.

Rabbits received pre-anesthesia medication [subcutaneous injection of 0.75 mg/kg acepromazine (Atravet, Ayerst, Montreal, QC, Canada) and 0.01 mg/kg glycopyrrolate], following which anaesthesia was induced with an intravenous injection of 5 mg/kg propofol (Propofol, Novopharm, Toronto, ON, Canada) and maintained using 2% isoflurane in 100% oxygen. Cardiac pulse, oxygen saturation and body temperature were continuously monitored with a multi-parameter physiologic monitor (LW6000, Digicare Biomedical Technology, Boynton Beach, FL). Body temperature was maintained at 37 ± 1 ^{o}C using a circulating water blanket and a snuggle safe. Normal saline (i.e., 0.9% NaCl) was continuously infused at a rate of 10 ml/kg/hour. The left jugular vein and contralateral common carotid artery were exposed and canulated with 22 G (0.95 mm diameter) catheters (Smiths Medical ASD, Southington, CT). Thirty percent of total blood volume, estimated at 6% of body weight, was exchanged with coated blood warmed to 37 °C by simultaneous venous injection and arterial withdrawal using a Harvard double

syringe pump (PHD2000, Harvard Apparatus, Holliston, MA) at a flow rate of 20 ml/min. The left jugular vein and common carotid artery catheters were then removed, these vessels ligatured and the surgical opening sutured.

The DVT model used herein involved venous flow reduction and endothelial damage. Flow reduction was achieved by creating a 0.7 cm diameter stenosis in the femoral vein (Figure 5-2). The intervention consisted in: (i) isolating the LV 1.5 cm proximal to the saphenous-popliteal bifurcation (vein diameter about 2mm); (ii) placing a 24 G (0.7 mm diameter) catheter (Smiths Medical ASD) along the vein; (iii) and tying up both vein and catheter together using a silk suture; (iv) gently pulling the catheter out thus creating an approximately 88 % cross-sectional surface stenosis and reducing the flow upstream of the suture. To further promote thrombosis, two separate endothelial injuries, 2 mm apart, were created by clamping the femoral vein with forceps upstream of the suture. To standardize the protocol, the forceps were closed to the first locked position for 2 seconds followed by immediate release, and the procedure was repeated at the second position; hemorrhage from the vessel was never observed. The surgical opening was then flushed with normal saline to remove air bubbles and closed. For one animal in each group (acute response), concomitant partial stenosis and endothelial damage were performed on both LV and RV.

5.4.3 *In vivo* monitoring using ultrasound

An ultrasound biomicroscope (Vevo660, Visualsonics, Toronto, ON, Canada) equipped with a 35 MHz center frequency probe (RMV703) was used to image venous flow. The B-mode, pulse-wave Doppler-mode and the new SFSAE-mode images respectively characterized the presence of thrombi, flow velocity and EA. The SFSAE [66;189] parameter is based on a spectral model that allows extracting attenuation compensated mean aggregate diameter *D*, in terms of number of erythrocytes, from analysis of the radiofrequency echoes backscattered by blood. The SFSAE images were

computed slightly upstream of the stenosis using 400 x 400 um regions of interest averaged over 30 images acquired at a frame rate of 5 Hz. Ultrasound measurements were performed at each time point: pre-intervention (d0), 30 minutes post-intervention (d1), days 4 (d4), 9 (d9) and 14 (d14). For the acute study, ultrasound measurements were performed at pre-intervention (d0) and 30 minutes post-intervention (d1) for both LV and RV.

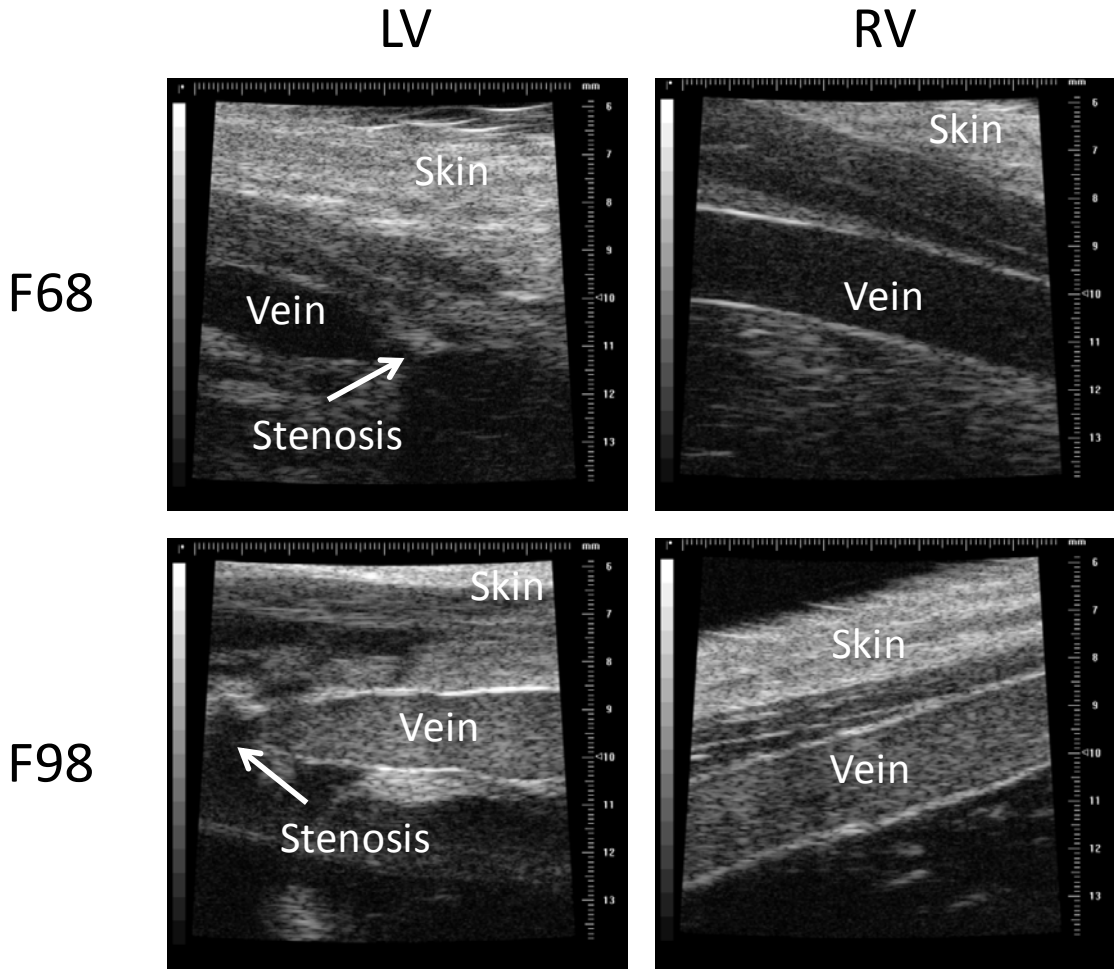

Figure 5-2 : B-mode ultrasound image of prothrombotic left vein (LV) and contralateral control right vein (RV) for F98 transfused rabbit and F68 transfused rabbit. The stenosis is indicated by an arrow in LV.

5.4.4 Laboratory blood tests

White cell, RBC and platelet counts, hemoglobin, hematocrit, prothrombin time and fibrinogen concentration were measured using standard hematology and clinical laboratory methods on samples obtained by venipuncture of the central ear artery on days d0, d1, d9 and d14.

5.4.5 Histology

On d14, a 2 cm section of tissue including the silk suture and the distal portion of the vein of interest was isolated and fixed in formalin for 48 hours. The tissues were then washed, embedded in wax and serially sliced (5 µm) in the axial plane at intervals of 50 µm along the vessel length and stained with H&E. Bright field microscopy examination by 3 independent experts (see acknowledgements) confirmed thrombus presence and general composition.

5.4.6 Statistical analyses

The design included double controls: an inter-individual control group (F98 versus F68) and an intra-individual control side (LV versus RV). All data are means ± standard errors. Aggregation data were analyzed with ANOVA computed using the generalized linear model in SPSS (v.17, SPSS Inc, Chicago, IL), with time and side as repeated measures and group as the independent factor. When interactions were present, local analyses were performed by successively isolating interacting factors. The threshold of significance was set at 5%.

5.5 Results

5.5.1 Blood velocity in veins and thrombus formation

Pre-intervention Doppler mean velocities were 10.0 ± 0.3 cm/s in the left and right femoral veins. In the two acute animals, on d1, a thrombus that stopped flow formed in both veins of the F98 animal but no thrombus was observed for the F68 animal, for which the velocities were reduced by the presence of the stenosis to 4 cm/s.

For the chronic F68 group, the velocity on d1 was similar to acute values at 9.4 ± 0.4 cm/s ($p = 0.73$) in the control RV and significantly reduced to 2.3 ± 0.7 cm/s ($p < 0.001$) in the prothrombotic LV upstream of the stenosis. One animal had a thrombus on d1. After two weeks (d14), the initial thrombus was still present in that animal and no thrombi were found in the other 4 rabbits. Reverse flow was observed for another animal but no thrombus was detected on d1 or on follow-up exams on d4, d9 and d14. For the chronic F98 group on d1, the RV velocity was unchanged compared to d0 (8.2 ± 0.9 cm/s, $p = 0.10$) but complete stasis and thrombi were observed in 4 out of 5 prothrombotic LV on d1. Two of these thrombi were recanalized on d9. For the F98 animal without thrombosis post-intervention, the LV flow was reduced to 1 cm/s on d1 and a thrombus had formed by d9.

When all 7 prothrombotic veins in the F98 transfused group are considered, 6 developed a thrombus on d1, whereas for the F68 group, only 1 out of 7 prothrombotic veins had a thrombus after 30 minutes (Table 1a). These proportions are statistically significant (Fisher exact test, $p = 0.03$), whereas the proportions of thrombi on d14 were not significantly different (Table 1b, $p = 0.52$). As also indicated in Table 1c, the presence of occluding thrombi was confirmed by histology with Haematoxilin / Eosin staining. For the F68 group, 4 out of 5 prothrombotic LV were normal or presented slight neointimal hyperplasia with neoendothelialization that remained confined close to the vessel wall

(Figure 5-3a). In the single F68-treated animal with thrombosis, a young disorganized blood clot was attached to the wall (Figure 5-3b). In the F98 group, prothrombotic LV cross-sections were almost completely obstructed by partially organized thrombi with neointima in 3 out of 5 rabbits (Figure 5-3c and d).

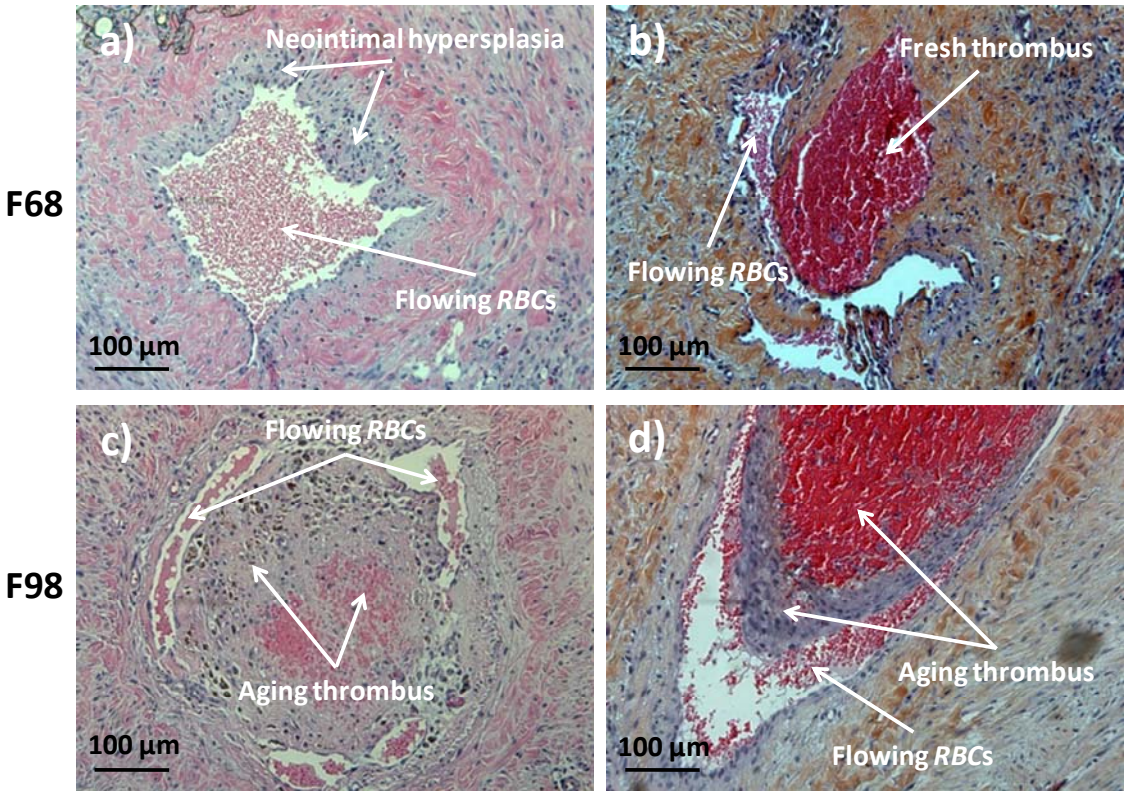

Figure 5-3 : Bright field microscopy of H&E stained cross sections of veins taken upstream of silk suture showing: (a) mural thrombus found in the F68 group LV; (b) disorganized young thrombus in the lone F68 group thrombosed LV; (c and d) completely obstructed lumen by partially organized thrombi from F98 group rabbit LV.

5.5.2 Blood tests

Laboratory measurements for the F98 and F68 groups on d0, d1, d9 and d14 are summarized in Table 2. Two-way ANOVA with time as the repeated factor revealed no statistical differences between F98 and F68 groups for all parameters except the white cell count and fibrinogen. White cell counts were higher in the F68 group on d1, and lower on d9, but only different from the d0 level on d9. Fibrinogen was higher in the F68 group on d1 and different from the d0 level, and was increased in the F98 group on d9 and different from the d0 level. Time following intervention influenced all parameters except prothrombin time: hemoglobin, hematocrit, white and red cell counts significantly decreased after d1, platelets decreased on d1 only in F98 and increased on d9 in F68.

(a)

d1*	Thr	No Thr
F68	1	6
F98	6	1

(b)

d14	Thr	No Thr
F68	1	4
F98	3	2

(c)

Histology	Thr	No Thr
F68	1	4
F98	3	2

Tab. 5-1 : Occluding thrombus (Thr) presence in instrumented veins: (a) 30 minutes post–intervention (i.e., d1) based on ultrasound assessment; (b) at day 14 (d14) pre-harvest based on ultrasound assessment; and (c) after tissue harvest and histology analysis. The proportions were only significantly different (*, $p < 0.05$) between the two groups on d1 based on the Fisher exact test ($p = 0.03$).

	Group	D0	D1	D9	D14
White cell count	F98	6.4 ± 0.7	5.2 ± 0.8	4.4 ± 0.9	2.0 ± 0.5°
			*	*	
[4.0 - 11.0 × 10^9/L]	F68	4.9 ± 0.6	7.3 ± 0.8	1.7 ± 0.5°	1.1 ± 0.3°
Red cell count	F98	5.9 ± 0.2	5.5 ± 0.1	4.5 ± 0.1°	4.0 ± 0.3°
	N.S.				
[4.0 - 5.9 × 10^{12}/L]	F68	6.0 ± 0.1	5.2 ± 0.5	4.8 ± 0.4°	4.5 ± 0.3°
Hemoglobin	F98	128 ± 1	118 ± 4	101 ± 2°	91 ± 6°
	N.S.				
[120 - 180 g/L]	F68	128 ± 2	113 ± 12	105 ± 7°	98± 7°
Hematocrit	F98	0.37 ± 0.01	0.34 ± 0.01	0.30 ± 0.01°	0.27 ± 0.02°
	N.S.				
[0.35 – 0.58]	F68	0.37 ± 0.02	0.33 ± 0.03	0.31 ± 0.02	0.29 ± 0.02°
Platelets	F98	345 ± 93	225 ± 23°	460 ± 45	429 ± 40
	N.S.				
[140 - 450 × 10^9/L]	F68	332 ± 34	304 ± 32	466 ± 25°	353 ± 36
Prothrombin time	F98	8.1 ± 0.1	8.1 ± 0.2	7.7 ± 0.1	7.8 ± 0.1
	N.S.				
[12 – 15 s]	F68	8.2 ± 0.2	7.7 ± 0.3	7.9 ± 0.1	8.0 ± 0.1
Fibrinogen	F98	2.5 ± 0.1	2.7 ± 0.3	4.0 ± 0.5°	3.1 ± 0.3
			*	*	
[2.0 – 4.5 g/L]	F68	2.4 ± 0.1	4.6 ± 0.7°	2.7 ± 0.2	2.4 ± 0.1

Tab. 5-2 : Blood analysis pre-intervention (d0), 30 minutes post-intervention (d1) and on days 9 (d9) and 14 (d14). ° indicates significant difference ($p<0.05$) from value at d0. * indicates significant difference ($p<0.05$) between F68 and F98 groups. N.S.: not significant. When interactions were present, local analyses were performed using Tukey multiple comparison procedures. Values are mean ± standard error, N = 5 / group.

5.5.3 *In vivo* RBC aggregation monitoring

Figure 5-4 shows examples of SFSAE images of parameter *D* in the control RV and upstream of the prothrombotic LV of a F98 transfused rabbit on d1.

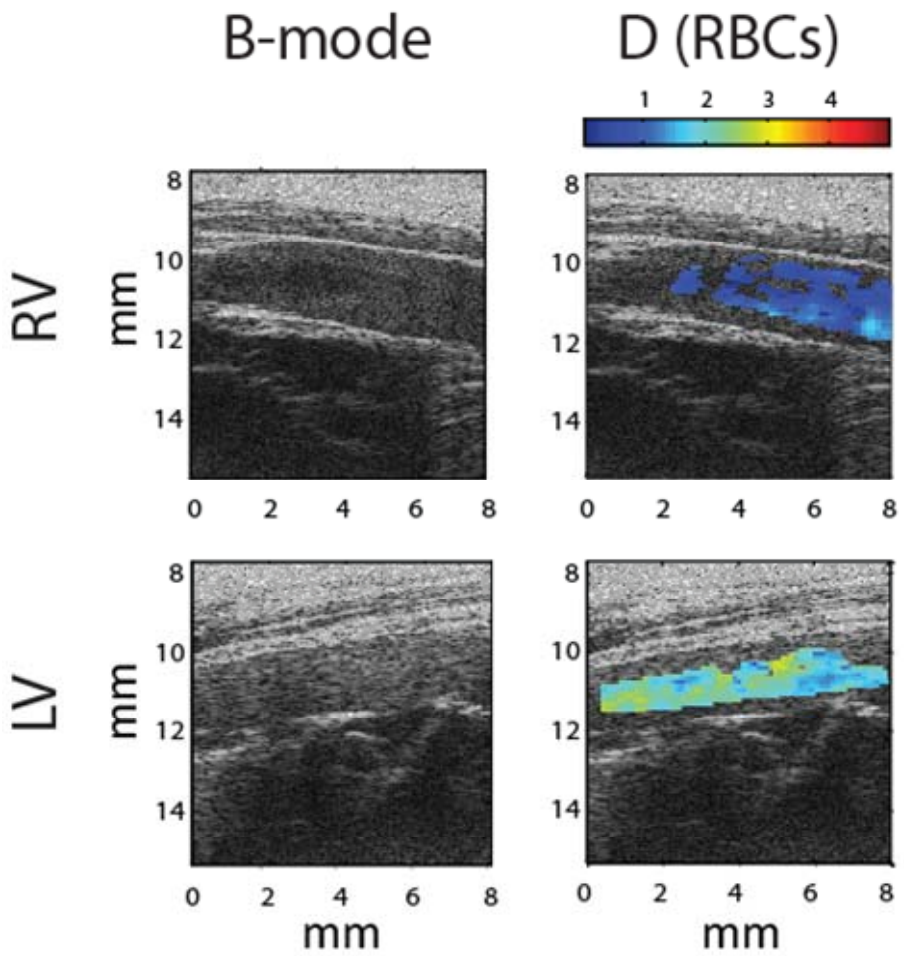

Figure 5-4 : B-mode image and superimposed parametrical images of *in situ* RBC aggregation level using structure parameter *D* for one F98 rabbit in LV and RV on d1. The SFSAE model was previously validated *in vitro* for $D < 8$ [66].

Spatially averaged values of *D* for all animals are reported in Figure 5-5. In RV, group and time had no effect on *D,* whereas in the LV, *D* values were significantly higher in F98 versus F68 on d1 only. In the F98 group, *D* was significantly higher in LV compared with RV on d1, d4 and d9 but not on d0 and d14. *D* of LV with F98 were significantly higher on d1 compared to all other measurement times. To summarize, the SFSAE could differentiate the level of aggregation through the skin *in vivo* and *in situ*: (i) between groups with different aggregation tendencies; (ii) for different flow conditions; and (iii) at different times for blood with hyperaggregation tendencies.

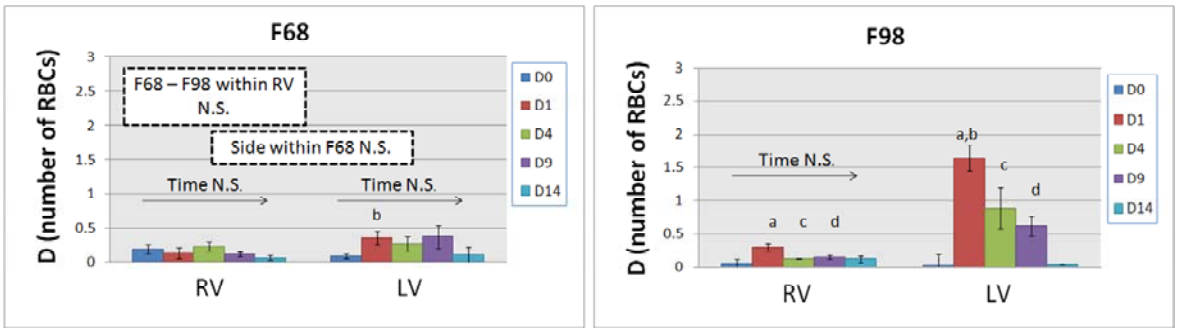

Figure 5-5 : Aggregate size *D* (estimated average aggregate diameter expressed in number of RBCs) pre-intervention (d0), 30 minutes post-intervention (d1), and on days 4 (d4), 9 (d9) and 14 (d14) for the control F68 group and the hyperaggregating F98 group. A stenosis and endothelial damage was performed in LV on d1 whereas no intervention was performed in RV. Significant differences were found for *D* in F98 group between LV and RV on d1 (a), d4 (c) and d9 (d), and between d1 and all other time points within LV in F98. On d1, significantly different values of *D* were found between F68 and F98 (b). N.S. represents non significant statistical difference.

5.6 Discussion

5.6.1 EA and acute DVT

This study was designed to experimentally assess whether abruptly increasing EA could provoke the formation of a DVT in a rabbit femoral vein subjected to calibrated partial occlusion and mechanical damage. Most DVT animal models are variants of the Wessler model [180], which consist in fully occluding the vessel and administrating a thrombogenic trigger, such as a local injection of thrombin or thromboplastin, or causing a mechanical, electrical or chemical vessel injury. Such models systematically form thrombi and are not well suited for our purpose. The DVT model used herein rather involved calibrated venous flow reduction and endothelial damage to preserve blood flow and mimic thrombogenic regions, such as a low flow recirculation zone behind a venous valve, for example. Such a model is better adapted for identifying hemorheological DVT risk factors such as EA.

The experimental protocol with blood exchange did not seem to induce confounding effects likely to explain this higher occurrence of thrombosis in F98 transfused animals. Indeed, as noted in Table 2, no differences were found between groups on d1 except for fibrinogen and white cell count that were significantly higher in F68 rabbits. The fibrinogen level also increased from d0 to d1 in that group. A mild surgery related inflammatory state increasing fibrinogen in both groups but with concomitant fibrinogen consumption during thrombus formation only in F98 animals could explain these variations. Similarly, the inflammatory-related increase in white cell counts in the F68 group on d1 could suggest a higher leukocyte recruitment and extravasation in F98 transfused rabbits. Indeed, enhanced leukocyte margination (i.e., displacement toward the wall) due to enhanced EA located mainly near the vessel center [73;77;131] could promote DVT through the accumulation of leukocytes on platelet thrombi [95] and

increased tissue factor expression by activated leukocytes [56;126]. From d0 to d1, the platelet count decreased in the F98 group. This can also be explained by enhanced platelet margination related to enhanced EA [72;73;122] promoting collisions, wall adhesion, activation of platelets and thrombus formation through the direct impact of increased EA.

Since an increase in EA was the sole factor preferentially promoting DVT in the F98 group, our results suggest that the viscosity increase caused by EA in that group further reduced the flow in the stenosed LV, thus inducing stasis and contributing to thrombosis [50], most likely also due to a synergistic role of blood viscosity on increased leukocyte and platelet margination. In the control F68 group, the prothrombotic threshold for an occluding thrombus to form was not met despite identical flow reducing and endothelial damaging interventions.

5.6.2 A new tool for local EA characterization

This study was also the first *in vivo* demonstration that quantitative ultrasound (SFSAE) can characterize EA with sufficient sensitivity to monitor its variations over time within different vascular beds (Figure 5-5). Measuring aggregate size *in situ* using ultrasound represents a major improvement over *in vitro* analyses of systemic EA with anticoagulated blood. Indeed, laboratory measures inherently overlook confounding variables such as flow conditions, vascular tone regulation, presence of collateral vascular beds or local release of pro-aggregating agents such as activated polymorphonuclear leukocytes [16] and superoxide anions [17], whereas the SFSAE can measure EA under actual flow conditions in the macrocirculation in a region of interest. The axial and lateral resolutions of SFSAE images at 35 MHz (400 × 400 µm) are still limited but permitted to characterize regional variations in this study.

It is expected that such local assessment of EA using ultrasound could shed some light on discrepancies previously reported on the effect of fibrinogen on DVT [50;52;173]. Based on our results, we hypothesize that it is not fibrinogen itself but rather its effect on

EA that is the risk factor triggering DVT in humans. Indeed, zones of reduced flow in the elderly , caused by a decreased flow mediated endothelium dependant dilation in that group age [130], could initiate a vicious cycle of increased EA, increased viscosity and further reduced flow leading to increase risk of DVT in that subgroup. In the younger patients, the viscosity increase could be efficiently offset by potent vascular dilation. The existence of compensatory interactions between EA induced hemodynamic perturbations and vascular bed dilation reserve have been suggested [117]. Similarly, locally reduced flow conditions, favorable to a first thrombus episode, could also plausibly explain why fibrinogen is a risk factor for DVT recurrence (i.e., same reduced flow conditions favorable to EA after thrombus lysis or recanalization) but not consistently for an initial DVT since local flow conditions can vary from patient to patient. These hypotheses can be elegantly tested non-invasively using the SFSAE.

5.6.3 Pluronics–coated RBC transfusions used as an hyper-EA animal model

There is growing evidence that inflammation promotes DVT by elevating tissue factor expression by the endothelium and leukocytes, fibrinogen synthesis, platelet reactivity and by down regulating fibrinolytic activity [55]. Because EA is also modulated by the plasmatic concentration of acute phase proteins such as fibrinogen, C-reactive protein, haptoglobin and ceruloplasmin [179], we modulated EA by transfusing Pluronic-coated erythrocytes in our animal model to essentially eliminate confounding effects due to inflammatory proteins. This approach does not, however, exclude the possibility that EA could amplify the inflammatory reaction (e.g., through leukocyte activation) but does demonstrate that the observations are not caused by inflammation alone. Other approaches include *in vivo* EA modulation using dextrans of different molecular weights [23]. However, dextran is also known to enhance fibrinolysis by activating the fibrinolytic pathway [91] and it affects plasma viscosity [8], as well as the obvious plasma dilution

effect of infusing a colloid, which may be confounding factors for DVT. Transfusions of Pluronic-coated red cells have been previously and successfully used to modulate EA *in vivo* [18;183;185], and has major advantages in that (i) the F98-coating enhances the intrinsic RBC aggregation properties alone without affecting plasma protein concentration; and (ii) the effect of the polymer coating can be controlled for by using a neutral, lower molecular weight molecule (F68). Pluronics are non toxic and have found numerous applications in areas of biomaterials, drug delivery and cardiovascular therapeutics [3].

In the present study, the long term effects of increased aggregation on thrombus evolution were monitored for two weeks. In this span, the effect of increased aggregation on DVT was not sustained in our experiments as 2 out of 5 thrombi from the F98 group had retracted at d9. This fading over time could have been due to the decrease in aggregation after d1 in the F98 group (Figure 5-5) due to accelerated clearance of F98 coated RBC. In a separate preliminary experiment (data not shown) blood was obtained by exsanguinations of exchange-transfused animals on d1, d9 and d14, adjusted to 40% hematocrit and EA levels were measured *in vitro* using the SFSAE method. In the F68 samples *D* was close to zero (no aggregation). In the F98 samples, *D* systematically decreased from d1 to d14, strongly suggesting clearing of coated cells. Clearance of coated cells has been shown in a similar rat transfusion protocol by a microscopy analysis [18]. In Table 2, clearing of coated RBC in both groups can also explain why RBC count, hemoglobin and hematocrit which decreased with time from d1. After d1, involvement of white cells in the RBC clearing process could explain the diminution of white cell count. A very mild inflammatory state, as mentioned before, could be responsible for elevated fibrinogen and white cell count in the F98 group on d9. The origin of this observation remains otherwise unexplained. The slight increase in platelets in the F68 group on d9 is not explained either but is very close to normal values and similar in both groups.

5.6.4 Clinical implications and conclusions

The determination of the optimal prophylactic oral anticoagulation duration is essential to prevent DVT recurrence and bleeding complications. Clinical studies have established that a 3 month duration was optimal for DVT provoked by transient risk factors [1;30]. For permanent risk factors, treatment duration can be established on specific individual risk profiles. For example, in the presence of active cancer, long term anticoagulation is indicated because the risk of recurrence is higher than the risk of bleeding [151]. However, some controversies remain concerning DVT of idiopathic origins. Some studies suggest increasing anticoagulation period [93] but others suggest that it only affects the risk versus time, as the incidence of recurrence in short and long term therapy groups after treatment discontinuation seems to balance out[1;2]. It is disconcerting to observe that idiopathic DVT is being considered as a risk factor in itself, especially when considering how often the situation occurs. Determining and understanding other mechanisms implicated in DVT would certainly improve risk profiling and anticoagulation therapy in clinical practice, but also open the way for new strategies in prevention and treatment not solely aimed on anticoagulation.

In conclusion, our study demonstrated that locally increased EA is not merely a secondary surrogate marker of inflammation but can itself trigger thrombus formation. Quantitative ultrasound is a unique tool allowing non-invasive, *in vivo* and *in situ* characterization of EA. Our results strongly suggest that monitoring hemorheology locally could help prevent triggering of thrombus formation and optimize prophylaxis strategies.

5.7 Acknowledgments

The authors wish to thank Dr. Hélène Héon, Dr. Shujie Qi and Ms. Nancy Beauchemin for their inestimable expertise in the animal procedures, Ms. Annie Major,

Dr. Igor Salazkin and Dr. Louis Gaboury for helping with histological analyses and Mr. Miguel Chagnon for help with the statistical analyses.

5.8 Sources of fundings

This work was supported by grants from the Canadian Institutes of Health Research (#MOP-84358 and #CMI-72323), Heart and Stroke Foundation of Canada (#PG-05-0313), National Institutes of Health of USA (#R01HL078655), and Natural Sciences and Engineering Research Council of Canada Ph.D. scholarship program (#ES D3-317051 - 2005).

5.9 Disclosures

None.

5.10 Online data supplement

5.10.1 Blood collection

Donor rabbits were used for blood supply. Blood was collected in 14% V/V citrate phosphate dextrose adenosine (CDPa, Baxter Corporation, Toronto, ON, Canada) by abdominal aorta exsanguination under anesthesia. Animals received a pre-medication subcutaneously consisting of 0.8 mg/kg metedomidine (Domitor, Pfizer Animal Health, New York, NY) and 0.01 mg/kg glycopyrrolate (Glycopyrrolate, Sandoz Canada, Boucherville, QC, Canada). Anesthesia was induced with an intravenous injection of 5 mg/kg ketamine (Ketalean, Bimeda-MTC Animal Health Inc., Lavaltrie, QC, Canada) and 0.5 mg/kg midazolam (Midazolam, Sandoz Canada, Boucherville, QC, Canada), and maintained with 2% isoflurane (Isoflo, Abbott Laboratories, St-Laurent, QC, Canada) in 100% oxygen until the sacrifice of the animal. Collected blood was then coated as described below.

5.10.2 Blood preparation

To control the aggregation tendency of erythrocytes, the covalent attachment of Pluronic copolymers F68 and F98 to the *RBC* surface was employed [8;18;183;185]. The protocol is described in detail in these articles. Briefly, Pluronics are block copolymers comprising a central poly(propylene glycol) -PPG- chain flanked by two poly(ethylene glycol) -PEG- chains. In aqueous solution, these copolymers micellize (self-aggregate) at a critical temperature primarily dependent on the molecular weight of the PPG core and copolymer concentration. By utilizing the known micellization behavior of Pluronics, following covalent attachment of its derivatized form to the RBC surface, it is possible to create erythrocytes with defined aggregation tendencies. Covalent attachment to the RBC surface was facilitated by first synthesizing a succinimidyl carbonate reactive derivative of the Pluronic prior to incubation with washed RBC [8;18;183;185]. In the present study, the concentration of the activated Pluronics during the coating process was 0.75 mg/ml of suspension at 10% hematocrit. At 37°C, this coating concentration of F98 increases RBC aggregation whereas F68 has essentially no effect on aggregation (Figure 5-1). Since rabbit blood forms few aggregates naturally, the F68 group can thus be considered as a low aggregating model and serves as an appropriate control for the polymer coating. Once the coating process was completed, RBC were refrigerated at 4°C overnight prior to transfusion.

6 Chapitre 6 : Discussion – conclusion

La caractérisation ultrasonore de l'agrégation érythrocytaire est un outil prometteur. Il est applicable *in vivo* et *in situ*, non invasif, rapide (d'où la possibilité d'une application en temps réel permettant un suivi en monitoring) et peu dispendieux (peut être intégré aux échographes cliniques ou à un appareil portable de monitoring). Pour caractériser le sang, un tissu dynamique dont les propriétés dépendent des conditions d'écoulement, ce sont des qualités fort intéressantes. Le développement d'un tel outil se heurte toutefois à deux problèmes fondamentaux : d'une part la caractérisation de l'agrégation par l'intensité du signal rétrodiffusé souffre de la complexité des relations hématocrite-fréquence lorsque les globules s'agrègent; et d'autre part l'atténuation des ondes ultrasonores par les tissus interposés modifie l'intensité et le contenu spectral du signal rétrodiffusé *in vivo*. L'approche spectrale préconisée dans ces travaux permet de surmonter ces limitations. Nous dressons dans ce chapitre le bilan des avancées ainsi que les limitations et perspectives de notre approche spectrale par le SFSE et le SFSAE. Quelques pistes pour améliorer le modèle et des perpectives futures sont également abordées.

6.1 Résumé et originalité du travail

Cette thèse décrit le développement et la validation de la caractérisation de l'agrégation érythrocytaire par une méthode ultrasonore spectrale quantitative paramétrique, menant à une application clinique sur la problématique de l'hyper-viscosité sanguine comme facteur de risque de la thrombose veineuse. Le problème a été considéré

sous les hypothèses de Born (diffuseurs faibles, pas de diffusions multiples) pour des globules rouges fluides (pas de comportement élastique). Le coefficient de rétrodiffusion est alors modélisé par le produit de la densité volumique *m*, de la section de rétrodiffusion $\sigma_b(k)$ et du facteur de structure $S(-2k)$. Ce modèle considère que la variation du *BSC* lorsqu'il y a agrégation érythrocytaire est due à un changement microstructurel dans le positionnement des globules, pris en compte entièrement par le facteur de structure. Ce dernier est lié au positionnement des globules *N(x,y)* et à la fonction de corrélation de paire *g(r)* par une transformée de Fourier. Cette approche intègre également les interactions partiellement cohérentes qui surgissent lorsque la densité des globules augmente à des hématocrites supérieurs à 5% pour des suspensions de globules rouges non agrégeants et, plus particulièrement, lorsque les globules s'agrègent. Cette approche est unique dans le domaine de la caractérisation tissulaire ultrasonore qui ne considère généralement que les interactions incohérentes et négligent du même fait l'impact de l'organisation structurelle des diffuseurs [159].

La validation expérimentale du modèle a été possible grâce à une approximation en série de Taylor au second ordre en fréquence du facteur de structure baptisée « *Structure Factor Size Estimator* », permettant la paramétrisation du problème à l'aide de deux paramètres microstructuraux, *W* et *D*. L'approche a tout d'abord été validée dans un écoulement cisaillé homogène à l'aide de trois transducteurs mono-éléments. Ces travaux ont été rapportés dans le chapitre 3 Cette étape a permis de valider la méthode de normalisation permettant d'obtenir le *BSC* à l'aide de plusieurs transducteurs focalisés large bande. Le paramètre *D* a pu alors être validé à faible hématocrite par une analyse en microscopie. La méthode a ensuite été généralisée et validée en 2D afin d'établir des images paramétriques pour des sangs présentant différentes tendances agrégeantes dans des écoulements tubulaire et à cisaillement homogène. Dans cette étude, rapportée dans le chapitre 4, la sensibilité du SFSE à la présence de niveaux d'agrégation transitoires, par

exemple au centre d'un tube (phénomène du « trou noir ») a également été démontrée. Cette propriété est fort importante car des niveaux d'agrégation transitoires sont vraissemblablement existant *in vivo* et impliqués dans la physiologie circulatoire. Nous remarquons ici que des cinétiques d'agrégation ont été mesurées *in vitro* et *in vivo* (voir les annexes A et B), ce qui contitue un autre témoignagne de la bonne résolution temporelle de la méthode. Par ailleurs, l'approximation au second ordre de *S(-2k)* par le SFSE et le SFSAE se révèle doublement intéressante : d'un côté elle permet de s'affranchir de grandeurs ultrasonores (coefficient de rétrodiffusion, pente spectrale, midband-fit) au profit de paramètres microstructuraux *W* et *D* décrivant l'organisation du tissu en des termes physiques; d'autres part l'approximation au second ordre s'avère suffisante pour permettre une estimation de l'atténuation α_0 causée par les tissus localisés entre la sonde et le sang, ce qui est incontournable pour une application *in vivo* cette approche ultrasonore paramétrique. Cette extension de la méthode a été nommée SFSAE ou « *Structure Factor Size and Attenuation Estimator »* [66]. La possibilité d'imager l'agrégation érythrocytaire *in situ* dans la macro-circulation est unique dans le domaine de la biorhéologie. Puisque la viscosité sanguine est principalement une fonction de l'agrégation, l'établissement par extrapolation de cartes locales de viscosité est également unique à la méthode ultrasonore et a été abordée au chapitre 4. Finalement, le SFSAE a été utilisé dans une étude expérimentale animale démontrant l'applicabilité *in vivo* de la méthode : l'agrégation a été quantifiée et démontrée significativement différente entre les deux groupes expérimentaux de lapins, entre les veines fémorales gauche et droite dans le groupe cible et dans le temps. L'intérêt d'une mesure locale *in vivo* de l'agrégation est évidente puisque qu'aucune différence d'agrégation n'a été mesurée du coté contra latéral de contrôle entre les deux groupes expérimentaux, et ce même pour le groupe hyperagrégeant. Si le sang avait été prélevé pour effectuer des analyses *in vitro* au laboratoire, de telles differences locales n'auraient pu être décelées. Une mesure *in vitro* en laboratoire rique donc de surestimer ou sous estimer l'impact réel local de l'agrégation

sur l'hémodynamie *in vivo* et la pathophysiologie de la thrombose veineuse. Cette étude suggère que les propriétés hémorhéologiques locales ont un impact sur la pathophysiologie aigue des thrombus veineux. et qu'elle porte une information nouvelle pertinente dans l'établissement du profil de risque de thrombose veineuse.

6.2 Propriétés, limites et perspectives des paramètres *W* et *D*

La caractérisation ultrasonore est encore peu utilisée aujourd'hui dans les domaines de la biorhéologie et de l'hémorhéologie clinique. Une des raisons est sans doute que la physique des interactions « ultrasons – globules rouges » est jugée trop complexe et dépendante de trop de paramètres (fréquence, hématocrite, atténuation). Sous l'hypothèse que l'hématocrite est connu, notre approche par le SFSE et le SFSAE permet de s'affranchir des deux autres facteurs confondants à l'aide de deux paramètres microstructuraux *W* et *D*.

6.2.1 Signification physique

Le facteur de structure $S(-2k)$ -comme son nom l'indique- reflète la structure microscopique des diffuseurs ultrasonores, c'est-à-dire de l'organisation spatiale des globules rouges.

En effet, des observations expérimentales ont démontré que *BSC(k)* variait avec l'agrégation des globules qui, si l'on se rapporte à la formulation de l'équation 2.13, est entièrement pris en compte par $S(-2k)$ puisque m et $\sigma_b(k)$ ne varient pas avec l'agrégation. Le SFSE est fondé sur une approximation au second ordre de $S(-2k)$ qui permet, dans la mesure où certaines hypothèses sont vérifiées (diffusion de Born, validité de l'approximation de $S(-2k)$ au second ordre, agrégats de conformations isotropes),

de décrire l'agrégation par *W* et *D.* Ces deux paramètres décrivent la microstructure des tissus en des termes ayant un sens physique qui dépasse les propriétés d'échogénicité du tissu.

6.2.1.1 Le facteur d'entassement *W :*

W est le facteur d'entassement. Il est relié à la compressibilité isothermale ξ_T par $W = mK_bT\xi_T$ [170] où K_b est la constante de Boltzmann et *T* la température absolue. Lorsqu'il n'y a pas d'agrégation, 0 < *W* < 1 et diminue avec la concentration des globules (voir figure 2.5). *W* s'exprime alors en fonction de *H*, ce qui lui confère une borne minimale à *H* fixe (voir les équations 2.8 et 2.9). Pour mieux comprendre et prédire *W* en fonction de l'agrégation et de l'hématocrite, on peut se rapporter à un modèle théorique d'adhésion de Baxter [140], qui s'applique à des sphères dures agrégeantes et qui possède une expression analytique du facteur de packing $W_{Baxter} = S(k \to 0)$ et qui peut être considéré en première approximation pour illustrer et interpréter le comportement de *W* en fonction de l'agrégation et de l'hématocrite:

$$S(0) = (2A)^{-2} \tag{6.1}$$

avec

$$A = 0.5(1 + 2H - \mu)(1 - H)^2$$
$$\mu = \iota H(1 - H)$$
$$\iota = \min\Big(6[\tau H^{-1} + (1 - H)^{-1}] \pm \{36[\tau H^{-1} + (1 - H)^{-1}]^2 -$$
$$12H-11+0.5H1-H-212$$

$A, \mu\ et\ \iota$ sont des paramètres du modèle qui dépendent de τ. τ^{-1} est le facteur de collage (« *stickiness parameter* ») du modèle. W_{Baxter} est représenté à la Figure 6-1 en fonction de τ^{-1} (lignes continues et pointillées). On peut observer que lorsqu'il y a

agrégation (augmentation de τ^{-1}), W_{Baxter} augmente et varie d'une manière unimodale en fonction de l'hématocrite avec un maximum autour de H = 20%. W_{Baxter} peut prendre des valeurs supérieures à 1 lorsqu'il y a agrégation, un phénomène que nous avons également observé expérimentalement pour W avec le modèle SFSE ou SFSAE.

Ainsi, il peut être théoriquement proposé, dans les limites d'applicabilité de l'approximation de notre problème par une suspension de sphères dures agrégeantes, de mesurer W en fonction de H afin de déterminer τ^{-1} qui est relié à l'énergie d'adhésion interglobulaire. Afin de vérifier la faisabilité de cette approche, quelques mesures expérimentales préliminaires de W ont été effectuées à l'aide du SFSE sur deux types de sang agrégeants, dans un écoulement au cisaillement homogène de Couette, mesurés à différents H. Ces résultats sont superposés sur les courbes théoriques dans la Figure 6-1. Dilution 1 est une suspension de globules rouges porcins dans une solution de dextran (poids moléculaire de 512 kDa) à une concentration plasmatique de 40 g/L constante; dilution 2 est une suspension de globules rouges porcins dans une solution à une concentration de dextran (poids moléculaire de 512 kDa) par globule rouge constante (ces deux types de sang ont été testé car les deux types de dilution peuvent être envisagées dans les études *in vitro* pour obtenir les différents hématocrites). Lorsqu'il y a peu d'agrégation (lorsque le cisaillement est supérieur à 10 s^{-1}, le modèle de Baxter prédit relativement bien le comportement de W evalué par le SFSE, particulièrement pour la dilution 2. Un cisaillement de 20 s^{-1} et de 10 s^{-1} avec pour la dilution 2 correspondent respectivement aux courbes de $\tau^{-1} = 0$ et $\tau^{-1} = 6$. Lorsque l'agrégation augmente encore (cisaillement de 2 s^{-1}), le modèle de Baxter ne correspond plus aux données expérimentales. On peut se demander si l'approximation par des sphères dures a atteint ses limites d'applicabilité. W_{Baxter} montre néanmoins un maximum de W vers H = 15% et une faible diminution à plus hauts hématocrites. Ce comportement en plateau pour H élévé a été observé pour du sang agrégeant en utilisant une technique ultrasonore

Doppler (puissance doppler) [157] dans un tube. Si ces résultats préliminaires demandent d'être confirmée par plus d'expériences, une tendance peut néanmoins être observée : dans la limite où les globules rouges peuvent être assimilés à des sphères dures, *W* semble mieux suivre les tendances prédites par W_{Baxter} lorsque la concentration de dextran par globule est contante. Pour une concentration de dextran constante dans du plasma, les données expérimentales à faible hématocrite suggèrent que l'on change de valeur de τ^{-1}, ce qui est cohérent avec la notion que la concentration de dextran par globule augmente lorsque *H* diminue. Cette approche est un premier pas vers une comparaison du niveau d'agrétation entre des échantillons agrégeants ayant des hématocrites différents.

La Figure 6-1 indique clairement que W_{Baxter} dépend fortement de *H*. L'estimation de *W* par le SFSE et le SFSAE permet donc de quantifier l'agrégation seulement pour *H* constant ou mieux lorsque *H* est connu. Lorsque *H* change, les comparaisons de niveaux d'agrégation en utilisant *W* sont plus complexes. Par exemple comment comparer une valeur de W_1 pour H = 25% chez le patient 1 avec W_2 pour H = 40% chez le patient 2 ? Des grilles en fonction de τ^{-1} telles qu'établies par le modèle de Baxter seraient une approche pouvant pallier à ce problème. Des modèles intégrants la déformation et la forme des globules serait toutefois souhaitables.

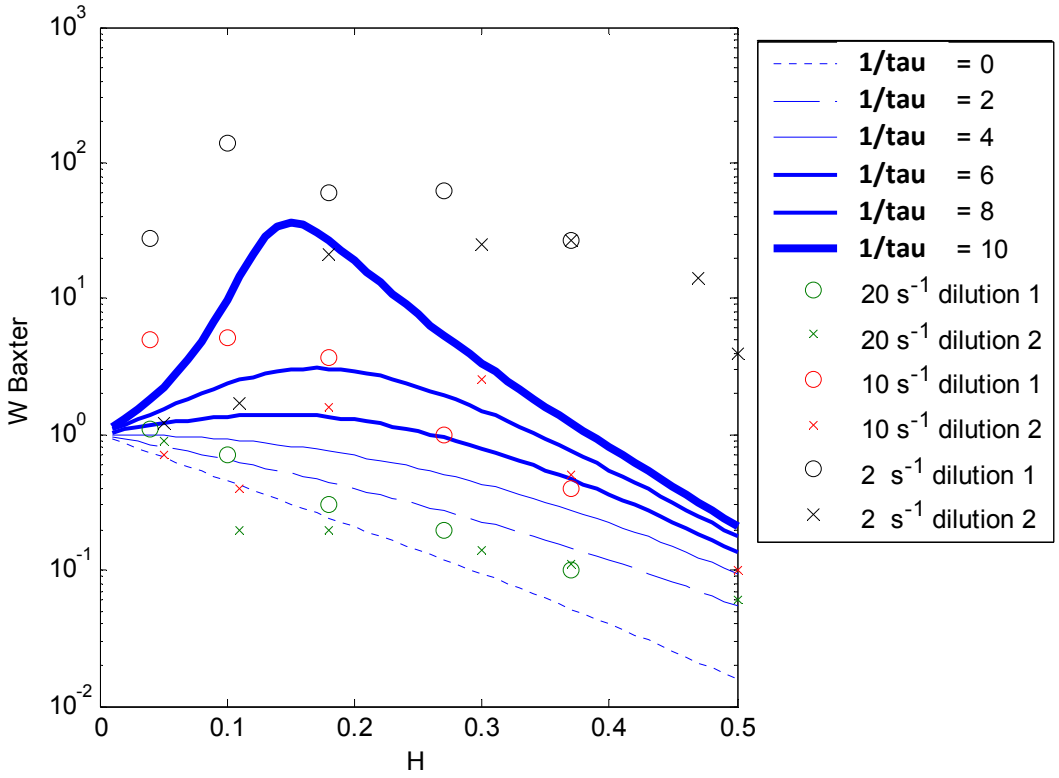

Figure 6-1 : W_{baxter} pour des sphères dures en fonction d'un index de collage de Baxter (« *stickiness parameter* ») en fonction de l'hématocrite *H*. Des mesures expérimentales obtenues dans le Couette à différents cisaillements sont superposées aux courbes théoriques pour deux types de sang. Dilution 1 est une suspension de globules rouges porcins dans une solution de dextran (poids moléculaire de 512 kDa) à une concentration plasmatique de 40 g/L constante. Dilution 2 est une suspension de globules rouges porcins dans une solution dont la concentration de dextran (poids moléculaire de 512 kDa) par globule est constante (40 g/L à *H* = 40% comme référence).

6.2.1.2 La taille moyenne des agrégats *D*

La paramétrisation du facteur de structure proposée dans ces travaux considère les diffuseurs élémentaires comme des diffuseurs de Rayleigh. Les globules rouges sont donc

approximés par des sphères dures de volume équivalent. Cela est juste du point de vue de la diffusion acoustique aux fréquences utilisées dans cette étude (voir paragraphe 2.3.1). On sait toutefois que les globules ne sont pas sphèriques mais ont plutôt une forme biconcave déformable. Leurs intéractions ne sont donc pas assimilables à celles de sphères dures, mais cette approximation a néanmoins été faite dans la détermination du paramètre *D*. Ce choix se justifie par le fait que la réelle structure tridimentionelle de rouleaux entrebranchés constitue une complexification importante du problème. Ainsi, le paramètre *D* a été abordé en toute première approximation comme le diamètre moyen isotrope équivalent à celui des réels agrégats entrebranchés. Si l'on se rappelle que se sont des caractéristiques de l'ensemble des diffuseurs contenus dans la fenêtre acoustique qui sont estimés, cette simplification est acceptable. Malgré cette limitation isotrope, le paramètre *D* a été validé par une évaluation optique pour du sang agrégeant à un hématocrite de 6% (voir chapitre 3) et en simulation 2D à l'aide du modèle de formation d'image ultrasonore linéaire de Bamber et Dickinson [12]. Dans les deux cas, *D* et R_g était significativement corrélés avec la taille des agrégats. Une validation plus précise du paramètre *D* pourrait être faite par des simulations en 3D [145] dans lesquels la densité microscopique *N(x,y,z)* est connue, ce qui pourrait permettre de déterminer avec plus de précision la relation entre R_g et *D.*

Il est toutefois évident qu'une approche permettant de prendre en compte la réelle structure des agrégats représente un beau défi à relever. Une description par des structures fractales serait sans doute souhaitable pour tenir compte de la morphologie complexe des agrégats. Une approche du type $D = N^{\frac{1}{d}}$ ou *N* est le nombre de globules de l'agrégat et *d* sa dimension fractale pourrait être considérée. Une dimension fractale *d* = 1 correspond à des agrégats linéaires et *d* = 3 à des agrégats sphériques compacts. Une valeur entre 1 et 3 correspond donc à des structures tridimentionnelles plus ou moins allongées. Une dimension fractale $2 < d < 2.3$ permet de décrire des structures

tridimensionnelles réversibles et poreuses [162]. Il serait donc aisé en posant cette hypothèse d'établir le lien entre *D* et le nombre de globules d'un agrégat. Cette approche n'a pas été retenue dans les résultats présentés dans cette thèse car la dimension fractale des agrégats porcins, différents des agrégats humains, n'est pas connue et dépend sous toute vraisemblance des conditions d'écoulement. On pourrait s'attendre à $2.3 < d$ puisque les agrégats porcins sont plus compacts que les agrégats humains mais la variation de *d* en fonction du cisaillement est inconnue. Ce projet peut passer par des travaux de simulation dans lesquels differentes structures plus ou moins isotropes seront étudiées et comparées. La sensibilité des ultrasons à l'anisotropie des agrégats a d'ailleurs été démontrée *in vitro* [5] et *in silico* [64]. Pour atteindre un tel degré de raffinement et de précision, il faudra considérer un montage expérimental permettant l'acquisition des signaux selon plusieurs angles, *in vitro* et surtout *in vivo*.

6.2.2 Limitations et projets futurs

6.2.2.1 Limite d'applicabilité en fréquence : effets sur le biais et la variance des estimés

Puisque le SFSE est une approximation au second ordre en fréquence du facteur de structure, il est évident qu'une borne supérieure en fréquence existe pour le modèle. En fait, cette limite peut être quantifiée en terme du produit adimensionnel *k*D*a*. Lorsque l'agrégation devient importante et que *D* augmente, on peut s'attendre à ce que la borne supérieure en fréquence d'applicabilité du modèle diminue. Il est proposé ici d'étudier l'effet d'une modification de la largeur de bande utilisé par le SFSE en réduisant artificiellement la limite supérieure des spectres, même si les acquisitions ont été faites avec toute la bande passante (9-28 MHz). On veut ainsi étudier les comportements de *W* et *D* en fonction de la largeur de bande utilisée par le SFSE. Un critère permettant de quantifier la performance du modèle est de calculer le coefficient de corrélation entre les

données expérimentales et les résultats de la modélisation par le SFSE. Des résultats expérimentaux typiques obtenus pour différents types de sang à l'aide du modèle SFSE sont présentés à la Figure 6-2 sur une échelle semi-logarithmique (ces données proviennent de la Figure 4-3). Sur une largeur de bande comprise entre 9 et 28 MHz, le SFSE suit bien la dépendance fréquentielle de *BSC(f)* puisque la corrélation $r^2 > 0.88$ lorsque $D < 13.7$. Cela correspond à $k*D*a < 4.3$ calculé à $f = 28$ MHz.

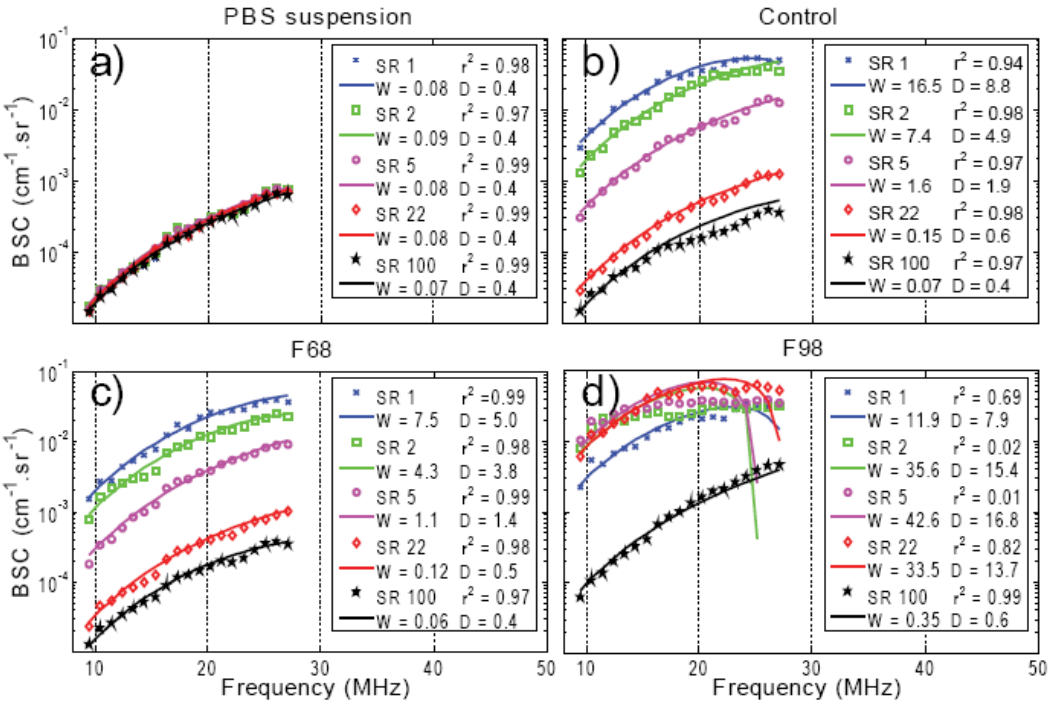

Figure 6-2 : Données expérimentales et courbes modélisées par le SFSE à différents taux de cisaillement (SR) pour: (a) une suspension non agrégeante, (b) du sang porcin dans du plasma, (c) des globules traitées avec du Pluronics F68 (contrôle) dans du plasma et (d) des globules rouges traités avec des Pluronics F98 (modèle hyperagrégeant) dans du plasma. Les valeurs de *W*, *D* et le coefficient de corrélation r^2 correspondant sont reportés dans la légende.

Afin d'illustrer l'effet du produit $k_{max}*D*a$ sur le SFSE, quatre exemples typiques ont été sélectionnés parmis les données de la Figure 6-2 pour des niveaux d'agrégation différents. k_{max} est le nombre d'onde correspondant à la fréquence maximale F_{max} de la bande passante utilisée pour le SFSE. La borne inférieure de fréquence demeure inchangée. Les mêmes données ont été utilisées pour tous les résultats mais sont exploités sur des bandes passantes différentes. Ces résultats sont présentés à la Figure 6-3 en fonction de F_{max}. On rappelle que $F_{max} = \frac{c}{2\pi} k_{max}$.

Pour les niveaux d'agrégation les plus faibles ($D < 14$), une diminution de k_{max} a peu d'effet sur D. Les courbes de *BSC(f)* en fonction de la fréquence sont superposées et r^2 est proche de 1. On peut noter une augmentation de la variance de D lorsque k_{max} diminue. Lorsqu'il y a une agrégation forte ($D > 14$), le SFSE ne donne pas de bons résultats puisque r^2 diminue pour tendre vers 0. En effet, les courbes de *BSC(f)* en fonction de f ne modélisent pas bien les valeurs expérimentales. Par contre, lorsque la limite supérieure k_{max} est diminuée, r^2 augmente et les valeurs de D se stabilisent. Si k_{max} est encore diminué, la variance de D augmente. Un compromis existe donc entre une largeur de bande réduite permettant la prise en compte de plus gros agrégats au prix d'une plus grande variance dans les estimations de D. Ce critère peut être testé à l'aide de r^2. Un comportement similaire a été constaté pour W. Cette approche pourrait être intégrée au modèle et permettre d'étendre l'application du SFSE à des niveaux d'agrégation supérieurs à $D = 14$. Cette figure illustre bien la relation entre la fréquence et la taille des agrégats.

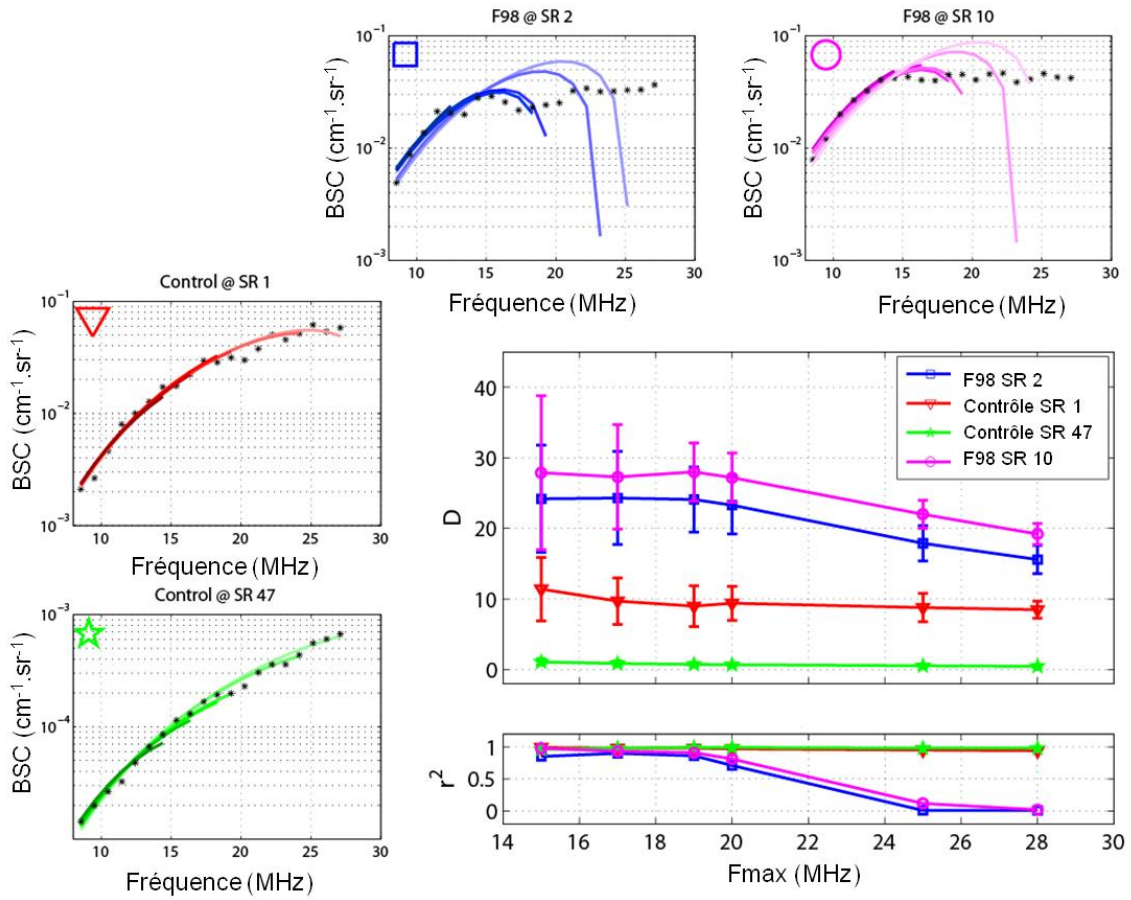

Figure 6-3 : Effet du produit $k_{max}*D*a$ sur le SFSE pour quatre niveaux d'agrégation : ☆ agrégation faible; △ agrégation modérée; □ agrégation forte; ○ agrégation très forte. Une augmentation de la limite supérieure F_{max} de la largeur de bande utilisée diminue la variance sur l'estimation de D mais au prix d'un biais qui se manifeste par une diminution de r^2 lorsque $k_{max}*D*a$ est trop grand. (k_{max} est le nombre d'onde correspondant à la borne supérieure de la bande passante utilisée pour le SFSE).

6.2.2.2 Effet de *H* sur l'agrégation et sur le modèle SFSE ou SFSAE

L'effet net de *H* sur l'agrégation n'est pas simple. Une augmentation de *H* favorise les interactions entre les globules et l'agrégation, mais augmente aussi la fréquence des collisions entre les agrégats et peut empêcher la formation libre de gros agrégats [162;163]. Expérimentalement, il est possible d'isoler l'effet de *H* en préparant des échantillons à différents hématocrite en diluant un échantillon avec du plasma (concentration plasmatique en macromolécule constante, i.e. dilution 1 à la Figure 6.1) ou en diluant avec de la saline (concentration en macromolécule par globule constante, i.e. dilution 2). Les résultats préliminaires de *W* en fonction *H* présentés à la Figure 6-1 semblent indiquer que c'est la concentration plasmatique en macromolécule par globule qui doit être maintenue constante pour demeurer sur la même courbe de τ^{-1}.

Indépendemment de ces considérations, le modèle de Baxter pour des sphères dures (Figure 6-1) montre bien la dépendance non linéaire de W_{Baxter} en fonction de *H* pour τ^{-1} constant. Si l'on se fie à cette figure, on peut s'attendre, lorsque l'on mesure *W* acoustiquement avec notre modèle, à de plus fortes variations de *W* à *H* = 20% qu'à *H* = 40% lorsque l'agrégation augmente due à la présence d'un pic autour de *H* = 20%.

L'effet de *H* sur *D* serait aussi très intéressant à évaluer mais demeure inconnu à ce jour. Si l'on pouvait trouver un moyen de bien contrôler le niveau d'agrégation en fonction de l'hématocrite (par des dilutions à concentration plasmatique constante ou à concentration macromoléculaire de protéines pro-agrégeantes constante par globule) en se référant à *W* et à la Figure 6-1 par exemple, il serait possible de décrire l'effet de *H* sur *D.* On peut espérer que *D* ne soit pas fonction de *H* mais les résultats du chapitre 3 dans lesquels *D* ~ 0.5 dans le cas non-agrégé à *H* = 40 % (plutôt que *D* ~ 1) est une indication que *D* est aussi une fonction de *H.* Encore une fois l'établissement de grilles exprimant *D* en fonction de *H* pour τ^{-1} constant peut être envisagé en faisant varier *H* pour un même

cisaillement. La comparaison de niveaux d'agrégation pour différents hématocrites est un problème difficile.

Toutefois, ces considérations demeurent de nature théorique, car il n'y a aucune raison de croire que l'hématocrite varie fortement en fonction de l'agrégation *in vivo*. Or, à hématocrite constant, *W* et *D* augmentent avec l'agrégation et possèdent tous deux une borne inférieure connue. *H* peut et doit être déterminé par une prise de sang et une microcentrifugation, tel qu'il a été fait dans ce travail.

6.2.2.3 Biais introduit par une erreur de mesure de *H* dans le modèle SFSE ou SFSAE

Puisque *H* est une variable d'entrée du modèle, il est important de quantifier le biais introduit par une surestimation ou une sous estimation de *H.* Si l'on examine l'équation 2.18, on constate que *H* est un facteur multiplicatif dans le modèle. Ainsi une erreur par un facteur $B = \frac{H_{estimé}}{H_{réel}}$ entraîne une erreur de $1/B$ pour *W* et de $\sqrt{1/B}$ pour *D.* Ces erreurs sont représentées à la Figure 6-4 pour des données obtenues dans le Couette avec le SFSE sur du sang porcin à 40% d'hématocrite provenant de l'étude du chapitre 4. Le SFSE est donc sujet à des erreurs provenant d'une mauvaise valeur d'entrée de *H*. Il faut donc porter une grande attention à la valeur de l'hématocrite.

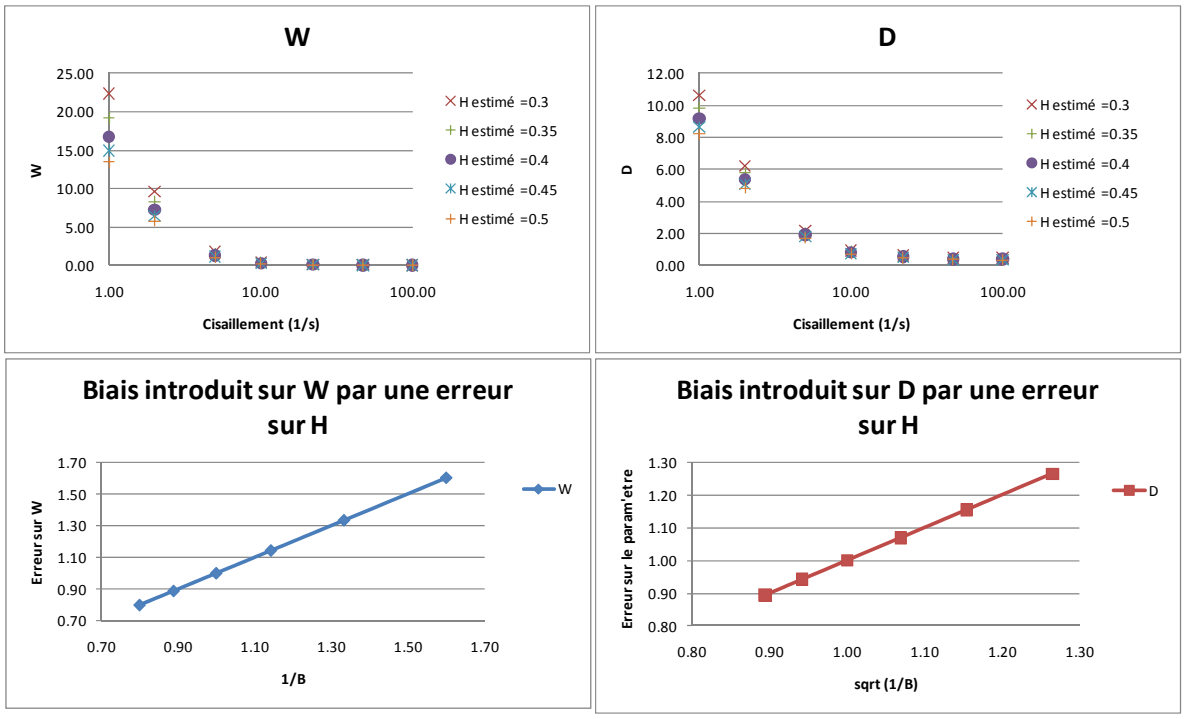

Figure 6-4 : Effet d'une erreur d'estimation de *H* par un facteur $B = \frac{H_{estimé}}{H_{réel}}$ sur *W* et *D* pour du sang porcin provenant de l'étude du chapitre 4 à 40% d'hématocrite dans le Couette par le modèle SFSE. Une surestimation par *B* de *H* entraîne une sous estimation de *W* par $^1/_B$ et de *D* par $\sqrt{^1/_B}$.

6.2.2.4 Sensibilité du modèle SFSE ou SFSAE aux artéfacts acoustiques et au bruit contenu dans le signal rétrodiffusé

Lorsque les conditions d'acquisition du signal ne sont pas optimales et que des artéfacts apparaissent dans le signal et entraîne l'apparition de données aberrantes. Notre approche spectrale est fortement sensible aux artéfacts et à la qualité des signaux. En effet, puisque la méthode repose sur un moyennage spectral à partir de plusieurs images numérisées successivement, la présence d'artéfacts dans quelques images peut faire diverger le modèle. Les réverbérations, mouvements de la sonde, les poils et les bulles

d'air sont particulièrement à éviter. Lorsqu'un vaisseau est imagé dans l'axe longitudinal, il est primordial que le signal sanguin ne soit pas superposé à du signal pariétal dû à proximité de la paroi. Une détection et un filtrage des données abhérentes (artéfacts de réverbération, lobes secondaires, etc.), un algorithme de recalage pour éliminer le mouvement dans les acquisitions *in vivo* devraient être considérés. Une analyse spectrale plus raffinée, passant par des filtres autorégressifs ou des analyses par ondelettes pourraient être envisagés afin de diminuer la variance et d'augmenter la résolution spatiale. Cette approche devra être effectuée avec minutie pour s'assurer de ne pas introduire de biais dans l'estimation spectrale.

6.2.3 Intérêt en médecine et en science fondamentale

Si des améliorations techniques ont été suggérées précedemment, c'est au niveau des implications cliniques que les perspectives sont les plus intéressantes. En effet, faute d'un outil adéquat, les implications de perturbations hémorhéologiques dans le développement des maladies cardiovasculaires ne sont pas encore bien comprises. La nature spécifique des locations de ces pathologies laisse espérer que des avancées technologiques permettant la caractérisation de la rhéologie sanguine *in vivo* et *in situ* permettent de mieux comprendre et de quantifier ces phénomènes fortement dépendants des conditions d'écoulement. L'étude expérimentale présentée au chapitre 5 illustre bien l'impact d'un tel outil : il a été possible de mettre en évidence, grâce au SFSAE, qu'une augmentation locale d'agrégation pouvait provoquer la formation d'un thrombus veineux. Ce genre d'étude suggère fortement que les paramètres hémorhéologiques (idéalement *in vivo* et *in situ*) devraient être pris en compte dans l'évaluation du risque de thrombose veineuse. Des travaux futurs comportant des études animales fondées sur des protocoles similaires à celui proposé au chapitre 5 peuvent être envisagés pour apronfondir la compréhension des impacts de l'hémorheologie sur la thrombose veineuse. L'expérience décrite au chapitre 5 a permis de mettre en évidence

l'implication de l'hyperagrégation sur la phase aigue de la formation d'un thrombus. Il serait intéressant de cibler l'impact de l'hyperagrégation sur l'activation et l'adhésion plaquettaire dans la formation de la thrombose veineuse par exemple. Des mécanismes favorisant la migration des plaquettes et des globules blancs ont été avancés mais n'ont pu être mis en évidence car les animaux ont été sacrifié après 14 jours. Il serait intéressant d'examiner les mécanismes cellulaires de manière plus précise par des analyses histologiques en phase aigue juste après la formation du thrombus.

Si les ultrasons ne permettent pas une résolution à l'échelle du globule rouge, une résolution de l'ordre de 400 µm a pu être mise en évidence dans ce travail, ce qui permet une cartographie acceptable dans des vaisseaux de 5 à 6 mm de diamètre. Dans la fémorale de lapin de 2 mm de diamètre, la méthode a néanmoins permis d'obtenir des niveaux d'agrégation moyens *in situ* dans des conditions d'écoulement *in vivo*. La méthode a été validée dans ce travail à des fréquences de 9-28 MHz. Cette gamme de fréquences s'applique principalement aux vaisseaus superficiels car les hautes fréquences sont rapidement atténuées durant la propagation. Pour de très gros agrégats, la méthode devrait pouvoir s'adapter à des fréquences plus faibles, malheureusement au prix d'une résolution plus faible. Sur l'humain, l'application de la méthode est pour l'instant limitée aux vaisseaux périphériques. Une application sur la veine fémorale devra se faire à plus faible fréquence car ces vaisseaux sont enfouis plus profondément sous la peau. L'applicabilité des résultats présentés ici demeure à être démontrée. Si elle est possible, on peut envisager une étude clinique sur l'humain pour évaluer si l'hyperagrégation mesurée par la méthode ultrasonore est impliquée dans le risque de formation de thrombus veineux.

En tirant profit de l'instantanéité d'une méthode d'imagerie par rapport aux tests en laboratoire, une application clinique en surveillance de l'inflammation en soins intensifs pourrait être développée, puisque plusieurs protéines inflammatoires induisent

l'agrégation (voir Tab. 1-2). Un transducteur placé sur un vaisseau périphérique du bras pourrait permettre une détection rapide de l'inflammation, ce qui est cliniquement primordial dans le traitement aigu du choc sceptique, par exemple. La nature non invasive des ondes ultrasonores constitue un atout intéressant à ce niveau.

6.3 Conclusions

L'étude du spectre du coefficient de rétrodiffusion du sang à l'aide du SFSE ou du SFSAE permet d'obtenir une information sur la microstructure sanguine. Cette information est intéressante car elle est à l'origine du comportement non newtonien du sang à faible cisaillements, qui fait augmenter la viscosité d'un ordre de grandeur. Une caractérisation *in vivo* et *in situ* de l'agrégation par les paramètres microstructuraux *W* et *D* a été réalisée dans ce travail. Le lien étiologique de l'hyperagrégation sur la thrombophlébite a également été démontrée et le niveau d'agrégation suivi et caractérisé dans le temps *in vivo*, montrant des perturbations localisées uniquement du coté thrombosé. Si des améliorations restent à être apportées à la méthode (structure fractale des agrégats, validation de *D*, lien entre *W* et τ^{-1}, indépendance à la fréquence) la démonstration de l'applicabilité de l'approche du problème par le SFSE ou le SFSAE à la caractérisation sanguine *in vitro* et *in vivo* a été clairement établie.

Bibliographie

[1] Agnelli, G. and Becattini, C., Treatment of DVT: how long is enough and how do you predict recurrence, *J.Thromb.Thrombolysis.*, **25** (2008), pp. 37-44.

[2] Agnelli, G., Prandoni, P., Santamaria, M. G., Bagatella, P., Iorio, A., Bazzan, M., Moia, M., Guazzaloca, G., Bertoldi, A., Tomasi, C., Scannapieco, G., and Ageno, W., Three months versus one year of oral anticoagulant therapy for idiopathic deep venous thrombosis. Warfarin Optimal Duration Italian Trial Investigators, *New England Journal of Medicine*, **345** (July2001), pp. 165-169.

[3] Ahmed, F., Alexandridis, P., and Neelamegham, S., Synthesis and Application of Fluorescein-Labeled Pluronic Block Copolymers to the Study of Polymer Surface Interactions, *Langmuir*, **17** (2001), pp. 537-546.

[4] Allard, L. and Cloutier, G., Power Doppler ultrasound scan imaging of the level of red blood cell aggregation : An in vitro study, *Journal of Vascular Surgery*, **30** (1999), pp. 157-168.

[5] Allard, L., Cloutier, G., and Durand, L. G., Effect of the insonification angle on the Doppler backscattered power under red blood cell aggregation conditions, *IEEE Transactions on Ultrasonics, Ferroelectrics, & Frequency Control*, **43** (1996), pp. 211-219.

[6] Alt, E., Banyai, S., Banyai, M., and Koppensteiner, R., Blood rheology in deep venous thrombosis--relation to persistent and transient risk factors, *Thromb Res.*, **107** (2002), pp. 101-107.

[7] Armstrong, J. K., Meiselman, H. J., and Fisher, T. C., Evidence against macromolecular "bridging" as the mechanism of red blood cell aggregation induced by nonionic polymers, *Biorheology*, **36** (1999), pp. 433-437.

[8] Armstrong, J. K., Meiselman, H. J., Wenby, R. B., and Fisher, T. C., Modulation of red blood cell aggregation and blood viscosity by the covalent attachment of Pluronic copolymers, *Biorheology*, **38** (2001), pp. 239-247.

[9] Armstrong, J. K., Wenby, R. B., Meiselman, H. J., and Fisher, T. C., The hydrodynamic radii of macromolecules and their effect on red blood cell aggregation, *Biophys J*, **87** (2004), pp. 4259-4270.

[10] Baddour, R. E. and Kolios, M. C., Investigating the Effect of Cell Size on the Backscatter from Suspensions of Varying Volume Fractions, *Ultrasonics Symposium*, (2006), pp. 637-640.

[11] Bagchi, P., Johnson, P. C., and Popel, A. S., Computational fluid dynamic simulation of aggregation of deformable cells in a shear flow, *J Biomech.Eng*, **127** (2005), pp. 1070-1080.

[12] Bamber, J. C. and Dickinson, R. J., Ultrasonic B-scanning: a computer simulation, *Physics in Medicine & Biology*, **25** (1980), pp. 463-479.

[13] Barber, J. O., Alberding, J. P., Restrepo, J. M., and Secomb, T. W., Simulated two-dimensional red blood cell motion, deformation, and partitioning in microvessel bifurcations, *Annals of Biomedical Engineering*, **36** (2008), pp. 1690-1698.

[14] Baskurt, O. K., Bor-Küçükatay, M., Yalçin, Ö., and Meiselman, H. J., Aggregation behavior and electrophoretic mobility of red blood cells in various mammalian species, *Biorheology*, **37** (2000), pp. 417-428.

[15] Baskurt, O. K., Farley, R. A., and Meiselman, H. J., Erythrocyte aggregation tendency and cellular properties in horse, human, and rat: a comparative study, *Am.J.Physiol*, **273** (1997), pp. H2604-H2612.

[16] Baskurt, O. K. and Meiselman, H. J., Activated polymorphonuclear leukocytes affect red blood cell aggregability, *Journal of Leukocyte Biology*, **63** (1998), pp. 89-93.

[17] Baskurt, O. K., Temiz, A., and Meiselman, H. J., Effect of superoxide anions on red blood cell rheologic properties, *Free Radical Biology & Medicine*, **24** (1998), pp. 102-110.

[18] Baskurt, O. K., Yalcin, O., Ozdem, S., Armstrong, J. K., and Meiselman, H. J., Modulation of endothelial nitric oxide synthase expression by red blood cell aggregation, *American Journal of Physiology (Heart & Circulatory Physiology)*, **286** (2004), pp. H222-H229.

[19] Bäumler, H., Neu, B., Donath, E., and Kiesewetter, H., Basic phenomena of red blood cell rouleaux formation, *Biorheology*, **36** (1999), pp. 439-442.

[20] Bell, D. N., Spain, S., and Goldsmith, H. L., The effect of red blood cells on the ADP-induced aggregation of human platelets in flow through tubes, *Thrombosis & Haemostasis*, **63** (1990), pp. 112-121.

[21] Bernstein, N. E., Demopoulos, L. A., Tunick, P. A., Rpsemzweig, B. P., and Kronzon, I., Correlates of spontaneous echo contrast in patients with mitral stenosis and normal sinus rhythm, *American Heart Journal*, **128** (1994), pp. 287-292.

[22] Bishop, J. J., Nance, P. R., Popel, A. S., Intaglietta, M., and Johnson, P. C., Effect of erythrocyte aggregation on velocity profiles in venules, *American Journal of Physiology (Heart & Circulatory Physiology)*, **280** (2001), pp. H222-H236.

[23] Bishop, J. J., Nance, P. R., Popel, A. S., Intaglietta, M., and Johnson, P. C., Erythrocyte margination and sedimentation in skeletal muscle venules, *American Journal of Physiology (Heart & Circulatory Physiology)*, **281** (2001), pp. H951-H958.

[24] Bishop, J. J., Popel, A. S., Intaglietta, M., and Johnson, P. C., Effects of erythrocyte aggregation and venous network geometry on red blood cell axial migration, *Am.J.Physiol Heart Circ.Physiol*, **281** (2001), pp. H939-H950.

[25] Boynard, M. and Lelievre, J. C., Size determination of red blood cell aggregates induced by dextran using ultrasound backscattering phenomenon, *Biorheology*, **27** (1990), pp. 39-46.

[26] Briley, D. P., Giraud, G. D., Beamer, N. B., Spear, E. M., Grauer, S. E., Edwards, J. M., Clark, W. M., Sexton, G. J., and Coull, B. M., Spontaneous echo contrast and hemorheologic abnormalities in cerebrovascular disease, *Stroke*, **25** (1994), pp. 1564-1569.

[27] Brooks, D. E., Russell, G., Janzen, G., and Janzen, J., "Mechanisms of erythrocyte aggregation," in: *Erythrocyte mechanics and blood flow,* Cokelet, G. R., Meiselman, H. J., and Brooks, D. E. (eds.), Liss,A.R., Inc., New York, 1980, pp. 119-140.

[28] Brooks, D. E. and Seaman, G. V. F., The effect of neutral polymers on the electrokinetic potential of cells and other charged particles. I. Models for the zeta potential increase, *Journal of Colloid & Interface Science*, **43(3)** (1973), pp. 670-686.

[29] Cabel, M., Meiselman, H. J., Popel, A. S., and Johnson, P. C., Contribution of red blood cell aggregation to venous vascular resistance in skeletal muscle, *American Journal of Physiology (Heart & Circulatory Physiology)*, **272** (1997), pp. H1020-H1032.

[30] Campbell, I. A., Bentley, D. P., Prescott, R. J., Routledge, P. A., Shetty, H. G., and Williamson, I. J., Anticoagulation for three versus six months in patients with deep vein thrombosis or pulmonary embolism, or both: randomised trial, *BMJ*, **334** (Mar.2007), pp. 674.

[31] Caro, C. G., Pedley, T. J., Schroter, R. C., and Seed, W. A., *The mechanics of the circulation*, 1 ed. Oxford, New York, Toronto: Oxford University Press, 1978, pp. 1-514.

[32] Castellini, M., Elsner, R., Baskurt, O. K., Wenby, R. B., and Meiselman, H. J., Blood rheology of Weddell seals and bowhead whales, *Biorheology*, **43** (2006), pp. 57-69.

[33] Charansonney, O., Mouren, S., Dufaux, J., Duvelleroy, M., and Vicaut, E., Red blood cell aggregation and blood viscosity in an isolated heart preparation, *Biorheology*, **30** (1993), pp. 75-84.

[34] Chen, S., Barshtein, G., Gavish, B., Mahler, Y., and Yedgar, S., Monitoring of red blod cell aggregability in a flow-chamber by computerized image analysis, *Clinical Hemorheology*, **14** (1994), pp. 497-508.

[35] Chen, S., Gavish, B., Zhang, S., Mahler, Y., and Yedgar, S., Monitoring of erythrocyte aggregate morphology under flow by computerized image analysis, *Biorheology*, **32** (1995), pp. 487-496.

[36] Chien, S., Blood viscosity: Influence of erythrocyte aggregation, *Science*, **157** (1967), pp. 829-831.

[37] Chien, S., "Biophysical behavior of red cells in suspensions," in: *The red blood cell,* Surgenor, D. M. (ed.), Academic Press, New York, San Francisco, London, 1975, pp. 1031-1133.

[38] Christiansen, S. C., Cannegieter, S. C., Koster, T., Vandenbroucke, J. P., and Rosendaal, F. R., Thrombophilia, clinical factors, and recurrent venous thrombotic events, *JAMA-J.Am.Med.Assoc.*, **293** (2005), pp. 2352-2361.

[39] Cloutier, G., Daronat, M., Savery, D., Garcia, D., Durand, L. G., and Foster, F. S., Non-Gaussian statistics and temporal variations of the ultrasound signal backscattered by blood at frequencies between 10 and 58 MHz, *J Acoust Soc Am*, **116** (2004), pp. 566-577.

[40] Cloutier, G. and Qin, Z., Ultrasound backscattering from non-aggregating and aggregating erythrocytes - A review, *Biorheology*, **34** (1997), pp. 443-470.

[41] Cloutier, G. and Qin, Z., Shear rate dependence of ultrasound backscattering from blood samples characterized by different levels of erythrocyte aggregation, *Annals of Biomedical Engineering*, **28** (2000), pp. 399-407.

[42] Cloutier, G., Qin, Z., Durand, L. G., and Teh, B. G., Power Doppler ultrasound evaluation of the shear rate and shear stress dependences of red blood cell aggregation, *IEEE Transaction on Biomedical Engineering*, **43** (1996), pp. 441-450.

[43] Cloutier, G., Zimmer, A., Yu, F. T., and Chiasson, J. L., Increased shear rate resistance and fastest kinetics of erythrocyte aggregation in diabetes measured with ultrasound, *Diabetes Care*, **31** (2008), pp. 1400-1402.

[44] Cokelet, G. R., Brown, J. R., Codd, S. L., and Seymour, J. D., Magnetic resonance microscopy determined velocity and hematocrit distributions in a Couette viscometer, *Biorheology*, **42** (2005), pp. 385-399.

[45] Copley, A. L., King, R. G., and Huang, C. R., "Erythrocyte sedimentation of human blood at varying shear rates," in: *Microcirculation,* Grayson, J. and Zingg, W. (eds.), Plenum Press, New York, 1976, pp. 133-134.

[46] Daniel, W. G., Nellessen, U., Schröder, E., Nonnast-Daniel, B., Bednarski, P., Nikutta, P., and Lichtlen, P. R., Left atrial spontaneous echo contrast in mitral valve disease: An indicator for an increased thromboembolic risk, *Journal of the American College of Cardiology*, **11** (1988), pp. 1204-1211.

[47] De Gennes, P. G., "Model polymers at interfaces," in: *Physical basis for cell-cell adhesion,* Bongrand P. (ed.), Boca Raton, 1989, pp. 39-60.

[48] De Kroon, M. G. M., Slager, C. J., Gussenhoven, W. J., Serruys, P. W., Roelandt, J. R. T. C., and Bom, N., Cyclic changes of blood echogenicity in high-frequency ultrasound, *Ultrasound in Medicine & Biology*, **17** (1991), pp. 723-728.

[49] deFilippi, C. R., Lacker, M., Grayburn, P. A., and Brickner, M. E., Spontaneous echo contrast in the descending aorta detected by transesophageal echocardiography, *American Journal of Cardiology*, **74** (1994), pp. 410-411.

[50] Dormandy, J. A., Annotation - Hemorheological Aspects of Thrombosis, *British Journal of Haematology*, **45** (1980), pp. 519-522.

[51] Dormandy, J. A., Influence of blood cells and blood flow on venous endothelium, *Int.Angiol.*, **15** (1996), pp. 119-123.

[52] Dormandy, J. A. and Edelman, J. B., High blood viscosity: an aetiological factor in venous thrombosis, *British Journal of Surgery*, **60** (1973), pp. 187-190.

[53] Dotevall, A., Johansson, S., and Wilhelmsen, L., Association between fibrinogen and other risk factors for cardiovascular disease in men and women. Results from the Göteborg Monica survey 1985, *Annals of Epidemiology*, **4** (1994), pp. 369-374.

[54] Elsner, R. and Meiselman, H. J., Splenic oxygen storage and blood viscosity in seals, *Marine Mammal Science*, **11** (1995), pp. 93-96.

[55] Esmon, C. T., Coagulation and inflammation, *J.Endotoxin.Res.*, **9** (2003), pp. 192-198.

[56] Esmon, C. T., Inflammation and thrombosis, *J.Thromb.Haemost.*, **1** (July2003), pp. 1343-1348.

[57] Fahraeus, R., The suspension stability of the blood, *Physiological Reviews*, **IX** (1929), pp. 241-275.

[58] Fahraeus, R. and Lindqvist, T., Viscosity of blood in narrow capillary tubes, *Am.J.Physiol*, **96** (1931), pp. 562-568.

[59] Fang, J. and Owens, R. G., Numerical simulations of pulsatile blood flow using a new constitutive model, *Biorheology*, **43** (2006), pp. 637-660.

[60] Feleppa, E. J., Porter, C. R., Ketterling, J., Lee, P., Dasgupta, S., Urban, S., and Kalisz, A., Recent developments in tissue-type imaging (TTI) for planning and monitoring treatment of prostate cancer, *Ultrasonic Imaging*, **26** (2004), pp. 163-172.

[61] Flory, P. J. and Fox, T. G. J., Treatment of intrinsic viscosity, *J.Am.Chem.Soc*, **73** (1951), pp. 1904-1906.

[62] Fontaine, I., Bertrand, M., and Cloutier, G., A system-based approach to modeling the ultrasound signal backscattered by red blood cells, *Biophysical Journal*, **77** (1999), pp. 2387-2399.

[63] Fontaine, I. and Cloutier, G., Modeling the frequency dependence (5-120 MHz) of ultrasound backscattering by red cell aggregates in shear flow at a normal hematocrit, *J Acoust Soc Am*, **113** (2003), pp. 2893-2900.

[64] Fontaine, I., Savéry, D., and Cloutier, G., Simulation of ultrasound backscattering by red cell aggregates: Effect of shear rate and anisotropy, *Biophysical Journal*, **82** (2002), pp. 1696-1710.

[65] Foster, F. S., Obara, H., Bloomfield, T., Ryan, L. K., and Lockwood, G. R., Ultrasound backscatter from blood in the 30 to 70 MHz frequency range, *IEEE Ultrasonics Symposium Proceedings*, (1994), pp. 1599-1602.

[66] Franceschini, E., Yu, F. T. H., and Cloutier, G., Simultaneous estimation of attenuation and structure parameters of aggregated red blood cells from backscatter measurements, *J Acoust Soc Am*, **123** (2008), pp. EL85-EL91.

[67] Franceschini, E., Yu, F. T. H., Destrempes, F., and Cloutier, G., Ultrasound characterization of red blood cell aggregation with intervening tissue-mimicking phantoms using the Structure Factor Size and Attenuation Estimator, *J.Acoust.Soc Am.*, **submitted** (2009).

[68] Fromageau, J., Gennisson, J. L., Schmitt, C., Maurice, R. L., Mongrain, R., and Cloutier, G., Estimation of polyvinyl alcohol cryogel mechanical properties with four ultrasound elastography methods and comparison with gold standard testings, *IEEE Trans.Ultrason.Ferroelectr.Freq.Control*, **54** (2007), pp. 498-509.

[69] Fung, Y. C., *Biomechanics: circulation*, 2nd ed. New York, Berlin, Heidelberg ...: Springer, 1997, pp. 1-571.

[70] Giglio, V., Pasceri, V., Messano, L., Mangiola, F., Pasquini, L., Dello, R. A., Damiani, A., Mirabella, M., Galluzzi, G., Tonali, P., and Ricci, E., Ultrasound tissue characterization detects preclinical myocardial structural changes in children affected by Duchenne muscular dystrophy, *J Am Coll.Cardiol.*, **42** (2003), pp. 309-316.

[71] Gijsen, F. J., van de Vosse, F. N., and Janssen, J. D., The influence of the non-Newtonian properties of blood on the flow in large arteries: steady flow in a carotid bifurcation model, *Journal of Biomechanics*, **32** (1999), pp. 601-608.

[72] Goldsmith, H. L., Bell, D. N., Braovac, S., Steinberg, A., and McIntosh, F., Physical and chemical effects of red cells in the shear-induced aggregation of human platelets, *Biophysical Journal*, **69** (1995), pp. 1584-1595.

[73] Goldsmith, H. L., Bell, D. N., Spain, S., and McIntosh, F. A., Effect of red blood cells and their aggregates on platelets and white cells in flowing blood, *Biorheology*, **36** (1999), pp. 461-468.

[74] Goldsmith, H. L., Kaufer, E. S., and McIntosh, F. A., Effect of hematocrit on adenosine diphosphate-induced aggregation of human platelets in tube flow, *Biorheology*, **32** (1995), pp. 537-592.

[75] Goldsmith, H. L. and Marlow, J., Flow behaviour of erythrocytes. I. Rotation and deformation in dilute suspensions, *Proc Royal Soc (London)*, **182** (1972), pp. 351-384.

[76] Goldsmith, H. L. and Marlow, J. C., Flow behavior of erythrocytes. II. Particle motions in concentrated suspensions of ghost cells, *Journal of Colloid & Interface Science*, **71** (1979), pp. 383-407.

[77] Goldsmith, H. L. and Spain, S., Margination of leukocytes in blood flow through small tubes, *Microvascular Research*, **27** (1984), pp. 204-222.

[78] Goss, S. A., Johnston, R. L., and Dunn, F., Compilation of empirical ultrasonic properties of mammalian tissues. II, *Journal of the Acoustical Society of America*, **68** (1980), pp. 93-108.

[79] Greenleaf, J. F., *Tissue characterization with ultrasound I*, 1 ed. Boca Raton, Florida: CRC Press, Inc., 1986, pp. 1-212.

[80] Greenleaf, J. F., *Tissue characterization with ultrasound II*, 1 ed. Boca Raton, Florida: CRC Press, 1986, pp. 1-245.

[81] Guinier, A. and Fournet, J., *Small anglescattering of X-rays*. NewYork: Wiley Interscience, 1955.

[82] Gustafsson, L., Appelgren, L., and Myrvold, H. E., Effects of increased plasma viscosity and red blood cell aggregation on blood viscosity in vivo, *Am.J.Physiol*, **241** (1981), pp. H513-H518.

[83] Gustafsson, L., Falk, A., Haglund, U., and Myrvold, H. E., Intestinal hemodynamic effects of dextran-induced hyperviscosity in the cat, *Int.J.Microcirc.Clin.Exp.*, **4** (1985), pp. 183-190.

[84] Hanss, M. and Boynard, M., "Ultrasound backscattering from blood: Hematocrit and erythrocyte aggregation dependence," in: *Ultrasonic Tissue Characterization II,* Linzer, M. (ed.), National Bureau of Standards, Gaithersburg, Maryland, 1979, pp. 165-169.

[85] Hitosugi, M., Niwa, M., and Takatsu, A., Rheologic changes in venous blood during prolonged sitting, *Thrombosis Research*, **100** (2000), pp. 409-412.

[86] Huang, C., Wang, S. H., and Tsui, P. H., Detection of blood coagulation and clot formation using quantitative ultrasonic parameters, *Ultrasound in Medicine & Biology*, **31** (2005), pp. 1567-1573.

[87] Hwang, J. J., Kuan, P., Chen, J. J., Ko, Y. L., Cheng, J. J., Lin, J. L., Tseng, Y. Z., and Lien, W. P., Significance of left atrial spontaneous echo contrast in rheumatic mitral valve disease as a predictor of systemic arterial embolization: A

transesophageal echocardiographic study, *American Heart Journal*, **127** (1994), pp. 880-885.

[88] Iliceto, S., Antonelli, G., Sorino, M., Biasco, G., and Rizzon, P., Dynamic intracavitary left atrial echoes in mitral stenosis, *American Journal of Cardiology*, **55** (1985), pp. 603-606.

[89] Insana, M. F., Wagner, R. F., Brown, D. G., and Hall, T. J., Describing small-scale structure in random media using pulse-echo ultrasound, *Journal of the Acoustical Society of America*, **87** (1990), pp. 179-192.

[90] Johnston, B. M., Johnston, P. R., Corney, S., and Kilpatrick, D., Non-Newtonian blood flow in human right coronary arteries: transient simulations, *J Biomech.*, **39** (2006), pp. 1116-1128.

[91] Jones, C. I., Payne, D. A., Hayes, P. D., Naylor, A. R., Bell, P. R., Thompson, M. M., and Goodall, A. H., The antithrombotic effect of dextran-40 in man is due to enhanced fibrinolysis in vivo, *Journal of Vascular Surgery*, **48** (2008), pp. 715-722.

[92] Kaymaz, C., Ozdemir, N., Kirma, C., and Ozkan, M., Spontaneous echo contrast in the descending aorta in patients without aortic dissection: associated clinical and echocardiographic characteristics, *Int.J Cardiol.*, **90** (Aug.2003), pp. 147-152.

[93] Kearon, C., Gent, M., Hirsh, J., Weitz, J., Kovacs, M. J., Anderson, D. R., Turpie, A. G., Green, D., Ginsberg, J. S., Wells, P., MacKinnon, B., and Julian, J. A., A comparison of three months of anticoagulation with extended anticoagulation for a first episode of idiopathic venous thromboembolism, *New England Journal of Medicine*, **340** (Mar.1999), pp. 901-907.

[94] Khodabandehlou, T. and Le Devehat, C., Hemorheological disturbances as a marker of diabetic foot syndrome deterioration, *Clinical Hemorheology & Microcirculation*, **30** (2004), pp. 219-223.

[95] Kirchhofer, D., Riederer, M. A., and Baumgartner, H. R., Specific accumulation of circulating monocytes and polymorphonuclear leukocytes on platelet thrombi in a vascular injury model, *Blood*, **89** (Feb.1997), pp. 1270-1278.

[96] Kitamura, H. and Kawasaki, S., Detection and clinical significance of red cell aggregation in the human subcutaneous vein using a high-frequency transducer (10 MHZ): A preliminary report, *Ultrasound in Medicine & Biology*, **23** (1997), pp. 933-938.

[97] Kitamura, H., Sigel, B., Machi, J., Feleppa, E. J., Sokil-Melgar, J., Kalisz, A., and Justin, J., Roles of hematocrit and fibrinogen in red cell aggregation determined by ultrasonic scattering properties, *Ultrasound in Medicine & Biology*, **21** (1995), pp. 827-832.

[98] Kolios, M. C., Czarnota, G. J., Lee, M., Hunt, J. W., and Sherar, M. D., Ultrasonic spectral parameter characterization of apoptosis, *Ultrasound Med Biol.*, **28** (2002), pp. 589-597.

[99] Krieger, E., van Der, L. B., Amann-Vesti, B. R., Rousson, V., and Koppensteiner, R., C-reactive protein and red cell aggregation correlate with late venous function after acute deep venous thrombosis, *J Vasc.Surg.*, **40** (2004), pp. 644-649.

[100] Landau L.D. and Lifshitz E.M., in: *Electrodynamics of Continuous Media,* Pergamon, Oxford, 1960, pp. 368-376.

[101] Laugier, P., Instrumentation for in vivo ultrasonic characterization of bone strength, *IEEE Trans.Ultrason.Ferroelectr.Freq.Control*, **55** (2008), pp. 1179-1196.

[102] Le Devehat, C., Vimeux, M., and Khodabandehlou, T., Blood rheology in patients with diabetes mellitus, *Clinical Hemorheology & Microcirculation*, **30** (2004), pp. 297-300.

[103] Lee, A. J., Mowbray, P. I., Lowe, G. D. O., Rumley, A., Fowkes, F. G. R., and Allan, P. L., Blood viscosity and elevated carotid imtima-media thickness in men and women. The Edinburgh artery study, *Circulation*, **97** (1998), pp. 1467-1473.

[104] Libby, P., Inflammation in atherosclerosis, *Nature*, **420** (2002), pp. 868-874.

[105] libgot, R., Ossant, F., and Gruel, Y. L. P. P. F., High frequency US characterization of the blood clotting process : intra and inter individual variations, *Ultrasonics Symposium*, **4** (2005), pp. 2259-2262.

[106] Lim, B. and Cobbold, R. S., On the relation between aggregation, packing and the backscattered ultrasound signal for whole blood, *Ultrasound in Medicine & Biology*, **25** (1999), pp. 1395-1405.

[107] Lizzi, F. L., Greenebaum, M., Feleppa, E. J., Elbaum, M., and Coleman, D. J., Theoretical framework for spectrum analysis in ultrasonic tissue characterization, *Journal of the Acoustical Society of America*, **73** (1983), pp. 1366-1373.

[108] Lizzi, F. L., Ostromogilsky, M., Feleppa, E. J., Rorke, M., and Yaremko, M. M., Relationship of ultrasonic spectral parameters to features of tissue microstructure, *Ultrasonics*, **33** (1986), pp. 319-329.

[109] Lockwood, G. R., Ryan, L. K., Hunt, J. W., and Foster, F. S., Measurement of the ultrasonic properties of vascular tissues and blood from 35-65 MHz, *Ultrasound in Medicine & Biology*, **17** (1991), pp. 653-666.

[110] Lowe, G. D., Etiopathogenesis of cardiovascular disease: hemostasis, thrombosis, and vascular medicine, *Ann.Periodontol.*, **3** (1998), pp. 121-126.

[111] Lowe, G. D. O., Fowkes, F. G. R., Dawes, J., Donnan, P. T., Lennie, S. E., and Housley, E., Blood viscosity, fibrinogen, and activation of coagulation and leukocytes in peripheral arterial disease and the normal population in the Edinburgh artery study, *Circulation*, **87** (1993), pp. 1915-1920.

[112] Lowe, G. D. O., Lee, A. J., Rumley, A., Price, J. F., and Fowkes, F. G. R., Blood viscosity and risk of cardiovascular events: the Edinburgh artery study, *British Journal of Haematology*, **96** (1997), pp. 168-173.

[113] MacRury, S. M., Lennie, S. E., McColl, P., Balendra, R., MacCuish, A. C., and Lowe, G. D. O., Increased red cell aggregation in diabetes mellitus: Association with cardiovascular risk factors, *Diabetic Medicine*, **10** (1993), pp. 21-26.

[114] Madsen, E. L., Insana, M. F., and Zagzebski, J. A., Method of data reduction for accurate determination of acoustic backscatter coefficients, *Journal of the Acoustical Society of America*, **76** (1984), pp. 913-923.

[115] Mamou, J., Oelze, M. L., O'Brien, W. D., Jr., and Zachary, J. F., Identifying ultrasonic scattering sites from three-dimensional impedance maps, *J Acoust Soc Am*, **117** (2005), pp. 413-423.

[116] Maruvada, S., Shung, K. K., and Wang, S., High-frequency backscatterer and attenuation measurements of porcine erythrocyte suspensions between 30-90 MHz, *Ultrasound in Medicine & Biology*, **28** (2002), pp. 1081-1088.

[117] Meiselman, H. J. and Baskurt, O. K., Hemorheology and hemodynamics: Dove andare?, *Clinical Hemorheology & Microcirculation*, **35 IP - 1-2** (2006), pp. 37-43.

[118] Milnor, W. R., *Hemodynamics*, 2 ed. Baltimore, Hong Kong, London, Sydney: Williams & Wilkins, 1989, pp. 1-387.

[119] Mo, L. Y. L. and Cobbold, R. S. C., A stochastic model of the backscattered Doppler ultrasound from blood, *IEEE Transaction on Biomedical Engineering*, **BME-33** (1986), pp. 20-27.

[120] Mo, L. Y. L. and Cobbold, R. S. C., "Theoretical models of ultrasonic scattering in blood," in: *Ultrasonic scattering in biological tissues,* Shung, K. K. and Thieme, G. A. (eds.), CRC Press, Boca Raton, Ann Arbor, London, Tokyo, 1993, pp. 125-170.

[121] Mo, L. Y. L., Yip, G., Cobbold, R. S. C., Gutt, C., Joy, M., Santyr, G., and Shung, K. K., Non-newtonian behavior of whole blood in a large diameter tube, *Biorheology*, **28** (1991), pp. 421-427.

[122] Nash, G. B., Watts, T., Thornton, C., and Barigou, M., Red cell aggregation as a factor influencing margination and adhesion of leukocytes and platelets, *Clinical Hemorheology & Microcirculation*, **39** (2008), pp. 303-310.

[123] Neu, B. and Meiselman, H. J., Depletion-mediated red blood cell aggregation in polymer solutions, *Biophysical Journal*, **83** (2002), pp. 2482-2490.

[124] Neu, B., Wenby, R., and Meiselman, H. J., Effects of dextran molecular weight on red blood cell aggregation, *Biophysical Journal*, **95** (2008), pp. 3059-3065.

[125] Nguyen, L. C., Yu, F. T., and Cloutier, G., Cyclic changes in blood echogenicity under pulsatile flow are frequency dependent, *Ultrasound Med Biol*, **34** (2008), pp. 664-673.

[126] Niemetz, J., Tissue-factor-endowed leukocytes do cause thrombosis, *Blood*, **106** (Aug.2005), pp. 1506-1507.

[127] Oelze, M. L., O'Brien, W. D., Jr., Blue, J. P., and Zachary, J. F., Differentiation and characterization of rat mammary fibroadenomas and 4T1 mouse carcinomas using quantitative ultrasound imaging, *IEEE Trans Med Imaging.*, **23** (2004), pp. 764-771.

[128] Oger, E., Incidence of venous thromboembolism: a community-based study in Western France. EPI-GETBP Study Group. Groupe d'Etude de la Thrombose de Bretagne Occidentale, *Thromb Haemost*, **83** (2000), pp. 657-660.

[129] Padilla, F., Akrout, L., Kolta, S., Latremouille, C., Roux, C., and Laugier, P., In vitro ultrasound measurement at the human femur, *Calcif.Tissue Int.*, **75** (2004), pp. 421-430.

[130] Parker, B. A., Ridout, S. J., and Proctor, D. N., Age and flow-mediated dilation: a comparison of dilatory responsiveness in the brachial and popliteal arteries, *American Journal of Physiology (Heart & Circulatory Physiology)*, **291** (Dec.2006), pp. H3043-H3049.

[131] Pearson, M. J. and Lipowsky, H. H., Influence of erythrocyte aggregation on leukocyte margination in postcapillary venules of rat mesentery, *American Journal of Physiology (Heart & Circulatory Physiology)*, **279** (2000), pp. H1460-H1471.

[132] Popel, A. S., Johnson, P. C., Kameneva, M. V., and Wild, M. A., Capacity for red blood cell aggregation is higher in athletic mammalian species than in sedentary species, *Journal of Applied Physiology*, **77** (1994), pp. 1790-1794.

[133] Pribush, A., Meiselman, H. J., Meyerstein, D., and Meyerstein, N., Dielectric approach to the investigation of erythrocyte aggregation: I. Experimental basis of the method, *Biorheology*, **36** (1999), pp. 411-423.

[134] Pribush, A., Meyerstein, N., and Meyerstein, D., Dielectric approach to investigation of erythrocyte aggregation. II. Kinetics of erythrocyte aggregation-disaggregation in quiescent and flowing blood, *Biorheology*, **37** (2000), pp. 429-441.

[135] Pries, A. R., Neuhaus, D., and Gaehtgens, P., Blood viscosity in tube flow: dependence on diameter and hematocrit, *Am.J.Physiol*, **263** (Dec.1992), pp. H1770-H1778.

[136] Qin, Z., Durand, L. G., and Cloutier, G., Kinetics of the "black hole" phenomenon in ultrasound backscattering measurements with red blood cell aggregation, *Ultrasound in Medicine & Biology*, **24** (1998), pp. 245-256.

[137] Quemada, D., Towards a unified model of elasto-thixotropy of biofluids, *Biorheology*, **21** (1984), pp. 423-436.

[138] Rampling, M. W., Hyperviscosity as a complication in a variety of disorders, *Seminars Thrombosis & Hemostasis*, **29** (2003), pp. 459-465.

[139] Rampling, M. W., Meiselman, H. J., Neu, B., and Baskurt, O. K., Influence of cell-specific factors on red blood cell aggregation, *Biorheology*, **41** (2004), pp. 91-112.

[140] Regnaut C. and Ravey J.C., Application of the adhesive sphere model to the structure of colloidal suspensions, *Journal of Chemical Physics*, **91** (1989), pp. 1211-1221.

[141] Renner, W., Cichocki, L., Forjanics, A., Koppel, H., Gasser, R., and Pilger, E., G-455A polymorphism of the fibrinogen beta gene and deep vein thrombosis, *Eur.J.Clin.Invest*, **32** (Oct.2002), pp. 755-758.

[142] Riha, P., Donner, M., and Stoltz, J. F., Time-dependant formation of red blood cell aggregates and its influence on blood rheological behaviour, *Journal of Biological Physics*, **19** (1993), pp. 65-70.

[143] Rosendaal, F. R., Risk factors for venous thrombotic disease, *Thromb Haemost*, **82** (1999), pp. 610-619.

[144] Rouffiac, V., Péronneau, P., Hadengue, A., Barbet, A., Delouche, P., Dantan, P., Lassau, N., and Levenson, J., A new ultrasound principle for characterizing erythrocyte aggregation - In vitro reproducibility and validation, *Investigative Radiology*, **37** (2002), pp. 413-420.

[145] Saha R.K. and Cloutier, G., Monte Carlo study on ultrasound backscattering by three-dimensional distributions of red blood cells, *Physical Review E*, **78** (2008).

[146] Savéry, D., "Modélisation de la rétrodiffusion des ultrasons par le sang : application à la mesure de l'agrégation érythrocytaire." Ph.D. Université de Montréal, 2003.

[147] Savéry, D. and Cloutier, G., A point process approach to assess the frequency dependence of ultrasound backscattering by aggregating red blood cells, *Journal of the Acoustical Society of America*, **110** (2001), pp. 3252-3262.

[148] Savéry, D. and Cloutier, G., Effect of red cell clustering and anisotropy on ultrasound blood backscatter: a Monte Carlo study, *IEEE Trans Ultrason.Ferroelectr.Freq.Control*, **52** (2005), pp. 94-103.

[149] Savéry, D. and Cloutier, G., High-frequency ultrasound backscattering by blood: analytical and semianalytical models of the erythrocyte cross section, *J.Acoust.Soc Am.*, **121** (2007), pp. 3963-3971.

[150] Schmid-Schönbein, H., Gaehtgens, P., and Hirsch, H., On the shear rate dependence of red cell aggregation in vitro, *Journal of Clinical Investigation*, **47** (1968), pp. 1447-1454.

[151] Schulman, S. and Ogren, M., New concepts in optimal management of anticoagulant therapy for extended treatment of venous thromboembolism, *Thrombosis & Haemostasis*, **96** (Sept.2006), pp. 258-266.

[152] Schulman, S., Rhedin, A. S., Lindmarker, P., Carlsson, A., Larfars, G., Nicol, P., Loogna, E., Svensson, E., Ljungberg, B., and Walter, H., A comparison of six weeks with six months of oral anticoagulant therapy after a first episode of venous thromboembolism. Duration of Anticoagulation Trial Study Group, *New England Journal of Medicine*, **332** (1995), pp. 1661-1665.

[153] Sewchand, L. S., Masri, M. A., Fritz, O. G., Boyd, N. G., and Rowlands, S., Fibrinogen and the ultralong-range interaction of human erythrocytes, *Cell Biophysics*, **6** (1984), pp. 215-221.

[154] Shehada, R. E. N., Cobbold, R. S. C., and Mo, L. Y. L., Aggregation effects in whole blood: Influence of time and shear rate measured using ultrasound, *Biorheology*, **31** (1994), pp. 115-135.

[155] Sherar, M. D., Noss, M. B., and Foster, F. S., Ultrasound backscatter microscopy images the internal structure of living tumour spheroids, *Nature*, **330** (1987), pp. 493-495.

[156] Shung, K. K., On the ultrasound scattering from blood as a function of hematocrit, *IEEE Transactions on Sonics Ultrasound*, **SU-29** (1982), pp. 327-331.

[157] Shung, K. K., Cloutier, G., and Lim, C. C., The effects of hematocrit, shear rate, and turbulence on ultrasonic Doppler spectrum from blood, *IEEE Transaction on Biomedical Engineering*, **39** (1992), pp. 462-469.

[158] Shung, K. K., Sigelmann, R. A., and Reid, J. M., Scattering of ultrasound by blood, *IEEE Transaction on Biomedical Engineering*, **BME-23** (1976), pp. 460-467.

[159] Shung, K. K. and Thieme, G. A., *Ultrasonic scattering in biological tissues*, 1 ed. Boca Raton, Ann Arbor, London, Tokyo: CRC Press, 1993, pp. 1-486.

[160] Sigel, B., Machi, J., Beitler, J. C., Justin, J. R., and Coelho, J. C. U., Variable ultrasound echogenicity in flowing blood, *Science*, **218** (1982), pp. 1321-1323.

[161] Sigelmann, R. A. and Reid, J. M., Analysis and measurement of ultrasound backscattering from an ensemble of scatterers excited by sine-wave bursts, *Journal of the Acoustical Society of America*, **53** (1973), pp. 1351-1355.

[162] Snabre, P. and Mills, P., Rheology of weakly flocculated suspension of rigid particles, *J Phys III France*, **6** (1996), pp. 1811-1834.

[163] Snabre, P. and Mills, P., Rheology of weakly flocculated suspensions of viscoelastic particles, *J Phys III France*, **6** (1996), pp. 1835-1855.

[164] Stoltz, J. F. and Donner, M., Red blood cell aggregation: Measurements and clinical applications, *Tr J of Medical Sciences*, **15** (1991), pp. 26-39.

[165] Swarnamani, S. and Singh, M., Analysis of erythrocyte aggregation mechanism in presence of dextran and magnetic field by ultrasound scattering in blood., *Biorheology*, **26** (1989), pp. 847-862.

[166] Teh, B. G. and Cloutier, G., Modeling and analysis of ultrasound backscattering by spherical aggregates and rouleaux of red blood cells, *IEEE Transactions on Ultrasonics, Ferroelectrics, & Frequency Control*, **47** (2000), pp. 1025-1035.

[167] Trahey, G. E., Allison, J. W., and von Ramm, O. T., Angle independent ultrasonic detection of blood flow, *IEEE Trans.Biomed.Eng*, **34** (1987), pp. 965-967.

[168] Tunis, A. S., Czarnota, G. J., Giles, A., Sherar, M. D., Hunt, J. W., and Kolios, M. C., Monitoring structural changes in cells with high-frequency ultrasound signal statistics, *Ultrasound Med Biol.*, **31** (2005), pp. 1041-1049.

[169] Twersky, V., Transparency of pair-correlated, random distributions of small scatterers, with application to the cornea, *Journal of the Optical Society of America*, **65** (1975), pp. 524-530.

[170] Twersky, V., Low-frequency scattering by correlated distributions of randomly oriented particles, *Journal of the Acoustical Society of America*, **81** (1987), pp. 1609-1618.

[171] Ueda, M. and Ozawa, Y., Spectral analysis of echos for backscattering coefficient measurement, *Journal of the Acoustical Society of America*, **77** (1985), pp. 38-47.

[172] Van Der Heiden, M. S., De Kroon, M. G. M., Bom, N., and Borst, C., Ultrasound backscatter at 30 MHz from human blood: influence of rouleau size affected by blood modification and shear rate, *Ultrasound in Medicine & Biology*, **21** (1995), pp. 817-826.

[173] Van Hylckama, V. and Rosendaal, F. R., High levels of fibrinogen are associated with the risk of deep venous thrombosis mainly in the elderly, *J.Thromb.Haemost.*, **1** (2003), pp. 2677-2678.

[174] Vander, A. J., Sherman, J. H., and Luciano, D. S., *Human physiology. The mechanisms of body function*, 6 ed. New York, St. Louis, San Francisco, London, Toronto, Tokyo: McGraw-Hill, Inc., 1997, pp. 1-754.

[175] Vaya, A., Mira, Y., Martinez, M., Villa, P., Ferrando, F., Estelles, A., Corella, D., and Aznar, J., Biological risk factors for deep vein trombosis, *Clinical Hemorheology & Microcirculation*, **26** (2002), pp. 41-53.

[176] Vicaut, E., Opposite effects of red blood cell aggregation on resistance to blood flow, *Journal of Cardiovascular Surgery*, **36** (1995), pp. 361-368.

[177] Wang, S. H. and Shung, K. K., An approach for measuring ultrasonic backscattering from biological tissues with focused transducers, *IEEE Trans Biomed Eng*, **44** (1997), pp. 549-554.

[178] Wear, K. A., Stiles, T. A., Frank, G. R., Madsen, E. L., Cheng, F., Feleppa, E. J., Hall, C. S., Kim, B. S., Lee, P., O'Brien, W. D., Jr., Oelze, M. L., Raju, B. I., Shung, K. K., Wilson, T. A., and Yuan, J. R., Interlaboratory Comparison of Ultrasonic Backscatter Coefficient Measurements From 2 to 9 MHz, *J Ultrasound Med*, **24** (2005), pp. 1235-1250.

[179] Weng, X., Cloutier, G., Beaulieu, R., and Roederer, G. O., Influence of acute-phase proteins on erythrocyte aggregation, *American Journal of Physiology (Heart & Circulatory Physiology)*, **271** (1996), pp. H2346-H2352.

[180] Wessler, S., Studies in intravascular coagulation. I. Coagulation changes in isolated venous segments, *J Clin.Invest*, **31** (1952), pp. 1011-1014.

[181] Westergren, Studies of the suspension stability of the blood in pulmonary tuberculosis, *Acta Medica Scandinavica*, **54** (1921), pp. 247-281.

[182] Windberger, U., Bartholovitsch, A., Plasenzotti, R., Korak, K. J., and Heinze, G., Whole blood viscosity, plasma viscosity and erythrocyte aggregation in nine mammalian species: reference values and comparison of data, *Exp.Physiol*, **88** (2003), pp. 431-440.

[183] Yalcin, O., Aydin, F., Ulker, P., Uyuklu, M., Gungor, F., Armstrong, J. K., Meiselman, H. J., and Baskurt, O. K., Effects of red blood cell aggregation on myocardial hematocrit gradient using two approaches to increase aggregation, *American Journal of Physiology (Heart & Circulatory Physiology)*, **290** (2006), pp. H765-H771.

[184] Yalcin, O., Ulker, P., Yavuzer, U., Meiselman, H. J., and Baskurt, O. K., Nitric oxide generation of endothelial cells exposed to shear stress in glass tubes perfused with red blood cell suspensions : role of aggregation, *Am J Physiol Heart Circ.Physiol*, **294** (2008), pp. H2098-H2105.

[185] Yalcin, O., Uyuklu, M., Armstrong, J. K., Meiselman, H. J., and Baskurt, O. K., Graded alterations of RBC aggregation influence in vivo blood flow resistance, *American Journal of Physiology (Heart & Circulatory Physiology)*, **287** (2004), pp. H2644-H2650.

[186] Yarnell, J. W., Baker, I. A., Sweetnam, P. M., Bainton, D., O'Brien, J. R., Whitehead, P. J., and Elwood, P. C., Fibrinogen, viscosity, and white blood cell

count are major risk factors for ischemic heart disease. The Caerphilly and Speedwell collaborative heart disease studies, *Circulation*, **83** (1991), pp. 836-844.

[187] Yu, F., Gennisson, J. L., and Cloutier, G., A new method to assess the kinetics of rouleaux formation in human subcutaneous veins using high frequency parametric imaging: Preliminary results, *IEEE Ultrasonics Symposium*, **2** (2005), pp. 870-873.

[188] Yu, F., Savery, D., Amararene, A., Foster, F. S., and Cloutier, G., Attenuation compensated spectral slopes during the kinetics of rouleaux formation for porcine whole blood in couette flow at 10-70 MHz, *Ultrasonics Symposium*, **2** (2004), pp. 842-845.

[189] Yu, F. T. H. and Cloutier, G., Experimental ultrasound characterization of red blood cell aggregation using the structure factor size estimator, *Journal of the Acoustical Society of America*, **122** (2007), pp. 645-656.

[190] Yuan, Y. W. and Shung, K. K., The effect of focusing on ultrasonic backscatter measurements, *Ultrasonic Imaging*, **8** (1986), pp. 121-130.

[191] Yuan, Y. W. and Shung, K. K., Ultrasonic backscatter from flowing whole blood. I: Dependence on shear rate and hematocrit, *Journal of the Acoustical Society of America*, **84** (1988), pp. 52-58.

[192] Yuan, Y. W. and Shung, K. K., Ultrasonic backscatter from flowing whole blood. II: Dependence on frequency and fibrinogen concentration, *Journal of the Acoustical Society of America*, **84** (1988), pp. 1195-1200.

[193] Yuan, Y. W. and Shung, K. K., Echoicity of whole blood, *Journal of Ultrasound Medicine*, **8** (1989), pp. 425-434.

[194] Zhang, J., Johnson, P. C., and Popel, A. S., Red blood cell aggregation and dissociation in shear flows simulated by lattice Boltzmann method, *J Biomech.*, **41** (2008), pp. 47-55.

[195] Zuccarelli, F., Taccoen, A., Razavian, M., and Chabanel, A., Increasing erythrocyte aggregability with the progressive grades of chronic venous insufficiency: importance and mechanisms, *Journal of Cardiovascular Surgery*, **36** (1995), pp. 387-391.

7 Annexe A – Articles de conférence

2004 IEEE Ultrasonics Symposium

Attenuation Compensated Spectral Slopes during the Kinetics of Rouleaux Formation for Porcine Whole Blood in Couette Flow at 10–70 MHz

F. Yu*[1], D. Savéry[2], A.. Amararene[1], F.S. Foster[3], G. Cloutier[1]
[1]Laboratory of Biorheology and Medical Ultrasonics (LBMU), University of Montreal Hospital, Montreal, Canada
[2]Formerly with LBMU, now with Philips Research, New York, U.S.A
[3]Sunnybrook Health Science Centre, University of Toronto, Toronto, Canada

Abstract—**The characterization of red blood cell (RBC) aggregation using ultrasound is a promising technique allowing *in vivo* and *in situ* assessment of its level in the human body. It is known that pathological levels of RBC aggregation are correlated with diseases involving hemorheological disorders. Important efforts have thus been targeted towards theoretical and empirical studies on ultrasonic absolute RBC backscatter. In this study, we present ultrasonic absolute backscatter values (BSC), and spectral slope (SS) dependencies as a function of temporal shear rate variations. Porcine anti-coagulated blood at 40% hematocrit was placed in a modified Couette flow system at 37 °C. Backscattered RF data were digitized and analyzed, using three wide-band focused transducers of central frequencies 10, 35 and 55 MHz. BSC and SS were calculated for each transducer to provide kinetic profiles during aggregation and disaggregation of RBCs. The reference medium used for absolute BSC values was a 6 % hematocrit suspension of RBCs in Ringer solution (no aggregation). Frequency dependent beam variations were taken in account using a diffraction correction factor. Different results on BSC and SS sensitivity for "small aggregates" and "large aggregates" are described as a function of frequency. The size of the aggregates was varied by modifying the flow shear rate. According to these experimental results, it is shown that spectral slopes between 10-70 MHz could be of clinical relevance for *in vivo* detection of red blood cell aggregation. This index may be of interest to display parametric images of RBC aggregates.**

Keywords - ultrasound blood characterization, high frequency imaging, spectral slope, backscatter coefficient, red blood cell aggregation.

I. INTRODUCTION

RBC aggregation is a reversible phenomenon that occurs naturally in the circulation. However, an abnormal level of aggregation has been clinically correlated with hyperlipidemia, atherosclerosis, diabetes and myocardial infarction. Ultrasonic characterization of blood has been extensively explored in the last three decades both theoretically and experimentally since it is the only means for characterizing RBC aggregation both *in vivo* and *in situ* non-invasively [1]. However, if the characterization of RBC suspensions in saline is well understood and well explained theoretically by the Rayleigh scattering model [2], quantitative results on the characterization of whole blood is far more complex and understood in a lesser extent. The objective of characterizing RBC aggregation *in vivo* [3;4] calls for more quantitative exploration of the backscattering characteristics of whole blood. The main difficulty in tissue characterization is to isolate the different variables that intervene in the data acquisition process. The experimental setup of the present study has therefore been designed to control these parameters at the rheological and acoustical levels. As it is well known that the level of aggregation is strongly modulated by the flow shear rate (γ), results on absolute backscatter (BSC) frequency dependence are presented in this paper for whole blood sheared in a Couette flow system. In order to provide absolute tissue characteristics, a normalization procedure is presented for a single transducer, based on the use of a low density 6% hematocrit suspension of RBCs, as a reference medium [5]. Frequency dependent attenuation and diffraction are also corrected in the above method. Paired results obtained by using the same blood sample for three broadband transducers are presented to compare results in different frequency bands. The backscatter measurements presented in this study are reported in terms of absolute BSC and spectral slope (SS).

II. MATERIALS AND METHODS

Fresh porcine whole blood was obtained from a local slaughter house, anti-coagulated with 3 g/L of EDTA, and the hematocrit was adjusted to 40 %. A 60 ml sample was then taken and sheared in a Couette flow system, as in [6]. The whole setup was placed in an oven to stabilize the temperature at 37 °C throughout the measurements. Also, a 6 % hematocrit saline suspension (H6) was prepared separately with the same blood sample, as used as a reference medium for BSC.

Three broadband transducers were successively used in this experiment (10, 35 and 55 MHz). It is important to note at this point that the same blood sample was used for all three transducers and therefore all results were paired. The pulse-echo acquisition system was composed of an Avtech pulse generator, a Ritec diplexer, a 10 dB Mitec linear amplifier, a Panametric 5900PR pulser-receiver (used in reception mode for band pass filtering and 20-54 dB amplification), and an 8 bits 500 MHz sampling frequency GageScope acquisition board.

0-7803-8412-1/04/$20.00 (c)2004 IEEE.

2004 IEEE International Ultrasonics, Ferroelectric and Frequency Control Joint 50th Anniversary Conferen

We first acquired 100 RF lines in the H6 suspension and we repeated the procedure on a stainless steel plane reflector submerged in degasified water for each transducer positioned in its focal plane. Each transducer was then successively placed in the inner cylinder of the Couette system so that its focal plane matched the center of the 2 mm gap filled by blood. An agar gel was used to fill the gap between the transducer and the surface of the inner cylinder of the Couette system to minimize flow disturbance produced by the hole in which the transducer was installed and to provide acoustic impedance matching. We then acquired 20 RF lines every 125 ms during the kinetics of RBC aggregation. For every kinetic, the blood was first sheared for 30 s to disrupt all aggregates. The shear rate was then changed to different values for a plateau lasting 15 s. A window of 512 points in each line was selected in the focal zone of the transducer, zero padded, Fourier transformed and the amplitude squared to get the power spectrum of the backscattered signal. These spectra were then averaged in windows of 1 s. The normalization method is based on results published in two papers:

- It was suggested in [5] that with focalized transducers, a low density 6% hematocrit RBC suspension provided a better normalization medium than a planar reflector. If this H6 medium is well characterized, the absolute BSC can be obtained by :

$$BSC_{Blood} = BSC_{H6} \times \frac{S_{Blood}}{S_{H6}} \times e^{-4L(\alpha_{Blood} - \alpha_{H6})} \qquad (1)$$

where S_x, BSC_x and α_x are respectively the power spectra, the absolute backscatter coefficients, and the attenuation coefficients of whole blood and H6 reference media.

- A mathematical expression [7] that is applicable in the focal plane of a focused transducer for Rayleigh diffusers (for a correlation length of the scatterers much less than the acoustic wavelength), and by considering the Born conditions (weak scattering), the following equation states that :

$$BSC_{H6} = \frac{S_{H6}(f,F)}{S_{plane}(f,F)} \times \frac{1}{0.63^2} \times \frac{R_p{}^2 k^2 a^2}{8\pi d\left[1+\left(\frac{ka^2}{4F}\right)^2\right]} \times \exp(4\alpha_{H6}(f)d) \qquad (2)$$

where S_{plane}, R_p, k, a, F and d are respectively the planar reflector power spectrum, the reflection coefficient of the planar reflector (here 1), the wave vector, the transducer radius, the transducer focal length and the inspected depth.

At it has been shown [5] [8], suspended H=6% RBCs are Rayleigh scatterers in the range of frequencies considered here. Least mean squared linear regression of BSC as a function of the frequency (log-log scale) were calculated to compute SS. Values of α_{H6} = 0.03 dB/cm/MHz [5] and α_{Blood} = 0.22 dB/cm/MHz [9] were taken as first approximations.

III. RESULTS

A. *Verification of the normalization method for BSC*

Figure 1 shows the frequency dependence of BSC_{H6} calculated by using equation (1) for each transducer in its respective bandwidth. The results follow a power law in f^4 as expected for Rayleigh scatterers. The results are thus in good accordance with the literature [5] [8].

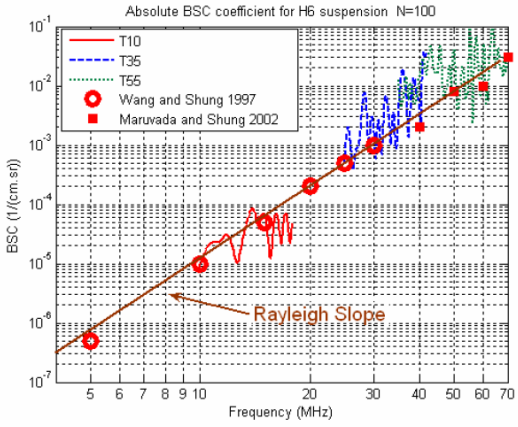

Figure 1. *: Frequency dependence of BSC_{H6} measured with all three transducers (T10, T35 and T55 MHz) and compared with the litterature.*

B. *Kinetics*

Using equation 2, we then computed BSC_{Blood} for different time variation patterns of the shear rate γ.

1) *For "small aggregates" (γ- pattern → 10 - 50 - 10 s^{-1})*

We first varied the shear rate to promote the formation of "small aggregates": We sheared the blood at 500 s^{-1} for 30 s to disrupt all aggregates. We then started acquiring data for 65 s as it was described before. After 5 s the shear rate was abruptly changed to 10 s^{-1} for 15 s, then changed to 50 s^{-1} for another 15 s, and again modified back to 10 s^{-1} for 15 s, and finally a shear rate of 500 s^{-1} was applied to disrupt the aggregates at the end. The evolution of BSC_{Blood} and SS are represented for each transducer in Figure 2.

With the 10 MHz transducer, at a shear rate of 500 s^{-1}, the absolute BSC was minimum (3.2×10^{-6} $cm^{-1}.sr^{-1}$) and the frequency dependence showed a SS close to 3. The shear rate was then abruptly changed to 10 s^{-1}: the BSC followed a sigmoid shape to reach a value of 1.4×10^{-4} $cm^{-1}.sr^{-1}$ (increase of 16.5 dB). When the shear was changed to 50 s^{-1}, the BSC decreased to 6.3×10^{-6} $cm^{-1}.sr^{-1}$ (decrease of 13.5 dB). When changed back to 10 s^{-1}, the BSC returned to the previous value in a predictable way. The SS showed no significant variation at this frequency.

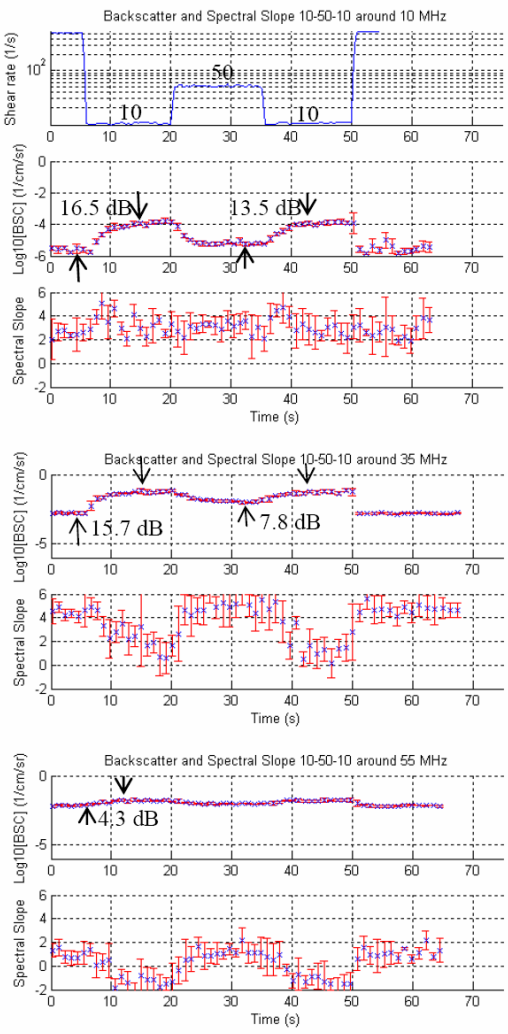

Figure 2. *BSC and SS kinetics for a shear rate variation pattern of 10-50-10 s^{-1} for each frequency transducer. These levels of shear rate were labeled as "small aggregates" formation in this study.*

With the 35 MHz transducer, the general pattern for BSC was similar to the previous observations: at 500 s^{-1} the BSC was $1.6x10^{-3}$ $cm^{-1}.sr^{-1}$. When the shear rate was abruptly changed to 10 s^{-1}, the BSC followed a sigmoid shape to reach a value of $6x10^{-2}$ $cm^{-1}.sr^{-1}$ (increase of 15.7 dB). When the shear was changed to 50 s^{-1}, the BSC decreased to $1x10^{-2}$ $cm^{-1}.sr^{-1}$ (decrease of 7.8 dB). However at this frequency, SS variations could be observed: SS decreased from 4.5 to 1 when the shear was changed from 500 s^{-1} to 10 s^{-1}. At 50 s^{-1}, the slope reached a value of 5. Although both BSC and SS curves show symmetrical behavior, the dynamic range of the BSC variation decreased compared to the results at 10 MHz, and the sensitivity of the SS parameter to the level of RBC aggregation seemed to be improved at this frequency.

With the 55 MHz transducer, similar observations can be made : whereas the BSC dynamic range decreased (from $6x10^{-3}$ $cm^{-1}.sr^{-1}$ to $1.6x10^{-2}$ $cm^{-1}.sr^{-1}$ for a variation of 4.3 dB when the shear rate was varied from 500 s^{-1} to 10 s^{-1}), SS varied from 1 to -2 for a consistent dynamic range of 3. The dynamic range of the BSC variation was very small with γ changing from 10 to 50 s^{-1}. However, as for the 35 MHz transducer, the SS variation was important at this frequency.

2) For "large aggregates" (γ- pattern $\rightarrow$ 2 - 10 - 2 s^{-1})

The same results are plotted in Figure 3 for a shear rate pattern of 2-10-2 s^{-1}, to promote the formation of "bigger aggregates". The variation of BSC was rather small for all frequencies when the shear rate was changed from 2 to 10 and then back to 2 s^{-1}: the dynamic range of BSC was very small at 10 MHz (3 dB). At higher frequencies, this variation was even smaller. However, the SS variation shows an interesting behavior: When the shear was changed from 500 s^{-1} to 2 s^{-1}, SS varied from 4 to 1 at 10 MHz and 35 MHz, and from 1 to -2 at 55 MHz. Also, SS was sensitive to the shear rate variation from 2 s^{-1} to 10 s^{-1} at 10 MHz. All these results are discussed in the next section.

IV. Discussion

A. *Terminology : "large" and "small" aggregates*

The terms "large" and "small" aggregates refer to relative size estimations that are only based on the well known shear rate versus rouleaux size relationship [10]. Absolute RBC aggregate size estimations have not been assessed so far.

B. *Spectral slope sensitivity*

From the previous results, it can be said that SS sensitivity increases with frequency for "small aggregates", whereas it decreases with frequency for "big aggregates". The very straightforward explanation for this observation is to consider the ratio between the ultrasonic wavelength and the scatterer size. When the scatterers are very small compared to the wavelength, we are in the presence of Rayleigh scatterers and SS is close to 4. This is the situation with small aggregates at 10 MHz. However, at 35 MHz and 55 MHz, because the wavelength decreases, the scatterers are no longer in the Rayleigh scattering regime and SS decreases when the shear rate diminishes. With the bigger aggregates, at 10 MHz and 10 s^{-1}, the scatterers are probably at the limit of the Rayleigh regime and SS is sensitive to aggregate size variations. At higher frequencies, the aggregates are already in the non-Rayleigh regime at 10 s^{-1} ($SS << 4$) and SS is not sensitive to the aggregate size variation for shear rates going from 2 s^{-1}, to 10 s^{-1} and back to 2 s^{-1}.

C. *Negative slope at 55 MHz*

If this result looks surprising at a first glance, it can be related to mathematical simulation models of aggregating RBCs that have been published in the literature. In these models, the BSC was shown to increase with frequency, to

reach a maximum and then to decrease as the frequency was further increased, thus resulting in the presence of a negative slope at high frequencies [11].

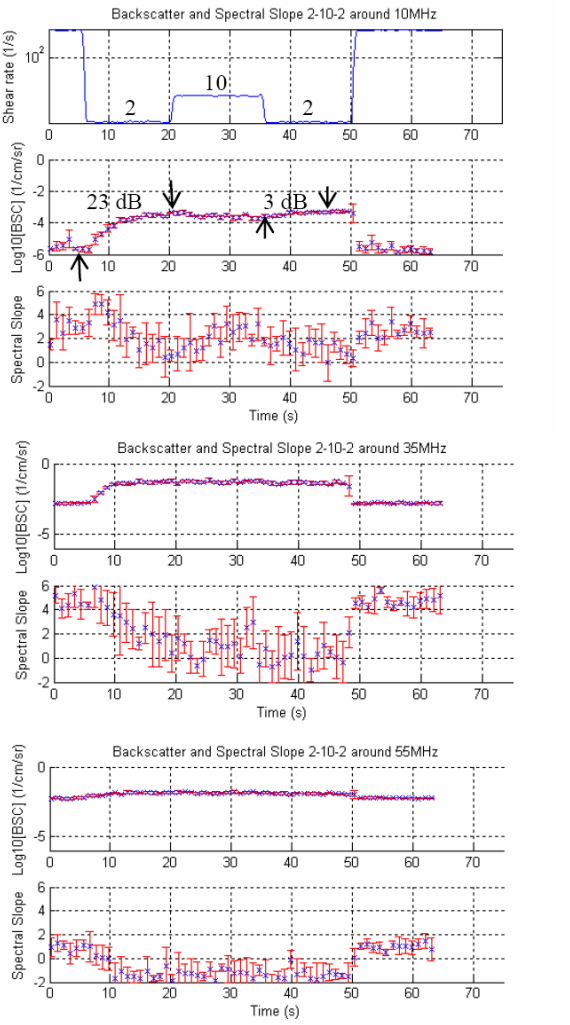

Figure 3. *BSC and SS kinetics for a shear rate variation pattern of 2-10-2 s^{-1} for each frequency transducer. These levels of shear rate correspond to the formation of "large aggregates".*

D. Problems with the 10 MHz transducer

The meticulous reader will notice on Figure 1 that the 10 MHz transducer bandwidth was not centered around 10 MHz. This discrepancy was caused by an error in the pulse generator settings for this transducer. The frequency band from 10 MHz to 18 MHz was selected based on the spectrum of the H6 reference solution, which reflects the conditions of acquisition better than the characteristics of the transducer. Because of this technical problem, more investigation must be done to confirm our lower frequency results. For instance the SS of 3 with this transducer must be further examined.

V. CONCLUSION

This study presented quantitative assessments of BSC and SS between 10 to 70 MHz as a function of the shear rate precisely controlled in a Couette flow system. A normalization method was introduced and validated with experimental data from the literature. It has been shown that SS sensitivity to RBC aggregation was increased at shear rates higher that 10 s^{-1} by using high frequency transducers. This suggests the use of parametric images of SS at high frequencies to map the phenomenon of red cell aggregation *in vivo*.

ACKNOWLEDGMENT

The authors would like to thank M. J. Brochu and M. R. Renaud from "Les Viandes ULTRA Meats Inc." for blood supplies. This research was supported by a grant from the Canadian Institutes of Health Research (MOP-36467).

REFERENCES

[1] G. Cloutier, and Z. Qin., "Ultrasound backscattering from non-aggregating and aggregating erythrocytes - A review," Biorheology, vol. 34, no. 6, pp. 443-470, 1997.

[2] K. K. Shung, R. A. Sigelmann, and J. M. Reid, "Scattering of ultrasound by blood," IEEE Trans. Biomed. Eng., vol. BME-23, no. 6, pp. 460-467, 1976.

[3] H. Kitamura and S. Kawasaki, "Detection and clinical significance of red cell aggregation in the human subcutaneous vein using a high-frequency transducer (10 MHZ): A preliminary report," Ultrasound Med. Biol., vol. 23, no. 6, pp. 933-938, 1997.

[4] M.G.M. De Kroon, C.J. Slager, W.J. Gussenhoven, P.W. Serruys, J.R.T..C. Roelandt, , and N. Bom, "Cyclic changes of blood echogenicity in high-frequency ultrasound," Ultrasound Med. Biol., vol. 17, no. 7, pp. 723-728, 1991.

[5] S.H. Wang and K.K. Shung, "An approach for measuring ultrasonic backscattering from biological tissues with foccussed transducers," IEEE Trans. Biomed. Eng., vol. 44, no. 7, pp. 549-554, Jan.1997.

[6] M.S. Van Der Heiden, M.G.M. De Kroon, N. Bom, and C. Borst, "Ultrasound backscatter at 30 MHz from human blood: influence of rouleau size affected by blood modification and shear rate," Ultrasound Med. Biol., vol. 21, no. 6, pp. 817-826, 1995.

[7] M. Ueda and Y. Ozawa, "Spectral analysis of echos for backscattering coefficient measurement," J. Acoust. Soc. Am., vol. 77, no. 1, Jan.2004.

[8] S. Maruvada, K.K. Shung, and S.H. Wang, "High-frequency backscatterer and attenuation measurements of porcine erythrocyte suspensions between 30-90 MHz," Ultrasound Med. Biol., vol. 28, no. 8, pp. 1081-1088, 2002.

[9] J.A. Jensen, Estimation of blood velocities using ultrasound. A signal processing approach, 1st ed. New York, Australia: Cambridge University Press, 1996, pp. 1-289.

[10] S. Chien, "Blood viscosity: Influence of erythrocyte aggregation," Science, vol. 157 pp. 829-831, 1967.

[11] D. Savéry and G. Cloutier, "A point process approach to assess the frequency dependence of ultrasound backscattering by aggregating red blood cells," J. Acoust. Soc. Am., vol. 110, no. 6, pp. 3252-3262, 2001.

A new method to assess the kinetics of rouleaux formation in human subcutaneous veins using high frequency parametric imaging: preliminary results

François Yu, Jean-Luc Gennisson and Guy Cloutier
Laboratory of Biorheology and Medical Ultrasonics, University of Montreal Hospital Research Center, Montreal, Canada

Abstract— **Laser erythroaggregameter is considered as the gold standard method for *in vitro* red blood cell (RBC) aggregation characterization. With this method, a high shear rate is first applied on the blood sample to disrupt the aggregates and to provide a common reference level prior to the aggregation phases. *In vivo*, it is very difficult to have a standard protocol that would allow studying the kinetics of rouleaux formation following prior disruption of the aggregates. We propose a new approach using low frequency shear waves to initially disrupt the aggregates, followed by the measurement of the kinetics of aggregation with high-frequency ultrasound in a peripheral subcutaneous vein following flow stoppage. Radio frequency (RF) data was recorded and absolute backscatter coefficient (BSC) and spectral slope (SS) were calculated on video sequences of 25 s for two normal individuals. BSC and SS varied over time ($p < 0.001$) and differed between subjects ($p < 0.001$), due to the different aggregability of RBCs between the two individuals. This later result was corroborated by the laser aggregameter method. Immediately after the transmission of shear waves, no significant differences between groups were found for BSC and SS, suggesting that this approach effectively provides a common reference level of disaggregation. In conclusion, it is shown that shear wave propagation in the subcutaneous vein allows disaggregation of RBCs and the obtaining of a common reference level to allow reproducible measurements of BSC and SS during the kinetic of rouleaux formation. It is believed that this method could be of clinical significance for *in vivo* measurements in pathologies associated with hyper-aggregation of erythrocytes.**

Keywords - ultrasound tissue characterization, high-frequency imaging, spectral slope, backscatter coefficient, red blood cell aggregation, in vivo study, parametric imaging.

I. Introduction

Red blood cell aggregation (RCA) occurs naturally in the human circulation. Under normal conditions, erythrocytes pile up and form reversible complex networks of rouleaux that disaggregate when passing microvessels. Although the exact physiological role of RBC aggregation has not been clear elucidated yet, it is well known that pathological levels RCA are observed in atherosclerosis, thrombosis, diabete hypertension, hyperlipidemia and many other vascul disorders. Ultrasonic imaging holds the perspective of furth elucidating the role of RCA on the etiology of these diseas *in vivo*.

In the field of ultrasound (US) tissue characterization, t ultrasonic signal scattered by an insonicated tissue is analyz to reveal its physical and structural properties. The first a foremost used US parameter is the B-mode power intensity the US signal. More quantitative and normalized paramete from RF measurements have since been proposed [including BSC and SS. Ultrasound characterization of blo has captivated many scientists in the last three decad because of its unique potential to assess the level of RCA bc *in vivo* and *in situ*. The dependence of blood echogenicity parameters such as the hematocrit, shear rate, plasr macromolecule concentration, flow disturbance and flc pulsatility has been studied extensively *in vitro* [2]. T backscattered signal at high frequencies has also be explored in order to take advantage of a better resolution. *vivo*, the task of quantifying the level of aggregation has be proven more difficult. The first study of *in vivo* B-mo imaging of aggregation in anesthetized dogs was conducted Sigel and al. [3]. Kitamura and al. [4] measured a sen quantitative 18 dB increase of blood echogenicity in B-mo following flow stoppage in a subcutaneous vein of the hum forearm. These measures showed good correlation wi plasma fibrinogen, serum total cholesterol and serum prote fraction excluding albumin. Both teams concluded on t necessity of exploiting absolute quantitative US indices achieve relevant clinical diagnosis. Using a 10 MHz cathet directly positioned into the vena cava and the aorta of you pigs, Wang and al. [5] were the firsts to report absolu quantitative measures of BSC *in vivo*, using a 6% hematoc reference RBC suspension (H6). They confirmed th differences of RCA in flowing blood between veins a arteries could be measured at 10 MHz. Exploiting pow Doppler measurements on normal and hyperlipidemic patien Cloutier and al. [6] had shown earlier significantly differe backscattered power between veins and arteries at the ilia femoral and popliteal sites. However, with the exception of t

femoral vein, the two populations could not be distinguished in this study.

In this work, we describe preliminary results on the potential of using high-frequency ultrasound (40 MHz) to differentiate the level of aggregation *in vivo* in the forearm subcutaneous vein of two individuals. The protocol relies on the kinetic profiles of quantitative BSC and SS measured under complete stasis of the flow. An initial disaggregation phase was obtained by sending low-frequency shear waves in the region of interest.

II. Materials and Methods

A. Population

Two healthy male volunteers, non smokers, not under medication and presenting no medical history of known pathology associated with increased erythrocyte aggregation were asked to participate in the study. To assess the repeatability of the method, five exams were conducted after an overnight fast on five different days for each subject. Two sequences of RF data were acquired on each exam.

B. RBC agregation

To assess the aggregation properties of erythrocytes, on three of these exams, 1.5 ml of EDTA (Ethylene Diamine Tetra-acetic Acid dipotassium salt) anticoagulated blood samples were withdrawn and rotated in a Couette flow instrument based on laser light scattering (erythro-aggregameter, Regulest, Florange, France). The indices measured with this instrument are described in [7]. They are considered as the gold standard for assessing kinetic indices and adhesion energy levels of RCA.

C. Ultrasound acquisition and signal processing

Complete flow stoppage in the forearm was obtained with proximal and distal constrictions of the region of interest, similarly to the manner reported in [4]. Acquisition of RF data was made using a VisualSonics wideband 40 MHz system (Vevo 660, Toronto, Canada) connected to an acquisition board (Gagescope 5800, 250 MHz sampling frequency). The focal point at 6 mm was positioned inside the lumen of the vessel, imaged in cross-section. Complete flow stoppage was visually inspected by speckle tracking on B-mode images. For all measurements, the power setting of the Vevo660 system was set at 32 % and the gain was 24 dB. Ten 25 s sequences of RF data were acquired for each patient. During the first 5 s, shear waves were externally applied on the vessel using a mini shaker (Type 4810, Brüel & Kjæl, Denmark) manually positioned near the region of interest. The shear waves were generated by exciting the mini shaker with a 60 Hz 10 Vpp sinusoidal signal. The vibration was then stopped and the remaining 20 s of acquisition corresponded to the aggregation phase. To provide parametric images of BSC and SS, sets of 10 images of 384 lines were registered, Fourier transformed, averaged in the spectral domain, normalized with respect to a 6 % hematocrit reference RBC suspension at 37°C, and compensated for attenuation. BSC and SS calculations are described in detail in [8]. The attenuation was compensated using an arbitrary standard value of 0.2 dB/MHz/cm [9].

D. Statistical tests

All results were expressed as mean ± 1 standard deviation (SD). Two way ANOVA (N=10) tests were used to analyze the BSC and SS results (Sigma Stat, Jandel Scientific, San Rafael, Ca, USA). A multiple pair wise comparison procedure was also performed using the Tukey algorithm.

III. Results

A. Parametric images

Figure 1 presents typical parametric images of BSC and SS images, a) at the beginning (3rd s) and b) the end (20th s)of an acquisition.

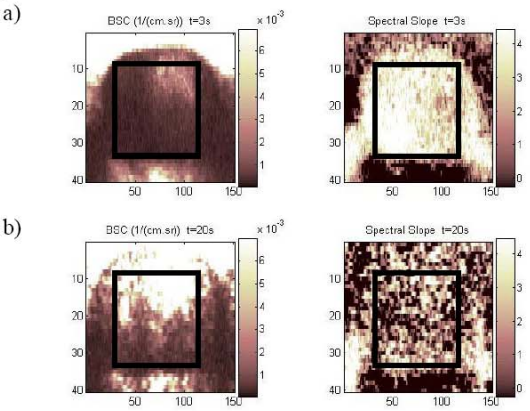

Figure 1 : Images of BSC and SS in the subcutaneous vein: a) at the 3rd s and b) at the 20th s of the acquisition. The shear waves were transmitted between 0 s < t < 5 s. Axes are in pixels. The diameter of the vessel is 2 mm. The focal point is at 6 mm.

Mean values of BSC and SS were calculated on the largest square manually selected within the vessel to extract mean kinetic curves for each sequence.

B. H6 reference medium

Figure 2 shows the frequency dependence of the BSC in a 6% hematocrit porcine RBC suspension.

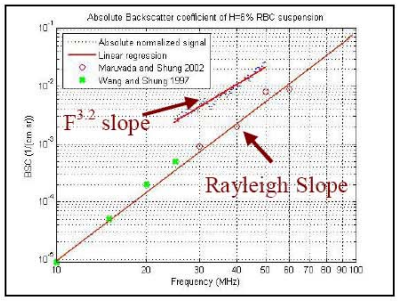

Figure 2 : BSC of a H6 suspension at 37°C, showing a SS of 3.2. Published experimental measurements are also presented for reference. The Rayleigh F^4 frequency dependence slope curve is also traced.

The use of such a reference medium was proposed in [8;10] The theoretical Rayleigh F^4 slope is traced for reference purpose. The linear regression used to determine the slope is also traced on the graph. A slope of 3.2 was found for the reference medium in the range of frequencies considered.

C. *Kinetics of RBC aggregation*

Figure 3 shows the effect of rouleaux formation on the BSC and the SS. Shear waves were applied on the vein of interest during the first 5 s, provoking an initial state of RBC disaggregation in the stagnant blood. At that point, the mean level of BSC for subjects 1 and 2 were, respectively, of $4.1\times10^{-4} \pm 6.1\times10^{-5}$ $cm^{-1}.sr^{-1}$ and $5.8\times10^{-4} \pm 3.1\times10^{-4}$ $cm^{-1}.sr^{-1}$. SS values were respectively 4.5 ± 0.3 and 4.2 ± 0.7. The mini shaker was then removed and the process of rouleaux formation began. BSC values increased to $1.1\times10^{-3} \pm 2.9\times10^{-4}$ $cm^{-1}.sr^{-1}$ (+4.1 dB) and $2.9\times10^{-3} \pm 1.7\times10^{-3}$ $cm^{-1}.sr^{-1}$ (+7 dB) for subjects 1 and 2, respectively; they were stable at that level after 20 seconds. SS decreased to 2.2 ± 0.4 and 1.0 ± 0.6 for these two individuals. However, the SS curves did not reach a plateau by the end of the 25 s of acquisition. These values are summarized in Table 1. The reported measures were computed over the first and last three seconds of acquisition.

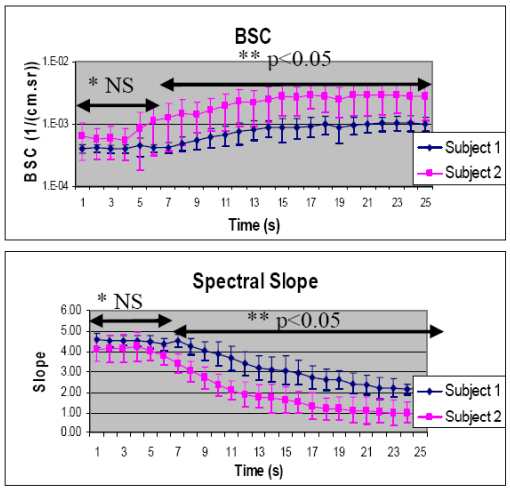

Figure 3 : Variation of BSC and SS in time. Shear waves were applied during the first 5 s. The results are expressed as mean ± 1 SD. N=10 for each subject. *indicates non significant (p>0.05) differences between subjects at a particular time. ** indicates significant (p<0.05) differences between subjects at a particular time.

Two way ANOVA tests on BSC and SS indicate: (1) that the difference in the mean values among the two subjects is statistically significant ($p<0.001$) after allowing for effects of differences in time; (2) that the difference in the mean values among the different time levels is also statistically significant ($p<0.001$) after allowing for effects of differences between subjects. These results show that SS and BSC are modified by the application of shear waves at the beginning of the experiment. The Tukey pair wise multiple comparison procedure showed that the BSC and SS between both groups at each moment are significantly different ($p<0.05$), between 5 s < t < 25 s (Figure 3).

			Mean	SD	SD/Mean
Beginning of kinetic	BSC	Subject 1	4.09×10^{-4}	6.12×10^{-5}	15 %
		Subject 2	5.79×10^{-4}	3.07×10^{-5}	53 %
	Slope	Subject 1	4.5	0.3	6 %
		Subject 2	4.2	0.7	16 %
End of kinetics	BSC	Subject 1	1.05×10^{-3}	2.85×10^{-4}	27 %
		Subject 2	2.89×10^{-3}	1.71×10^{-3}	59 %
	Slope	Subject 1	2.2	0.4	18 %
		Subject 2	1.0	0.6	59 %

Table 1 : Summary of BSC and SS levels across the vessel at the beginning (first 3 s) and at the end (last 3 s) of the measurements. SD/Mean is the coefficient of variation.for 10 scannings of a given subject.

	tA	S10	γD	H
Subject 1	7.7 ± 0.9	11.6 ± 0.6	20.7 ± 0.3	47.3 ± 0.6
Subject 2	3.2 ± 0.3	19.9 ± 2.0	37.5 ± 5.3	41.7 ± 2.1

Table 2 : Physiological parameters related to the rheology of blood measured by the laser erythroaggregameter at room temperature. These results are the mean of three measurements on three different days. Parameters : tA = primary aggregation time; S10 = mean kinetic index at 10 s ; γD = partial dissociation threshold ; H= hematocrit.

IV. Discussion

A. *Interpretation of the RBC aggregation kinetics*

As shown in Figure 3, the significantly higher BSC value and lower SS value at the end of the experiments suggest the existence of a higher level of aggregation for subject 2. This suggestion is confirmed by the *in vitro* laser aggregameter indices; for instance, a lower value of tA and higher S10 and γD indicate a higher level of aggregation for subject 2 (see Table 2). Moreover, these results (Figure 3) also suggest that the level of disaggregation induced by the application of shear waves was comparable between the two individuals. The application of shear waves could thus provide a common reference level prior to kinetic US measurements *in vivo*. The mechanisms explaining the effect of shear waves on RBC disaggregation will need further investigations.

In Figure 3, lower BSC values, corresponding to a disaggregated state, were associated with SS near 4. Higher BSC, corresponding to higher levels of aggregation, were associated with lower SS values. These variations in BSC and SS are coherent for both individuals regarding Rayleigh and specular scattering theories. It is interesting to note that BSC curves reached a plateau at the 20th second, while SS curves were still decreasing. This suggests a higher sensitivity of SS to the formation of aggregates, emphasizing the importance of developing parametric imaging for the ultrasound characterization of blood.

Absolute *in vitro* BSC values were published for human blood as a function of the shear rate [11]. Using a 50 MHz wideband transducer, Foster et al. measured BSC in the range of 4×10^{-3} $cm^{-1}.sr^{-1}$ to 8×10^{-2} $cm^{-1}.sr^{-1}$ at 35 MHz. Our absolute BSC values are lower than those reported in that study. One possible explanation is the use of a lower attenuation coefficient of 0.2 dB/MHz/cm (compared to 3 dB/mm at 50 MHz in their study). In that same study, BSC variations of 14.3 dB were measured between low and high levels of residual shear rate in blood subjected to a Couette flow. It is well known that aggregation is higher under low residual shear than under conditions [12]. That could explain parts of our lower 4.1 to 7 dB BSC variations.

B. 6% hematocrit reference medium

This medium would have expected to present a SS of 4, in accordance with the Rayleigh theory. In our results, there was however an overestimation of the BSC as compared to values published by [10;13] and a SS of 3.2 was found. One explanation for this discrepancy is that a broadband band excitation pulse was used rather than a sinusoidal tone pulse. Another explanation is that the suspension of washed RBCs could have contained some residual plasma protein therefore promoting a little aggregation. Notice, however, that for the purpose of this paper, the same reference medium was used for all experiments. Thus, this factor did not interfere with the comparative study reported here.

C. Repeatability

The coefficients of variation in Table 1 showed higher values at the end of the kinetics of aggregation. This can be explained by the complex nature of 3D rouleaux since different aggregate sizes may be present in the region of interest and at different spatial orientations. The effect of anisotropy on BSC has been documented in the literature. Furthermore, the acquisitions were performed on five different days, which also could induce higher variabilities.

D. Preliminary results

This study constitutes preliminary results as they were only performed on two subjects. More extensive studies of two populations with circulatory related disorders would be required, following FDA approval of the apparatus.

V. Conclusion

Different levels of RCA in two individuals were quantitatively assessed *in vivo* non-invasively. The application of shear waves at the beginning of the acquisition provided a common reference level prior to quantitative US kinetic measurements. These preliminary results strongly support that this method could be of clinical significance for reproducible *in vivo* measurements in pathologies associated with hyper-aggregation of erythrocytes.

Acknowledgments

This research was supported by a grant from the Canadian Institutes of Health Research (MOP-36467), and by a National Scientist award from the Fonds de la Recherche en Santé du Québec (to G.C.). This work was also supported by a doctoral scholarship from the National Sciences and Engineering Council of Canada.

References

[1] F. L. Lizzi, , M. Greenebaum, E.J. Feleppa, M. Elbaum and D.J. Coleman, "Theoretical framework for spectrum analysis in ultrasonic tissue characterization," *J Acoust Soc Am, ;73(4):1366-73,1983.*

[2] G. Cloutier and Z. Qin, "Ultrasound backscattering from non-aggregating and aggregating erythrocytes - A review," *Biorheology*, vol. 34, no. 6, pp. 443-470, 1997.

[3] B. Sigel, J. Machi, J.C. Beitler, J.R. Justin and J.C.U. Coelho, "Variable ultrasound echogenicity in flowing blood," *Science*, vol. 218, pp. 1321-1323, 1982.

[4] H. Kitamura and S. Kawasaki, "Detection and clinical significance of red cell aggregation in the human subcutaneous vein using a high-frequency transducer (10 MHz): A preliminary report," *Ultrasound in Medicine & Biology*, vol. 23, no. 6, pp. 933-938, 1997.

[5] S.H. Wang and K.K. Shung, "*In vivo* measurements of ultrasonic backscattering in blood," *IEEE Transactions on Ultrasonics, Ferroelectrics, & Frequency Control*, vol. 48, no. 2, pp. 425-431, 2001.

[6] G. Cloutier, X. Weng, G.O. Roederer, L. Allard, F. Tardif and R. Beaulieu, "Differences in the erythrocyte aggregation level between veins and arteries of normolipidemic and hyperlipidemic individuals," *Ultrasound in Medicine & Biology*, vol. 23, no. 9, pp. 1383-1393, 1997.

[7] M. Donner, M. Siadat and J.F. Stoltz, "Erythrocyte aggregation: Approach by light scattering determination," *Biorheology*, vol. 25, pp. 367-375, 1988.

[8] F. Yu, D. Savery, A. Amararene, F. S. Foster, and G. Cloutier. Attenuation compensated spectral slopes during the kinetics of rouleaux formation for porcine whole blood in couette flow at 10-70 MHz. Proceedings - IEEE Ultrasonics Symposium . 2004.

[9] J.A. Jensen, *Estimation of blood velocities using ultrasound. A signal processing approach*, 1st ed. New York, Australia: Cambridge University Press, 1996, pp. 1-289.

[10] S.H. Wang and K.K. Shung, "An approach for measuring ultrasonic backscattering from biological tissues with focused transducers," *IEEE Trans Biomed Eng ;44(7):549-54.*, vol. :549-54. pp. -54, 1997.

[11] F.S. Foster, H. Obara, T. Bloomfield, L.K. Ryan and G.R. Lockwood, "Ultrasound backscatter from blood in the 30 to 70 MHz frequency range," *IEEE Ultrasonics Symposium Proceedings*, pp. 1599-1602, 1994.

[12] V. Rouffiac, P. Peronneau, J.P. Guglielmi, M. Del Pino, N. Lassau and J. Levenson, "Comparison of new ultrasound index with laser reference and viscosity indexes for erythrocyte aggregation quantification," *Ultrasound Med Biol, 29(6):789-99.*, vol. :789-99. pp. -99, 2003.

[13] S. Maruvada, K.K. Shung and S.H. Wang, "High-frequency backscatterer and attenuation measurements of porcine erythrocyte suspensions between 30-90 MHz" *Ultrasound in Medicine & Biology*, vol. 28, no. 8, pp. 1081-1088, 2002.

8 Annexe B – Articles de revue scientifique

Franceschini *et al.*: JASA Express Letters [DOI: 10.1121/1.2896115] Published Online 20 March 20

Simultaneous estimation of attenuation and structure parameters of aggregated red blood cells from backscatter measurements

Emilie Franceschini, François T. H. Yu, and Guy Cloutier
Laboratory of Biorheology and Medical Ultrasonics, University of Montreal Hospital Research Center, 2099 Alexandre de Sève (room Y-1619), Montréal, Québec, H2L 2W5, Canada

Abstract: The analysis of the ultrasonic frequency-dependent backscatter coefficient of aggregating red blood cells reveals information about blood structural properties. The difficulty in applying this technique *in vivo* is due to the frequency-dependent attenuation caused by intervening tissue layers that distorts the spectral content of backscattering properties from blood microstructures. An optimization method is proposed to simultaneously estimate tissue attenuation and blood structure factor. With *in vitro* experiments, the method gave satisfactory estimates with relative errors below 22% for attenuations between 0.101 and 0.317 dB/cm/MHz, signal-to-noise ratios >28 dB and $kR<2.7$ (k being the wave number and R the aggregate radius).

PACS numbers: 43.80.Qf, 43.80.Cs, 43.35.Bf, 43.35.Yb [CC]
Date Received: October 5, 2007 **Date Accepted:** January 15, 2008

1. Introduction

Ultrasonic (US) backscattered echoes from blood contain frequency-dependent information that can be used to obtain quantitative parameters reflecting the aggregation state of red blood cells (RBCs). Recently, two parameters describing RBC aggregation, the packing factor and mean fractal aggregate diameter, were extracted from the structure factor size estimator (SFSE).[1] The SFSE is a second-order data reduction model based on the structure factor and adapted to a dense medium such as blood. This approach is based on the analysis of the backscattered power spectrum that contains information about the size, spatial organization, concentration and mechanical properties of scatterers (i.e., RBCs). The difficulty in applying the SFSE *in vivo* is that the spectral content of backscattered echoes is also affected by attenuation caused by intervening tissue layers between the probe and the blood flow. More generally, ultrasound scatterer size estimation techniques for tissue characterization (such as liver, kidney, prostate or breast) are facing similar challenges.[2,3] To correctly evaluate microstructural parameters, it is thus of major interest to take into account tissue attenuation effects. A few groups[2,4,5] developed measurement techniques to evaluate the frequency-dependent attenuation in order to compensate *a posteriori* the backscattered power spectrum. The goal of this letter is to further develop this strategy for *in vivo* measures of RBC scatterer sizes. We propose to simultaneously determine blood structural parameters and total attenuation by using an optimization method, termed the structure factor size and attenuation estimator (SFSAE).

This method consists in fitting the spectrum of the backscattered radio-frequency (rf) echoes from blood to an estimated spectrum by a modified SFSE model. This approach is similar to that presented by Bigelow *et al.*,[3] who estimated the effective radius of tissue microstructure and total attenuation from simulated backscattered signals. Herein, *in vitro* experimental evaluation of the SFSAE is performed. Porcine RBCs were sheared in a Couette flow system, and ultrasonic rf echoes were obtained using a 25 MHz center-frequency transducer. Since skin is one of the most attenuating tissue layers during *in vivo* scanning, three skin-mimicking phantoms with different attenuation coefficients were successively introduced between the

Franceschini *et al.*: JASA Express Letters [DOI: 10.1121/1.2896115] Published Online 20 March 2008

transducer and the blood flow. This study shows the SFSAE ability to evaluate three parameters (the packing factor, mean fractal aggregate diameter, and total attenuation).

2. Structure factor size and attenuation estimator

Blood can be seen as a very dense suspension of red cells. These RBCs cannot be treated as independent scatterers since particle interactions (collision, attraction, deformation, flow dependent motions) are strong. The theoretical model of ultrasound backscattering by blood that we developed[1] is based on the particle approach,[6,7] which consists of summing contributions from individual RBCs and modeling the RBC interaction by a particle pair-correlation function. Assuming that the Born approximation is valid (weak scattering), the model proposed in Ref. 1 can be modified to predict the theoretical backscatter coefficient from blood

$$BSC_{\text{theor}}(k) = m\sigma_b(k)S(k)A(k), \tag{1}$$

where k is the wave vector, m is the number density of RBCs in blood estimated by measuring the hematocrit H by microcentrifugation ($m=H/V_s$, where V_s is the volume of a RBC), σ_b is the backscattering cross section of a single RBC, S is the structure factor describing the spatial organization of RBCs, and A is the frequency-dependent attenuation function. The backscattering cross section σ_b of a weak scattering particle small compared to the wavelength (Rayleigh scatterer) can be determined analytically as follows: $\sigma_b(k)=1/(4\pi^2)k^4V_s^2\gamma_z^2$, where γ_z is the variation of impedance between the RBC and its suspending medium (i.e., the plasma). The structure factor S is by definition the Fourier transform of the pair-correlation function[7] g and can be approximated by its second-order Taylor expansion[1] in k as

$$S(k) = 1 + m\int (g(r)-1)e^{-2jkr}dr \approx W - \frac{12}{5}(kR)^2. \tag{2}$$

In this expression, $g(r)$ represents the probability of finding two particles separated by a distance r. W is the low-frequency limit of the structure factor ($S(k)|_{k\to 0}$) called the packing factor.[7,8] R is the radius of three-dimensional (3D) RBC aggregates assumed to be isotropic. We introduce $D=R/a$ as the isotropic diameter of an aggregate (expressed in number of RBCs) with a the radius of one RBC sphere-shaped model of volume V_s. The attenuation function A is given by: $A(k)=e^{-4\alpha_0 f}$, where f is the frequency and α_0 is the attenuation coefficient (in dB/MHz) defined by: $\alpha_0=\Sigma_i\alpha_i e_i$, where α_i and e_i are, respectively, the intervening tissue layer attenuations (in dB/cm/MHz) and thicknesses. According to the above equation, we thus assume, as a first approximation, that the attenuation linearly increases with the frequency: $\alpha(f)=\alpha_0 f$.

The measured backscatter coefficient reported in this study was computed as

$$BSC_{\text{meas}}(k) = BSC_{\text{ref}}(k)\frac{\overline{P_{\text{meas}}(k)}}{\overline{P_{\text{ref}}(k)}}. \tag{3}$$

In Eq. (3), the mean backscattered power spectrum $\overline{P_{\text{means}}}$ was obtained by averaging the power spectra of 400 backscattered echoes from blood. The mean power spectrum $\overline{P_{\text{ref}}}$ was obtained from a reference sample of non-aggregated RBCs at a low hematocrit of 6% (i.e., Rayleigh scatterers).[9] In this case, 400 echoes were also averaged. The backscatter coefficient of this reference sample BSC_{ref} was estimated using the "Rayleigh estimation" approach used by Yu and Cloutier,[1] which theoretical value is given by Eq. (13) in Ref. 8 (three-dimensional Perkus Yevick packing factor for cylinders). This reference sample was used to compensate the backscattered power spectrum $\overline{P_{\text{meas}}}$ for the electromechanical system response, and the depth-dependent diffraction and focusing effects caused by the US beam.

The packing factor W, aggregate diameter D and total attenuation along the propagation path α_0 were determined by matching the measured BSC_{meas} given by Eq. (3) with the theoretical BSC_{theor} given by Eq. (1). For this purpose, we searched values of W, D, and α_0

Franceschini *et al.*: JASA Express Letters [DOI: 10.1121/1.2896115] Published Online 20 March 2008

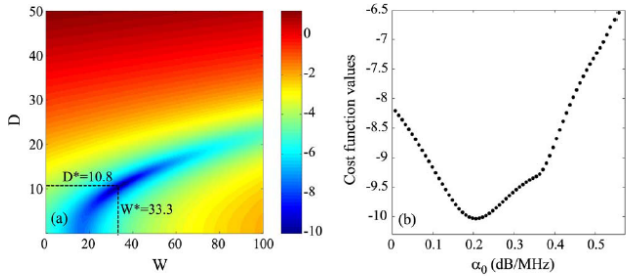

Fig. 1. (Color online) (a) Typical aspect of the logarithm of the cost function $F(W,D,\alpha_0)$ for a fixed value of α_0. The logarithm is shown here in order to enhance the visual contrast. This cost function has one minimum denoted (W^*,D^*) that depends on α_0. (b) Typical aspect of the function $\log(F(W^*,D^*,\alpha_0))$ for varying values of α_0 (W^* and D^* being calculated for each α_0). This cost function has a single minimum.

minimizing the cost function $F(W,D,\alpha_0)-\|BSC_{\text{meas}}-BSC_{\text{theor}}\|^2$. In all studied cases, the cost function seemed to have a unique global minimum, as was observed by plotting the cost function surface $F(W,D)$ with varying values of α_0. An example is given in Fig. 1.

3. Methods

3.1 Experimental setup

US measurements were performed in a Couette flow system to produce a linear blood velocity gradient at a given shear rate (see Fig. 1 in Ref. 10). The system consisted of a rotating inner cylinder with a diameter of 160 mm surrounded by a fixed concentric cylinder of diameter 164 mm. A 60 ml blood sample was sheared in the 2 mm annular space between the two coaxial cylinders. The US scanner (Vevo 770, Visualsonics, Toronto, Canada) equipped with the RMV 710 probe was used in M mode for this study. The single-element focused circular transducer had a center frequency of 25 MHz, a diameter of 7.1 mm and a focal depth of 15 mm. We operated at a sampling frequency of 250 MHz with 8 bits resolution (Gagescope, model 8500CS, Montreal, Canada). The probe was mounted in the sidewall of the fixed outer cylinder and was positioned to have its focal zone at the center of both cylinders. To ensure ultrasonic coupling, the hole within the outer stationary cylinder (containing the probe) was filled with a liquid agar gel based mixture. When solidified, this gel was cut to match the curvature of the cylinder to avoid any flow disturbance. The gel was a mixture of distilled water, 3% (w/w) agar powder (A9799, Sigma Chemical, Saint Louis, MO), 8% (w/w) glycerol, and a specific concentration of 50 μm cellulose scattering particles (S5504 Sigmacell, Sigma Chemical, Saint Louis, MO) that determined the attenuation coefficient. Four experiments were performed with four mixtures having Sigmacell (SC) concentrations varying from 0% to 0.75% (w/w). The 0% concentration constituted the nonattenuating gel and the three other mixtures mimicked skin attenuations.

3.2 Attenuation measurements

The attenuation coefficients of the reference (0%) and three skin-mimicking phantoms α_p were determined by using a standard substitution method. Two transducers with center frequencies of 25 MHz (Vevo 770, Visualsonics, Toronto, Canada) and 20 MHz (V317-SM Panametrics, Waltham, MA) were coaxially aligned facing each other for transmission measurements. Transmitted signals were recorded both with and without the agar gel sample in the acoustic path. The attenuation coefficient was then estimated using a log spectral difference technique.[11] For a given concentration of SC, measurements were obtained from two different sample thicknesses, and for each, four regions were scanned for averaging purpose. Values obtained were 0.007 ± 0.002, 0.101 ± 0.028, 0.208 ± 0.029, and 0.317 ± 0.039 dB/cm/MHz for SC concentrations of 0, 0.25, 0.50, and 0.75%, respectively. The thickness of the skin-mimicking phantoms

Franceschini *et al.*: JASA Express Letters [DOI: 10.1121/1.2896115] Published Online 20 March 2008

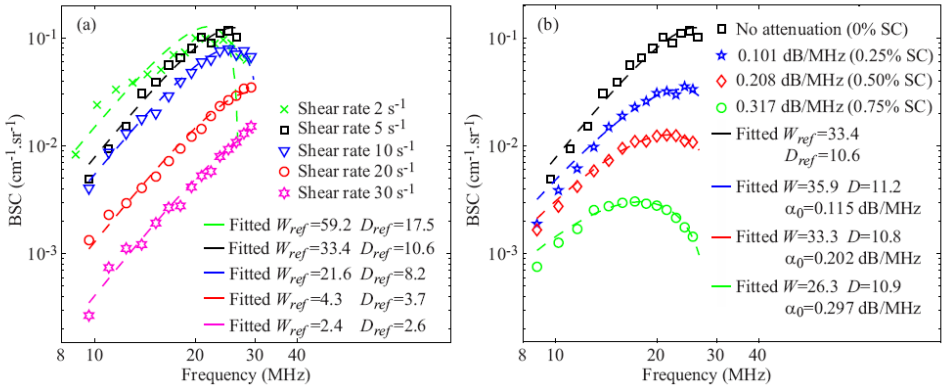

Fig. 2. (Color online) (a) Backscatter coefficients for blood sheared at different residual shear rates and measured with the 0% Sigmacell (SC) concentration phantom (no attenuation), and corresponding fitting with the classical SFSE with no compensation for attenuation. (b) Backscatter coefficients for blood sheared at 5 s^{-1} and measured with each of the four phantoms. The corresponding fitted models are the SFSE for the 0% SC phantom, and the SFSAE for the three other skin-mimicking phantoms (0.25, 0.5, and 0.75% SC).

e_p being fixed to 1 cm, their attenuation coefficients were thus in the same range as the human dermis (0.21 dB/MHz at 14–50 MHz considering a 1 mm dermis thickness[12]).

3.3 Blood preparation and measurement protocol

Fresh porcine whole blood was obtained from a local slaughterhouse, centrifuged and the plasma and buffy coat were removed. Two blood samples were then prepared: (i) a H6 reference sample, which was a 6% hematocrit non-aggregating RBCs resuspended in saline solution; and (ii) a 40% hematocrit T40 test sample, which consisted of RBCs resuspended in plasma to promote aggregation. The H6 sample was sheared at 50 s^{-1} and coupled with the 0% SC concentration agar gel. Echoes were selected with a rectangular window of length 0.8 mm at four depths every 0.2 mm (i.e., with 75% overlap between windows). For each depth, the power spectra of the backscattered echoes were averaged over 400 acquisitions to provide $\overline{P}_{\text{ref}}$. Then, the H6 sample was removed and the T40 blood was introduced in the Couette device. In the first 30 s, a shear rate of 500 s^{-1} was applied to disrupt RBC aggregates. The shear rate was then reduced to residual values of 2, 5, 10, 20, and 30 s^{-1} for 90 s. After that, for each shear rate, acquisitions of 400 rf lines were performed for 80 s. Echoes were windowed as for the H6 sample at the same depths and their power spectra were averaged to obtain $\overline{P}_{\text{meas}}$. This protocol was repeated four times with the four agar-based phantoms.

3.4 Reference measurements with the 0% SC concentration phantom

The experiment with the 0% SC phantom was realized in order to have reference results on packing factors W_{ref} and aggregate diameters D_{ref} obtained from the classical SFSE.[1] These parameters were assumed to be true values of packing factors and aggregate diameters for all shear rates, and will be compared in the next section with packing factors and diameters estimated by the SFSAE and by the SFSE when skin-mimicking phantoms are used.

It is important to emphasize the fact that the H6 reference sample was also measured with the 0% SC phantom. The phantom attenuation, although small with no SC, therefore affected equivalently both spectra $\overline{P}_{\text{meas}}$ and $\overline{P}_{\text{ref}}$ in Eq. (3). The resulting measured backscatter coefficient BSC_{ref} was thus not biased by attenuation. The terminology "no attenuation" was used for this experiment in the following.

4. Results and discussion

Figure 2(a) reports results on W_{ref} and D_{ref} for the SFSE in the case of no attenuation. Typical results of the SFSAE minimization procedure for the different agar phantoms at a shear rate of

Franceschini *et al.*: JASA Express Letters [DOI: 10.1121/1.2896115] Published Online 20 March 2008

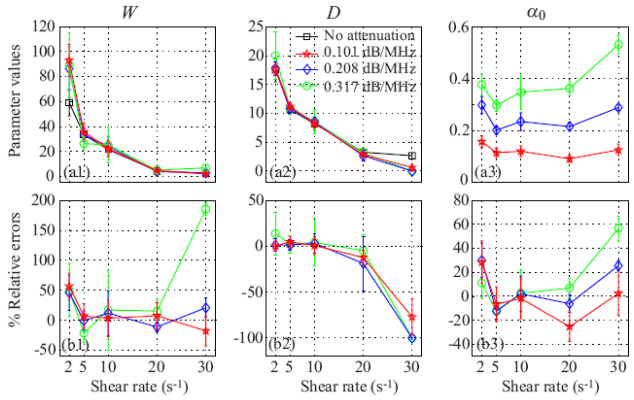

Fig. 3. (Color online) (a) Values of W, D, and α_0 (in dB/MHz) for different residual shear rates estimated by the classical SFSE for the 0% SC concentration and by the SFSAE for the three skin-mimicking phantoms. (b) Corresponding relative errors.

5 s^{-1} are given in Fig. 2(b). All results on W, D, and α_0 from the SFSAE are summarized in Fig. 3 for all residual shear rates. In this figure, the relative errors for each parameter correspond to: $(W-W_{\text{ref}})/W_{\text{ref}}$, $(D-D_{\text{ref}})/D_{\text{ref}}$, and $(\alpha_0-\alpha_{\text{ref}})/\alpha_{\text{ref}}$, with α_{ref} measured in transmissions. More specifically, α_{ref} corresponds to $\Sigma_i \alpha_i e_i = (\alpha_p e_p + \alpha_{\text{blood}} e_{\text{blood}})$, where $\alpha_p e_p$ is the skin-mimicking phantom attenuation estimated in transmission, and $\alpha_{\text{blood}} e_{\text{blood}}$ is the blood attenuation taken equal to 0.022 dB/MHz (Ref. 1) for all shear rates. To underline the necessity to take into account the attenuation, parameters W_{nocomp} and D_{nocomp} were evaluated with the SFSE without attenuation compensation when skin-mimicking phantoms were used. Because of the frequency-dependent distortion produced by the attenuating medium, large relative errors can be seen in Fig. 4(a) for both parameters. However, by compensating the backscatter coefficients

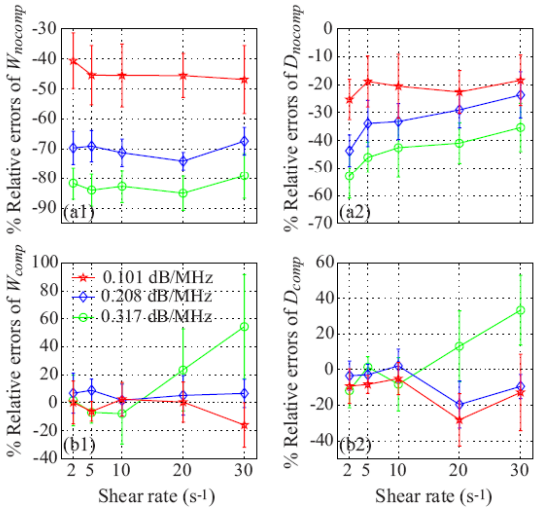

Fig. 4. (Color online) Relative errors of the packing factor and aggregate diameter for the three skin-mimicking phantoms obtained with the SFSE (a) with no compensation for attenuation (W_{nocomp} and D_{nocomp}), and (b) with attenuation compensation using the attenuation values estimated in transmission (W_{comp} and D_{comp}). Parameters W_{nocomp} and W_{comp} and similarly D_{nocomp} and D_{comp} are compared with W_{ref} and D_{ref}, respectively.

Franceschini *et al.*: JASA Express Letters [DOI: 10.1121/1.2896115] Published Online 20 March 2008

in the SFSE with the value measured in transmission (Sec. 3.2), relative errors in Fig. 4(b) are largely reduced to values comparable to those estimated with the SFSAE [see Fig. 3(b)].

The SFSAE (Fig. 3) gave quantitatively satisfactory estimates of W, D, and α_0 with relative errors below 22%, for shear rates between 5 and 20 s^{-1}. The SFSE with attenuation compensation [Fig. 4(b)] gave estimates of W_{comp} and D_{comp} with relative errors below 12% for shear rates between 2 and 10 s^{-1}, and below 28% for the shear rate of 20 s^{-1}. However, for the SFSAE, the average estimates for the shear rate of 2 s^{-1} were less accurate (relative errors below 57% for W and below 30% for α_0). The estimation of D was satisfactory at that shear rate (relative errors below 14%). The worse results of W, D, and α_0 were obtained at 30 s^{-1} for the highest attenuation.

The apparent limit of applicability of the SFSAE method for shear rates of 2 and 30 s^{-1} may be explained by considering the following. At 2 s^{-1}, for the frequency bandwidth considered (9–30 MHz), the SFSE and consequently the SFSAE seem to reach their limit of applicability for large aggregate sizes (typically D_{ref}=17.5 in Fig. 2(a), i.e., kR=4.8). This limit is illustrated by the bad fit of the SFSE model in Fig. 2(a) at 2 s^{-1}. The bad estimations of the SFSAE at 30 s^{-1} are explained by the fact that the aggregate diameters were estimated to zero and attenuations were overestimated. At this high shear rate, RBC aggregation is partially inhibited and the signal-to-noise ratio (SNR) of our measurements was reduced ($\approx$−4 dB between 20 and 30 s^{-1} for all phantoms). The accuracy of the estimates was thus degraded with increasing attenuations, as can be seen from the large relative errors at the highest attenuation with the SFSAE but also with the SFSE with attenuation compensation (W_{comp} and D_{comp}).

To conclude, the SFSAE performed well for $kR<2.7$ (i.e., D=10 at 5 s^{-1}) and under the condition that the SNR is sufficiently good (SNR>28 dB corresponding to the SNR at 30 s^{-1} for the 0.25% SC). Although the SFSAE gave less accurate estimates for 2 and 30 s^{-1}, the estimated parameter values presented in Fig. 3(a) show that the SFSAE gave qualitatively satisfactory estimates for the three SC skin-mimicking phantoms at all shear rates, since the estimates of W and D versus shear rates had the same behaviors as W_{ref} and D_{ref}.

5. Conclusions

The performance of the new SFSAE was assessed with experimental measurements on blood in a Couette flow device. The accuracy of the estimates obtained with the SFSAE was not as satisfactory as those obtained with the SFSE with attenuation compensation (i.e., when *a priori* are known about the attenuation). Nevertheless, the SFSAE has the major advantage to be easily applicable *in vivo* because of the simultaneous estimation of the blood structural properties and total attenuation (contrary to the SFSE attenuation-compensation method, needing the attenuation and thickness of the tissue intervening layers to be known). This work thus confirms the *in vivo* applicability of RBC aggregate size and structure estimations. Complementary studies are nevertheless required to determine the validity domain of the SFSAE according to kR and attenuation.

Acknowledgments

This work was supported by the Canadian Institutes of Health Research (Grant Nos. MOP-84358 and CMI-72323), by the Heart and Stroke Foundation of Canada (Grant No. PG-05-0313), and by the National Institutes of Health of USA (Grant No. RO1HL078655). Dr. Cloutier is recipient of a National Scientist award of the Fonds de la Recherche en Santé du Québec. The authors are also thankful to Dr. F. Destrempes for his helpful discussion on the optimization tool.

References

[1]F. T. H. Yu and G. Cloutier, "Experimental ultrasound characterization of red blood cell aggregation using the structure factor size estimator," J. Acoust. Soc. Am. **122**, 645–656 (2007).
[2]V. Roberjot, S. L. Bridal, P. Laugier, and G. Berger, "Absolute backscatter coefficient over a wide range of frequencies in a tissue-mimicking phantom containing two populations of scatterers," IEEE Trans. Ultrason. Ferroelectr. Freq. Control **43**, 970–978 (1996).
[3]T. A. Bigelow, M. L. Oelze, and W. D. O'Brien, "Estimation of total attenuation and scatterer size from

backscatter ultrasound waveforms," J. Acoust. Soc. Am. **117**, 1431–1439 (2005).
[4]P. He and J. F. Greenleaf, "Application of stochastic analysis to ultrasonic echoes—Estimation of attenuation and tissue heterogeneity from peaks of echo envelope," J. Acoust. Soc. Am. **79**, 526–534 (1986).
[5]B. J. Oosterveld, J. M. Thijssen, P. C. Hartman, R. L. Romijn, and G. J. E. Rosenbusch, "Ultrasound attenuation and texture analysis of diffuse liver disease: Methods and preliminary results," Phys. Med. Biol. **36**, 1039–1064 (1991).
[6]L. Y. L. Mo and R. S. C. Cobbold, "Theoretical models of ultrasonic scattering in blood," in *Ultrasonic Scattering in Biological Tissues*, edited by K. K. Shung and G. A. Thieme (CRC, Boca Raton, FL, 1993), Chap. 5, pp. 125–170.
[7]V. Twersky, "Low-frequency scattering by correlated distributions of randomly oriented particles," J. Acoust. Soc. Am. **81**, 1609–1618 (1987).
[8]K. K. Shung, "On the ultrasound scattering from blood as a function of hematocrit," IEEE Trans. Sonics Ultrason. **SU-29**, 327–331 (1982).
[9]S. H. Wang and K. K. Shung, "An approach for measuring ultrasonic backscattering from biological tissues with focused transducers," IEEE Trans. Biomed. Eng. **44**, 549–554 (1997).
[10]L.-C. Nguyen, F. Yu, and G. Cloutier, "*In vitro* study of frequency-dependent blood echogenicity under pulsatile flow," Proc.-IEEE Ultrason. Symp. 2007, 2507–2510.
[11]R. Kuc and M. Schwartz, "Estimating the acoustic attenuation coefficient slope for liver from reflected ultrasound signals," IEEE Trans. Sonics Ultrason. **SU-26**, 353–362 (1979).
[12]B. I. Raju and M. A. Srinivasan, "High-frequency ultrasonic attenuation and backscatter coefficients of *in vivo* normal human dermis and subcutaneous fat," Ultrasound Med. Biol. **27**, 1543–1556 (2001).

Pathophysiology/Complications
BRIEF REPORT

Increased Shear Rate Resistance and Fastest Kinetics of Erythrocyte Aggregation in Diabetes Measured With Ultrasound

GUY CLOUTIER, PHD[1,2]
AUDREY ZIMMER, MSC[1]
FRANÇOIS T.H. YU, MSC[1]
JEAN-LOUIS CHIASSON, MD[3]

OBJECTIVE — To measure with ultrasound the increased erythrocyte aggregation (EA) kinetics and adhesion energy between erythrocytes in patients with type 2 diabetes and poor metabolic control.

RESEARCH DESIGN AND METHODS — Blood samples were analyzed in a Couette rheometer at 32 MHz following shear rate reductions from 500 s^{-1} to residual shears of 0 (stasis), 1, 2, 10, 50, 100, and 200 s^{-1}. The increase in EA was determined with the integrated backscatter coefficient as a function of time and shear rate.

RESULTS — The time required to form aggregates was shorter in diabetic patients at shear rates below 200 s^{-1} ($P < 0.01$). Erythrocytes formed larger aggregates in diabetic patients than in control subjects ($P < 0.05$ at 2 to 100 s^{-1}).

CONCLUSIONS — Ultrasound can potentially noninvasively demonstrate, in vivo and in situ, the impact of local abnormal EA on arteriovenous flow disorders in diabetes.

Diabetes Care 31:1400–1402, 2008

Flow disorders in diabetes often lead to severe outcomes in various organs and tissues; abnormal rheology of erythrocytes (RBC) likely impairs macro- and microcirculatory blood flow, tissue oxygenation, and vascular tone regulation in affected patients (1–3). Diabetic retinopathy is attributed to microvascular flow disorders and enhanced RBC aggregation (4). Erythrocyte aggregation (EA) and plasma viscosity are also predictive of diabetic foot syndrome deterioration (5). EA is a reversible phenomenon responsible for increased blood viscosity at low shear rates. RBC hyperaggregation can also promote flow stasis and thrombosis in macrocirculation. This study proposes an ultrasound method that has the potential to noninvasively detect early rheological disorders in situ in blood vessels. The method is based on backscattering of ultrasound by blood; it measures the extent of EA and its shear rate dependency.

RESEARCH DESIGN AND METHODS

Populations

Recruited individuals were nonsmoking males. They completed a questionnaire on current medications and medical history. BMI and blood pressure were measured. Nine patients with type 2 diabetes and eight healthy control subjects gave informed consent to the approved protocol. Patients with poor metabolic control were intentionally chosen. Lipid profile and inflammatory proteins (fibrinogen, Von Clauss method; haptoglobin and immunoglobin G, immunonephelometric method; and C-reactive protein, latex agglutination technique) were determined for each participant.

Six patients were on oral antidiabetic and aspirin medications, three were on insulin, five were on cholesterol-lowering therapy, and four were treated for hypertension. Those on insulin had a history of coronary artery disease, and two of them had suffered from myocardial infarction. Distal angiopathy or cutaneous trophic disorders were not present. Mean ± SD age of patients was 58.3 ± 8.8 years (range 41–70). Healthy subjects were age matched (51.1 ± 8.7 years [range 41–64]), did not take regular medications, and had no history of cardiovascular disease. None had lipid disorders or hypertension.

Couette experiments

A Couette instrument made of two concentric cylinders and installed in an incubator at 37°C generated homogeneous shear rates via a rotating outer cylinder. Fifty milliliters of EDTA anticoagulated blood at 40% hematocrit was introduced between both cylinders. The stationary inner cylinder held an ultrasound transducer perpendicular to flow. The 32-MHz polyvinylidine flouride ultrasound transducer (Visualsonics, Toronto, Canada) had a −6 dB bandwidth of 15–45 MHz. It was pulsed with bipolar square waves (model no. AVB2-TA-C-CRIMA; Avtech, Ottawa, Canada). Received radio frequency (RF) echoes (model no. AU-3A-0120; Miteq, Hauppauge, NY) were amplified by 54 dB, filtered between 10 and 50 MHz (model no. 5900 PR; Panametrics, Waltham, MA), and digitized at 250 MHz (model no. 8500 CS; GageScope, Montreal, Canada).

The protocol consisted of imposing a 500 s^{-1} shear rate for 120 s to disrupt aggregates. Then, aggregation kinetics were recorded for 380 s at randomly applied reduced shear rates of 0, 1, 2, 10, 50, 100, and 200 s^{-1}. One hundred RF echoes were acquired every 2 s. For each blood sample, the protocol was repeated three times for averaging. RF signals were adjusted to compensate for blood attenuation at each shear rate and integrated backscatter coefficient (IBSC) was deter-

From the [1]Laboratory of Biorheology and Medical Ultrasonics, Research Center, University of Montreal Hospital, Montreal, Quebec, Canada; the [2]Department of Radiology, Radio-Oncology and Nuclear Medicine and the Institute of Biomedical Engineering, University of Montreal, Quebec, Canada; and the [3]Research Center, University of Montreal Hospital, Montreal, Quebec, Canada, and the Department of Medicine, University of Montreal, Montreal, Quebec, Canada.

Received 12 September 2007 and accepted 26 March 2008.
Published ahead of print at http://care.diabetesjournals.org on 28 March 2008. DOI: 10.2337/dc07-1802.

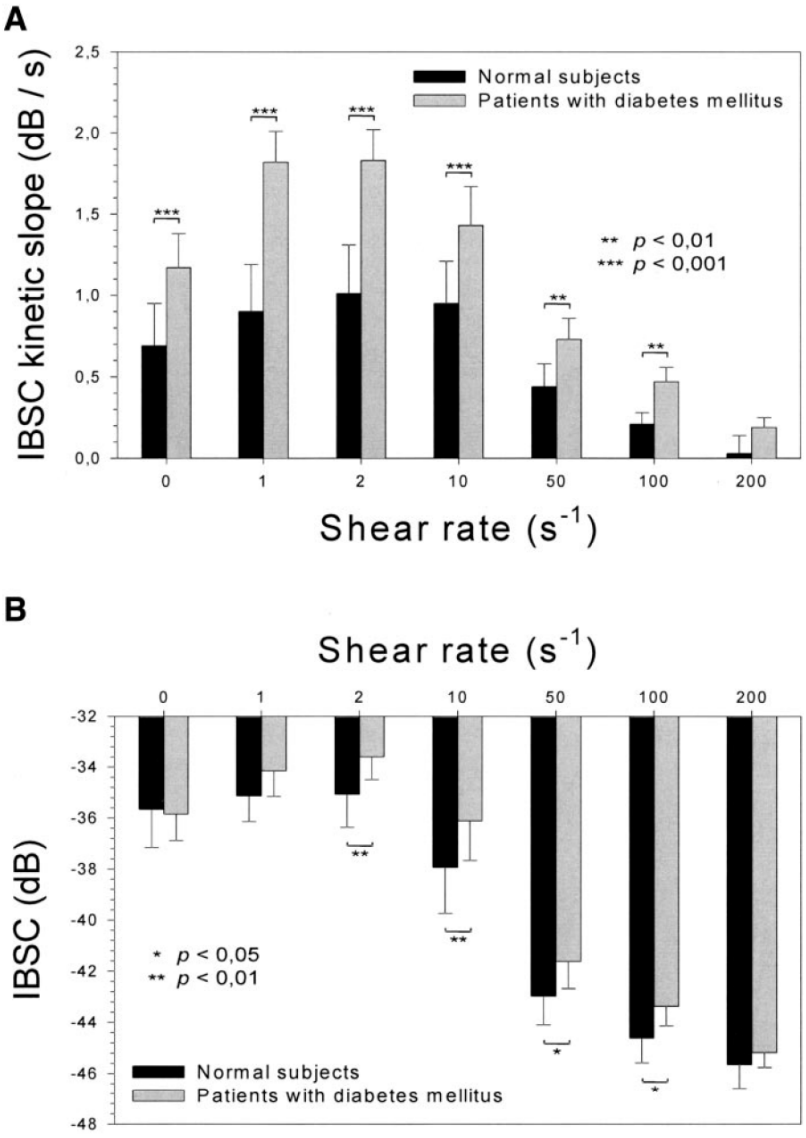

Figure 1—A*: Raising slopes from 2 to 8 s of the IBSC as a function of the shear rate applied to blood samples (means ± SD).* B*: IBSC at the plateau of RBC aggregation as a function of the shear rate. The power of 0 dB corresponds to that of a perfect flat stainless steel reflector. Two-way analyses of variance (Tukey method for multiple comparisons) confirmed impact of shear rate* ($P < 0.001$) *and population* ($P < 0.001$) *on IBSC slopes and IBSC at plateaus. The* P *values shown on the figure correspond to multiple comparisons between populations. IBSC slopes at 2* s^{-1} *were correlated with physiological variables (Pearson coefficient* $r = 0.59$, $P = 0.02$ *for A1C;* $r = 0.53$, $P = 0.03$ *for fibrinogen;* $r = 0.54$, $P = 0.02$ *for immunoglobin G; and* $r = 0.72$, $P = 0.001$ *for haptoglobin). Forward-stepwise regressions explained IBSC kinetic slopes at 2* s^{-1} *by the following model (*$r = 0.94$*): IBSC kinetic =* -1.00 ($P = 0.009$) + 0.67 *haptoglobin* ($P < 0.001$) + 0.11 *immunoglobin G* ($P = 0.003$) + 5.60 *A1C* ($P = 0.048$). *Only immunoglobin G was positively correlated with the plateau of IBSC at 2* s^{-1} *(Pearson coefficient* $r = 0.49$, $P = 0.046$*).*

mined as previously described (6). IBSC reflects the number of RBC per aggregate (7).

RESULTS— BMI, blood pressure, triglycerides, total cholesterol, HDL and LDL cholesterol, fibrinogen, and C-reactive protein were not different between groups ($P > 0.05$; unpaired *t* tests), whereas immunoglobin G (8.4 ± 1.0 vs. 11.3 ± 1.8 g/l, $P < 0.001$), haptoglobin (1.0 ± 0.4 vs. 1.6 ± 0.5 g/l, $P < 0.05$), and A1C (5.5 ± 0.8 vs. 8.8 ± 2.1%, $P < 0.01$) were significantly higher in diabetic patients than in control subjects. Couette flow protocol resulted in disaggregation of RBC and minimum IBSC at 500 s^{-1}, formation of aggregates and rapid increase in IBSC depending on reduced applied shear (Fig. 2 of ref. 7), and development of stable aggregate sizes and plateaus of IBSC after a few seconds for most shears to minutes at 0 s^{-1}.

Figure 1*A* summarizes mean raising slopes of IBSC between 2 and 8 s after shear rate reductions. In control subjects, maximum slope at 2 s^{-1} was not different from that at 1 and 10 s^{-1} ($P > 0.89$), whereas in diabetic patients, maximum slope of IBSC occurring at 2 s^{-1} was similar to that at 1 s^{-1} ($P = 1.0$). Except for that at 200 s^{-1} ($P = 0.11$), kinetic slopes were always faster in diabetic patients, which is indicative of higher rates of neighboring RBC clustering.

IBSC at plateaus averaged between 180 and 380 s after shear rate reductions as presented in Fig. 1*B*. In control subjects, maximum IBSC at 2 s^{-1} was similar to those at 0 and 1 s^{-1} ($P > 0.95$). Similarly, IBSCs at 1 and 2 s^{-1} were similar in diabetic patients ($P > 0.95$). IBSCs were statistically higher in diabetic patients between 2 and 100 s^{-1}, which reflects stronger adhesions and bigger steady-state aggregate sizes in diabetes.

CONCLUSIONS— Statistically significant differences in Fig. 1 were noted for shears between 2 and 100 s^{-1}, which correspond to normal flow at center streams and pathological flow stasis in recirculation zones of large systemic veins and arteries. Accordingly, EA in diabetes can be related to lower-limb artery ischemic events, microangiopathy in foot extremities, and retinopathy. Inflammation is involved in pathogenesis of type 2 diabetes and RBC aggregation, which agrees with our results (legend of Fig. 1). Subacute inflammatory state promoting RBC aggregation is also associated with obesity (8) and metabolic syndrome (9). Thus, reducing inflammation (and indirectly aggregation) with statins and A1C with antidiabetic medication and/or diet are indicated because both have known benefits to cardiovascular consequences of diabetes. We reported measurements from a laboratory instrument, but a short-term objective is sizing RBC aggregates in vivo with ultrasound (10). At 32 MHz, superficial (5–6 mm depth) vessels can be scanned. The proposed noninvasive method should be

investigated further because it may have potential benefit for diagnosis and follow-up of diabetic foot complications and for monitoring therapy.

Acknowledgments— This study was supported by operating grants MOP-36467 and MOP-84358 of the Canadian Institutes of Health Research and the National Scientist award of the Fonds de la Recherche en Santé du Québec (to G.C.).

We thank Dr. F.S. Foster for providing the Couette flow system and D. Poisson for her assistance in blood sampling.

References

1. McMillan DE: Plasma protein changes, blood viscosity, and diabetic microangiopathy. *Diabetes* 25:855–864, 1976
2. Demiroglu H, Gürlek A, Barista I: Enhanced erythrocyte aggregation in type 2 diabetes with late complications. *Exp Clin Endocrinol Diabetes* 107:35–39, 1999
3. Salazar-Vazquez BY, Rodriguez-Moran M, Intaglietta M, Guerrero-Romero F: Blood pressure and hematocrit in diabetes and the role of endothelial responses in the variability of blood viscosity. *Diabetes Care* 29:1523–1528, 2006
4. Satoh M, Imaizumi K, Bessho T, Shiga T: Increased erythrocyte aggregation in diabetes mellitus and its relationship to glycosylated haemoglobin and retinopathy. *Diabetologia* 27:517–521, 1984
5. Khodabandehlou T, Le Devehat C: Hemorheological disturbances as a marker of diabetic foot syndrome deterioration. *Clin Hemorheol Microcirc* 30:219–223, 2004
6. D'Astous FT, Foster FS: Frequency dependence of ultrasound attenuation and backscatter in breast tissue. *Ultrasound Med Biol* 12:795–808, 1986
7. Yu F, Cloutier G: Experimental ultrasound characterization of red blood cell aggregation using the structure factor size estimator. *J Acoust Soc Am* 122:645–656, 2007
8. Samocha-Bonet D, Lichtenberg D, Tomer A, Deutsch V, Mardi T, Goldin Y, Abu-Abeid S, Shenkerman G, Patshornik H, Shapira I, Berliner S: Enhanced erythrocyte adhesiveness/aggregation in obesity corresponds to low-grade inflammation. *Obes Resh* 11:403–407, 2003
9. Toker S, Rogowski O, Melamed S, Shirom A, Shapira I, Berliner S, Zeltser D: Association of components of the metabolic syndrome with the appearance of aggregated red blood cells in the peripheral blood: an unfavorable hemorheological finding. *Diabetes Metab Res Rev* 21:197–202, 2005
10. Franceschini E, Yu FTH, Cloutier G: Simultaneous estimation of attenuation and structure parameters of aggregated red blood cells from backscatter measurements. *J Acoust Soc Am* 123:EL85–EL91, 2008

Ultrasound in Med. & Biol., Vol. 34, No. 4, pp. 664–673, 2008

0301-5629/08/$–see front matter

ELSEVIER

doi:10.1016/j.ultrasmedbio.2007.10.002

● *Original Contribution*

CYCLIC CHANGES IN BLOOD ECHOGENICITY UNDER PULSATILE FLOW ARE FREQUENCY DEPENDENT

Linh Chi Nguyen,* François T. H. Yu,* and Guy Cloutier*†

*Laboratory of Biorheology and Medical Ultrasonics, Centre hospitalier de l'Université de Montréal (CHUM)–Hôpital Notre-Dame, Montréal, Québec, Canada, and †Department of Radiology, Radio-Oncology and Nuclear Medicine, and Institute of Biomedical Engineering, Université de Montréal, Montréal, Québec, Canada

(*Received* 14 *August* 2007; *in final form* 4 *October* 2007)

Abstract—Previous *in vivo* and *in vitro* studies have demonstrated that blood echogenicity varies under pulsatile flow, but such changes could not always be measured at physiological stroke rates. The apparent contradiction between these studies could be a result of the use of different ultrasound frequencies. Backscattered signals from porcine blood were measured in a pulsatile Couette flow apparatus. Cyclic changes in shear rate for stroke rates of 20 to 70 beats per minute (BPM) were applied to the Couette system, and different blood samples were analyzed (normal blood and blood with hyperaggregating erythrocytes promoted with dextran). To confirm that cyclic echogenicity variations were observable, spectral analysis was performed to verify if changes in echo-amplitude corresponded to the stroke rate applied to the flow. Echogenicity was measured with two single-element transducers at 10 and 35 MHz. At 35 MHz, cyclic variations in backscatter were observed from 20 to 70 BPM. However at 10 MHz, they were detected only at 20 BPM. For all cases except for hyperaggregating red blood cells (RBCs) at 20 BPM, the magnitude of the cyclic variations were higher at 35 MHz. We conclude that cyclic variations in RBC aggregation exist at physiological stroke rates, unlike what has been demonstrated in previous *in-vitro* studies at frequencies of 10 MHz. The increased sensitivity at 35 MHz to small changes in aggregate size might be the explanation for the better characterization of RBC aggregation at high stroke rates. Our results corroborate *in-vivo* observations of cyclic blood echogenicity variations in patients using a 30-MHz intravascular ultrasound catheter. (E-mail: guy.cloutier@umontreal.ca)

Key Words: **Red blood cell aggregation, Cyclic echogenicity variations, Pulsatile flow, High-frequency ultrasound, Backscattering coefficient.**

INTRODUCTION

Red blood cell (RBC) aggregation is a natural, reversible phenomenon that occurs in human blood vessels and plays an important role in blood flow properties. During the aggregation process, RBCs form reversible rouleaux or complex 3-D networks that result from an equilibrium between aggregating forces, such as interactions between RBCs and plasmatic macromolecules, and disaggregation forces such as the shear force of flow. Interestingly, elevated levels of RBC aggregation have been related to different circulatory pathologies, such as vascular thrombosis (Chabanel et al. 1994), coronary artery disease (Neumann et al. 1989, 1991), diabetes mellitus (Hayakawa and Kuzuya 1991; Le Dévéhat et al. 1996, 2000), obesity (Poggi et al. 1994; Samocha-Bonet et al. 2003), myocardial infarction and cerebrovascular accidents (Hayakawa and Kuzuya 1991; Vayá et al. 2004).

Most techniques for measuring RBC aggregation are only applicable under *in-vitro* conditions. Ultrasound imaging is a promising tool to characterize RBC aggregation because it provides real-time observations of this process *in vivo* and *in situ*. Several studies have shown that blood echogenicity is highly related to the state of RBC aggregation. They have demonstrated that echogenicity is dependent on the shear rate and on macromolecules at a sufficient concentration, such as neutral dextran and plasma fibrinogen. However, the relationship between RBC aggregation and blood echogenicity is complex because of the non-Rayleigh backscattering effect. Understanding the acoustic properties of blood is therefore necessary to characterize, *in situ*, the dynamics

Address correspondence to: Dr. Guy Cloutier, Director, Laboratory of Biorheology and Medical Ultrasonics, University of Montréal Hospital Research Center, 2099 Alexandre de Sève (Room Y-1619), Montréal, Québec, Canada, H2L 2W5.

of RBC aggregation and other hemorheological mechanisms that occur in blood vessels.

Previous results on blood echogenicity under pulsatile flow

Few studies have characterized RBC aggregation *in vivo* and *in situ*. De Kroon et al. (1991) were the first to report *in-vivo* cyclic variations of blood echogenicity by using a 30-MHz intravascular ultrasound device. The catheter was placed in the iliac artery of patients with coronary artery disease and cyclic changes in blood echo-density were measured. They suggested that the echo-density variations were associated with changes in the state of RBC aggregation related to the flow rate increase and decrease during a cardiac cycle. Concurrently and following this *in-vivo* investigation, several *in-vitro* studies have been performed with porcine blood in pulsatile mock flow by using 10-MHz Doppler transducers. However, no cyclic variation of blood echogenicity was evident from these *in-vitro* results under physiological stroke rates. Cloutier and Shung (1991, 1993) discerned cyclic changes in Doppler power at 20 beats per minute (BPM), but no variation was apparent at 70 BPM. Moreover, Wu and Shung (1996) and Lin and Shung (1999) also demonstrated that cyclic changes in Doppler power existed only at low pulsatility. Other studies have examined the effect of acceleration during systole on RBC aggregation and found no obvious variations of echogenicity at 60 BPM (Paeng et al. 2001; Paeng and Shung 2003). To explain the absence of cyclic variations in blood echogenicity at high stroke rates, these authors suggested that RBCs do not have time to aggregate or disaggregate during the different phases of the flow cycle.

The apparent contradiction between *in-vivo* and *in-vitro* studies at physiological stroke rates could be related to the use of different ultrasound frequencies or characteristics. Thus, our hypothesis is that high-frequency transducers might have an improved detection to small RBC aggregate size variations at high stroke rates and could outperform low-frequency transducers for this application. Another hypothesis that might explain differences between *in-vivo* and *in-vitro* results is that blood from patients with coronary artery disease, as studied by De Kroon et al. (1991), is likely more prone to be hyperaggregating than porcine blood. Consequently, RBC aggregation and disaggregation at high stroke rates might occur with pathologic blood because of the higher aggregation kinetics and larger size of RBC clusters.

Objectives of the present study

The focus was to compare cyclic variations of blood echogenicity obtained with high-frequency (35 MHz) and lower-frequency (10 MHz) transducers. It also examined the effect of stroke rate and different blood types (normal and hyperaggregating RBCs) on echogenicity under pulsatile flow.

Table 1. Description of studied blood samples

Name	Acronym	Hematocrit (%)	Suspending medium
Total blood	TH40	40	Plasma
Dextran blood	DH40	40	Isotonic saline water with dextran 512 kDa at 30 g/L
H6 suspension	H6	6	Isotonic saline water

MATERIALS AND METHODS

Blood preparation

Because porcine blood is known to have similar RBC aggregation properties to normal human blood (Weng et al. 1996), it was used in this study. Fresh porcine blood was collected from a local slaughterhouse and anticoagulated with 3 *g*/L of ethylene diamine tetra acetic acid (EDTA). Then, blood samples were centrifuged for 15 min at 3,000 RPM (1,855*g*) at room temperature, the buffy coat layer containing white cells and platelets was removed, the plasma was separated from RBCs and replaced with isotonic saline solution for a second centrifugation, and then three 70-mL blood samples were prepared as described in Table 1.

The TH40 was referred to normal blood, whereas DH40 corresponded to hyperaggregating RBCs (Boynard and Lelievre 1990; Meiselman 1993). The DH40 samples were prepared by mixing washed RBCs with a dextran 512 kDa saline solution. The dextran powder (lot 124H0055, Sigma Chemical, St. Louis, MO, USA) was dissolved into saline at a concentration of 30 *g*/L of solution. The TH40 and DH40 samples were studied for the kinetics of RBC aggregation under pulsatile flow. The H6 suspension was used as a reference medium (nonaggregating Rayleigh suspension) for signal normalization (see Signal processing). All hematocrits were measured by microcentrifugation. Experiments were performed within 48 h of blood collection.

Pulsatile Couette flow system

The acoustic properties of blood were measured in a Couette flow system illustrated in Fig. 1. The rotating inner cylinder had an external diameter of 160 mm, and the stationary outer cylinder had an internal diameter of 164 mm. The rotating cylinder was attached to a stepper motor driven by a controller (Zeta 6104, Compumotor, Rohnert Park, CA, USA). Unlike Poiseuille tube flow, the shear rate in a Couette apparatus is spatially homogeneous within the 2-mm gap, for the design of Fig. 1, separating the two cylinders. Consequently, this set-up

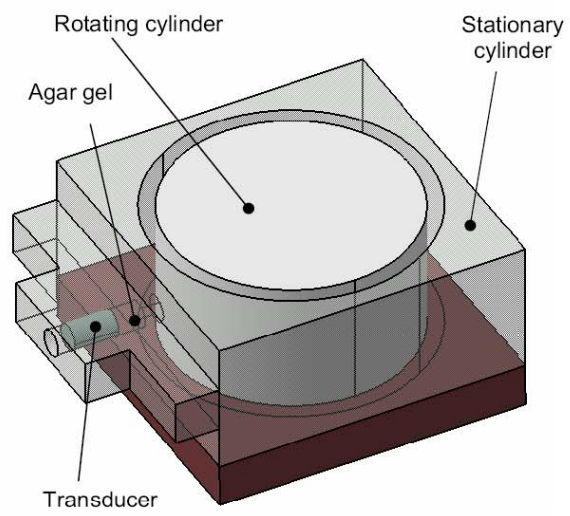

Fig. 1. Couette flow system for blood echogenicity measurements.

was ideal to precisely modulate the shear rate-dependent RBC aggregation process. The blood sample was introduced between the two concentric cylinders and submitted to cyclic variations in shear rate. Figure 2 shows the cyclic variations in shear rate applied to blood samples. For each aggregation kinetics, a shear rate of 500 s^{-1} was first applied for 35 s to attain an initial disaggregated state. Then, the shear rate was changed from 2 s^{-1}during diastole to 100 s^{-1} during systole at stroke rates of 20, 45 and 70 BPM, with a duty cycle of 10%. The duty cycle was defined as the ratio between systolic time and the duration of one pulsatile cycle. The time origin of zero was set after 35 s, when cyclic variations in shear rate started to be applied. The H6 suspension was also sheared in the Couette system at 50 s^{-1} for reference measurements. The Couette flow system was housed in a chamber and maintained at a constant temperature of 37° C.

Ultrasound recordings

Two single-element transducers were used to compare the backscattering properties of blood: a 35-MHz center frequency-focused transducer, with a −6 dB bandwidth from 28 MHz to 45 MHz (model PVDF 054-40-6, Visualsonics, Toronto, Ontario, Canada) and a 10-MHz center-frequency plane transducer, with a −6 dB bandwidth from 9 MHz to 14 MHz (V312-SU, Panametrics, Waltham, MA, USA). Both transducers were positioned at 90 degrees with respect to the flow. The 35-MHz transducer with a 3-mm diameter was positioned for measurements at the center of the co-axial cylinder gap, at its focal length (6 mm), whereas the 10-MHz transducer with a 6-mm diameter was adjusted for recordings at 15 mm. A gel obtained by mixing agar powder at a concentration of 30 *g* per liter into a 8 mL/100 mL glycerol/distilled water mixture, served as a coupling medium between the transducer and the blood sample. The solidified gel filling the transducer cavity was also useful to avoid any blood flow disturbance in the Couette system (Fig. 1).

The pulse-echo acquisition system consisted of an Avtech pulse generator (AVB2-TA-C-CRIMA, Ottawa, Ontario, Canada), a Ritec diplexer (RDX-6, Warwick, RI, USA), a 10-dB Mitec linear amplifier (model AU-A3-0120, Hauppauge, NY, USA), and a Panametrics pulser receiver (5900 PR, Waltham, MA, USA) that was used for further amplification and bandpass filtering. The radiofrequency (RF) acoustic signals were digitized with an 8-bits Gagescope acquisition board (8500CS, Montreal, Quebec, Canada) at a sampling frequency of 500 MHz. The RF signals were recorded from the test samples (TH40 and DH40), the H6 suspension and from a plane reflector used for calibration (see Signal processing). For the kinetic experiments, three RF lines were recorded every 0.1 s starting at $t = 0$ s (see Fig. 2), when cyclic variations in shear rate were applied to the flow. Every kinetics was then repeated 20 times for each stroke rate to increase the signal-to-noise ratio (SNR) of any given experiment. All measurements were averaged over five TH40 and five DH40 blood samples collected from different animals. A minimum of 10 cycles were recorded for every kinetic measurement. For the plane reflector and the H6 suspension stirred in a beaker, 100 consecutive RF lines were acquired, whereas 20 RF lines were recorded for the H6 suspension placed in the Couette setup. The H6 suspensions within the beaker were used in eqn (1), whereas the H6 suspensions within the Couette apparatus were utilized in eqn (2) given below.

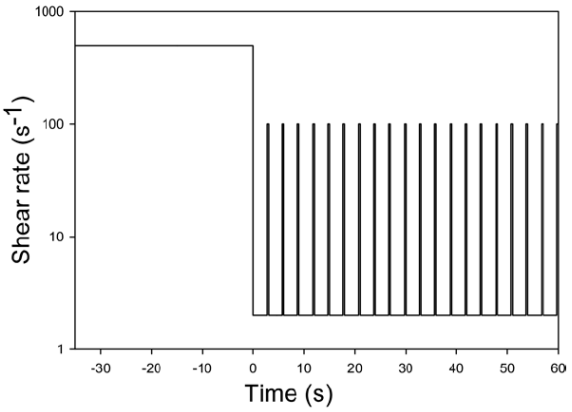

Fig. 2. Shear rate pattern applied to each blood sample to initially disaggregate RBCs and then induce pulsatile flow. This example is for a stroke rate of 20 BPM.

Signal processing

The backscattering coefficient of blood (BSC_{blood}) was calculated according to the modified substitution method, as in Yu and Cloutier's (2007) work using eqn (1):

$$BSC_{blood} = BSC_{H6} \times \frac{S_{blood}}{S_{H6,1}} \times \exp(4d(\alpha_{blood} - \alpha_{H6})) \quad (1)$$

Here, BSC_{H6} is the BSC of the H6 reference suspension in a beaker computed using eqn (2). S_{blood} and $S_{H6,1}$ are, respectively, the power spectrum of the backscattered signal from the test sample and from the H6 medium measured in the Couette system. The parameters d, α_{blood} and α_{H6} are the inspected depth, attenuation coefficients of blood and of the H6 medium, respectively. The values of α_{blood} and α_{H6} were approximated at 0.22 dB/cm/MHz (Greenleaf 1986) for blood and 0.03 dB/cm/MHz (Wang and Shung 1997) for the H6 medium. BSC_{H6} was computed as:

$$BSC_{H6} = \frac{S_{H6,2}}{S_{plane}} \times \frac{1}{0.63^2} \times \frac{Rp^2k^2a^2}{8\pi d\left(1 + \left(\frac{ka^2}{4d}\right)^2\right)} \times \exp(4\alpha_{H6}d) \quad (2)$$

where $S_{H6,2}$ is the H6 suspension stirred in a beaker with a magnetic agitator to avoid sedimentation and S_{plane} is the power spectrum of the reflected signal from a stainless steel plane submerged in distilled water. Variables R_p, k and a, respectively, represent the reflection coefficient from the planar reflector (assumed to be 1), the wave number and the transducer radius. For each medium, the power spectrum was windowed at 1,024 points, zero padded to 2,048 points, fast Fourier transformed (FFT) and then averaged over the RF lines to provide a mean power spectrum.

Fitting of the aggregation kinetic curves

The aggregation kinetics were characterized by computing the relative BSC (ΔBSC) in dB, which allowed comparisons between both transducers. The absolute BSC was first calculated from eqn (1) and expressed in $cm^{-1}sr^{-1}$. For each transducer, the absolute BSC after applying a shear rate of 500 s^{-1}, which corresponds to an initial disaggregated state (at $t = 0$ s), was set at the 0-dB reference. We then modeled the temporal evolution of ΔBSC with a sigmoid curve (Fig. 3), as in the work of Rouffiac et al. (2002). As seen on this figure, the sigmoid curve has two distinctive zones, a transition regime (TR) and a permanent regime (PR). The sigmoid was fitted on the mean ΔBSC and therefore ignored the cyclic echogenicity variations within PR. The sigmoid in Fig. 3 was defined by the following equation:

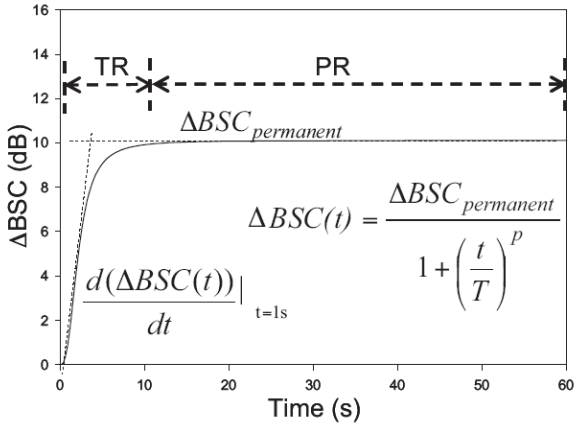

Fig. 3. Aggregation kinetic modeling using a sigmoid fitting. Two parameters are obtained from the fitting: $\Delta BSC_{permanent}$ and the aggregation kinetic slope computed from the derivative of the sigmoid curve at $t = 1$ s. Two regimes are defined on this figure, a transition regime (TR) and a permanent regime (PR).

$$\Delta BSC_{blood}(t) = \frac{\Delta BSC_{permanent}}{1 + \left(\frac{t}{T}\right)^p} \quad (3)$$

where $\Delta BSC_{permanent}$, t, T and p are, respectively, the ΔBSC_{blood} reached during the permanent regime, the time and two constants obtained from the sigmoid fitting. $\Delta BSC_{permanent}$, T and p were solved by least mean-squared fitting with Sigma Plot 2000 (v. 6.00, Systat Software, San Jose, CA, USA). Two parameters from eqn (3) were used to compare the aggregation kinetics: $\Delta BSC_{permanent}$ and the aggregation kinetic slope computed from the derivative of eqn (3) at $t = 1$ s. $\Delta BSC_{permanent}$ and the aggregation kinetic slope allowed comparison of the transducer sensitivity to RBC aggregation. $\Delta BSC_{permanent}$ is an index that is determined by the mean aggregate sizes and non-Rayleigh backscattering behavior, whereas the aggregation kinetic slope is a measure of the blood sample "aggregability" from a disaggregated state.

Computation of the mean cyclic variations in echogenicity

Within PR, BSC averaging was performed over the last 10 cycles from five different experiments ($n = 50$) by registering the maxima of a fitted sinusoidal function at known pulse rates of 20, 45 or 70 BPM, depending on the stroke rate applied to the flow. To improve averaging at high stroke rates, oversampling of the data was performed by convolving the zero-padded data with a sine cardinal. The data were interpolated by double oversampling at 45 BPM (double zero padding) and triple oversampling at 70 BPM (triple zero padding).

Spectral analysis was performed to confirm that cyclic variations of BSC_{blood} were not artifactual and

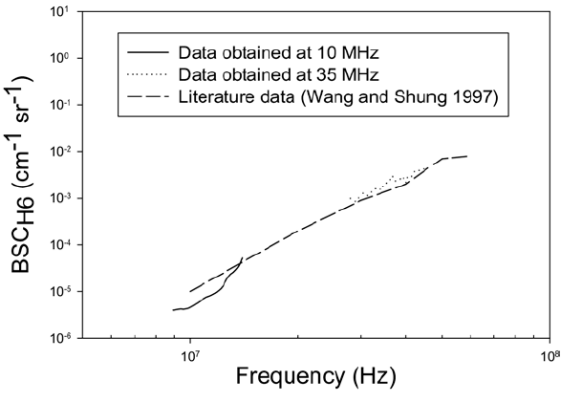

Fig. 4. Backscattering coefficient of the H6 suspension (BSC_{H6}) and comparison with the literature (Wang and Shung 1997), showing Rayleigh scattering behavior (BSC ~ f^4).

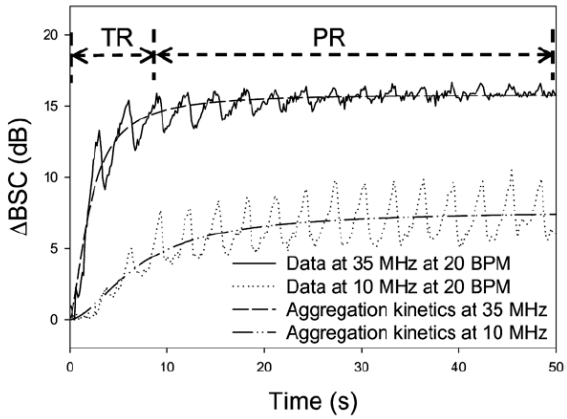

Fig. 5. Aggregation kinetics of hyperaggregating RBCs under pulsatile flow at 20 BPM obtained with the 35-MHz and 10-MHz transducers. Two regimes are identified on this figure, a transition (TR) and a permanent (PR) regimes.

therefore related to cyclic changes in shear rate. Variations of echogenicity were considered observable if the main frequency component (frequency with the highest magnitude) of the FFT spectrum corresponded to the stroke rate.

Statistical analysis

Three-way analyses of variance (ANOVA, SigmaStat, v. 3.11, Systat) with the Tukey test for multiple comparisons were performed to compare the effect of the transducer, blood type and stroke rate. These statistical tests were conducted on $\Delta BSC_{permanent}$, aggregation kinetic slopes, and cyclic variations of BSC. A significance level of $p < 0.05$ was considered to be statistically significant.

RESULTS

H6 data

To validate the modified substitution method described by eqns (1) and (2), we compared in Fig. 4 our BSC_{H6} data with previous results from the literature (Wang and Shung 1997). These authors had shown that Rayleigh behavior (BSC ~ f^4) was respected at a low hematocrit for frequencies up to 30 MHz. It can be seen that our BSC_{H6} is comparable to these results.

RBC aggregation kinetics

Examples of aggregation kinetics under pulsatile flow are presented in Fig. 5. Figures 6 and 7 report the $\Delta BSC_{permanent}$ and aggregation kinetic slope values obtained by the sigmoid fitting of eqn (3). ANOVA tests confirmed that the $\Delta BSC_{permanent}$ (Fig. 6) and the aggregation slope (Fig. 7) were significantly higher at 35 MHz than at 10 MHz ($p < 0.001$). Also, $\Delta BSC_{permanent}$ for DH40 samples were significantly higher than TH40 ($p < 0.001$), for all stroke rates. For the aggregation kinetic slope, DH40 samples had higher values than TH40 ($p < 0.001$) at 35 MHz only, for all stroke rates. Finally, the stroke rate did not have a significant effect on both $\Delta BSC_{permanent}$ ($p = 0.103$, Fig. 6) and the aggregation slope ($p = 0.675$, Fig. 7).

Cyclic variations of blood echogenicity

Cyclic changes of BSC during the PR phase are presented in Figs. 8 and 9 for stroke rates of 20 and 70 BPM. The mean value of BSC was set to 0 dB. To

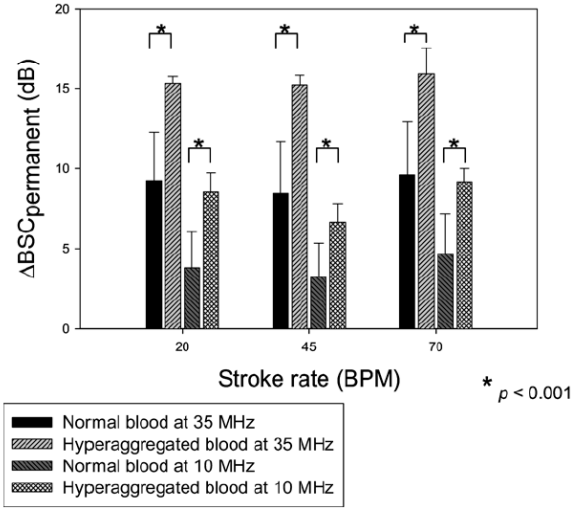

Fig. 6. Relative backscattering coefficient in PR ($\Delta BSC_{permanent}$) obtained at 35 MHz and 10 MHz for normal blood and hyperaggregating RBCs. Each result represents the mean ± one standard deviation computed over five experiments.

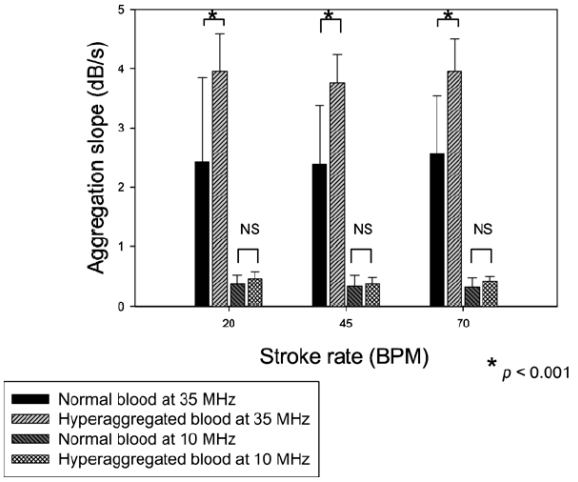

Fig. 7. Aggregation kinetic slope obtained at 35 MHz and 10 MHz for normal blood and hyperaggregating RBCs. Each result represents the mean ± one standard deviation computed over five experiments.

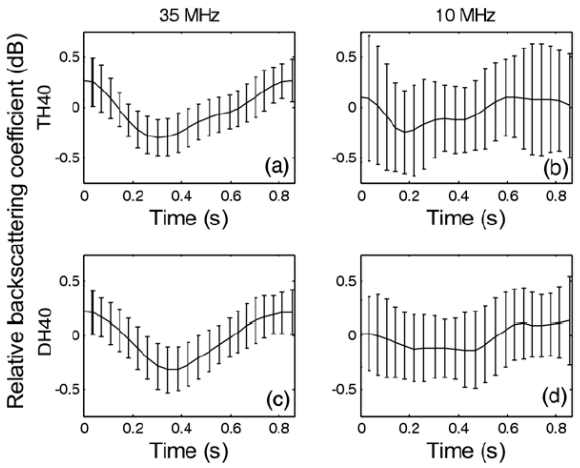

Fig. 9. Variations of the relative backscattering coefficient at a stroke rate of 70 BPM. (a, b) At 35 and 10 MHz, respectively, with normal blood samples, and (c, d) at the same frequencies with hyperaggregating RBCs. Each result represents the mean ± one standard deviation computed over 50 cycles from five experiments.

verify if these cyclic variations were not artifactual, Figs. 10 (20 BPM) and 11 (70 BPM) show mean spectrograms of BSC for five pulsatile cycles within the PR phase that were averaged over five experiments. The standard deviations are not shown on spectrograms for clarity.

Cyclic variations were reliable if the main frequency component corresponded to the stroke rate applied to the flow. For a pulsatile flow at 20 BPM, the main frequency component was observed at 0.33 Hz (20 BPM) for both transducers and both blood types (Fig. 10). At 70 BPM, the main frequency component corresponded to 1.2 Hz (70 BPM) at 35 MHz (Fig. 11a, c), but this was not the case at 10 MHz (0.24 Hz, 14 BPM, Fig. 11b, d). Therefore, at 10 MHz and 70 BPM, the cyclic variations reported in Fig. 9b and d are artifactual. Table 2 summarizes values of the mean cyclic BSC changes in dB at all stroke rates and the main frequency component

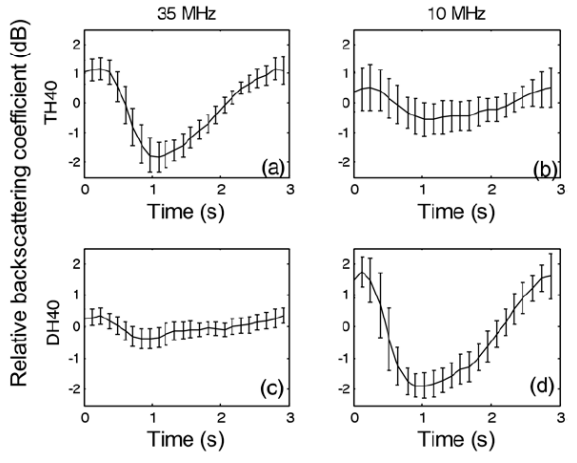

Fig. 8. Variations of the relative backscattering coefficient at a stroke rate of 20 BPM. (a, b) At 35 and 10 MHz, respectively, with normal blood samples, and (c, d) at the same frequencies with hyperaggregating RBCs. Each result represents the mean ± one standard deviation computed over 50 cycles from five experiments.

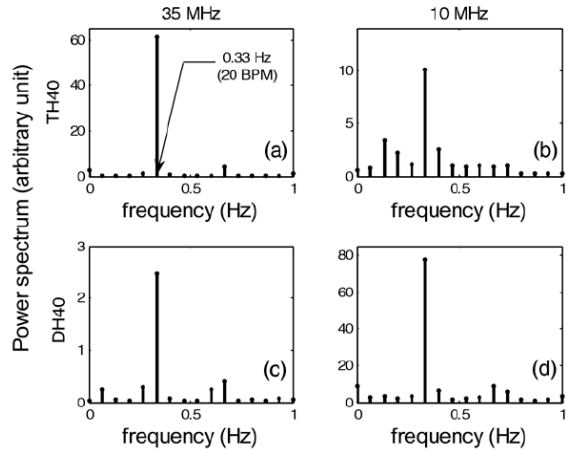

Fig. 10. Mean spectrograms of the ΔBSC for five pulsatile cycles at 20 BPM. (a, b) At 35 and 10 MHz, respectively, with normal blood samples, and (c, d) at the same frequencies with hyperaggregating RBCs. Each result was averaged for five pulsatile cycles and five experiments.

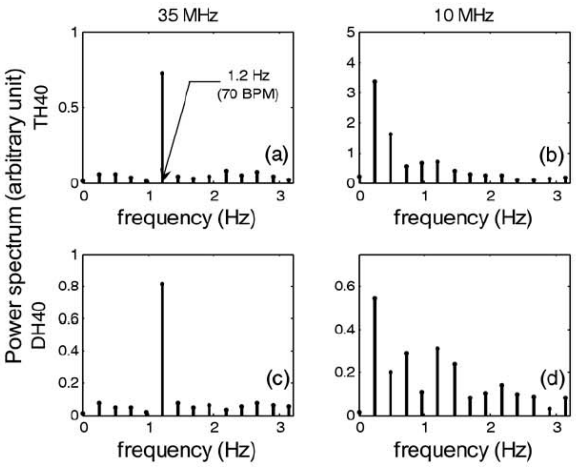

Fig. 11. Mean spectrograms of the ΔBSC for five pulsatile cycles at 70 BPM. (a, b) At 35 and 10 MHz, respectively, with normal blood samples, and (c, d) at the same frequencies with hyperaggregating RBCs. Each result was averaged for five pulsatile cycles and five experiments.

of the cyclic variations for both transducers and blood types. The three-way ANOVA revealed that the stroke rate and transducer's frequency had a significant effect on cyclic variations of BSC ($p < 0.001$) but not the blood type ($p = 0.509$). More specifically, cyclic variations decreased with increasing stroke rate, except for DH40 at 35 MHz, where variations at 20 BPM were not significantly different from those at 70 BPM.

DISCUSSION

Measurements of the aggregation kinetics

Effect of the transducer. As shown in Figs. 6 and 7, the 35-MHz transducer provided significantly higher values of $\Delta BSC_{permanent}$ and aggregation kinetic slope than the 10-MHz probe for both TH40 and DH40 bloods. After a disaggregation phase at 500 s^{-1}, the flow was reduced to a mean shear rate of 11.8 s^{-1} (100 s^{-1} during the mimicked systole and 2 s^{-1} during diastole with a duty cycle of 10%). To explain and confirm the sensitivity difference to aggregation between both transducers, we performed complementary experiments at a constant step shear rate change (*i.e.*, no pulsatility, see Fig. 12a and b). A shear rate of 100 s^{-1} was first applied, as for the mimicked systole, followed by the phase of aggregation kinetic at a constant shear rate of 2 s^{-1}, which corresponds to the mimicked diastolic shear rate of our pulsatile flow experiments. Note that a second objective of these other measures was to prove that the higher $\Delta BSC_{permanent}$ and aggregation kinetic slope at 35 MHz (focused probe) could not be attributed to the fact that measurements at 10 MHz were performed with a nonfocused transducer. Additional recordings were thus realized with a focalized-10 MHz probe (model V312-SM, Panametrics), as shown in Fig. 12b.

According to this figure (panel b), focusing of the 10-MHz transducer does not modify the aggregation kinetic profile. However, Fig. 12a and b shows that aggregation kinetics differ considerably between 35 MHz and 10 MHz transducers, and between TH40 and DH40 bloods. In Fig. 12a with normal RBCs, only one zone exists with ΔBSC higher at 35 MHz (zone 1a). In Fig. 12b with hyperaggregating RBCs, two zones can be observed: a first one where ΔBSC are higher at 35 MHz (zone 1b), and a second one with ΔBSC higher at 10 MHz (zone 2). The existence of higher ΔBSC at 10 MHz (zone 2) is well known from the literature, and an explanation is the existence of non-Rayleigh backscattering at 35 MHz that reduces the intensity of echoes when

Table 2. Cyclic variation of the backscattering coefficient for normal blood (TH40) and hyperaggregating RBCs (DH40) at 35 MHz and 10 MHz, for different stroke rates

Blood sample	Stroke rate (BPM)	Transducer (MHz)	Main frequency component (BPM)	Cyclic variation (dB)		
TH40	20	35	20	3.0 ± 0.8		
		10	20	1.1 ± 1.3		
	45	35	45	1.1 ± 0.3		
		10	18	Not observable		
	70	35	70	0.6 ± 0.3	NS	
		10	14	Not observable		
DH40	20	35	20	0.7 ± 0.5		
		10	20	3.6 ± 0.6	NS	
	45	35	45	1.0 ± 0.3		NS
		10	9	Not observable		
	70	35	70	0.5 ± 0.4		
		10	14	Not observable		

Each cyclic variation value represents the mean ± one standard deviation computed over 50 cycles from five experiments. Each pair of multiple comparisons were significantly different ($p < 0.002$) except for those indicated by NS (non-significant).

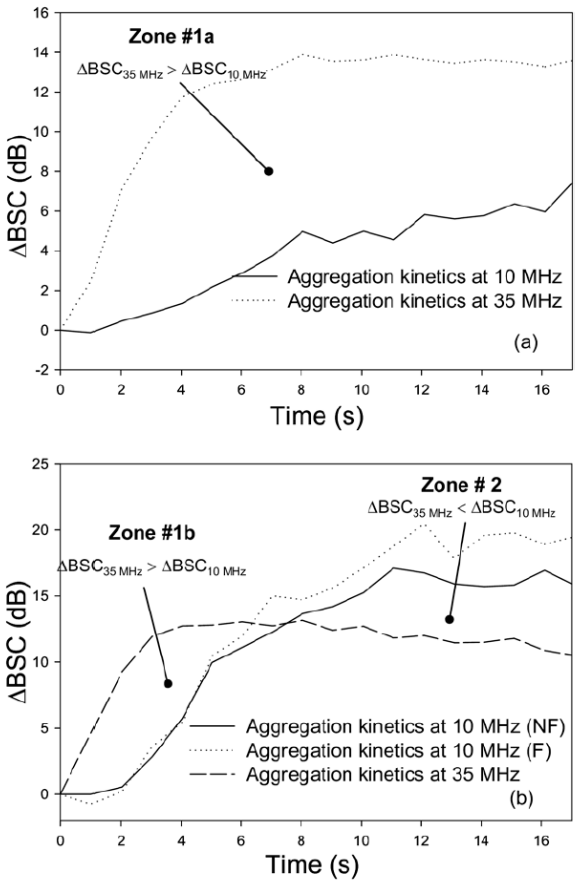

Fig. 12. Aggregation kinetics under steady flow with a step shear rate change from 100 s^{-1} to 2 s^{-1} (at $t = 0$ s) obtained with the 35- and 10-MHz transducers. (a) With normal blood samples (in zone 1a, ΔBSC is higher at 35 MHz during the whole kinetic); (b) with hyperaggregating RBCs (in zone 1b, ΔBSC is higher at 35 MHz and in zone 2 ΔBSC is higher at 10 MHz). Note that the 10-MHz nonfocused transducer (NF) gave a similar kinetic than the 10-MIIz focused transducer (F).

large RBC aggregates are present (Fontaine and Cloutier 2003; Cloutier et al. 2004). Higher ΔBSC at 35 MHz (zones 1a and b) have also been documented (Cloutier et al. 2004; Yu and Cloutier 2007), but a clear explanation is still missing.

Cloutier et al. (2004) suggested that high-frequency transducers with large bandwidth might have decreased time responses to changes in aggregate sizes and might thus detect more rapidly growths of small RBC clusters than lower frequency transducers. However, this hypothesis alone cannot explain zone 1a of Fig. 12a. Additional suppositions are that low-frequency transducers may have insufficient spatial resolutions to detect changes in small structures (Cloutier and Qin 1997; Huang et al. 2005), as it was probably the case for normal TH40 blood. Further investigations are therefore needed to better understand the higher sensitivity to changes in small aggregate sizes at high frequency.

The results of Fig. 12 are now used to interpret our pulsatile flow observations of Fig. 5. The aggregation kinetic profiles under pulsatile flow had the same tendency as in Fig. 12a, with the maximum backscatter at 35 MHz and no crossing of the 35-MHz and 10-MHz kinetic profiles over time. Therefore, this finding and Figs. 6 and 7 suggest that, for a mean shear rate of 11.8 s^{-1}, aggregates of both TH40 and DH40 bloods were not large enough to produce non-Rayleigh effect at 35 MHz under pulsatile flow.

Effect of the blood sample. As observed in Figs. 6 and 7, DH40 had significantly greater $\Delta BSC_{permanent}$ than TH40, whatever the ultrasound frequency and stroke rate. The aggregation kinetic slopes were higher for DH40 at 35 MHz at all stroke rates. The higher $\Delta BSC_{permanent}$ suggests that DH40 formed larger aggregates than TH40, whereas the steepest slopes indicate larger growth in size of aggregates over time. These observations are consistent with previous studies on RBCs suspended in large-molecular-weight dextran *vs.* control RBCs in native plasma (Bauersachs et al. 1989; Meiselman 1993).

Effect of the stroke rate. As reported earlier, the stroke rate applied to the flow did not significantly affect $\Delta BSC_{permanent}$ (Fig. 6, $p = 0.103$) and the aggregation slope (Fig. 7, $p = 0.675$). For any given blood sample, the flow shear rate is recognized as a main determinant of RBC aggregation (Schmid-Schönbein et al. 1968), under both steady and pulsatile flows. Because the mean shear rate remained the same in our experiments (11.8 s^{-1}), whatever the stroke rate as the duty cycle was held fixed at 10%, our findings again support the hypothesis that similar mean aggregate sizes were obtained for a given set of experiments with TH40 or DH40 blood samples.

Cyclic variations of echogenicity

According to Table 2, no cyclic variation of BSC could be observed at 10 MHz for 45 BPM and 70 BPM, whatever the blood type. For these cases, the stroke rate did not correspond to the main frequency component of the cyclic variation and the BSC variations could not be related to changes in shear rate. This agrees with previous studies where RBC aggregation and disaggregation were not observed at high stroke rates with a 10-MHz transducer (Cloutier and Shung 1993; Wu and Shung 1996; Lin and Shung 1999; Paeng et al. 2001). However, we explain the absence of cyclic variations not because RBCs do not have time to aggregate but because the sensitivity of the 10-MHz transducer to cluster size changes is insufficient. At 35 MHz and 70 BPM, even if cyclic variations were small (<0.6 dB), spectrograms of BSC revealed consistent pulsations (Fig. 11a and c).

Effect of the transducer. We now compare the effect of the transducer at 20 BPM for both blood types. We noted that TH40 had a higher cyclic variation at 35 MHz than at 10 MHz (Fig. 8a, b), but this was not the case for DH40 (Fig. 8c, d). To discuss these results, we again refer to Fig. 12a, b. Note, however, that comparing these steady flow measures to the condition of our pulsatile flow experiments is not straightforward. In Fig. 12, the shear rate was reduced from 100 to 2 s^{-1} and observations lasted 17 s. For unsteady flow experiments as in Fig. 5, pulsatility between 100 and 2 s^{-1} was maintained for at least 22 s before analyzing BSC of the last 10 cycles. Consequently, each measure of cyclic variation in backscatter experienced a "time history" of ~22 s at a mean shear rate of 11.8 s^{-1}. Similarities thus exist between conditions of Figs. 5 and 12.

For TH40, we found larger cyclic changes at 35 MHz than at 10 MHz for all stroke rates (Table 2). This can be explained by the fact that small changes in aggregate size between 100 and 2 s^{-1} are better detected at 35 MHz (zone 1a of Fig. 12a). Of course, increasing the observation period in permanent regime before analyzing cyclic changes in BSC could have modified conclusions for TH40. For instance, as seen on Fig. 12a, the plateau of ΔBSC was not reached after 17 s at 10 MHz. For DH40, which forms larger aggregates than TH40, the 10-MHz transducer could better sense cyclic variations in permanent regime at 20 BPM (*i.e.*, after more than 22 s of cyclic shearing, which corresponds to zone 2 of Fig. 12b). However, as the stroke rate was increased to 45 and 70 BPM, detecting small changes in large aggregate size was not possible at 10 MHz. In addition to the "time history" in permanent regime, it is clear that the pulsation rate influences the detectability of RBC aggregation and disaggregation at 10 MHz. As introduced earlier, this may be explained by the slower transient time response at 10 MHz (5-MHz bandwidth) than at 35 MHz (17-MHz bandwidth).

Comparison with previous studies on cyclic echogenicity variations

Cyclic variations in this study were small when compared with previous results obtained with whole porcine blood at 10 MHz (Cloutier and Shung 1993; Wu and Shung 1996; Lin and Shung 1999; Paeng et al. 2001), whereas they cannot quantitatively be compared with De Kroon et al. (1991). First, in the current paper the pulsatile flow was investigated in a Couette system instead of a mock tube flow loop or *in-vivo* conditions. Second, blood echogenicity variations were determined differently from one study to another. De Kroon et al. (1991) quantified them from B-mode grey scale images at 30 MHz, whereas Shung's group and our group previously examined Doppler power at 10 MHz. Our current data at 10 and 35 MHz were obtained from RF signals with different SNR and transducer characteristics than previous studies.

CONCLUSION

Backscattered signals from porcine blood were measured in a pulsatile Couette flow apparatus to compare the effect of the transducer frequency, stroke rate and blood type on echogenicity variations. Two single-element 10-MHz and 35-MHz transducers were used with normal porcine blood and porcine RBCs suspended in dextran to promote hyperaggregation. For both blood types, cyclic variations of echogenicity were observed up to 70 BPM at 35 MHz, whereas cyclic changes were not found at stroke rates higher than 20 BPM at 10 MHz. Unlike what has been proposed in previous studies at a frequency of 10 MHz, RBC aggregation and disaggregation are detectable at a higher frequency of 35 MHz and exist at a physiological stroke rate of 70 BPM. Therefore, the present investigation has shown that high-frequency transducers have a better sensitivity to detect rapid changes in RBC aggregate sizes and can lead to better characterization of RBC aggregation under physiological conditions.

Acknowledgments—This work was supported by the Canadian Institutes of Health Research (grant No. MOP-84358). Dr. Cloutier is recipient of the National Scientist award of the Fonds de la Recherche en Santé du Québec (2004-2009). Ms. Nguyen received an undergraduate studentship award from the Natural Sciences and Engineering Research Council of Canada. The authors also acknowledge Les Viandes ULTRA Meats Inc., Saint-Esprit, Quebec, Canada for the supply of blood, and Mr. Ovid Da Silva, Research Support Office, Research Centre, CHUM, for editing this manuscript.

REFERENCES

Bauersachs RM, Wenby RB, Meiselman HJ. Determination of specific red blood cell aggregation indices via an automated system. Clin Hemorheol 1989;9:1–25.

Boynard M, Lelievre JC. Size determination of red blood cell aggregates induced by dextran using ultrasound backscattering phenomenon. Biorheology 1990;27:39–46.

Chabanel A, Horellou MH, Conard J, Samama MM. Red blood cell aggregability in patients with a history of leg vein thrombosis: influence of post-thrombotic treatment. Br J Haematol 1994;88: 174–179.

Cloutier G, Shung KK. Cyclic variation of Doppler backscattering power from porcine blood in a pulsatile flow model. IEEE Ultrason Symp 1991;1301–1304.

Cloutier G, Shung KK. Study of red cell aggregation in pulsatile flow from ultrasonic Doppler power measurements. Biorheology 1993; 30:443–461.

Cloutier G, Qin Z. Ultrasound backscattering from non-aggregating and aggregating erythrocytes—A review. Biorheology 1997;54: 443–470.

Cloutier G, Daronat M, Savery D, Garcia D, Durand LG, Foster FS. Non-Gaussian statistics and variations of the ultrasound signal backscattered by blood at frequencies between 10 and 58 MHz. J Acoust Soc Am 2004;116:566–577.

De Kroon MGM, Slager CJ, Gussenhoven WJ, Serruys PW, Roelandt JRTC, Bom N. Cyclic changes of blood echogenicity in high-frequency ultrasound. Ultrasound Med Biol 1991;17:723–728.

Fontaine I, Cloutier G. Modeling the frequency dependence (5-120 MHz) of ultrasound backscattering by red cell aggregates in shear flow at a normal hematocrit. J Acoust Soc Am 2003;113:2893–2900.

Greenleaf JF. Tissue characterization with ultrasound I, 1st ed. Boca Raton, FL: CRC Press, 1986:1–245.

Hayakawa M, Kuzuya F. Effects of Ticlopidine on erythrocytes aggregation in thrombotic disorders. Angiology 1991;42:747–753.

Huang CC, Tsui PH, Wang SH, Chiu CY. Detecting the process of coagulation and clot formation with high frequency ultrasound. J Med Biol Eng 2005;25:171–177.

Le Dévéhat C, Khodabandehlou T, Vimeux M, Aouane F. Diabetes mellitus: Its effects on blood rheological properties and microcirculatory consequences. Clin Hemorheol 1996;16:677–683.

Le Dévéhat C, Khodabandehlou T, Vimeux M. Diabète sucré et fibrinogène: Conséquences hémorhéologiques et microcirculatoires. J Mal Vasc 2000;25:53–57.

Lin YH, Shung KK. Ultrasonic backscattering from porcine whole blood of varying hematocrit and shear rate under pulsatile flow. Ultrasound Med Biol 1999;25:1151–1158.

Meiselman HJ. Red blood cell role in RBC aggregation: 1963–1993 and beyond. Clin Hemorheol 1993;13:575–592.

Neumann FJ, Tillsmanns H, Roebruck P, Zimmermann R, Haupt HM, Kübler W. Hemorrheological abnormalities in unstable angina pectoris: A relation independent of risk factor profile and angiographic severity. Br Heart J 1989;62:421–428.

Neumann FJ, Katus HA, Hoberg E, Roebruck P, Braun M, Haupt HM, Yillmanns H, Kübler W. Increased plasma viscosity and erythrocyte aggregation: Indicators of an unfavorable clinical outcome in patients with unstable angina pectoris. Br Heart J 1991;66:425–430.

Paeng DG, Cao PJ, Shung KK. Doppler power variation from porcine blood under steady and pulsatile flow. Ultrasound Med Biol 2001;27:1245–1254.

Paeng DG, Shung KK. Cyclic and radial variation of the Doppler power from porcine whole blood. IEEE Trans Ultrason Ferroelect Freq Cont 2003;50:614–622.

Poggi M, Palareti G, Biagi R, Parenti M, Babini AC, Coccher S. Prolonged very low calory diet in highly obese subjects reduces plasma viscosity and red cell aggregation but not fibrinogen. Int J Obes 1994;18:490–496.

Rouffiac V, Péronneau P, Hadengue A, Barbet A, Delouche P, Dantan P, Lassau N, Levenson J. A new ultrasound principle for characterizing erythrocyte aggregation. Invest Radiol 2002;37:413–420.

Samocha-Bonet D, Lichtenberg D, Tomer A, Deutsch V, Mardi T, Goldin Y, Abu-Abeid S, Shenkerman G, Patshornik H, Shapira I, Berliner S. Enhanced erythrocyte adhesiveness/aggregation in obesity corresponds to low-grade inflammation. Obes Res 2003;11:403–407.

Schmid-Schönbein H, Gaehtgens P, Hirsch H. On the shear rate dependence of red cell aggregation in vitro. J Clin Invest 1968;47:1447–1454.

Vayá A, Falcó C, Réganon E, Vila V, Martínez-Sales V, Corella D, Contreras MT, Aznar J. Influence of plasma and erythrocyte factors on red blood cell aggregation in survivors of acute myocardial infarction. Thromb Haemost 2004;91:354–359.

Wang SH, Shung KK. An approach for measuring ultrasonic backscattering from biological tissues with focused transducers. IEEE Trans Biomed Eng 1997;44:549–554.

Weng X, Cloutier G, Pibarot P, Durand LG. Comparison and simulation of different levels of erythrocyte aggregation with pig, horse, sheep, calf, and normal human blood. Biorheology 1996;33:365–377.

Wu SJ, Shung KK. Cyclic variation of Doppler power from whole blood under pulsatile flow. Ultrasound Med Biol 1996;22:883–894.

Yu F, Cloutier G. Experimental ultrasound characterization of red blood cell aggregation using the structure factor size estimator. J Acoust Soc Am 2007;122:645–656.